GIS AND REMOTE SENSING OF LANDSCAPE-LEVEL DISTURBANCES

GIS AND REMOTE SENSING TECHNIQUES TO QUANTIFY VEGETATION RESPONSES TO LANDSCAPE-LEVEL DISTURBANCES

By PRABHA AMALI RUPASINGHE, M.Sc., B.Sc.

Faculty of Science

Department of Biology

A Thesis Submitted to the School of Graduate Studies

in Partial Fulfillment of the Requirements for the Degree

DOCTOR OF PHILOSOPHY

February 2021

DOCTOR OF PHILOSOPHY (2021)	McMaster University
Department of Biology	Hamilton, Ontario
TITLE:	GIS and Remote Sensing Techniques to Quantify Vegetation Responses to Landscape-Level Disturbances
AUTHOR:	Prabha Amali Rupasinghe M.Sc. (Bowling Green State University) B.Sc. (University of Peradeniya)
SUPERVISOR:	Dr. Patricia Chow-Fraser
NUMBER OF PAGES:	xxix, pp. 258

Lay Abstract

Ecosystem stress is caused by natural or anthropogenic factors and results degradation of ecosystems. I investigated the spatial and temporal dynamics of ecosystem stress on aquatic and terrestrial ecosystems using Remote Sensing and Geographic Information Systems techniques. I mapped *Phragmites australis,* a notorious invasive grass, in wetlands to aid the *Phragmites* management programs. My research shows that images collected in late summer or fall provide high *Phragmites* mapping accuracy. Furthermore, I successfully mapped small, low-density *Phragmites* stands in the early stages of invasions. I also investigated the pre-and post-fire vegetation dynamics in the boreal forests of Alberta. I show that the species composition and water features influence the burn severity. The human influence on these ecosystems alters the natural post-fire vegetation recovery processes. Overall, my thesis advances the use of novel remote-sensing techniques to investigate the ecosystem stress factors on wetland and boreal ecosystems in Canada.

Abstract

Ecosystems respond to stress factors that may have a natural or anthropogenic origin. Natural stress factors include flood, wildfire, drought, insect infestations, etc. and anthropogenic stress factors include pollution, land cover changes, and the introduction of alien invasive species. These stressors can degrade ecosystems and result in biodiversity loss and lowered resilience. In this thesis, I investigate the spatial and temporal dynamics of ecosystem stress caused by natural and anthropogenic factors in both aquatic and terrestrial ecosystems. The large study areas and long-term changes in my research have mandated the use of Remote Sensing (RS) and Geographic Information Systems (GIS) techniques in ways that have not been previously considered in ecological studies. In the first two chapters, I developed new approaches to monitor *Phragmites australis*, one of the most aggressive alien plant species that has invaded wetland ecosystems throughout N. America, as well as roadside ditches where management is costly and logistically challenging. I have developed innovative methods to accurately map invasive *Phragmites* under two conditions: 1) when plant biomass and densities are high so that managers can evaluate the effectiveness of treatment methods and 2) when plant biomass and densities are small and sparse so that these stands can be quantified and eradicated. I found that freely available, low to moderate resolution satellite imagery (Landsat 7/8 and Sentinel 2), acquired in late July or early August, can be used to produce highly accurate maps of dense *Phragmites* populations. I also found that commercial satellite imagery (WorldView 2/3) can be used to map *Phragmites* in the early stages of invasion and when

plants have regenerated following herbicide treatment. In the latter half of my thesis, I examined how pre-fire canopy species composition and forest health influence the response of boreal forests to wildfires in Alberta, Canada. Forest fires occur naturally in boreal forests and usually affect very large spatial extents that remove accumulated fire fuel from the system. Following these outbreaks, the forests will regenerate and eventually become restored to their initial state. Climate-change induced droughts and flooding may change the frequency and location of these forest fires. To quantify the burn severity of each fire, I used Landsat images to calculate the differenced Normalized Burn Ratio (dNBR); then combined dNBR for all affected areas to develop the Standardized Burn Impact Score (SBIS), which quantifies the average impact of each fire based on the size of the burned area and the mean burn severity per pixel. In general, pre-fire dominance of coniferous species (jack pine and spruce) led to higher SBIS values while pre-fire dominance of broad-leaved species (aspen, birch, and poplar) led to lower values. Mean burn severity and SBIS values increased significantly when fire outbreaks occurred at a distance of 1 km or greater from water features (e.g. lakes, rivers, streams, wetlands). I also investigated the post-fire recovery process using indices of vegetation health and accounting for the effect of distance from the water features with respect to different levels of human activity. My results show that the post-fire recovery patterns are altered due to human activities and can affect the long-term fire regimes in boreal forests of northern Alberta. Overall, my thesis has advanced the use of novel remote-sensing techniques to study ecosystem stress factors on wetland and boreal ecosystems in Canada.

Acknowledgments

I would like to express my heartfelt gratitude to my supervisor, Dr. Pat Chow-Fraser. First, thank you so much for giving me the opportunity to be a part of your amazing lab. You gave me the freedom to explore my own research ideas, shaped them up, and showed me the right path. I appreciate the limitless support you gave me when I was lost and overwhelmed. Most importantly, thank you for being patient with me and encouraging me. Being an international student away from home, you were a friend and a parent to me when I was feeling down and stressed. You were a truly exceptional, caring, and an inspiring mentor. Thank you for everything.

I would also like to extend my gratitude to my supervisory committee, Dr. Michael Waddington, Dr. Darren Scott, and Dr. Jonathon Stone for providing me great insights and constructive criticism to improve my research.

I am grateful to all the PCF lab members for the care and support, and for making my time at McMaster a joyful and memorable time. A special thanks to James and Chantel for sharing your work and supporting me to develop my thesis chapters. And thank you to all the lab friends, Dan, Lindsey, Nick, Morgan, Alana, Dani, Sawsan, Steve, and Sarah for all the care, friendship, and for providing invaluable suggestions for my lab talks. You all helped me so much to adapt to a new city and country. A big thank you to all the PCF lab undergraduates during my time, especially Jordan, Sherry, Yuxin, Iris, Matthew, Kristen, and Grace for the assistance with fieldwork, downloading and preprocessing images, and digitizing.

Many thanks to the School of Graduate Studies (SGS) and the Department of Biology at McMaster University for the financial and official support. I would also like to thank all the institutions who have funded, supported, provided data, and/or collaborated during the last four years, namely, Boreal Water Futures, Global Water Futures, Ministry of Transportation, Ontario, Nature Conservancy of Canada, Ontario Parks, Canadian Wildlife Service, and Ministry of Environment and Climate Change Canada. I also like to thank Ms. Jennifer Angoh (Trent University) and Dr. Christina Davy (Trent University and Ontario Ministry of Natural Resources and Forestry) for sharing field data and for the great collaboration.

I am eternally grateful to my wonderful parents. Ammi and Thaththi, thank you for the love, faith, and trust you had in your little girl and for raising me to be the person I am today. Your love had no limits, and I am truly blessed to have such amazing parents like you. A big, heartfelt thank to my one and only sister, who is also my best friend and partner in crime. Akki, you were the one who listened to all my nonsense, worries, and sorrows. Simply thank you for being with me ever since I can remember. Also, a heartfelt thank to my grandparents for the love, care, and affection.

A special thanks to Charmini, Eureka, Dilusha, Kasuni, Guvanthi, Sanchala, and Chathushka for the amazing friendship during my time in Hamilton. You all are lifetime friends. Also, a big thank to Ramadha and Chethana for the support with my research work.

Last, but not least, a huge thank to my loving husband Dayal. You were right next to me all these years. Thank you for being that loving, caring, supportive, funny, loud, and hungry person, and simply for being there for me. I would not have made it this far without you.

Thank you all.

.

Table of Content

List of Figures

List of Tables

List of Abbreviations

ASTER	Advances in Spaceborne Thermal Emission and Reflection Radiometer
ATS	Alberta Township Systems
AVIRIS	Airborne Visible InfraRed Imaging Spectrometer
BCNWA	Big Creek National Wildlife Area
BL	Bistcho Lake
BWF	Boreal Water Futures
CASI	Compact Airborne Spectrographic Imager
CBI	Composite Burn Index
CM	Crown Marsh
dNBR	differenced Normalized Burn Ratio
ESA	European Space Agency
ETM	Enhanced Thematic Mapper
GIS	Geographic Information System
GWF	Global Water Futures
HyMap	Hydrological Modeling and Analysis Platform
LAI	Leaf Areas Index
LiDAR	Light Detection and Ranging
LP	Long Point
LPI	Largest Patch Index
LSL	Lesser Slave Lake
LSU	Linear Spectral Unmixing
MF	Match Filtering
ML	Maximum Likelihood
MNF	Minimum Noise Fraction
MODIS	Moderate-resolution Imaging Spectroradiometer
MT	Mixture Tuning

MTO	Ministry of Transportation, Ontario
MTMF	Mixture-Tuned Match Filtering
NASA	National Aeronautics and Space Administration
NCC	Nature Conservancy Canada
NDVI	Normalized Difference Vegetation index
NDWI	Normalized Difference Water Index
NFDB	National Wildfire Database
NIR	Near InfraRed
OLI	Operations Land Imager
OMNRF	Ontario Ministry of Natural Resources and Forestry
PALSAR	Phased Array type L-band Synthetic Aperture Radar
PCA	Principal Component Analysis
RBM	Rondeau Bay Marsh
RBR	Relativized Burn Ratio
RC	Richardson
RdNBR	Relativized dNBR
ROI	Regions Of Interest
RS	Remote Sensing
S2	Sentinel 2
SAM	Spectral Angle Mapper
SAR	Synthetic Aperture Radar
SBIS	Standardized Burn Impact Score
SPOT	Satellite Pour l'Observation de la Terre
SVM	Support Vector Machines
SWIR	ShortWave InfraRed
SWOOP	South West Ontario Orthophotography Project
TM	Thematic Mapper
UAV	Unmanned Aerial Vehicle

USGS	United States Geological Survey
WB	Wood Buffalo National Park
WV	WorldView

Declaration of Academic Achievement

This thesis is presented in sandwich thesis format with six chapters and one appendix. Chapter 1 provides a general introduction. Chapters 2 and 3 are published in peer-review scientific journals, Chapter 4 is under peer-review in a scientific journal and Chapter 5 is presented as a manuscript. Chapter 6 provides general conclusions. Appendix A is a published internal report from the Ministry of Transportation, Ontario, and is extended work from Chapter 3.

Chapter 1: **General Introduction**

Author: Prabha Amali Rupasinghe

Chapter 2: **Identification of Most Spectrally Distinguishable Phenological Stage of Invasive *Phragmites australis* in Lake Erie wetlands (Canada) for Accurate Mapping Using Multispectral Satellite Imagery**

Authors: Prabha Amali Rupasinghe and Patricia Chow-Fraser

Date accepted: June 20, 2019

Journal: Wetlands Ecology and Management, 27(4), 513–538.

https://doi.org/10.1007/s11273-019-09675-2

Reproduced with permission from Springer Nature (License Number: 5003780817826)

Comments P. A. R. conducted image processing, data analysis, and wrote the

manuscript under the supervision of P. C-F

Chapter 3: **Mapping *Phragmites* cover using WorldView 2/3 and Sentinel 2 images at Lake Erie Wetlands, Canada**

Authors: Prabha Amali Rupasinghe and Patricia Chow-Fraser

Date accepted: December 04, 2020

Journal: Biological Invasions. https://doi.org/10.1007/s10530-020-02432-0

Reproduced with permission from Springer Nature (License Number: 5003780193196)

Comments P. A. R. conducted data collection, image processing, data analysis, and wrote the manuscript under the supervision of P. C-F

Chapter 4: **Relating pre-fire canopy species and proximity to water features to burn severity of boreal wildfires in northern Alberta, Canada**

Authors: Prabha Amali Rupasinghe and Patricia Chow-Fraser

Journal: Forest Ecology and Management (Under review, manuscript number FORECO-D-21-00141)

Comments P. A. R. conducted data collection, image processing, data analysis, and wrote the manuscript under the supervision of P. C-F

Chapter 5: **Effect of anthropogenic impact on post-fire vegetation recovery of Alberta's boreal forests using time-series Landsat data**

Authors: Prabha Amali Rupasinghe and Patricia Chow-Fraser

Journal: Presented as a manuscript

Comments P. A. R. conducted data collection, image processing, data analysis, and wrote the chapter under the supervision of P. C-F

Chapter 6: General Conclusions

Author Prabha Amali Rupasinghe

Chapter 7/ Appendix A: Use of World View 3 (WV 3) satellite imagery for early detection of invasive *Phragmites australis* in roadway corridors in Ontario

Authors: Prabha Amali Rupasinghe and Patricia Chow-Fraser

Date Accepted: October 2018

Publisher: Ontario Ministry of Transportation (MTO) (Report Number: 2015-15)

Comments: P. A. R. conducted data collection, image processing, data analysis, and wrote the chapter under the supervision of P. C-F

Chapter 1. Introduction

1.1. Ecosystem health and stress

A healthy ecosystem can be defined as a stable and sustainable system that is maintaining its organization autonomously through time and is resilient to stress (glossary) (Costanza, 1992; Lu et al., 2015; Rapport et al., 2001; Rapport, Costanza, & McMichael, 1998). Ecosystems go through stress periodically. Various studies have attempted to define ecosystem stress (Kolasa & Pickett, 1992; Rapport et al., 1985; Ulanowicz, 1996). According to Rapport et al., (1985), ecosystem stress is defined as "an external force or factor, or stimulus that causes changes in the ecosystem, or causes the ecosystem to respond, or entrains ecosystemic dysfunctions that may exhibit symptoms" (Glossary). The response of an ecosystem to stress could be determined through comparison to the normal state (O'Neill & Reichle, 1979). Rapport et al., (1985) classifies ecosystem stressors into five categories; 1) harvesting of renewable resources, 2) pollution of water, air, or land, 3) land-use changes caused by human activity, 4) introduction of exotic plant or animal species, and 5) extreme natural events such as volcanic eruptions, earthquakes, and climatic shifts. Tracking the ecosystem response to these stressors are often challenging and requires frequent ecosystem monitoring and assessment through ecosystem health indicators. These ecosystem responses could be tracked through various factors such as changes in nutrient cycling, primary productivity, species diversity, decline or the shift of species composition, and the changes in the size

distribution of species (Allan et al., 2013; Kolasa & Pickett, 1992; Likens et al., 1978; Rapport et al., 1985; Regier & Hartman, 1973).

Periodic disturbances are natural in nearly all types of ecosystems and the common examples are flood, drought, fire, and insect infestation (Vogl, 1980, Glossary). Depending on the severity of the stressor and the pre-disturbance health status and resilience, ecosystem recovery is determined. In a healthy ecosystem, post-disturbance recovery is generally faster (Odum, 2014). In some cases, these natural stress factors are not necessarily destructive but help the regeneration and nutrient recycling within the system. In contrast to natural stressors, anthropogenic stressors are often devastating (Rapport & Whitford, 1999). Ecosystems cannot adapt to human-induced stressors such as land cover changes, the introduction of exotic species, and overharvesting, and this results in further degradation of the ecosystem and often fail to recover back to its original state (Rapport & Whitford, 1999). Furthermore, anthropogenic activity enhances and increases the frequency of natural disturbances such as wildfire and flood, through processes such as human-induced climate change and disrupt the natural disturbance-recovery patterns.

1.2. Geographic Information Systems (GIS) and Remote Sensing (RS)

Bonham-Carter, (1994) defines GIS as “a computer system for managing spatial data”. GIS is (Bonham-Carter, 1994). These systems aid in combining different types of spatial data layers such as aerial or satellite images, topographic data, and climatic data and producing meaningful outputs, and support decision making. GIS has broad applications in many fields including environmental analysis such as hazard analysis and

prediction, site selection, resource exploration, and ecosystem monitoring (Bonham-Carter, 1994; Downey, 2006).

RS has many definitions, yet could be simply introduced as “gathering of information at a distance” (Campbell, 2002). In a broader sense, Gupta, (2017), defines RS as “the technology of acquiring data through a device which is located at a distance from the object, and analysis of the data for interpreting the physical attributes of the object”. RS technology is mainly developed through the analysis and interpretation of satellite or aerial images. In the past five decades, this technology has drastically developed with broad applications in many disciplines such as resource exploitation, mapping and monitoring the earth's environment on both local and global scales, atmospheric and climatic sciences, and many other (Gupta, 2017; Thenkabail, 2016).

Assessment of ecosystem health and response to stressors is challenging, especially when larger spatial extends are affected and with altered temporal patterns as a response to stressors with a direct or indirect anthropogenic origin. Conventional field assessments are often valuable in characterizing the ecosystem disturbances accurately. However, GIS- and RS-based methods provide the advantage of assessing the stress factors as well as the ecosystem responses in larger spatial and temporal scales, hence can give a more comprehensive idea on long-term stress dynamics (Gouveia et al., 2009; Zarco-Tejada et al., 2002; Zhang et al., 2010). These techniques could be used to both regular monitoring of ecological health indices such as species richness, ecosystem productivity, and vigor, and ecosystem resilience (Glossary) and evaluate the changes following natural or human-induced disturbances (Kerr & Ostrovsky, 2003). RS data can

also be effectively used to identify the human interactions with the physical environment through various mapping and modeling approaches (Hurtt et al., 2001). Despite the broad applicability of RS and GIS in ecological research, effective and reliable methods need to be developed on a case by case basis to address the issues such as scale, data availability, and uncertainties in retrieving health indicators due to the complexity and uniqueness of ecological problem assessment (Li et al., 2014).

1.3. Invasive *Phragmites australis*

Phragmites australis (Cav.) Trin. ex Steud. subspecies *australis* (common reed; hereafter *Phragmites*) is a perennial grass and one of the worst plant invaders in wetlands of North America (Packer et al., 2017). It is a cosmopolitan species that grows in wetlands, lakeshores, estuaries, and roadside ditches (DeVries et al., 2020; McNabb & Batterson, 1991). Other than the introduced, invasive lineage, two other lineages of *Phragmites* are identified in North America; native *P. australis* subsp. *Americanus* and *P. australis* subsp. *berlandieri* (Kettenring et al., 2012). The introduced, invasive haplotype is of European origin and has been distributed through the temperate parts of North America since the early 1800s (Saltonstall, 2002; Saltonstall & Meyerson, 2016). Furthermore, hybridization between the introduced and native North American lineages has been also confirmed (Saltonstall & Meyerson, 2016). The invasive *Phragmites* haplotype has aggressively colonized through North American east coast, the gulf coast, the Great Lakes region, and southwestern U.S. (Chambers et al., 1999; Meyerson et al., 2010; Saltonstall, 2002).

Invasive *Phragmites* is a robust grass with a broader level of salinity tolerance that can successfully grow in a range of ecosystems including fresh, brackish, and saltwater marshes, riverbanks as well as roadside ditches (Brisson et al., 2010; Meyerson et al., 2000; Saltonstall, 2002; Tewksbury et al., 2002). *Phragmites* reproduce both sexually through wind-pollinated seeds and asexually through underground rhizomes (Markle & Chow-Fraser, 2018; Meyerson et al., 2000; Packer et al., 2017). Seed dispersal could occur through both wind and water while vegetative propagation could occur through the dispersal of fragments of rhizomes by water currents, animals, or construction equipment (Tewksbury et al., 2002). Once established, *Phragmites* form dense monocultures through an extensive below-ground rhizome system with roots growing up to 4 m below surface and shoots growing 3 to 4 m above ground height with over 70 stem shoots (Gilbert et al., 2014; Packer et al., 2017).

Rapid invasion of *Phragmites* has caused many negative environmental impacts such as alterations of resource utilization, trophic structure modifications, changes in disturbance regimes, reduce light at the marsh surface soil and air temperatures, inhibition of the germination of other plant species, slow decomposition of organic matter and many other (D'antonio & Dudley, 1995; Mack, 1996; Marks et al., 1994; Meyerson et al., 2000). Due to high biomass production and litter accumulation, *Phragmites* increase the marsh elevation to a greater extent than other marsh species, hydrological flow is modified and may lead to loss of first-order streams (Lathrop et al., 2003; Meyerson et al., 2000). Invasions could also lead to rapid changes in wetland plant communities where mixed plant communities could turn into tall, *Phragmites* mono stands (Meyerson et al.,

2009). Unlike vegetation communities, *Phragmites* have both negative and positive effects on fauna that utilize the invaded habitats. Approximately fifty bird species were recorded to use *Phragmites* stands in North America and *Phragmites* provide protective cover to species such as muskrat, wading birds, and some duck species during summer (Berthold et al., 1993; Lynch et al., 1947; Parsons, 2003). On the other hand, *Phragmites* have detrimental effects on fish communities due to habitat alterations (Able & Hagan, 2000). According to Markle & Chow-Fraser, (2018), *Phragmites* reduce the effective habitat for the at-risk turtle species.

Due to strong establishment, effective *Phragmites* treatment requires multiple different, repeated treatments (Gilbert, 2015). In Ontario, *Phragmites* management is mainly conducted through chemical treatment using glyphosate or imazapyr (Avers et al., 2007; Gilbert, 2015). Mechanical control measures include various approaches such as cutting, drowning, smothering, excavating, and burning (Gilbert et al., 2014). *Phragmites* eradication after being well-established takes an enormous amount of effort, time, and cost. Controlling *Phragmites* at earlier stages of invasions could significantly reduce the efforts and is relatively more effective (Ontario Ministry of Natural Resources, 2011). For effective treatment, identification of well-established, young, and mixed stands of *Phragmites* in the affected areas is equally essential. RS-based approaches provide the best means to map *Phragmites* over large spatial extents including the areas that are physically inaccessible.

1.4. Boreal forests and wildfires

Boreal forests are the northernmost forests of the world and encompass approximately 30% of the worlds' forested areas (Gauthier et al., 2015). Boreal forests are bordered to the south by arid steppe, prairie, or semi-desert ecosystems and to the north by subarctic woodlands with patchy treeless and stunted forested stands (Apps et al., 1993). These regions are characterized by short summers and long, extreme winters. Boreal forests are dominated by coniferous species with occasional deciduous stands. Other than the forested regions, these ecosystems contain a large number of wetlands and many water bodies such as lakes and rivers (Mery et al., 2010).

Wildfires are the most common, large-scale, natural disturbance in these ecosystems and are an essential part of boreal forest dynamics (Terrier et al., 2013). They increase the landscape-level productivity, shape the structure, and composition, and renew the boreal stands (Terrier et al., 2013). Wildfire recurrence interval in these forests is approximately 29 to 300 years, and this is strongly affected by factors such as climate and anthropogenic activity (Fastie & Mann, 1993; Kasischke et al., 1995, 2000). The intensity of fires (Glossary) is determined by the fire interval as this determines the level of fuel loading and the local weather and regional climate and also may be affected by the fuel type, topography, and characteristics of previous disturbances (Weber & Flannigan, 1997).

The wildfire activity in the boreal region has drastically increased in the past few decades as a result of global climate change (Flannigan et al., 2005; Peng et al., 2011). Increased global temperatures have increased the drought frequency, and created extreme

fire-weather (Glossary) days and thereby extend the fire season (Flannigan et al., 2009). This further increases the number of ignitions as well as the longer burning leading to larger fire outbreaks (Wang et al., 2017). In Canada, 35% of the wildfires have resulted from lightning, yet accounts for 85% of the total area burned (Weber & Flannigan, 1997). According to Wang et al., (2017), a warm, moist atmosphere may lead to more lightening and Wotton et al., (2010) suggest an increase in the ignition from about 75% to 140% by the end of the century. Kirschbaum & Fischlin, (1996) predicts an increase of temperature in 1900 to 2050 in order of 1-2 °C in summer and 1-3 °C in winter, approximately 20% change in precipitation, and drier summer soils with 2-8 mm less water. Therefore, North American fire regimes are expected to increase dramatically due to global climate change.

The changes in fire regimes (Glossary) may alter the post-fire recovery trajectories. The size of fire determines the patchiness of the landscape and affects the propagules dispersal into the burned areas for the forest regeneration (Weber & Flannigan, 1997). Furthermore, the alterations of fire regimes may lead to widespread conversion of vegetation types such as conifer dominant to deciduous dominant forests or eventual shift to prairie grasslands (Johnstone et al., 2010; Mbogga et al., 2010; Rehfeldt et al., 2012; Stralberg et al., 2018). On the other hand, increased fire activity may require more sophisticated fire management strategies. Fire suppression costs are usually high and the fires could be disastrous if they are to occur in remotely populated areas and reduce the harvestable forested areas (Terrier et al., 2013). To overcome the possible challenges of fire management in the future, a better understanding of the underlying causes of wildfires as the post-fire vegetation successional dynamics are essential. To get

a more generalized idea of these dynamic processes, wildfire activity needs to be studied in large spatial extend through long periods.

1.5. Thesis Objectives

Environmental stress and ecosystem response assessment and monitoring require collaboration between both RS specialists and ecologists. My thesis aims to bridge the spheres of knowledge by using RS and GIS techniques to understand and manage ecosystem stress and responses. The overall objective of my thesis is to develop RS- and GIS-based methodologies to understand and manage ecosystem stress on larger spatial and temporal scales. I investigate two major ecosystem stress factors of anthropogenic and natural origin, that have become serious concerns in two different Canadian ecosystems. The first half of my thesis focuses on developing RS-based techniques to optimize accurate mapping of one of the worst invasive plant species of North America, *Phragmites australis*, as an ecosystem stress factor with anthropogenic origin affecting aquatic ecosystems. The second half of my thesis investigates the factors that affect the wildfires and post-fire recovery of boreal forests in Alberta as a natural stress factor on terrestrial ecosystems.

In Chapter 2, we use time series of freely available, moderate resolution satellite data to map the distribution of mature *Phragmites* stands in Lake Erie Wetlands. Here, we investigate the phenological stage of *Phragmites* which produce the most unique reflectance signal to accurately identify the invaded areas using RS images.

In Chapter 3, we investigate the use of commercially available high-resolution multispectral and freely available moderate resolution satellite imagery to detect smaller

Phragmites patches in wetlands, since studies have shown that treatment of small clumps has the highest efficacy. Here, we investigate the usage of subpixel image classification techniques to identify young, less dense *Phragmites* patches at the early stages of invasion.

In Chapter 4, we investigate the factors that affect the burn severity in boreal forests of Alberta and provide a simple cost-effective approach to quantify burn impact using freely available satellite data over long periods and larger spatial scales. Here, we evaluate the effect of the distribution of canopy species, the number of burned days and the proximity to water features on burn severity.

In Chapter 5, we study the post-fire recovery rates and patterns following the same wildfire outbreaks investigated in Chapter 4. Here, we evaluate the influence of anthropogenic activity (proximity to human settlements and density of seismic lines) on the post-fire recovery process using RS-based vegetation indices and species-level recovery, and proximity to water features.

The thesis consists of one appendix. Here we used high-resolution satellite imagery to map small patches of *Phragmites* on roadsides and wetlands using a similar mapping approaches developed in Chapter 3 of this thesis. The appendix is presented in the format of an internal report of the Ministry of Transportation of Ontario.

1.6. Literature cited

Able, K. W., & Hagan, S. M. (2000). Effects of common reed (*Phragmites australis*) invasion on marsh surface macrofauna: Response of fishes and decapod crustaceans. *Estuaries*, *23*(5), 633–646.

Allan, J. D., McIntyre, P. B., Smith, S. D. P., Halpern, B. S., Boyer, G. L., Buchsbaum, A., Burton, G. A., Campbell, L. M., Chadderton, W. L., Ciborowski, J. J. H., Doran, P. J., Eder, T., Infante, D. M., Johnson, L. B., Joseph, C. A., Marino, A. L., Prusevich, A., Read, J. G., Rose, J. B., … Steinman, A. D. (2013). Joint analysis of stressors and ecosystem services to enhance restoration effectiveness. *Proceedings of the National Academy of Sciences*, *110*(1), 372–377. https://doi.org/10.1073/pnas.1213841110

Apps, M. J., Kurz, W. A., Luxmoore, R. J., Nilsson, L. O., Sedjo, R. A., Schmidt, R., Simpson, L. G., & Vinson, T. S. (1993). Boreal forests and tundra. *Water, Air, and Soil Pollution*, *70*(1), 39–53.

Avers, B., Fahlsing, R., Kafcas, E., Schafer, J., Collin, T., Esman, L., Finnell, E., Lounds, A., Terry, R., & Hazelman, J. (2007). A guide to the control and management of invasive Phragmites. *Michigan Department of Environmental Quality, Lansing*.

Berthold, P., Kaiser, A., Querner, U., & Schlenker, R. (1993). Analysis of trapping figures at mettnau station, s germany, with respect to the population development in small birds-a 20 years summary 34 report of the mri-program. *Journal Fur Ornithologie*, *134*(3), 283–299.

Bonham-Carter, G. F. (1994). *Geographic Information Systems for Geoscientists: Modelling with GIS* (First Edition, Vol. 13). Elsevier.

Brisson, J., de Blois, S., & Lavoie, C. (2010). Roadside as invasion pathway for common reed (*Phragmites australis*). *Invasive Plant Science and Management*, *3*(4), 506–514. https://doi.org/10.1614/IPSM-09-050.1

Campbell, J. B. (2002). *Introduction to remote sensing 3rd ed* (3rd ed.). The Guilford Press. New York, New York, USA.

Chambers, R. M., Meyerson, L. A., & Saltonstall, K. (1999). Expansion of *Phragmites australis* into tidal wetlands of North America. *Aquatic Botany*, *64*(3–4), 261–273. https://doi.org/10.1016/S0304-3770(99)00055-8

Costanza, R. (1992). Toward an operational definition of ecosystem health. *Ecosystem Health: New Goals for Environmental Management*, *239*, 269.

D'antonio, C. M., & Dudley, T. L. (1995). Biological invasions as agents of change on islands versus mainlands. In *Islands* (pp. 103–121). Springer.

DeVries, A. E., Kowalski, K. P., & Bickford, W. A. (2020). Growth and behavior of North American microbes on *Phragmites australis* leaves. *Microorganisms*, *8*(5), 690.

Downey, L. (2006). Using Geographic Information Systems to Reconceptualize Spatial Relationships and Ecological Context. *American Journal of Sociology*, *112*(2), 567–612. https://doi.org/10.1086/506418

Fastie, C. L., & Mann, D. H. (1993). *A preliminary fire history for the Caribou-Poker Creeks Research Watershed, Alaska*.

Flannigan, M. D., Krawchuk, M. A., de Groot, W. J., Wotton, B. M., & Gowman, L. M. (2009). Implications of changing climate for global wildland fire. *International Journal of Wildland Fire*, *18*(5), 483–507.

Flannigan, Mike D., Logan, K. A., Amiro, B. D., Skinner, W. R., & Stocks, B. J. (2005). Future area burned in Canada. *Climatic Change*, *72*(1–2), 1–16.

Gauthier, S., Bernier, P., Kuuluvainen, T., Shvidenko, A. Z., & Schepaschenko, D. G. (2015). Boreal forest health and global change. *Science*, *349*(6250), 819–822. https://doi.org/DOI: 10.1126/science.aaa9092

Gilbert, J. (2015). *Rondeau Provincial Park Invasive Phragmites Management Program 2008–2014 Summary Report and Recommended Next Steps*. Unpublished manuscript.

Gilbert, J., Vidler, N., Cloud Sr, P., Jacobs, D., Slavik, E., Letourneau, F., & Alexander, K. (2014). *Phragmites australis* at the crossroads: Why we cannot afford to ignore this invasion. *Proceedings of Great Lakes Wetlands Day*, 78–84.

Gouveia, C., Trigo, R. M., & DaCamara, C. C. (2009). Drought and vegetation stress monitoring in Portugal using satellite data. *Natural Hazards and Earth System Sciences*, *9*(1), 185–195. https://doi.org/10.5194/nhess-9-185-2009

Gupta, R. P. (2017). *Remote Sensing Geology* (3rd Edition). Springer. https://books.google.ca/books?id=lERADwAAQBAJ&printsec=copyright&source=gbs_pub_info_r#v=onepage&q&f=false

Hurtt, G. C., Rosentrater, L., Frolking, S., & Moore III, B. (2001). Linking remote-sensing estimates of land cover and census statistics on land use to produce maps

of land use of the conterminous United States. *Global Biogeochemical Cycles*, *15*(3), 673–685.

Johnstone, J. F., Hollingsworth, T. N., Chapin III, F. S., & Mack, M. C. (2010). Changes in fire regime break the legacy lock on successional trajectories in Alaskan boreal forest. *Global Change Biology*, *16*(4), 1281–1295.

Kasischke, E. S., Christensen Jr, N. L., & Stocks, B. J. (1995). Fire, global warming, and the carbon balance of boreal forests. *Ecological Applications*, *5*(2), 437–451. https://doi.org/10.2307/1942034

Kasischke, E. S., French, N. H., O'Neill, K. P., Richter, D. D., Bourgeau-Chavez, L. L., & Harrell, P. A. (2000). Influence of fire on long-term patterns of forest succession in Alaskan boreal forests. In *Fire, climate change, and carbon cycling in the boreal forest* (pp. 214–235). Springer.

Kerr, J. T., & Ostrovsky, M. (2003). From space to species: Ecological applications for remote sensing. *Trends in Ecology & Evolution*, *18*(6), 299–305.

Kettenring, K. M., de Blois, S., & Hauber, D. P. (2012). Moving from a regional to a continental perspective of Phragmites australis invasion in North America. *AoB PLANTS*, *2012*. https://doi.org/10.1093/aobpla/pls040

Kirschbaum, M. U. F., & Fischlin, A. (1996). *Climate change impacts on forests*. https://www.osti.gov/etdeweb/biblio/441883

Kolasa, J., & Pickett, S. T. A. (1992). *Ecosystem stress and health: An expansion of the conceptual basis*. *1*(1), 7–13.

Lathrop, R. G., Windham, L., & Montesano, P. (2003). Does *Phragmites* expansion alter the structure and function of marsh landscapes? Patterns and processes revisited. *Estuaries*, *26*(2), 423–435. https://doi.org/DOI: 10.1007/BF02823719

Li, Z., Xu, D., & Guo, X. (2014). Remote sensing of ecosystem health: Opportunities, challenges, and future perspectives. *Sensors*, *14*(11), 21117–21139.

Likens, G. E., Bormann, F. H., Pierce, R. S., & Reiners, W. A. (1978). Recovery of a deforested ecosystem. *Science*, *199*(4328), 492–496.

Lu, Y., Wang, R., Zhang, Y., Su, H., Wang, P., Jenkins, A., … Squire, G. (2015). Ecosystem health towards sustainability. *Ecosystem Health and Sustainability*, *1*(1), 1–15.

Lynch, J. J., O'Neil, T., & Lay, D. W. (1947). Management significance of damage by geese and muskrats to Gulf Coast marshes. *The Journal of Wildlife Management*, *11*(1), 50–76.

Mack, R. N. (1996). Predicting the identity and fate of plant invaders: Emergent and emerging approaches. *Biological Conservation*, *78*(1–2), 107–121.

Markle, C. E., & Chow-Fraser, P. (2018). Effects of European common reed on Blanding's turtle spatial ecology. *The Journal of Wildlife Management*, *82*(4), 857–864. https://doi.org/10.1002/jwmg.21435

Marks, M., Lapin, B., & Randall, J. (1994). *Phragmites australis* (*P. communis*): Threats, management and monitoring. *Natural Areas Journal*, *14*(4), 285–294.

Mbogga, M. S., Wang, X., & Hamann, A. (2010). Bioclimate envelope model predictions for natural resource management: Dealing with uncertainty. *Journal of Applied Ecology*, *47*(4), 731–740.

McNabb, C. D., & Batterson, T. R. (1991). Occurrence of the common reed, *Phragmites australis*, along roadsides in Lower Michigan. *Michigan Academician (USA)*, *23*, 211–220.

Mery, G., Katila, P., Galloway, G., Alfaro, R. I., Kanninen, M., Lobovikov, M., & Varjo, J. (2010). *Forests and society-responding to global drivers of change* (Vol. 25). International Union of Forest Research Organizations (IUFRO). https://core.ac.uk/download/pdf/48018311.pdf

Meyerson, L. A., Saltonstall, K., Windham, L., Kiviat, E., & Findlay, S. (2000). A comparison of *Phragmites australis* in freshwater and brackish marsh environments in North America. *Wetlands Ecology and Management*, *8*(2–3), 89–103. https://doi.org/10.1023/A:1008432200133

Meyerson, L. A., Viola, D. V., & Brown, R. N. (2010). Hybridization of invasive Phragmites australis with a native subspecies in North America. *Biological Invasions*, *12*(1), 103–111.

Meyerson, L., Saltonstall, K., & Chambers, R. (2009). *Phragmites australis* in Eastern North America: A Historical and Ecological Perspective. In *Human Impacts on Salt Marshes: A Global Perspective* (p. 432). University of California Press.

Odum, E. P. (2014). The strategy of ecosystem development. In *The Ecological Design and Planning Reader* (pp. 203–216). Springer.

O'Neill, R. V., & Reichle, D. E. (1979). *Dimensions of ecosystem theory*. Oak Ridge National Lab.(ORNL), Oak Ridge, TN (United States).

Ontario Ministry of Natural Resources. (2011). *Invasive Phragmites – Best Management Practices* (Peterborough, Ontario).

Packer, J. G., Meyerson, L. A., Skálová, H., Pyšek, P., & Kueffer, C. (2017). Biological Flora of the British Isles: Phragmites australis. *Journal of Ecology*, *105*(4), 1123–1162. https://doi.org/10.1111/1365-2745.12797

Parsons, K. C. (2003). Reproductive success of wading birds using *Phragmites* marsh and upland nesting habitats. *Estuaries*, *26*(2), 596–601.

Peng, C., Ma, Z., Lei, X., Zhu, Q., Chen, H., Wang, W., Liu, S., Li, W., Fang, X., & Zhou, X. (2011). A drought-induced pervasive increase in tree mortality across Canada's boreal forests. *Nature Climate Change*, *1*(9), 467–471.

Rapport, D. J., Costanza, R., & McMichael, A. J. (1998). Assessing ecosystem health. *Trends in Ecology & Evolution*, *13*(10), 397–402.

Rapport, D. J., Fyfe, W. S., Costanza, R., Spiegel, J., Yassie, A., Bohm, G. M., … Whitford, W. G. (2001). Ecosystem health: definitions, assessment and case studies. *Our Fragile World: Challenges and Opportunities for Sustainable Development. EOLSS, Oxford*, 21–42.

Rapport, D. J., & Whitford, W. G. (1999). How ecosystems respond to stress: Common properties of arid and aquatic systems. *BioScience*, *49*(3), 193–203.

Rapport, J. D., Regier, H. A., & Hutchinson, T. C. (1985). Ecosystem Behavior Under Stress. *The American Naturalist*, *125*(5), 617–640. JSTOR.

Regier, H. A., & Hartman, W. L. (1973). Lake Erie's fish community: 150 years of cultural stresses. *Science*, *180*(4092), 1248–1255.

Rehfeldt, G. E., Crookston, N. L., Sáenz-Romero, C., & Campbell, E. M. (2012). North American vegetation model for land-use planning in a changing climate: A solution to large classification problems. *Ecological Applications*, *22*(1), 119–141.

Saltonstall, K. (2002). Cryptic invasion by a non-native genotype of the common reed, Phragmites australis, into North America. *Proceedings of the National Academy of Sciences*, *99*(4), 2445–2449. https://doi.org/10.1073/pnas.032477999

Saltonstall, K., & Meyerson, L. A. (2016). Phragmites australis: From genes to ecosystems. *Biological Invasions*, *18*(9), 2415–2420.

Stralberg, D., Wang, X., Parisien, M.-A., Robinne, F.-N., Sólymos, P., Mahon, C. L., Nielsen, S. E., & Bayne, E. M. (2018). Wildfire-mediated vegetation change in boreal forests of Alberta, Canada. *Ecosphere*, *9*(3), e02156. https://doi.org/10.1002/ecs2.2156

Terrier, A., Girardin, M. P., Périé, C., Legendre, P., & Bergeron, Y. (2013). Potential changes in forest composition could reduce impacts of climate change on boreal wildfires. *Ecological Applications*, *23*(1), 21–35. https://doi.org/10.1890/12-0425.1

Tewksbury, L., Casagrande, R., Blossey, B., Häfliger, P., & Schwarzländer, M. (2002). Potential for Biological Control of *Phragmites australis* in North America. *Biological Control*, *23*(2), 191–212. https://doi.org/10.1006/bcon.2001.0994

Thenkabail, P. S. (2016). *Remote Sensing Handbook; Volume 3: Remote Sensing of Water Resources, Disasters, and Urban Studies.* Taylor & Francis.

Ulanowicz, R. E. (1996). Trophic Flow Networks as Indicators of Ecosystem Stress. In G. A. Polis & K. O. Winemiller (Eds.), *Food Webs* (pp. 358–368). Springer US. https://doi.org/10.1007/978-1-4615-7007-3_35

Vogl, R. J. (1980). The ecological factors that produce perturbation-dependent ecosystems. *The Recovery Process in Damaged Ecosystems*, 63–94.

Wang, X., Parisien, M.-A., Taylor, S. W., Candau, J.-N., Stralberg, D., Marshall, G. A., Little, J. M., & Flannigan, M. D. (2017). Projected changes in daily fire spread across Canada over the next century. *Environmental Research Letters*, *12*(2), 025005.

Weber, M. G., & Flannigan, M. D. (1997). *Canadian boreal forest ecosystem structure and function in a changing climate: Impact on fire regimes*. *5*, 22.

Wotton, B. M., Nock, C. A., & Flannigan, M. D. (2010). Forest fire occurrence and climate change in Canada. *International Journal of Wildland Fire*, *19*(3), 253–271.

Zarco-Tejada, P. J., Miller, J. R., Mohammed, G. H., Noland, T. L., & Sampson, P. H. (2002). Vegetation Stress Detection through Chlorophyll a + b Estimation and Fluorescence Effects on Hyperspectral Imagery. *Journal of Environmental Quality*, *31*(5), 1433–1441. https://doi.org/10.2134/jeq2002.1433

Zhang, X., Goldberg, M., Tarpley, D., Friedl, M. A., Morisette, J., Kogan, F., & Yu, Y. (2010). Drought-induced vegetation stress in southwestern North America. *Environmental Research Letters*, *5*(2), 024008. https://doi.org/10.1088/1748-9326/5/2/024008

Chapter 2. Identification of Most Spectrally Distinguishable Phenological Stage of Invasive *Phragmites australis* in Lake Erie wetlands (Canada) for Accurate Mapping Using Multispectral Satellite Imagery

By,

Prabha Amali Rupasinghe and Patricia Chow-Fraser

Rupasinghe, P. A., & Chow-Fraser, P. (2019). Identification of most spectrally distinguishable phenological stage of invasive *Phramites australis* in Lake Erie wetlands (Canada) for accurate mapping using multispectral satellite imagery. *Wetlands Ecology and Management*, *27*(4), 513–538. https://doi.org/10.1007/s11273-019-09675-2

2.1. Abstract

Phragmites australis (Cav.) Trin. ex Steudel subspecies *australis* is one of the worst plant invaders in wetlands of North America. Remote sensing is the most cost-effective method to track its spread given its widespread distribution and rapid colonization rate. We hypothesize that the morphological and/or physiological features associated with different phenological states of *Phragmites* can influence their reflectance signal and thus affect mapping accuracies. We tested this hypothesis by comparing classification accuracies of cloud-free images acquired by Landsat 7, Landsat 8, and Sentinel 2 at roughly monthly intervals over a calendar year for two wetlands in southern Ontario. We used the Support Vector Machines classification and employed field observations and image acquired from unmanned aerial vehicle (8 cm) to perform accuracy assessments. The highest *Phragmites* producer's, user's, and overall accuracy (96.00%, 91.11%, and 88.56% respectively) were provided by images acquired in late summer and fall period. During this period, green, Near Infrared, and Short-Wave Infrared bands generated more unique reflectance signals for *Phragmites*. Both Normalized Difference Vegetation Index and Normalized Difference Water Index showed significant difference between *Phragmites* and the most confused classes (cattail; *Typha latifolia* L., and meadow marsh) during the late summer and fall period. Since meadow marsh separated out best from *Phragmites* and cattail in the February image, we used it to mask the meadow marsh in the July image to reduce confusion. The unique reflectance signal of *Phragmites* in late summer and fall is likely due to prolonged

greenness of *Phragmites* when compared to other wetland vegetation, large, distinct inflorescence, and the water content of *Phragmites* during this period.

Key Words: *Phragmites*, Wetlands, multispectral images, SVM classification

2.2. Introduction

Phragmites australis subsp. *Australis* (Cav.) Trin. ex Steudel (the common reed) is a perennial grass that grows in aquatic, semi-aquatic, and terrestrial habitats throughout the world. Saltonstall (2002) identified 27 genetically distinct groups (haplotypes) worldwide, of which 11 have been found in North America. Over the past 2 decades, the European haplotype M began to make rapid incursions into Canada and the U.S., especially into coastal wetlands of the Laurentian Great Lakes (Wilcox et al. 2003; Tulbure et al. 2007; Wilcox 2012; Bourgeau-Chavez et al. 2015), and along highway corridors (Saltonstall 2002; Lelong et al. 2007). This haplotype exhibits invasive characteristics, including its ability to aggressively colonize exposed mud flats sexually (through seeds), and then expand asexually (through rhizomes) to form dense monocultures that inhibit biodiversity of other plants and wildlife (Meyerson et al. 2000; Markle and Chow-Fraser 2018). Its rapid spread has been attributed to it being a superior competitor against other emergent vegetation (Rickey and Anderson 2004; Uddin et al. 2014) and to being more tolerant of disturbances (e.g. road maintenance and changes in hydrologic regimes) and stress (e.g. increased salinity due to road de-icing salts) (McNabb and Batterson 1991; Marks et al. 1994; Chambers et al. 1999; Saltonstall 2002).

Due to its competitive traits against native wetland vegetation, the invasive haplotype (henceforth referred to as invasive *Phragmites*) has successfully invaded many wetlands in south western Ontario and have become the dominant species since the late 1990s. Despite the destructive nature of this invader, very little control of invasive *Phragmites* occurred in the province of Ontario until a pilot project in 2007 involving Roundup Ultrá (Gilbert 2015). Glyphosate, the active compound in Roundup Ultra2 had already been found to be effective in controlling the growth of invasive *Phragmites* in several jurisdictions within the USA (Gilbert 2015). Other than chemical control, mechanical control and prescribed burning is also being used currently for *Phragmites* management. To track the rapid rate of colonization and to assess the effectiveness of control strategies implemented, frequent monitoring and mapping of wetland vegetation has become an essential aspect of sustainable marsh management (Adam et al. 2010).

Traditional floristic mapping requires extensive field work, collection of taxonomic information, ancillary data analysis, and visual estimation of percentage cover of each species, which are costly and labor intensive (Lyon and McCarthy 1995). Due to these limitations, traditional mapping programs have been limited to studies at the site level. For mapping wetland at the regional level, more cost-effective remote sensing techniques can be used because they require comparatively less but more strategic field surveys, and less time required for mapping protocols. An additional benefit is that remotely sensed imagery is acquired repeatedly and provide archived data, which can be easily incorporated into a Geographic Information System (GIS) for further analyses and to study the spatial dynamics of plant assemblages (Ozesmi and Bauer 2002). Such

approaches have been used successfully to map invasive plant species in marshes, where the absence of tree cover gives the sensor an unblocked view of the target species (Laba et al. 2008; Hestir et al. 2008; Bourgeau-Chavez et al. 2015).

Mapping individual species in marshes have several challenges. First, meteorological conditions can lead to lower accuracy because the specular reflectance of sunlight by the water surface often mixes with the signature of other land-cover classes (Bostater et al. 2004; Morel and Bélanger 2006). Water depth, presence of suspended and dissolved materials in the water column, and flow conditions can also affect reflectance by water, which would eventually affect land-cover classification (Hestir et al. 2008). Previous researchers have dealt with these water-related challenges by using different empirical criteria, image correction with field spectrometer measurements, and adjusting image acquisition time in case of air borne data (Bostater et al. 2004; Morel and Bélanger 2006). Other than the physical conditions, biological heterogeneity may also affect mapping accuracy of wetland vegetation.

Differences in phenological stage (i.e. timing of flowering, senescence, and changes in leaf and canopy structure) can also influence the reflectance signatures of co-occurring species (Hestir et al. 2008). Since most of the wetland species share similar habitats and are adapted to the same environmental conditions, they share similar morphological features such as leaf arrangement and canopy architecture that are difficult to distinguish visually. By identifying the phenological stages of the target species that help them stand out from co-occurring species, however, it should be possible to improve mapping accuracy. According to Zhang et al. (2003), four transition dates define the key

phenological phases of a species: 1) green-up (date of onset of photosynthetic activity), 2) maturity (date when green leaf area is maximum), 3) senescence (rate at which greenness decreases), and 4) dormancy (date at which photosynthetic rate approaches zero). At regional and larger scales, variations in the composition of the community, micro- and regional climate regimes, soils, land management and plant-related features can lead to multiple modes of growth and senescence within a single annual cycle (Zhang et al. 2003). Therefore, use of appropriate type of remotely sensed imagery collected in the most spectrally distinguishable phenological state, data pre- and post-processing techniques, and the classification algorithms may all affect the outcome.

Successful mapping of wetlands at the species level has typically required data with high spatial and spectral resolution (Everitt et al. 1995, 1996, 2001; Fuller 2005). Some sensors that have been used previously used include airborne hyperspectral sensors such as AVIRIS (Airborne Visible InfraRed Imaging Spectrometer; 224 bands) (Williams and Hunt Jr 2002), CASI (Compact Airborne Spectrographic Imager; 288 bands) (Schmidt and Skidmore 2001), HyMap (Hydrological Modeling and Analysis Platform;126 bands) (Zhang and Xie 2013), and PROBE-1 (128 bands) (Lopez et al. 2004) and high resolution multispectral satellite imagery such as IKONOS (Fuller 2005; Flores et al. 2006) and QuickBird (Laba et al. 2008). Their relatively high cost and limited spatial cover (in the case of airborne data), however, make them unsuitable for frequent large-scale mapping that is required to track invasive *Phragmites* with high growth rates. By comparison, imagery with moderate spatial and spectral resolution (10 to 100 m spatial resolution and <100 bands) have been commonly used for community-level

mapping and have not been used for species-level mapping except when they occur as monocultures (Dewey et al. 1991; Sohn and McCoy 1997; Zhang et al. 2003). Some of the moderate-resolution data used for species identification include Landsat TM (Thematic Mapper; 7 bands) and ETM+ (Enhanced Thematic Mapper Plus; 8 bands) (Peterson 2005; Resasco et al. 2007; Huang and Asner 2009), SPOT (Satellite Pour l'Observation de la Terre; 4 bands) (Rasolofoharinoro et al 1998), and ASTER (Advances in Spaceborne Thermal Emission and Reflection Radiometer; 14 bands) (Gao and Liu 2008) and MODIS (Moderate-resolution Imaging Spectroradiometer; 36 bands) (Zhang et al. 2003).

Despite its moderate spatial resolution (i.e. 30 m), Landsat data had been used by many researchers around the globe for species-level mapping. These images are particularly useful because the imagery are free, available every 16 days, provide extensive coverage, and date back to 1984 (Peterson 2005; Resasco et al. 2007). Moreover, Sentinel 2, a relatively new sensor (with 10, 20, and 60 m spatial resolution) launched in 2015, has been used for the classification of crop and tree species, development of vegetation indices, Leaf Areas Index (LAI), and biophysical variables analysis etc. To date, however, it has not yet been used extensively in phenological studies (Delegido et al. 2011; Frampton et al. 2013; Hill 2013; Immitzer et al. 2016).

Besides selection of data, classification accuracy will depend on proper selection of the classification algorithm. Support Vector Machines (SVM) classification is a supervised, non-parametric, statistical learning technique developed by Vapnic in 1979 (Vapnik and Kotz 1982). As this method does not assume data normality distribution, it

usually performs better than many popular classifiers such as the maximum likelihood classification (Dalponte et al. 2008; Rupasinghe et al. 2018). The SVM performs better in terms of classification accuracy, computational time, and stability to parameter setting when compared with radial basis function neural networks and K-nearest neighbor classification methods (Melgani and Bruzzone 2004; Pal and Mather 2005). Moreover, this method can produce high classification accuracy using a relatively small training data set (Dalponte et al. 2008; Zheng et al. 2015). Consequently, over the past decade, SVM classification has gained popularity in the remote sensing community (Mountrakis et al. 2011). Many past investigators have successfully used the SVM classification in forest and crop classification, species-level mapping in wetlands, and in developing vegetation indices for different data sources such as hyperspectral (Gualtieri and Cromp 1999), LiDAR (Dalponte et al. 2008), and multispectral data including Landsat TM (Huang et al. 2008; Zheng et al. 2015) and Sentinel 2 (Stratoulias et al. 2015).

Previous studies have demonstrated that the moderate resolution multispectral images could be used to map invasive species that form large monocultures however, the reflectance signal of these invasive species are often very similar to the native species that share the same ecosystem. This may lead to low classification accuracy for both invasive and native species. Therefore, it is important to identify the vegetation categories that have similar reflectance signatures as the invasive species to develop more accurate classification protocols. Moreover, the effect of biological heterogeneity highly varies depending on the site conditions and the species composition of the study area. In this study, we address these issues and focus mainly on the effect of different phenological

states on mapping accuracy of selected Lake Erie wetlands, with special emphasis on invasive *Phragmites*. We evaluated the use of SVM classification to map large monocultures of *Phragmites* in two Lake Erie wetlands using Landsat 7, 8, and Sentinel 2 imagery. To minimize omission errors associated with classification of mixed pixels (*Phragmites* and similar land cover classes) when moderate resolution imagery are used for species level classification, and as limited spectral bands are available in multispectral imagery, we have analyzed the time series images collected over different months of the calendar year to determine the best time in the *Phragmites* growth cycle or the best phenological state when the plant will produce a reflectance signature that will be most unique when compared with co-occurring vegetation. For future applications with other image sources, we have also identified the bands that contributed most to distinguishing among *Phragmites* and other similar vegetation classes. In summary, this novel *Phragmites* mapping approach; 1. Will provide cost-effective method to identify *Phragmites* invaded wetlands using freely available, moderate-resolution satellite images for large-scale monitoring and treatment effectiveness monitoring programs, 2. Will provide the wetland management community with an accurate, cost-effective method to track changes in the distribution of invasive *Phragmites* at a regional scale, and 3. Support future research to accurately map *Phragmites* with other sensors which provide important spectral information and to collect images during the best period of the year and plan field work accordingly.

2.3. Methods

2.3.1. Study sites

We conducted the study in two Lake Erie wetlands, Big Creek National Wild Life Area (BCNWA) (49° 59’ N 80° 46’ W) and Rondeau Bay Marsh (RBM) (42° 17′ N 81° 52′ W) (Fig. 2.1). BCNWA is located on the North shore of Lake Erie, 3 km from the southwest Port Rowan and at the head of the Long Point Bay on Lake Erie, in the Regional Municipality of Haldimand-Norfolk county (Ashley and Robinson 1996; Environment and Climate Change Canada 2011). It is a 771-ha complex consisting of two sub-units, Big Creek unit (615 ha) and the Hahn Marsh Unit (156 Ha). Our study focused on the Big Creek unit, which is managed by the Environment and Climate Change Canada. Wetlands at this site is dominated by Bluejoint Grass (*Calamagrostis canadensis* (Michx.) P. Beauv.), cattails (*Typha latifolia* L.), and sedges (Ashley and Robinson 1996). The invasive species in this site includes *Phragmites*, European frog-bit (*Hydrocharis morsus-ranae* L.) and European Black Alder (*Alnus glutinosa* (L.) Gaertn.) (Environment and Climate Change Canada 2011).

RBM is a shallow coastal wetland, also on the northern shore of the central basin of the Lake Erie, approximately 100 km southeast of Windsor ON, Canada and Detroit, MI, USA (Meloche and Murphy 2006; Glass et al. 2012). It was established in 1894 and was Ontario’s second protected provincial park. It covers an area of 3257 ha and mainly consists of forests, sandy peninsula, and marsh. Forested land in RBM is characterized by rare Carolinian tree species, where it is the largest remaining representation of Carolinian forests in Canada and is a primeval or wilderness remnant of the vegetation of early

Ontario (Mann and Nelson 1980; McLaughlin 1993). Approximately 40% of the rare, threatened or endangered species in Canada are Carolinian and are present in RBM.

We used the BCNWA site for development of our classification protocols as this site had not been treated during the study period and there were no significant changes in *Phragmites* cover over the period studied. We used the RBM site for comparison of results obtained from the BCNWA site to evaluate the validity of our methods. We did not use this site for initial methods evaluation because the site had been treated for invasive *Phragmites* during the study period, and this limited the amount of time when our ground reference data were valid.

2.3.2. Ground reference data

As the ground reference for BCNWA, we used manually digitized land-cover maps that were created with field data collected from two previous studies (Marcaccio et al. 2016; Markle and Chow-Fraser 2018). One study was focused on habitat use by Blanding's turtles (*Emys blandingii* (Holbrook, 1838)) and included vegetation surveys conducted between 14 July and 14 August 2014. In this study, 176 quadrats (2 m × 2 m) were used to identify the vegetation data (Markle and Chow-Fraser 2018), which included aquatic marsh, cattail marsh, meadow marsh, mixed organic marsh, open water, invasive *Phragmite*s, treated invasive *Phragmite*s, upland, and other land-cover types (eg: swamp, thicket). Marcaccio et al. (2016) have created vegetation maps using imagery collected with a fixed-wing Unmanned Aerial Vehicle (UAV; Sensefly eBee Canon ELPH 110 HS, 4 cm spatial resolution for red, green and blue bands) on 4 September 2015 during clear-sky conditions based on the field surveys conducted by Markle and Chow-Fraser 2018).

As ground reference for the RBM site, we used manually digitized orthophotos (South West Ontario Orthophotography Project; SWOOP; 20 cm spatial resolution for red, green and blue bands) collected in 2010 and 2015 that has been used in same study by Markle and Chow-Fraser (2018). Field data from a vegetation survey conducted in summer 2011 and 2013 were used to create manually digitized maps for 20 land cover classes, including bulrush organic shallow marsh, campground, cattail organic shallow marsh, fen, floating leaved shallow marsh, meadow marsh, mixed forest, mixed shallow aquatic marsh, mixed woodlands, open beach, open field, open water, organic thicket swamp, invasive *Phragmites,* residential, road, rolled invasive *Phragmites*, shrub beach, shrubs, and trail. (Markle and Chow-Fraser 2018). Other than the field data, we also used locations of where invasive *Phragmites* had been treated between 2009 and 2014 (Gibert 2015) as ground reference.

For the current study, we used eleven land cover classes for the BCNWA (Agriculture, beach, cattail organic shallow marsh, constructed, floating vegetation, meadow marsh, open water, *Phragmites*, shallow marsh, and trees/shrubs) and eight classes for RBM (cattail organic shallow marsh, mixed forest, open beach, open water, organic thicket swamp, *Phragmites*, residential, and shrub beach).

2.3.3. Image data

Multispectral satellite data from Landsat 7, Landsat 8 and Sentinel 2 were used in this study (Table 2.1). Landsat is the longest continuous record of satellite observations owned by United States Geological Survey (USGS) and National Aeronautics and Space Administration (NASA). The Landsat mission consists of eight satellites, and currently

both Landsat 7 and 8 are active. Landsat 7 was launched in 1999 and Landsat 8 was launched in 2013. Sentinel 2 is a satellite owned by the European Space Agency (ESA), designed for studies based on terrestrial observations. It consists of two satellites, Sentinel-2A (launched in 2015) and Sentinel-2B (launched in 2017).

We downloaded all cloud-free images corresponding to the year when respective vegetation surveys had been conducted; when no cloud-free images for particular months were available that year, we sought image data acquired immediately prior to or following the survey year. We assumed that the changes in cover of *Phragmites* between two consecutive years are relatively small. For the both BCNWA and RBM sites, we used a total of fourteen Landsat 7, fourteen Landsat 8, and twelve Sentinel 2 images. We used ENVI 5.5 (Harris Geospatial 2018) to radiometrically and atmospherically (ENVI FLAASH atmospheric correction) correct images to obtain the surface reflectance from the digital numbers. For the Sentinel 2 images, six bands which had 20-m spatial resolution (Table 2.1) were resampled to 10 m and pre-processed separately. We then stacked the resampled bands with 10 m bands for the post-processing. We used reflectance images for all image classifications.

2.3.4. Image classification and phenological analysis

We used SVM classification to classify the time-series reflectance images of Landsat 7 and 8 and Sentinel 2 for BCWNA site for selected bands (Table 2.1). Using ArcGIS 10.5, we first generated random points within the manually digitized land cover maps from UAV and orthophotos using the vegetation survey data for both study sites separately (10 points per land cover class, located at the center of the polygons to avoid

mixed pixels at the edges; Fig. 2.1). We then used the random points to manually create Regions Of Interest (ROI) in ENVI 5.5, capturing 5 or more pixels per location (depending on the area occupied by the land-cover type under consideration) and used these as ground reference for image classification. We added more points for some classes during the classification process after evaluating the Jefferies-Matusita separability to increase the separability of classes with poor separability prior to the image classification. We conducted the image classification for both sites using the classes mentioned under the section 2.2. For accuracy assessment, we used a separate set of non-overlapping random points to create a minimum of 10 ROI's (Fig. 2.1), consisting of one to ten image pixels each, per vegetation class and information about the vegetation types collected in the field. We identified the months with highest classification accuracy in terms of overall accuracy and *Phragmites* user's and producer's accuracy.

We used the same set of ROIs used for the classification to analyze the Jefferies-Matusita separability of *Phragmites* with the other land-cover classes for the time series images. Jefferies-Matusita separability is a quantitative evaluation of spectral separability and it indicates how well the selected ROI pairs are statistically separate for images collected in different phenological stages. Separability values were plotted with Microsoft Excel 2016. Based on the separability values, we identified classes that were most confused with *Phragmites*.

Furthermore, we stacked the Landsat 8 images collected in each season (March to June: spring, June to September: summer, September to December: Fall, and December to March: winter) and repeated the SVM classification using the bands from all the images

per season combined as input. Here, we expect to combine fine spectral changes of species throughout the season to improve the classification and to minimize the effect from the changing water levels through each season. We also performed a Principal Component Analysis (PCA) on the stacked images and repeated the classification on all PCA bands. We used Minitab 18 to perform a two-way ANOVA followed by Tukey's test to determine significant differences across seasons and across satellites after pooling the results from single months, seasons combined, and a PCA of the pooled data as there were no significant difference across the groupings.

To identify what plant feature, greenness or the plant water status (i.e. Plant function) is responsible for *Phragmites* mapping accuracy we calculated the Normalized Difference Vegetation index (NDVI) and Normalized Difference Water Index (NDWI) for monthly Landsat 8 images in the time series. Moreover, to identify which spectral bands contributed most to *Phragmites* separability, we evaluated the reflectance changes of each band for Landsat 8 for the time series images. We generated 30 random points per vegetation class in ArcGIS (10.5), extracted the reflectance values for all the bands (Table 2.1), and calculated NDVI and NDWI per point. We calculated the mean values for reflectance, NDVI, and NDWI per vegetation class throughout the year, plotted the changes, and determined the time at which NDVI and NDWI were most different between *Phragmites* and the confused vegetation classes. We used One-way ANOVA and Tukey's test in Minitab 18 to identify significantly contributing bands and indices for *Phragmites* mapping accuracy. We also excluded one band at a time for Landsat 8 image

that provided the highest classification accuracy and repeated the SVM classification to identify the bands that contributed most to the *Phragmites* spectral signature.

To compare the results from BCNWA site, we repeated the image classification, the separability analysis, and conducted the analysis to determine the bands that contributed most to the indices in the RBM site. We did not perform the multi-temporal image classification for this site as RBM had been treated for invasive *Phragmites* during the study period. A summary of the methods used in this study is documented in Fig. 2.2.

2.3.5. Reduction of mapping confusion between *Phragmites* and meadow marsh mapping

Based on results from the "Image classification and phenological analysis", we identified that the meadow marsh was the most confused class with *Phragmites* and that the highest separability between classes occurred in February. We also found the highest accuracy for *Phragmites* and other land-cover classes to be in July. Therefore, we created a mask for meadow marsh based on the Landsat 8 images acquired in February, applied the mask to the July images and repeated the SVM classification without the meadow marsh ROIs. For this image classification, we used the bands listed in Table 2.1. We used the same ground reference information, and protocols for image classification and accuracy assessment as described under "Image classification and phenological analysis". We have also calculated the overlap area between *Phrgmites* and meadow marsh with comparison to manually digitized vegetation maps for February, July, and February-July combined maps using ArcGIS.

2.4. Results

2.4.1. Image classification and phenological analysis

The overall accuracy was the highest in late summer and early fall (July to October), tapering at both ends of the calendar year. We observed similar trends for all three sensors examined (Tables 2.2, 2.3 and 2.4; Fig. 2.3). Both the user's and producer's accuracies of *Phragmites* followed the same trend, peaking in late summer and early fall. When the three sensors were compared, Sentinel 2 provided the highest *Phragmites* user's and producer's accuracy, while Landsat 8 provided the highest overall accuracy and Landsat 7 provided the lowest accuracy in all cases. The classification for BCNWA resulted in higher accuracy for both Landsat 8 and Sentinel 2. When these results were compared with those for the RBM site, we observed a similar trend in classification accuracy with respect to the three sensors but a higher accuracy for Landsat 7.

The most confused classes with invasive *Phragmites* were meadow marsh and the cattail organic shallow marsh. Separability of *Phragmites* with all other landcover classes were greatest in July, except when it was compared with meadow marsh; for the meadow marsh, the highest separability with the two other classes was observed in February (Fig. 2.4). As demonstrated in the error matrices, most of the commission error for *Phragmites* was attributed to confusion with cattail and meadow marsh (Tables 2.5, 2.6 and 2.7). Other than for *Phragmites*, we also observed some confusion between agricultural lands and trees/shrubs, cattail and meadow marsh, and open water and shallow marsh (Tables 2.5, 2.6, and 2.7). When compared with the RBM site, cattail organic shallow marsh was the most confused class with *Phragmites*. We excluded meadow marsh from the RBM

site because meadow marsh occupied very little area and Landsat and Sentinel 2 spatial resolution did not capture this class accurately.

Classification of single images (single month) did not produce accuracies that differed significantly from classification of multiple images from different months that were combined into a single image (combined seasonal) or classification of pooled images after a PCA was run (PCA seasonal; Fig. 2.5). We did not observe a significant difference with respect to overall or *Phagmites* user's and producer's accuracies among the single month, combined seasonal or PCA seasonal treatments. Therefore, we pooled the data for three groupings and conducted statistical analysis to identify the seasons with highest classification accuracies. Our results indicated that summer and fall had homogeneous means when compared to the spring and winter. When considering the sensors, Sentinel 2 had the highest accuracy while Landsat 7 had lowest for overall and *Phragmites* user's accuracy. There were, however, no significant differences in the *Phragmites* producer's accuracy between sensors (Fig. 2.6).

Since cattail and meadow marsh were most confused with *Phragmites,* we examined how respectively reflectance, NDVI and NDWI values changed over the time series for these three classes. Visually, coastal aerosols, blue, green, red, and SWIR2 (ShortWave InfraRed) bands associated with the three classes showed no difference in reflectance. The NIR (Near InfraRed) reflectance was higher for *Phragmites* than for cattail in July and August while reflectance for meadow marsh in February was greater than those for *Phragmites* and cattails. The SWIR1 reflectance for meadow marsh was slightly higher than that for *Phragmites* in August (Fig.2.7). One-way ANOVA followed

by Tukey's test shows that the greatest number of significant p-values were recorded for green, NIR, and both SWIR bands when compared to the other bands. These results were consistent with the highest mapping accuracy of invasive *Phragmites* (i.e. the month associated with the greatest number of significant p-values) being recorded in July, August, and September in terms of separability between invasive *Phragmites* and cattail, whereas the highest mapping accuracy in regard to separability between invasive *Phragmites* and meadow marsh was recorded in February (Table 2.8).

Except for one band on a single occasion, accuracies associated with the image classification provided a similar trend. Exclusion of green, NIR, and SWIR1 bands resulted in greater than 2% reduction in overall and *Phragmites* user's accuracies; however, *Phragmites* producer's accuracy remained constant through all bands and single-band exclusions (Table 2.9). Overall, these results suggest that the green, NIR, and SWIR reflectance of *Phragmites* contributed most to the unique reflectance signature that resulted in higher classification accuracy, especially with respect to cattail when compared to the other spectral bands. The results also confirmed that the highest *Phragmites* mapping accuracy could be obtained in the late summer and early fall period. When these results were compared with the RBM site, the green, NIR, and SWIR2 bands provided the greatest number of significant p-values. Images acquired in August also provided the most significant p-values. Results of image classification with band exclusions for the RBM site did not show the same trend noted for the BCNWA site. There was more than 2% accuracy reduction for overall, *Phragmites* user's and producer's accuracy when the green band was excluded. Exclusion of NIR band only

reduced *Phragmites* producer's accuracy while exclusion of SWIR2 band reduced both producer's and user's accuracy.

Next, we compared the NDVI and NDWI values of *Phragmites*, cattail and meadow marsh for the time series images (Fig 2.8 and Table 2.10). The NDVI scores associated with August and September were significantly different from those of other months while NDWI scores associated with July, August and September were significantly different. The meadow marsh class was significantly different from *Phragmites* with respect to NDVI and NDWI scores in the February image. These results suggested that both greenness and plant water use efficiency may affect the spectral signature of invasive *Phragmites*. There were no clear patterns associated with RBM for NDVI and NDWI scores, but we observed the most significant p-values in June, August, September, and October.

2.4.2. Reduction of mapping confusion between *Phragmites* and meadow marsh mapping

When classified images of February and July were compared visually, we observed a higher *Phragmites* commission error in July (11.11%), compared with that in February (9.52%; Fig. 2.9; Tables 2.2, 2.3 and 2.4). There was also a 35 ha overlap between the mapped and actual meadow marsh in February compared with only a 30 ha overlap in July. Furthermore, only 13 ha of meadow marsh was mapped as false *Phragmites* in February while 26 ha was mapped in July. When we combined the meadow marsh mapped in February with the July image, we found that the overall accuracy was reduced to 85.4% (kappa coefficient = 0.83) in the combined image;

however, both *Phragmites* user's and producer's accuracies were increased to 92.3 % and 96.0%, respectively. By combining images collected in these two months, the overlap between the mapped and actual meadow marsh was increased to 39 ha, while the commission error for meadow marsh was reduced to 15 ha.

2.5. Discussion

In this paper, we developed a novel approach to map *Phragmites* using freely available multispectral imagery by identifying the best phenological period during which the plants produced their most distinguishable signature compared to background land-cover classes (especially cattails and meadow marsh). Variation in surface reflectance of marsh vegetation associated with phenological changes over the year were captured in remotely sensed imagery (Zhang et al. 2003; Tuanmu et al. 2010). We were able to monitor these phenological changes in our wetlands using satellite data with moderate spatial resolution that included Landsat 7, 8 and Sentinel 2. Classified images of all three satellite platforms resulted in maps of *Phragmites* of acceptable accuracy (>80% average accuracy of overall and *Phragmites* user's and producer's accuracy) when classifications were performed on images acquired in late summer or fall. Of all three satellites, the accuracy of classified Landsat 7 images was lowest, in part because of data gaps; Landsat 8 provided the highest overall accuracy while Sentinel 2 provided highest *Phragmites* user's and producer's accuracy.

The data source, classification algorithm, and use of timely ground reference data can all affect the accuracy of image classification, especially for fine-scale species mapping. Ensuring that ground reference collection and image acquisition are completed

in the same year is probably most important, especially when complex vegetation features such as wetlands are considered. We obtained lower classification accuracy overall for RBM than for BCNWA using either Landsat 8 or Sentinel 2, partly because of mismatched timing between field surveys (all collected in 2011) and image acquisition (2014 for Landsat 8 and 2016 for Sentinel 2 images, respectively). Landsat 7 images, on the other hand, provided higher classification accuracy because the satellite images had been acquired in 2009, 2010 and 2011, closer to the time of field surveys. Another reason for the poorer accuracies for Landsat 8 and Sentinel 2 was because a control program had been implemented in the fall of 2011, and many of the *Phragmites* stands that were present in the 2011 field surveys had been eradicated and were no longer present in the 2014 and 2016 images. We tried to improve accuracy in two ways, first by manually delineating *Phragmites* stands in a 2015 SWOOP image to provide more appropriate ground reference data for the 2014 and 2016 satellite images and secondly, by accounting for treatment locations. Due to the inconsistency of image and field reference data collection time, however, we can only use the RBM site to apply methodology developed for the BCNWA site, and we believe that the mismatch of field reference and image dates for RBM did not materially affect conclusions drawn from the BCNWA data.

Marcaccio and Chow-Fraser (2016) found various degrees of accuracies when they compared four mapping options and data sources for mapping BCNWA. In the first option, Ontario Ministry of Natural Resources and Forestry (OMNRF) classified Landsat data using an NDVI-based hierarchical image object-based decision tree (Young et al. 2011). The data sources were Landsat 5 and 7 images acquired in summer 1993, 1999,

and 2010; Marcaccio and Chow-Fraser obtained an overall accuracy of 57%, with associated *Phragmites* producer's and user's accuracy of 56% and 77% respectively for this option. This is lower than our results where the overall accuracy was 75 and 86% for Landsat 7, 71% and 88% for Landsat 8, and >80% *Phragmites* accuracy for most of the cases with the SVM classification. This is likely because the OMNRF study did not include any ground reference in their classification whereas here we used a number of ground reference points for both classification and accuracy assessment.

The second option in Marcaccio and Chow-Fraser's study involved use of PALSAR (Phased Array type L-band Synthetic Aperture Radar; Bourgeau-Chavez et al. 2015). In this approach, all landcover within a 10-km buffer of the Great Lakes shoreline was mapped, including several classes of emergent vegetation, particularly *Phragmites*. Landsat 7 data collected in spring, summer and fall from 2008 to 2011 had been used to delineate landscape features; the authors used random forests isodata and the maximum likelihood classification methods, as well as field reference data for both classification and accuracy assessment. When this approach was applied to BCNWA, Marcaccio and Chow-Fraser (2016) obtained 77% overall accuracy, and *Phragmites* producer's and user's accuracies of 86% and 77%, respectively. This compares favorably with the 77% that we obtained for producer's and user's accuracy in this study. Although radar data appear to be advantageous for mapping *Phragmites* and the PALSAR data are now freely available, we will not be able to use these image data for mapping updates because the mission ended in 2011.

Marcaccio and Chow-Fraser (2018) have used the image object-oriented classification method for SWOOP images collected in spring 2006, 2010, and 2015 to map *Phragmites* along major highways of southern and central Ontario. When this approach was applied to mapping BCNWA, the overall classification accuracy was 62%, while the producer's accuracy was 90% and the user's accuracy was 58%. Although the 20-cm spatial resolution has obvious advantages, the SWOOP images are only available every 5 years. Marcaccio et al. (2016) also used UAV data (spatial resolution of 8 cm) to manually delineate land cover types based on extensive field surveys of the BCNWA. This method provided the highest user's and producer's accuracy of 100% while the overall accuracy was 87%. The method was highly accurate but also the most labor intensive.

Stratoulias et al. (2015) developed a simulation of the bands of Sentinel 2 based on the satellite's response function and airborne hyperspectral data collected from the sensor AISA for lakeshore mapping at Lake Balaton, Hungary. They also used the SVM classification and have reported that Sentinel 2 can perform satisfactorily in classifying wetland ecosystems, including *Phragmites*. They suggested, however, that the *Phragmites* mapping accuracy could be reduced if higher inter-class spectral variability were present. They first predicted the strong capability of Sentinel 2 imagery for fine-habitat monitoring for species such as *Phragmites*. Our study has confirmed this prediction and showed that Sentinel 2 imagery can be used to map wetlands with relatively high accuracies for both *Phragmites* and other land classes.

All previous *Phragmites* mapping techniques have demonstrated various pros and cons in terms of data sources and availability, mapping technique, and accuracy. Our method is advantageous over these published mapping options because we use freely available data within relatively short time intervals, with sensors that are still available (and will be for the foreseeable future). Moreover, mapping accuracy has been high, both with respect to overall accuracy as well as for *Phragmites* alone. The one limitation of this approach is the low spatial resolution, which limits the accuracy of mapping small stands of *Phragmites* or mixed assemblages of *Phragmites* with other emergent or meadow taxa. Our method also requires a large number of ground reference locations, collected in the same year when the image is acquired. This approach relies on availability of cloud-free images and can be an insurmountable problem as we discovered for RBM, when we could not find any cloud-free images in 2011. Nevertheless, the relatively high accuracy, zero cost of data acquisition and continuous availability of images, we believe our novel approach is best suited to tracking changes in distribution of *Phragmites* when monitoring for effectiveness of treatment programs.

The reflectance signature of a plant depends on many factors (Knipling 1970.) Reflectance in the visible region is mainly affected by the types of plant pigments (primarily chlorophyll) and their concentration, and some effect by carotenoids, xanthophylls, and anthocyanin. Leaf internal structure, specifically the cellular arrangement and layers, cell wall cellulose structures, and air cavities can affect the reflectance in the NIR region (Wilstxtter and Stoll 1918; Mestre 1935; Sinclair 1968). Reflectance in the SWIR region is strongly influenced by the water content in plant

tissues, especially in wavelengths 1.45 μm and 1.94 μm (Fabre et al. 2011). Besides properties of a single leaf, other factors that can affect the plant's reflectance signature includes features such as leaf orientation, shadows, illumination angle, leaf density, and the size of leaves and the non-foliage background features such as soil (for the terrestrial species) or water (for the wetland species) (Knipling 1970). Hence, species with similar morphology and anatomy may share various degrees of similarity in reflectance signatures.

Both cattail and meadow marsh are highly confused with *Phragmites* in our classification approach. All three classes occupy similar habitats where the plants are partially submerged. Hence the background reflectance has the same effect on them and result in somewhat similar signals. For example, cattail and *Phragmites* both share similar morphological traits, being tall, unbranched shoots that form dense monospecific stands and have approximately similar leaf arrangement (Bellavance and Brisson 2010). Hence both species produced very similar reflectance signatures that caused confusion in image classification. There were differences, however, in how the two species senesced; cattail started yellowing by the end of July while *Phragmites* remained green until early September. Moreover, *Phragmites* produced its unique, and large inflorescence by the end of summer and throughout the fall. Hence *Phragmites* and cattail exhibited highest separability during late summer to fall, and this led to increased mapping accuracy. The NDVI time-series analysis mirrored this since both classes had a similar pattern throughout the year except in July to September, when they had highest divergence. We obtained significant separation between cattail and *Phramites* in June to September using

NDWI values and this indicates that plant-water features may also play a role in discriminating between these two classes.

The meadow marsh produced a relatively complicated signature, that reflected the assemblage of different plant species, including various grasses, sedges, emergent shrubs, and upland plant species (Wilcox n.d.). Furthermore, the meadow marsh community undergoes occasional flooding, and this leads to even more variability in their reflectance signals throughout the year. Therefore, the meadow marsh signal is confused not only with *Phragmites*, but also with other wetland landcover classes such as cattail and shallow marsh. In February, however, the meadow marsh tends to be completely covered by snow while the taller *Phragmites* and cattail stalks are only partially covered in snow. This difference in February can be used to increase the separability among these three classes. Although separability between *Phragmites* and meadow marsh was higher during the winter, the reflectance signal of meadow marsh still overlapped with that of other snow-cover features such as shallow marsh, beach, and frozen shallow water. Hence the overall accuracy was low. Additionally, the degree of separability between *Phragmites* and meadow marsh during the winter may depend on the amount of snow accumulation. There was a significant difference in NDVI between *Phragmites* and meadow marsh from February to July and significant NDWI difference from July to September. With respect to invasive *Phragmites* and meadow marsh, however, there was no clear pattern in NDVI and NDWI, and hence these may not help to separate these classes to improve mapping accuracy.

Many studies have explored the use of combined images collected in different seasons and have reported improved classification accuracy (Oetter et al. 2001; Guerschman et al. 2003; Tottrup 2004; Lu and Weng 2007). Use of multi-temporal images in classification not only incorporates fine phenological changes in the spectral data, but also helps to exclude the effect of the sun's angle and to provide a unique spectral response pattern (Tottrup 2004). We expected that use of multitemporal images for wetland classification may be useful in overcoming the effect of varying water levels within each season; however, we did not observe any evidence that overall classification accuracy would increase significantly by combining multiple images. According to Tottrup (2004) the acquisitions should not be too close in time as there are no clear changes in phenology and the sun's angle within a single season. Our results may have been different if we had combined multiple images for the same seasons; however, we did not explore this as our main objective was to determine the phenological states of *Phragmites* that produced the most unique reflectance signature for mapping. Finally, we should point out that use of a PCA to reduce the effect of redundant data did not yield a significant increase in accuracy as expected.

2.6. Conclusions

We accurately mapped large *Phragmites* patches in wetlands using Landsat and Sentinel 2 images acquired in late summer through fall, in combination with the SVM classification method. To achieve high classification accuracy, our protocol requires a large number of ground reference locations to be established. Our results indicate that the green, NIR, and SWIR bands are most useful in development of the unique *Phragmites*

reflectance signal during this period. We believe that the prolonged greenness of *Phragmites* when compared to other wetland vegetation, large, distinct inflorescence, and the water content of *Phragmites* during this period helps to produce the unique reflectance signature. Also, the prolonged greenness of *Phragmites* when compared to other classes help in the mapping process. Cattail and meadow marsh were the most confused classes with *Phragmites*, likely because all three landcover classes occupy similar habitats and have similar morphological features.

Although *Phragmites* best separated out from cattails and other classes in July to September, meadow marsh separated out best in February. Therefore, we recommend the use of February (snow covered) images in combination with summer time images to reduce the confusion among these three classes. This may be more useful when maps are produced for management purposes when the primary goal is to accurately map invaded areas. Use of multitemporal images for each season did not increase classification accuracy.

Overall, our study explored the use of freely available satellite data for mapping invasive *Phragmites*, which has become a serious management issue. Despite the moderate spatial resolution, images acquired in the correct phenological state can increase classification accuracy. Our novel approach provides a cost-effective and accurate *Phragmites* mapping method for different types of wetland ecosystems, when *Phragmites* needs to be frequently monitored and managed across large spatial extents.

2.7. Acknowledgements

Partial funding for this study came from a grant to PC-F from the Highway Infrastructure Innovation Funding Program from the Ministry of Transportation of Ontario. We thank C. Markle and J. Marcaccio for their assistance in assembling relevant data for this study. We are grateful to the helpful comments provided by anonymous reviewers on an earlier draft of this manuscript.

2.8. Literature Cited

Adam E, Mutanga O, Rugege D (2010) Multispectral and hyperspectral remote sensing for identification and mapping of wetland vegetation: a review. Wetl Ecol Manag 18:281–296

Ashley EP, Robinson JT (1996) Road mortality of amphibians, reptiles and other wildlife on the Long Point Causeway, Lake Erie, Ontario. Can Field Nat 110:403–412

Bellavance M-E, Brisson J (2010) Spatial dynamics and morphological plasticity of common reed (Phragmites australis) and cattails (Typha sp.) in freshwater marshes and roadside ditches. Aquat Bot 93:129–134

Bostater CR, Ghir T, Bassetti L, et al (2004) Hyperspectral remote sensing protocol development for submerged aquatic vegetation in shallow waters. In: Remote Sensing of the Ocean and Sea Ice 2003. International Society for Optics and Photonics, pp 199–216

Bourgeau-Chavez L, Endres S, Battaglia M, et al (2015) Development of a bi-national Great Lakes coastal wetland and land use map using three-season PALSAR and Landsat imagery. Remote Sens 7:8655–8682

Chambers RM, Meyerson LA, Saltonstall K (1999) Expansion of *Phragmites australis* into tidal wetlands of North America. Aquat Bot 64:261–273

Dalponte M, Bruzzone L, Gianelle D (2008) Fusion of hyperspectral and LIDAR remote sensing data for classification of complex forest areas. IEEE Trans Geosci Remote Sens 46:1416–1427

Delegido J, Verrelst J, Alonso L, Moreno J (2011) Evaluation of sentinel-2 red-edge bands for empirical estimation of green LAI and chlorophyll content. Sensors 11:7063–7081

Dewey SA, Price KP, Ramsey D (1991) Satellite remote sensing to predict potential distribution of dyers woad (*Isatis tinctoria*). Weed Technol 5:479–484

Environment and Climate Change Canada (2011) Big Creek National Wildlife Area. In: aem. https://www.canada.ca/en/environment-climate-change/services/national-wildlife-areas/locations/big-creek.html. Accessed 26 Mar 2018

Everitt JH, Anderson GL, Escobar DE, et al (1995) Use of Remote Sensing for Detecting and Mapping Leafy Spurge (Euphorbia esula). Weed Technol 9:599–609

Everitt JH, Escobar DE, Alaniz MA, et al (1996) Using Spatial Information Technologies to Map Chinese Tamarisk (Tamarix chinensis) Infestations. Weed Sci 44:194–201

Everitt JH, Escobar DE, Davis MR (2001) Reflectance and image characteristics of selected noxious rangeland species. J Range Manag 54:208–208

Fabre S, Lesaignoux A, Olioso A, Briottet X (2011) Influence of Water Content on Spectral Reflectance of Leaves in the 3–15 μm Domain. IEEE Geosci Remote Sens Lett 8:143–147

Flores ES, Gallegos HR, Yool SR (2006) Plant invasions in dynamic landscapes, A field and remote sensing assessment of predictive and change modeling. Multidimens Spat Charact Plant Invasions 'El Pinacate Gran Desierto Altar Reserve 115

Frampton WJ, Dash J, Watmough G, Milton EJ (2013) Evaluating the capabilities of Sentinel-2 for quantitative estimation of biophysical variables in vegetation. ISPRS J Photogramm Remote Sens 82:83–92

Fuller DO (2005) Remote detection of invasive Melaleuca trees (*Melaleuca quinquenervia*) in South Florida with multispectral IKONOS imagery. Int J Remote Sens 26:1057–1063

Gao, J, Liu, Y (2008) Mapping of land degradation from space: a comparative study of Landsat ETM+ and ASTER data. Int J Remote Sens, 29(14) 4029-4043

Gibert JM (2015) Rondeau Provincial Park Invasive *Phragmites* Management Program 2008 – 2014 Summary Report and Recommended Next Steps

Glass WR, Corkum LD, Mandrak NE (2012) Spring and summer distribution and habitat use by adult threatened spotted gar in Rondeau Bay, Ontario, using radiotelemetry. Trans Am Fish Soc 141:1026–1035

Gualtieri JA, Cromp RF (1999) Support vector machines for hyperspectral remote sensing classification. In: 27th AIPR Workshop: Advances in Computer-Assisted Recognition. International Society for Optics and Photonics, pp 221–233

Guerschman JP, Paruelo JM, Bella CD, et al (2003) Land cover classification in the Argentine Pampas using multi-temporal Landsat TM data. Int J Remote Sens 24:3381–3402

Harris Geospatial (2018) Fast Line-of-sight Atmospheric Analysis of Hypercubes (FLAASH) https://www.harrisgeospatial.com/docs/FLAASH.html Accessed 20 Jun 2018

Hestir EL, Khanna S, Andrew ME, et al (2008) Identification of invasive vegetation using hyperspectral remote sensing in the California Delta ecosystem. Remote Sens Environ 112:4034–4047. doi: 10.1016/j.rse.2008.01.022

Hill MJ (2013) Vegetation index suites as indicators of vegetation state in grassland and savanna: An analysis with simulated SENTINEL 2 data for a North American transect. Remote Sens Environ 137:94–111

Holbrook, J. E. (1838) North American herpetology, vol. 4. J. Dobson, Philadelphia

Huang C, Asner GP (2009) Applications of Remote Sensing to Alien Invasive Plant Studies. Sensors 9:4869–4889. doi: 10.3390/s90604869

Huang H, Gong P, Clinton N, Hui F (2008) Reduction of atmospheric and topographic effect on Landsat TM data for forest classification. Int J Remote Sens 29:5623–5642

Immitzer M, Vuolo F, Atzberger C (2016) First experience with Sentinel-2 data for crop and tree species classifications in central Europe. Remote Sens 8:166

Knipling EB (1970) Physical and physiological basis for the reflectance of visible and near-infrared radiation from vegetation. Remote Sens Environ 1:155–159

Laba M, Downs R, Smith S, et al (2008) Mapping invasive wetland plants in the Hudson River National Estuarine Research Reserve using quickbird satellite imagery. Remote Sens Environ 112:286–300

Lelong B, Lavoie C, Jodoin Y, Belzile F (2007) Expansion pathways of the exotic common reed (*Phragmites australis*): a historical and genetic analysis. Divers Distrib 13:430–437

Lopez RD, Edmonds CM, Slonecker TS, et al (2004) Accuracy assessments of airborne hyperspectral data for mapping opportunistic plant species in freshwater coastal wetlands. Remote Sens GIS Accuracy Assess 253–267

Lu D, Weng Q (2007) A survey of image classification methods and techniques for improving classification performance. Int J Remote Sens 28:823–870

Lyon JG, McCarthy J (1995) Wetland and environmental applications of GIS. CRC Press

Mann DL, Nelson JG (1980) Ideology and wildlands management: the case of Rondeau Provincial Park, Ontario. Environ Manage 4:111–124

Marcaccio JV, Chow-Fraser P (2016) Mapping options to track invasive *Phragmites australis* in the Great Lakes basin in Canada. Proceedings of 3rd International Conference "Water resources and wetlands". Tulcea, Romania

Marcaccio, Chow-Fraser P (2018) Mapping invasive *Phragmites australis* in highway corridors using provincial orthophoto databases in Ontario.

Marcaccio JV, Markle CE, Chow-Fraser P (2016) Use of fixed-wing and multi-rotor unmanned aerial vehicles to map dynamic changes in a freshwater marsh. J Unmanned Veh Syst 4:193–202

Markle CE, Chow-Fraser P (2018) Effects of European common reed on Blanding's turtle spatial ecology. J Wildl Manag. doi: 10.1002/jwmg.21435

Marks M, Lapin B, Randall J (1994) *Phragmites australis* (*P. communis*): threats, management and monitoring. Nat Areas J 14:285–294

McLaughlin C (1993) Ecosystem management in Rondeau Provincial Park. Altern J 19:6

McNabb CD, Batterson TR (1991) Occurrence of the common reed, *Phragmites australis*, along roadsides in Lower Michigan. Mich Acad USA

Melgani F, Bruzzone L (2004) Classification of hyperspectral remote sensing images with support vector machines. IEEE Transactions on geoscience and remote sensing, 42(8), 1778-1790. doi: 10.1109/TGRS.2004.831865

Meloche C, Murphy SD (2006) Managing Tree-of-Heaven (*Ailanthus altissima*) in Parks and Protected Areas: A Case Study of Rondeau Provincial Park (Ontario, Canada). Environ Manag N Y 37:764–72. doi: http://dx.doi.org/10.1007/s00267-003-0151-x

Mestre H (1935) The absorption of radiation by leaves and algae. In: Cold Spring Harbor symposia on quantitative biology. Cold Spring Harbor Laboratory Press, 191–209

Meyerson LA, Saltonstall K, Windham L, et al (2000) A comparison of *Phragmites australis* in freshwater and brackish marsh environments in North America. Wetl Ecol Manag 8:89–103

Morel A, Bélanger S (2006) Improved detection of turbid waters from ocean color sensors information. Remote Sens Environ 102:237–249

Mountrakis G, Im J, Ogole C (2011) Support vector machines in remote sensing: A review. ISPRS J Photogramm Remote Sens 66:247–259. doi: 10.1016/j.isprsjprs.2010.11.001

Oetter DR, Cohen WB, Berterretche M, et al (2001) Land cover mapping in an agricultural setting using multiseasonal Thematic Mapper data. Remote Sens Environ 76:139–155

Ozesmi SL, Bauer ME (2002) Satellite remote sensing of wetlands. Wetl Ecol Manag 10:381–402

Pal M, Mather PM (2005). Support vector machines for classification in remote sensing. International Journal of Remote Sensing, 26(5), 1007-1011.

Peterson EB (2005) Estimating cover of an invasive grass (*Bromus tectorum*) using tobit regression and phenology derived from two dates of Landsat ETM+ data. Int J Remote Sens 26:2491–2507. doi: 10.1080/01431160500127815

Rasolofoharinoro M, Blasco F, Bellan MF, Aizpuru M, Gauquelin T, Denis J (1998) A remote sensing based methodology for mangrove studies in Madagascar. Int J Remote Sens 19(10) 1873-1886

Resasco J, Hale AN, Henry MC, Gorchov DL (2007) Detecting an invasive shrub in a deciduous forest understory using late-fall Landsat sensor imagery. Int J Remote Sens 28:3739–3745

Rickey MA, Anderson RC (2004) Effects of nitrogen addition on the invasive grass *Phragmites australis* and a native competitor *Spartina pectinata*. J Appl Ecol 41:888–896

Rupasinghe PA, Simic Milas A, Arend K, Simonson MA, Mayer C, Mackey S (2018) Classification of shoreline vegetation in the Western Basin of Lake Erie using airborne hyperspectral imager HSI2, Pleiades and UAV data. Int J Remote Sens 1-21.

Saltonstall K (2002) Cryptic invasion by a non-native genotype of the common reed, *Phragmites australis*, into North America. Proc Natl Acad Sci 99:2445–2449

Schmidt KS, Skidmore AK (2001) Exploring spectral discrimination of grass species in African rangelands. Int J Remote Sens 22:3421–3434

Sinclair TR, Schreiber MM, Hoffer RM (1968) Pathway of solar radiation through leaves 1. Agronomy Journal, 65(2), 276-283

Sohn Y, McCoy RM (1997) Mapping desert shrub rangeland using spectral unmixing and modeling spectral mixtures with TM data. Photogramm Eng Remote Sens 63:707–716

Stratoulias D, Balzter H, Sykioti O, et al (2015) Evaluating sentinel-2 for lakeshore habitat mapping based on airborne hyperspectral data. Sensors 15:22956–22969

Tottrup C (2004) Improving tropical forest mapping using multi-date Landsat TM data and pre-classification image smoothing. Int J Remote Sens 25:717–730

Tuanmu M-N, Viña A, Bearer S, et al (2010) Mapping understory vegetation using phenological characteristics derived from remotely sensed data. Remote Sens Environ 114:1833–1844

Tulbure MG, Johnston CA, Auger DL (2007) Rapid invasion of a Great Lakes coastal wetland by non-native *Phragmites australis* and Typha. J Gt Lakes Res 33:269–279

Uddin M, Robinson RW, Caridi D, et al (2014) Suppression of native *Melaleuca ericifolia* by the invasive *Phragmites australis* through allelopathic root exudates. Am J Bot 101:479–487

Vapnik VN, Kotz S (1982) Estimation of dependences based on empirical data. Springer-Verlag New York

Wilcox DA (2012) Response of wetland vegetation to the post-1986 decrease in Lake St. Clair water levels: seed-bank emergence and beginnings of the *Phragmites australis* invasion. J Gt Lakes Res 38:270–277

Wilcox I (n.d.) Wetland Meadow Marsh Community - surface area, supply-based (Lake Ontario & Thousand Islands). http://www.losl.org/twg/pi/pi_meadowmarsh-e.html. Accessed 17 May 2018

Wilcox KL, Petrie SA, Maynard LA, Meyer SW (2003) Historical distribution and abundance of Phragmites australis at long point, Lake Erie, Ontario. J Gt Lakes Res 29:664–680

Williams AP, Hunt Jr ER (2002) Estimation of leafy spurge cover from hyperspectral imagery using mixture tuned matched filtering. Remote Sens Environ 82:446–456

Wilstxtter R, Stoll A (1918) Untersuchungen fiber die Assimilation derKohlensiiure. Julius Springer Berl 344

Young BE, Young G, Hogg AR (2011) Using Landsat TM NDVI change detection to identify *Phragmites* infestation in southern Ontario coastal wetlands. Ont. Min. Nat. Resour., Inventory Monitoring and Assessment, Peterborough: 32

Zhang X, Friedl MA, Schaaf CB, et al (2003) Monitoring vegetation phenology using MODIS. Remote Sens Environ 84:471–475

Zhang, C, Xie, Z (2013) Object-based vegetation mapping in the Kissimmee River watershed using HyMap data and machine learning techniques. Wetlands, 33(2), 233-244. doi: 10.1007/s13157-012-0373-x

Zheng B, Myint SW, Thenkabail PS, Aggarwal RM (2015) A support vector machine to identify irrigated crop types using time-series Landsat NDVI data. Int J Appl Earth Obs Geoinformation 34:103–112. doi: 10.1016/j.jag.2014.07.002

Table 2.1 Comparison of spectral bands of Landsat7, Landsat 8 and Sentinel 2. NIR=Near Infrared; SWIR=Short Wave InfraRed (bands used in the study are in bold)

	Landsat 7		**Landsat 8**		**Sentinel 2**	
Spectral Band	Wavelength (μm)	Spatial resolution (m)	Wavelength (μm)	Spatial resolution (m)	Wavelength (μm)	Spatial resolution (m)
Coastal aerosols	---	---	**0.433-0.453**	30	0.443	60
Blue	**0.45-0.52**	30	**0.450-0.515**	30	**0.490**	10
Green	**0.52-0.60**	30	**0.525-0.600**	30	**0.560**	10
Red	**0.63-0.69**	30	**0.630-0.680**	30	**0.665**	10
Vegetation Red Edge	---	---	---	---	**0.705**	20
Vegetation Red Edge	---	---	---	---	**0.740**	20
Vegetation Red Edge	---	---	---	---	**0.783**	20
NIR	**0.77-0.90**	30	**0.845-0.885**	30	**0.842**	10
Narrow NIR	---	---	---	---	**0.865**	20
Water vapor	---	---	---	---	0.945	60
Cirrus	---	---	1.360-1.390	30	---	---
SWIR-Cirrus	---	---	---	---	1.375	60
SWIR1	**1.55-1.75**	30	**1.560-1.660**	30	**1.610**	20
SWIR2	**2.90-2.35**	30	**2.100-2.300**	30	**2.190**	20
Long Wavelength Infrared	---	---	10.30-11.30	100	---	---
Thermal	10.40-12.50	60*(30)	---	---	---	---

Long Wavelength Infrared	---	---	11.50-12.50	100	---	---
Panchromatic	0.52-0.90	15	0.500-0.680	15	---	---

Table 2.2 Monthly changes in mapping accuracy (%) for the two study sites using Landsat 7 (Note: Producer's and User's accuracy pertain to invasive *Phragmites*. Overall accuracy pertains to all classified classes. The month with highest overall accuracy is bolded).

Big Creek					Rondeau Bay				
Date	Producer's	User's	Overall	Average	Date	Producer's	User's	Overall	Average
2014 Feb 15	58.00	63.04	62.93	61.32	2009 Mar 13	60.00	79.00	80.21	73.07
2015 Mar 23	88.00	42.31	62.59	64.30	2010 May 03	70.00	80.00	83.03	77.687
2014 Apr 24	84.00	37.50	64.99	62.16	2011 Jun 07	53.33	72.73	80.26	68.77
2015 Jul 13	66.00	44.00	73.86	61.29	2010 Jul 06	**90.00**	**81.82**	**85.96**	**85.93**
2015 Jul 29	**82.00**	**52.56**	**76.43**	**70.33**	2009 Aug 04	**76.67**	**79.31**	**81.14**	**79.04**
2014 Aug 21	**84.00**	**53.41**	**74.82**	**70.74**	2010 Nov 11	53.33	76.19	79.83	69.78
2015 Sep 15	**78.00**	**62.03**	**72.69**	**70.90**					
2015 Nov 02	74.33	66.67	62.49	67.83					

Table 2.3 Monthly changes in mapping accuracy (%) for the two study sites using Landsat 8 (Note: Producer's and User's accuracy pertain to invasive *Phragmites*. Overall accuracy pertains to all classified classes. The month with highest overall accuracy is bolded).

Big Creek					Rondeau Bay				
Date	Producer's	User's	Overall	Average	Date	Producer's	User's	Overall	Average
2015 Feb 27	76.00	90.48	66.13	77.54	2014 Jan 14	81.25	70.27	65.78	72.43
2014 May 31	84.00	52.81	74.60	70.47	2014 Feb 15	84.38	58.70	63.12	68.73
2014 Jun 03	86.00	51.19	74.83	70.67	2014 Mar 03	68.75	59.46	65.40	64.54
2015 Jul 21	**96.00**	**88.89**	**88.56**	**91.15**	2014 Jun 04	53.13	54.84	71.48	59.82
2014 Aug 19	**92.00**	**79.31**	**79.63**	**83.65**	2014 Aug 10	**79.59**	**73.58**	**75.00**	**76.06**
2014 Sep 04	**93.55**	**72.73**	**78.94**	**81.74**	2014 Sep 27	81.25	48.15	67.68	65.69
2014 Nov 20	94.00	54.65	76.43	75.03	2014 Oct 10	71.00	61.54	71.62	68.05

Table 2.4 Monthly changes in mapping accuracy (%) for the two study sites using Sentinel 2 (Note: Producer's and User's accuracy pertain to invasive *Phragmites*. Overall accuracy pertains to all classified classes. The months with highest overall accuracy is bolded).

Big Creek					Rondeau Bay				
Date	Producer's	User's	Overall	Average	Date	Producer's	User's	Overall	Average
2016 Apr 27	87.69	63.10	81.71	77.50	2016 Apr 27	77.10	62.43	69.89	69.81
2016 May 28	62.56	40.53	73.23	58.77	2016 May 28	84.55	55.03	72.89	70.82
2016 Jul 06	93.85	84.33	82.82	87.00	2016 Jun 29	80.56	56.68	74.61	70.62
2016 Jul 27	**95.35**	**91.11**	**84.00**	**90.15**	2016 Jul 06	**82.66**	**77.61**	**79.65**	**79.97**
2016 Sep 26	**92.82**	**87.44**	**86.11**	**88.79**	2016 Dec 10	72.98	60.74	72.83	68.85
2016 Oct 15	**87.18**	**72.34**	**82.88**	**80.80**					
2016 Dec 10	**89.23**	**79.82**	**85.94**	**85.00**					

Table 2.5 Error Matrix for Landsat 7 (2015 July 29) for the Big Creek (number of pixels)

		Reference data										
Classification results	Class	Agriculture	Beach	Cattail	Constructed	Floating	Meadow marsh	Open water	Phragmites	Shallow marsh	Trees/Shrubs	Total
	Agriculture	**67**	0	0	0	0	0	0	0	0	0	67
	Beach	1	**14**	0	1	0	0	1	0	0	0	17
	Cattail	0	4	**108**	1	2	2	3	2	0	0	122
	Constructed	1	3	0	**26**	0	0	0	0	0	0	30
	Floating	0	0	0	0	**9**	0	0	0	0	0	9
	Meadow marsh	0	2	0	0	0	**3**	0	1	1	0	7
	Open water	0	0	0	0	0	0	**44**	0	10	0	54
	Phragmites	0	1	6	0	0	19	0	**41**	3	8	78
	Shallow marsh	1	0	7	0	4	7	0	0	**13**	1	33
	Trees/shrubs	4	0	0	0	1	0	0	6	0	**9**	20
	Total	74	24	121	28	16	31	48	50	27	18	**437**

Number of correctly classified pixels for each land cover class are given in bold text

Table 2.6 Error Matrix for Landsat 8 (2015 July 21) for the Big Creek (number of pixels)

		Reference data										
Classification results	Class	Agriculture	Beach	Cattail	Constructed	Floating	Meadow marsh	Open water	*Phragmites*	Shallow marsh	Trees/shrubs	Total
	Agriculture	**70**	0	0	0	0	0	0	0	0	0	70
	Beach	0	**19**	1	1	0	0	0	0	0	0	21
	Cattail	0	0	**120**	0	0	8	1	2	0	0	131
	Constructed	0	1	0	**27**	0	0	0	0	0	0	28
	Floating	0	0	0	0	**10**	0	0	0	0	0	10
	Meadow marsh	0	2	0	0	0	**13**	0	0	0	0	15
	Open water	0	0	0	0	2	0	**43**	0	4	0	49
	Phragmites	0	2	0	0	0	2	2	**48**	0	0	54
	Shallow marsh	0	0	0	0	4	4	2	0	**19**	0	29
	Trees/shrubs	4	0	0	0	0	4	0	0	4	**18**	30
	Total	74	24	121	28	16	31	48	50	27	18	**437**

Number of correctly classified pixels for each land cover class are given in bold text

Table 2.7 Error Matrix for Sentinel 2 (2016 July 26) for the Big Creek (number of pixels)

		Reference data										
Classification results	Class	Agriculture	Beach	Cattail	Constructed	Floating	Meadow marsh	Open water	*Phragmites*	Shallow marsh	Trees/shrubs	Total
	Agriculture	**167**	0	0	0	0	1	0	0	0	0	168
	Beach	0	**78**	0	8	0	0	0	0	0	0	86
	Cattail	0	0	**347**	0	0	15	0	12	8	0	382
	Constructed	0	5	0	**112**	0	0	0	0	0	0	117
	Floating	0	0	1	0	**28**	0	0	0	0	0	29
	Meadow marsh	0	0	71	0	0	**97**	0	0	0	0	168
	Open water	4	0	0	1	0	0	**197**	0	37	0	239
	Phragmites	0	0	16	0	0	4	0	**246**	1	3	270
	Shallow marsh	0	0	1	0	12	2	16	0	**48**	8	87
	Trees/shrubs	13	0	0	0	0	1	0	0	0	**19**	33
	Total	184	83	436	121	40	120	213	258	94	30	**1579**

Number of correctly classified pixels for each land cover class are given in bold text

Table 2.8 P-Values for selection of most contributing bands for the *Phragmites* signature using one-way ANOVA and Tukey's test (Note: statistically significant values are given in bold text; P-C is *Phragmites* and Cattail organic shallow marsh comparison and P-M is *Phragmites* and meadow marsh comparison).

		BCNWA							Number of significant p-values
Band	Classes	Feb	May	Jun	Jul	Aug	Sep	Nov	
Coastal	P-C	0.076	**0.021**	0.579	0.100	0.060	0.051	0.189	1
aerosols	P-M	**0.000**	0.821	0.200	0.120	0.240	0.089	**0.010**	2
Blue	P-C	0.067	0.240	0.984	0.200	0.074	**0.001**	0.052	1
	P-M	**0.000**	0.996	0.882	1.000	0.989	**0.004**	0.056	2
Green	P-C	0.073	**0.040**	0.631	**0.002**	**0.041**	**0.000**	0.082	4
	P-M	**0.000**	0.634	0.114	0.102	0.142	0.377	**0.003**	2
Red	P-C	0.053	0.127	0.815	**0.004**	**0.009**	0.098	0.074	2
	P-M	**0.000**	0.445	**0.044**	0.994	0.113	0.012	0.057	2
NIR	P-C	**0.006**	0.963	0.621	**0.000**	**0.000**	**0.000**	0.500	4
	P-M	**0.000**	0.239	0.191	**0.022**	**0.022**	0.248	0.138	3
SWIR 1	P-C	0.081	0.378	0.97	**0.000**	**0.000**	**0.003**	0.47	3
	P-M	**0.048**	0.831	0.915	0.788	0.994	0.134	0.398	1
SWIR 2	P-C	**0.000**	0.214	0.638	**0.000**	**0.000**	**0.003**	0.219	4

	P-M	**0.000**	0.985	0.998	**0.000**	0.239	0.134	0.166	2
Number of significant p-values	P-C	2	2	0	5	5	5	0	
	P-M	7	0	1	2	1	1	2	
					RBM				
	Classes	Jan	Feb	Mar	Jun	Aug	Sep	Oct	
Coastal aerosols	P-C	0.124	0.172	0.398	0.331	0.109	0.435	0.655	0
Blue	P-C	0.384	0.154	0.383	0.377	0.377	0.748	0.225	0
Green	P-C	0.325	0.174	0.406	0.850	**0.007**	0.137	0.582	1
Red	P-C	0.290	0.173	0.413	0.653	0.687	0.236	**0.013**	1
NIR	P-C	0.159	0.167	0.462	0.447	**0.021**	**0.003**	**0.045**	3
SWIR 1	P-C	0.058	0.077	0.056	0.630	**0.001**	0.128	0.476	1
SWIR 2	P-C	0.061	0.120	0.100	0.560	0.103	0.698	0.287	0
Number of significant p-values	P-C	0	0	0	0	3	1	2	

Table 2.9 Accuracy (%) values for Landsat 8 July images when one band is excluded at a time (Note: Producer's and User's accuracy pertain to invasive *Phragmites*. Overall accuracy pertains to all classified classes. Bands that reduce the accuracy more than 2% when excluded is bolded.)

Image	*BCNWA*				*RBM*			
	Overall	Producer's	User's	Average	Overall	Producer's	User's	Average
With 7 bands	88.56	96.00	92.31	92.29	75.00	79.59	73.58	76.06
Without band 1	87.64	96.00	90.56	91.40	74.58	79.51	72.55	75.55
Without band 2	88.10	96.00	90.57	91.56	75.00	**77.55**	72.70	75.08
Without band 3	**86.27**	96.00	**88.71**	**90.33**	**72.46**	**73.47**	**71.26**	**72.40**
Without band 4	88.10	96.00	90.57	91.56	74.15	79.59	73.58	75.78
Without band 5	**85.58**	96.00	**85.71**	**89.10**	74.15	77.55	71.70	74.47
Without band 6	**86.19**	96.00	**85.12**	**89.10**	73.30	**71.43**	**70.00**	**71.58**

Without band 7	88.10	96.00	90.57	91.56	75.00	79.51	72.41	75.85
	Difference of accuracy from classification accuracy of all 7 bands							
Without band 1	0.92	0.00	1.75	0.89	0.42	0.08	1.03	0.51
Without band 2	0.46	0.00	1.74	0.73	0.00	**2.04**	0.88	0.98
Without band 3	**2.29**	0.00	**3.60**	1.96	**2.54**	**6.12**	**2.32**	**3.66**
Without band 4	0.46	0.00	1.74	0.73	0.85	0.00	0.00	0.28
Without band 5	**2.98**	0.00	**6.6**	**3.19**	0.85	**2.04**	1.88	1.59
Without band 6	**2.37**	0.00	**7.19**	**3.19**	1.70	**8.16**	**3.58**	**4.48**
Without band 7	0.46	0.00	1.74	0.73	0.00	0.08	1.17	0.21

Table 2.10 P-Values for monthly changes of NDVI and NDWI of *Phragmites*, cattail organic shallow marsh, and meadow marsh using one-way ANOVA and Tukey's test (Note: statistically significant values are given in bold text; P-C is *Phragmites* and Cattail organic shallow marsh comparison and P-M is *Phragmites* and meadow marsh comparison).

		BCNWA							Number of significant p-values
Band	Classes	Feb	May	Jun	Jul	Aug	Sep	Nov	
NDVI	P-C	0.060	0.550	0.304	0.140	**0.003**	**0.002**	**0.003**	3
	P-M	**0.000**	**0.000**	**0.000**	0.992	0.079	**0.048**	0.306	4
NDWI	P-C	0.078	0.254	**0.010**	**0.000**	**0.017**	**0.000**	0.181	4
	P-M	**0.000**	0.087	0.422	**0.000**	**0.000**	**0.000**	0.730	4
Number of significant p-values	PC	0	0	1	1	2	2	1	
	P-M	2	1	1	1	1	2	0	
		RBM							
	Classes	Jan	Feb	Mar	Jun	Aug	Sep	Oct	
NDVI	P-C	0.914	0.706	0.727	**0.045**	0.720	**0.029**	**0.030**	**3**
NDWI	P-C	0.169	0.862	0.959	0.136	**0.000**	0.058	0.053	1
Number of significant p-values	P-C	0	0	0	1	1	1	1	

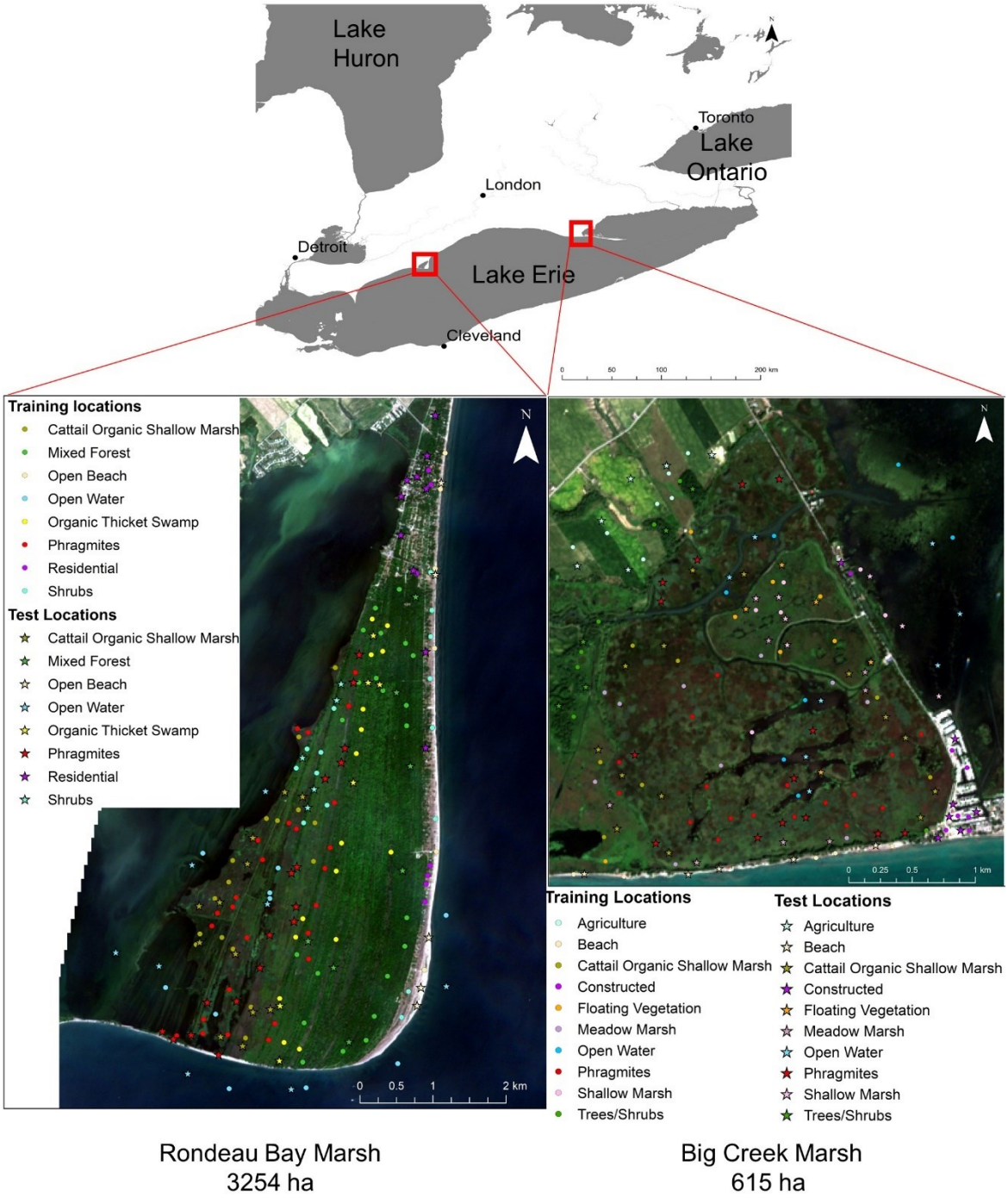

Fig. 2.1 Location of study sites and test and training locations used for classification

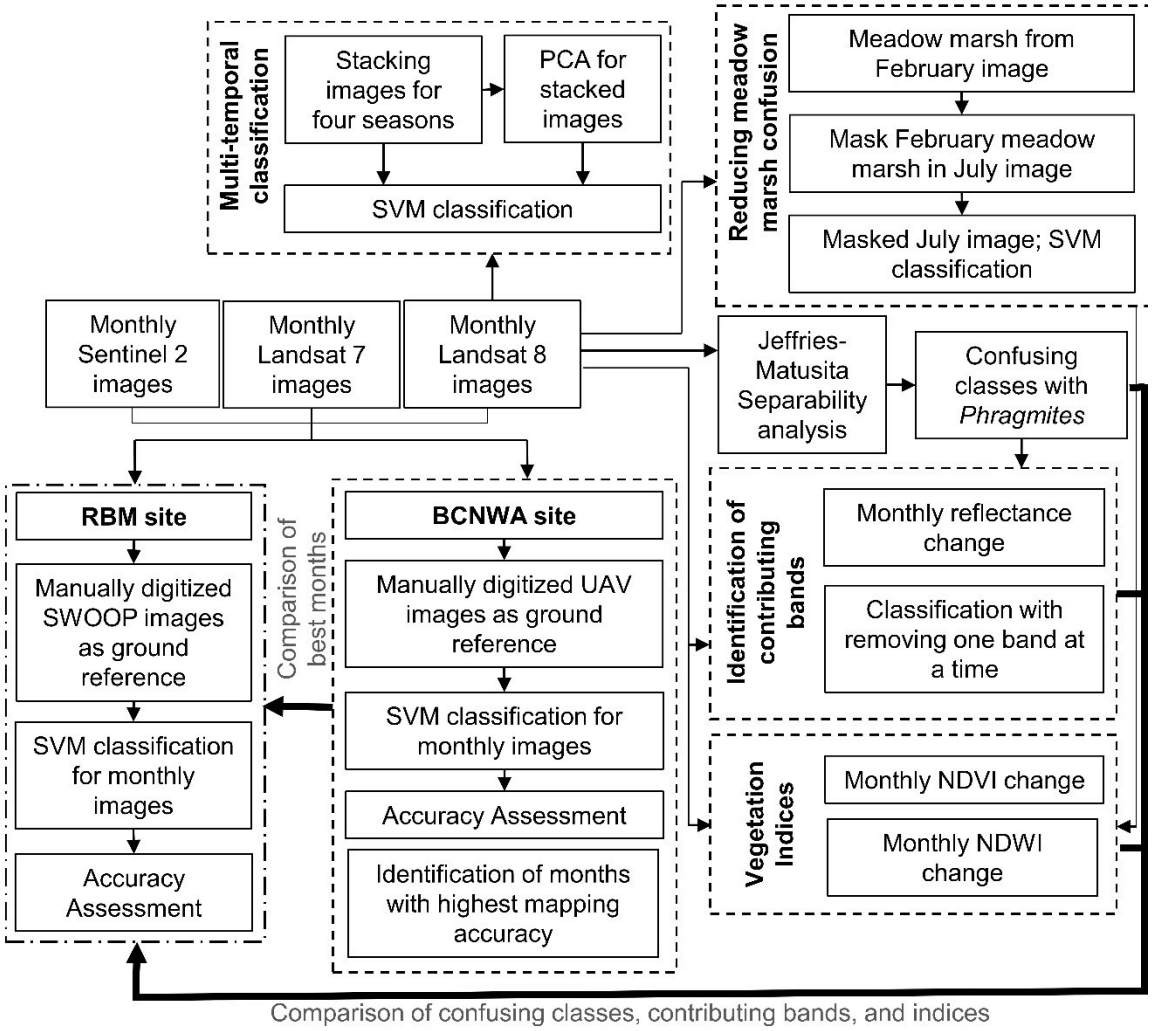

Fig. 2.2 Flow chart of the methods used in the study

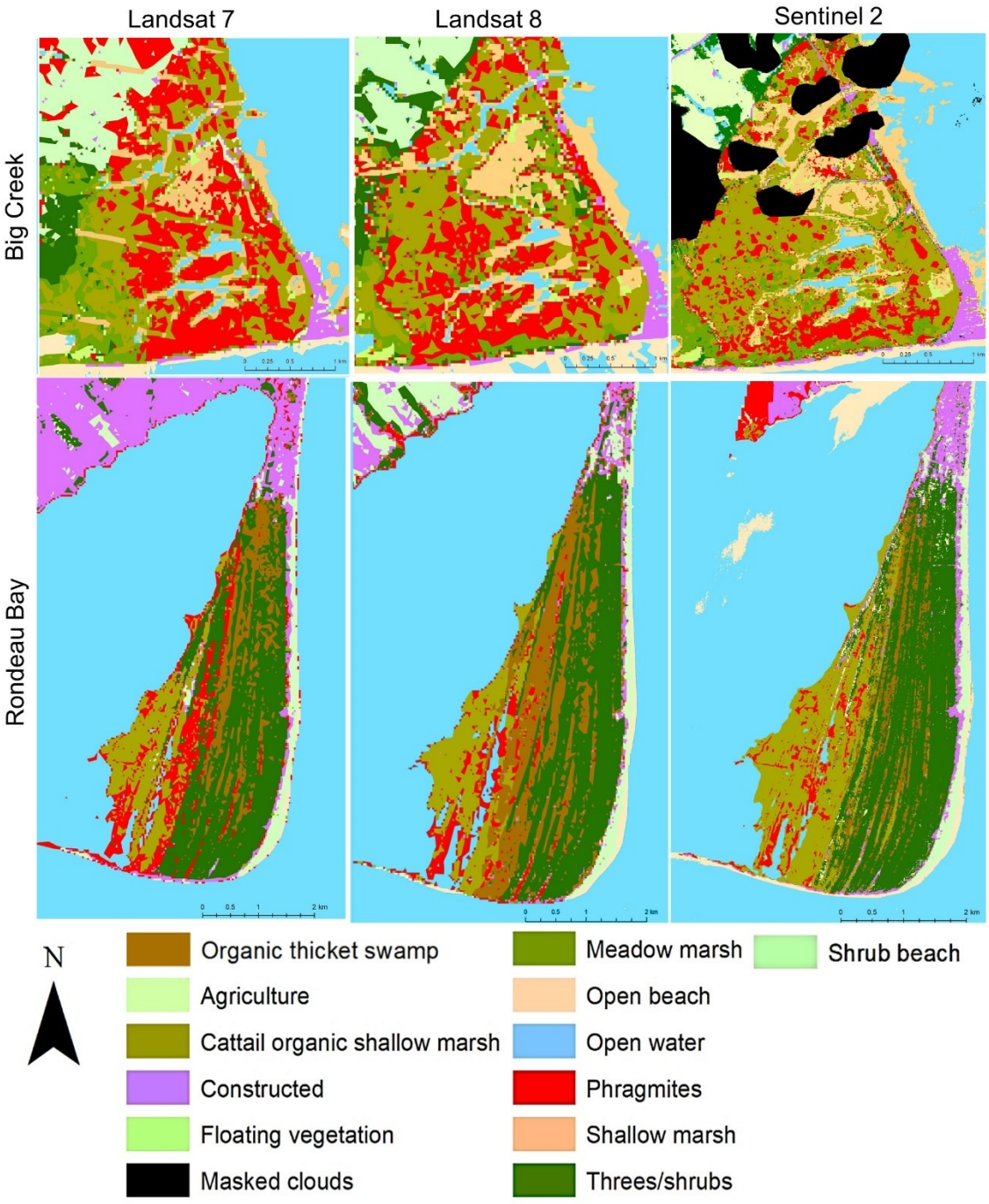

Fig. 2.3 Classified maps with SVM classification for Big Creek and Roundeau Bay, Lake Erie

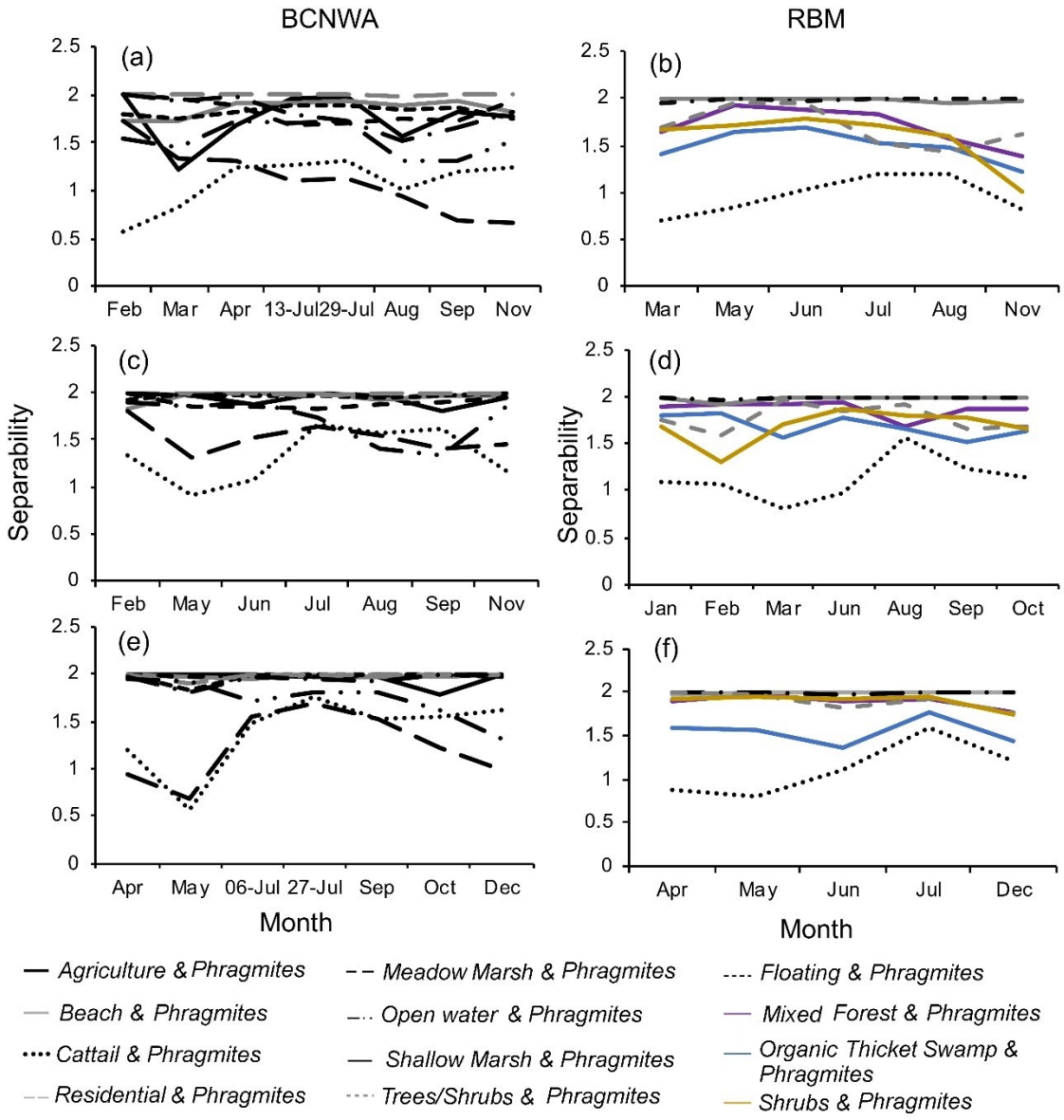

Fig. 2.4 Monthly changes in Jeffries-Matusita Separability of *Phragmites* in Big Creek wetland for (a) Landsat 7 (c) Landsat 8 and (e) Sentinel 2 data; For RBM (b) Landsat 7 (d) Landsat 8 and (f) Sentinel 2 data

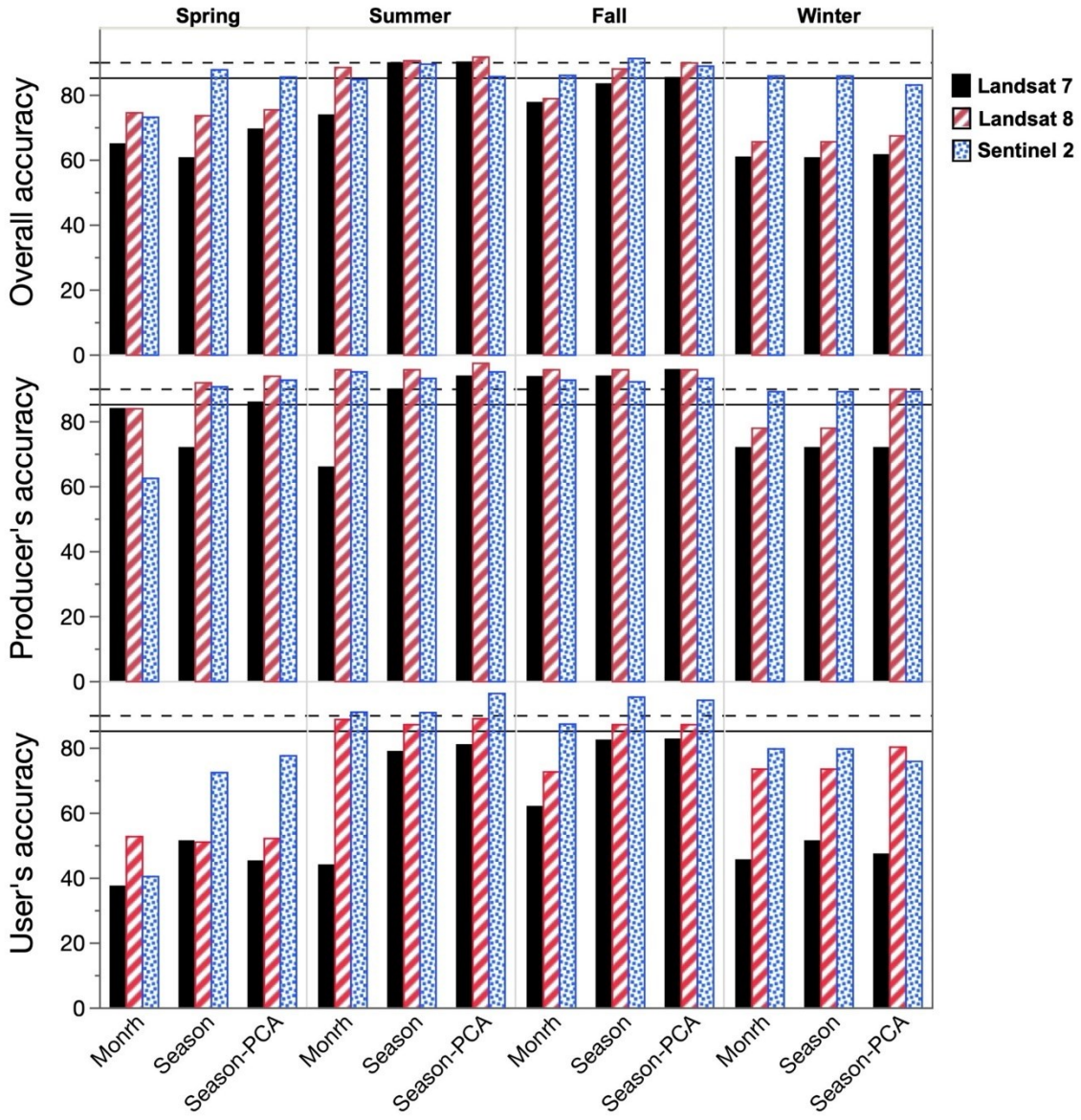

Fig. 2.5 Comparison of Overall, Producer's and User's accuracies for automated classifications of three different satellite images of Big Creek Wetland. Accuracies are sorted by three different methods. Month refers to a single month for a season. Solid line indicates 85% accuracy whereas the dotted line refers to 90% accuracy

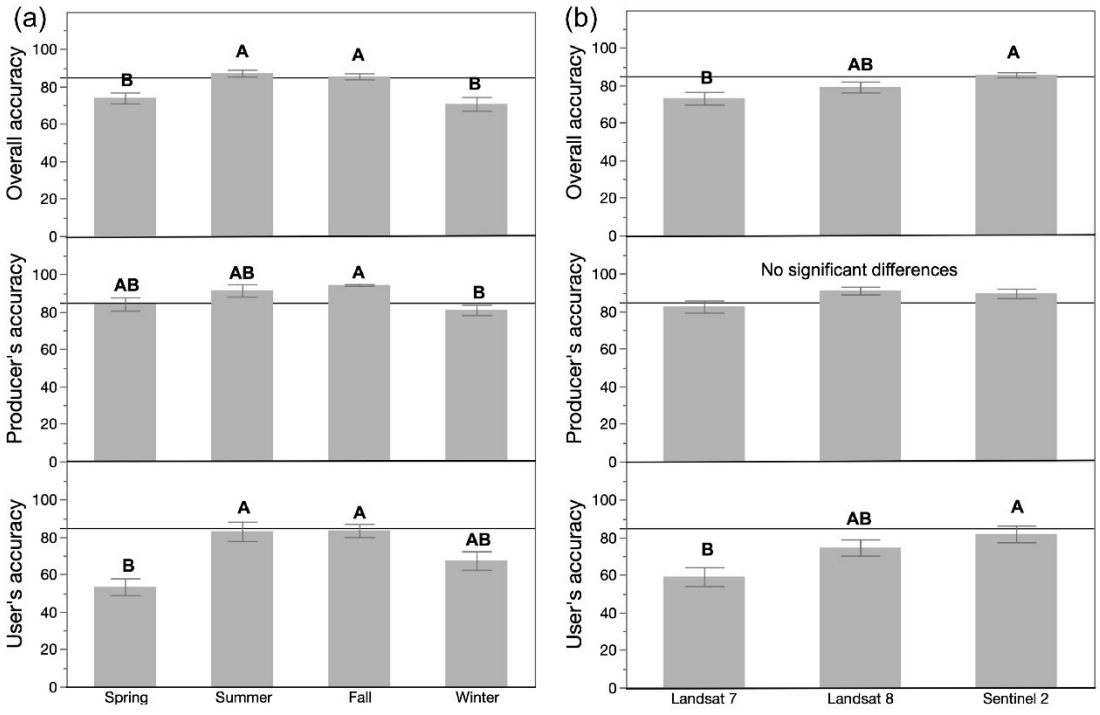

Fig. 2.6 Results of ANOVA comparing *Phragmites* user's, producer's and overall accuracies across a) four seasons and b) satellite sensors. Similar letters join statistically homogeneous means in each panel as indicated by a Tukey's comparison of multiple means

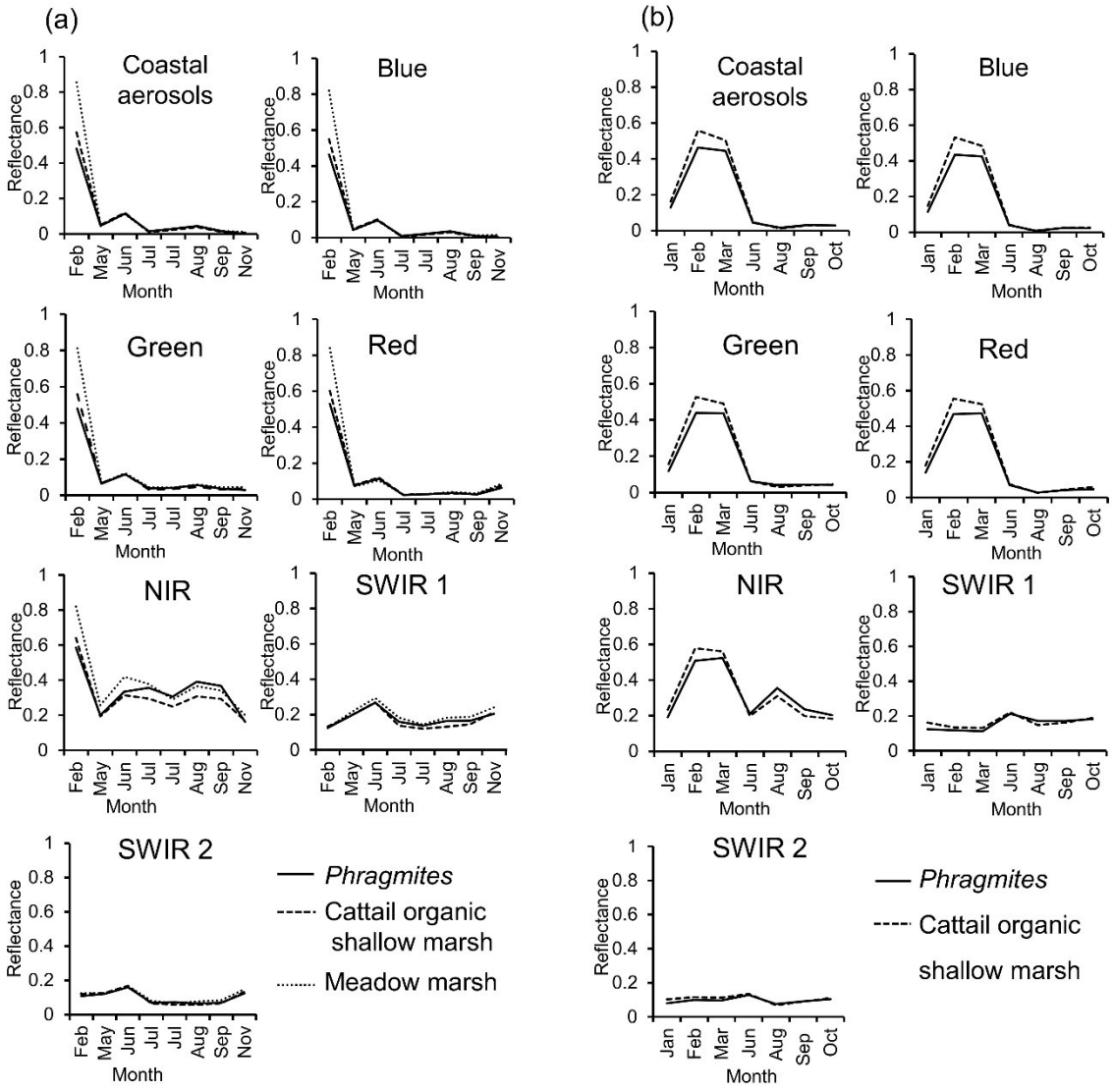

Fig. 2.7 Monthly changes in reflectance of (a) *Phragmites*, cattail organic shallow marsh and meadow marsh for BCNWA site and (b) *Phragmites* and cattail for RBM site for the 7 bands of Landsat 8

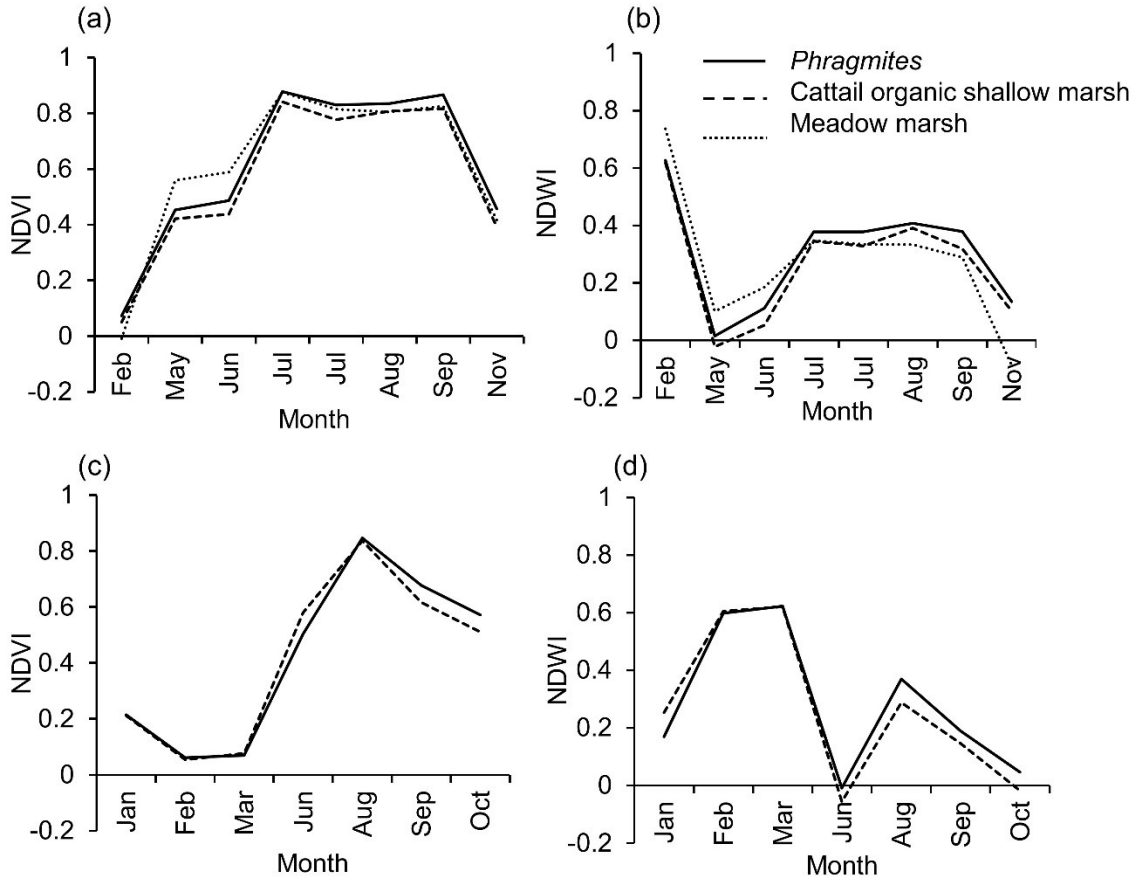

Fig. 2.8 Monthly changes in (a) NDVI and (b) NDWI for BCNWA and (c) NDVI and (d) NDWI for RBM for *Phragmites*, cattail organic shallow marsh and meadow marsh

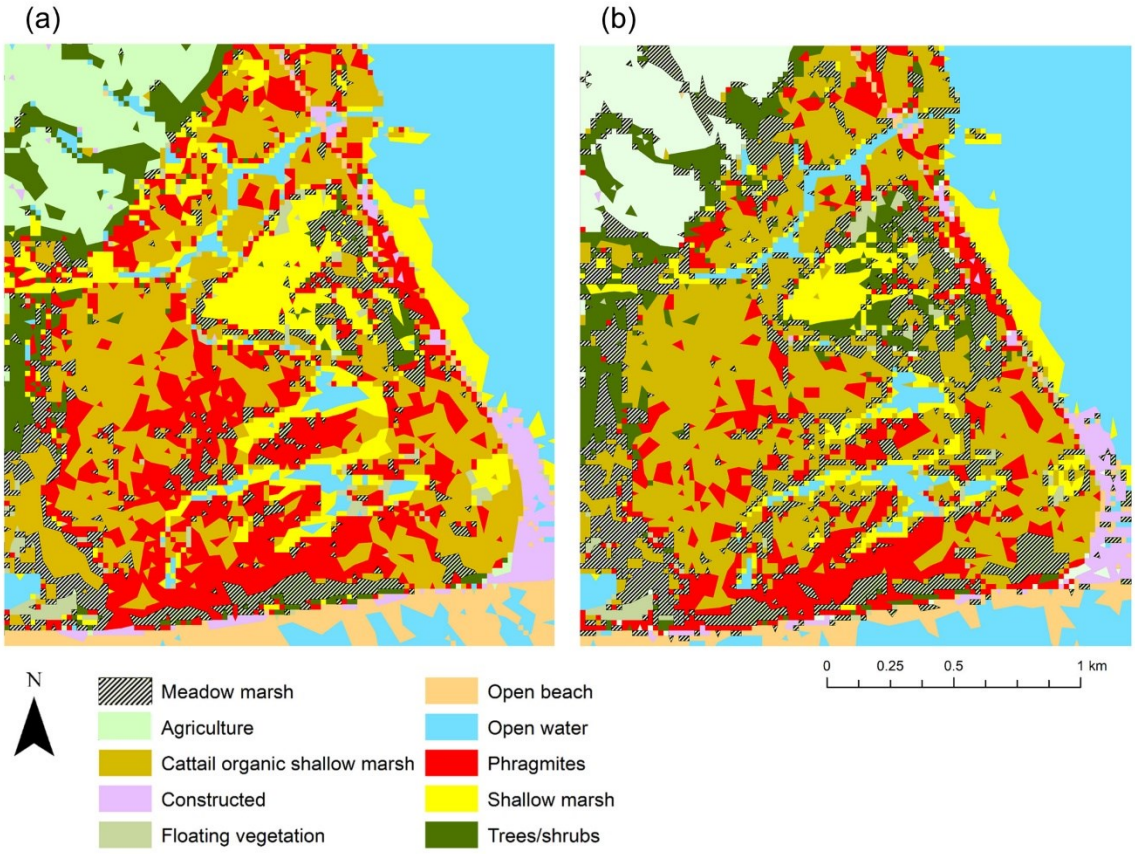

Fig. 2.**9** Landsat 8 images for mapping meadow marsh (a) using only July image and (b) using July image after masking meadow marsh with February image

Chapter 3. Mapping *Phragmites* cover using WorldView 2/3 and Sentinel 2 images at Lake Erie Wetlands, Canada

By,

Prabha Amali Rupasinghe and Patricia Chow-Fraser

Rupasinghe, P. A., & Chow-Fraser, P. (2021). Mapping *Phragmites* cover using WorldView 2/3 and Sentinel 2 images at Lake Erie Wetlands, Canada. *Biological Invasions*. https://doi.org/10.1007/s10530-020-02432-0

3.1. Abstract

Phragmites australis (Cav.) Trin. ex Steudel subspecies *australis* is an aggressive plant invader in North American wetlands. Remote sensing provides cost-effective methods to track its spread given its widespread distribution. We classified *Phragmites* in three Lake Erie wetlands (two in Long Point Wetland Complex (LP) and one in Rondeau Bay Marsh (RBM)), using commercial, high-resolution (WorldView2/3: WV2 for RBM, WV3 for LP) and free, moderate-resolution (Sentinel 2; S2) satellite images. For image classification, we used Mixture-Tuned Match Filtering (MTMF) and then either Maximum Likelihood (ML) or Support Vector Machines (SVM) classification methods. Using WV2/3 images with ML classification, we obtained higher overall accuracy for both LP sites (93.1%) compared with the RBM site (86.4%); both *Phragmites* users' and producers' accuracies were also higher for LP (89.3% and 92.7%, respectively) compared with RBM (84.3% and 88.4%, respectively). S2 images with SVM classification provided similar overall accuracies for LP (74.7%) and for the RBM (74.3%); *Phragmites* users' and producers' accuracies for LP were 85.3% and 76.3%, and for the RBM, 69.1% and 79.2%, respectively. Using WV2/3, we could quantify small patches (percentage cover ≥20%; shoots ≥1 m tall; stem counts >25) with accuracy > 80%, whereas parallel effort with S2 images only accurately quantified high density (>60% cover), mature shoots (>1m tall; Stem counts >100). By simultaneously mapping young or sparsely distributed *Phragmites* shoots and dense mature stands accurately, we show our approach can be used for routine mapping and regular updating purposes, especially for post-treatment effectiveness monitoring.

Key Words: MTMF, *Phragmites*, WorldView 2 and WorldView 3, Sentinel 2, wetlands, invasive species

3.2. Introduction

Phragmites australis (the common reed; hereafter *Phragmites)* is a taxonomically diverse perennial grass, with 27 genetically distinct groups throughout the world, 11 of which are found in North America. One of the European haplotypes, M, is an aggressive invader in coastal wetlands and roadway corridors and have been growing at the expense of native vegetation in many coastal marshes of the lower Great Lakes (Saltonstall 2002). This haplotype exhibits invasive characteristics, including its ability to aggressively colonize exposed mud flats sexually (through seeds), and then expand asexually (through rhizomes) to form dense monocultures that inhibit biodiversity of other plants and wildlife (Meyerson et al. 2000; Markle and Chow-Fraser 2018). Its rapid spread has been attributed to it being a superior competitor against other emergent vegetation (Meyerson et al. 2000; Uddin et al. 2014) and to being more tolerant of disturbances (e.g. road maintenance and changes in hydrologic regimes) and environmental stressors (e.g. increased salinity due to road de-icing salts) (McNabb and Batterson 1991; Marks et al. 1994; Chambers et al. 1999; Brisson et al. 2010; Taddeo and Blois 2012; Rodríguez and Brisson 2015). Once established, this aggressive invader has been known to reduce wetland plant diversity and alter vegetation structure (Ailstock et al. 2001; Mal and Narine 2004; Lambert et al. 2010; Gilbert et al. 2014), habitat for wetland fauna (Weinstein and Balletto 1999; Bolton and Brooks 2010; Gilbert et al. 2014; Cook et al. 2018; Markle and Chow-Fraser 2018), and modify hydrology and soil properties

(Chambers et al. 1999; Bolton and Brooks 2010), thus having an overall negative impact on ecosystem functions.

Optimal conditions for the growth of *Phragmites* are provided by water bodies with seasonal fluctuations of 30 cm (Deegan et al. 2007). New shoots of *Phragmites* arise in the spring and may grow up to 3-4 m tall during the summer, producing large inflorescences giving rise to thousands of seeds towards the late summer and early fall (Burgess and Evans 1989; Gilbert et al. 2014; Gagnon Lupien et al. 2015). According to (Albert et al. 2015), both seeds and vegetative propagation contribute to the new *Phragmites* establishment; however, 84% of the newly established *Phragmites* stands are formed through seed germination. Lathrop et al., (2003) have reported three patterns of *Phragmites* growth in brackish tidal marshes at eastern USA: i) colonization or new growth, ii) linear clonal growth along an axis, and iii) circular clonal patches (non-directional) with random spread. New *Phragmites* stands are characterized by low-density short shoots with a few small leaves. *Phragmites* grown in deep water also produce lower number of shoots and shorter rhizomes, thus limiting its vegetative expansion (Weisner and Strand 1996; Vretare et al. 2001). Linear *Phragmites* stands are mostly observed along the roadside in linear wetland corridors and along shores of water ways, while circular growths are mostly observed in wetlands with ideal growth conditions.

The distinctive growth patterns of *Phragmites* make them well suited to remote sensing approaches. A number of methods have been developed to map dense *Phragmites* with higher accuracy (i.e. >80%), involving satellite images of moderate 30-m Landsat and 10-m and 20-m Sentinel 2 (Rupasinghe & Chow-Fraser, 2019), and emergent

vegetation with 10-m and 20-m SPOT; 4-m IKONOS (Rutchey and Vilchek 1999; Sawaya et al. 2003; Phillips et al. 2005). Other methods are available that employ more expensive high resolution hyperspectral images acquired by commercial sensors such as AVIRIS, CASI, HyMap, and PROBE-1 (Schmidt and Skidmore 2001; Bachmann et al. 2002; Williams and Hunt Jr 2002; Lopez et al. 2004), that could be used for mapping low-density stands. For mapping invasive species, multispectral images have advantages over hyperspectral images because of their overall lower cost (some available at no cost or reduced cost), higher spatial coverage, and shorter durations between acquisitions that facilitate repeated mapping of the entire wetland for assessing treatment efficacy at the ecosystem scale. The main disadvantage, however, is that multispectral images produce lower accuracy compared with hyperspectral images, especially at early stages of invasion when plant densities are low (Adam et al. 2010).

Selection of hyperspectral or multispectral images and choosing the best classification algorithm is essential for accurate species-level mapping. Campbell, (2002) described two categories of classification algorithms that can be used in supervised classification methods: i) distance based or hard classifiers and ii) unmixing based or soft classifiers. In hard classifiers, the distance from a known reflectance value is used to determine the match between an unknown pixel. Maximum Likelihood classification (ML), Spectral Angle Mapper (SAM), and Minimum Distance classification are some of the examples for hard classifiers and they act as ‘first look’ tools to identify the presence of target species in the study area (Campbell 2002). The soft classifiers such as Linear Spectral Unmixing (LSU), Mixture Tuned Match Filtering (MTMF), and Bayesian

Probability use relative abundance of land cover classes within a pixel. In these techniques, mixed pixels that contain several landcover classes are decomposed into its original constituents, to develop a set of output images rather than a single classified image as in hard classifiers (Lass et al., 2005; Williams & Hunt Jr, 2004; Williams & Hunt Jr, 2002).

Despite the expansion of *Phragmites* in many Lake Ontario and Erie coastal marshes in the late 1990s (Wilcox et al. 2003), control programs were not implemented in Ontario until 2007 (Bourgeau-Chavez et al. 2015; Gilbert 2015). Non-chemical control methods such as cutting, drowning, smothering, covering, excavating, plowing, grazing, and burning have been tested in Ontario with varying success (Gilbert et al. 2014). In some instances, mechanical control cannot be implemented in natural ecosystems when the invaded area is large and inaccessible by either boat or road. In these instances, aerial application of either glyphosate or imazapyr has been used (Avers et al. 2007; Derr 2008; Gilbert et al. 2014; Gilbert 2015). Although glyphosate had been used widely within the United States to control the growth of invasive *Phragmites* (Gilbert 2015), its use in Ontario has been prohibited except by Emergency Use Registration, which requires first, an accurate map of *Phragmites* in the wetland to spray only the target area during aerial herbicide application and to avoid spraying on native vegetation and secondly, an accurate monitoring program to quantify the efficacy of the treatment program since complete removal of *Phragmites* in an area requires repeated applications over several years (Gilbert et al. 2014; Rupasinghe et al. 2017).

To meet treatment protocols such as Ontario's Emergency Use Registration requirements, managers must obtain high mapping accuracies for both the expansive mature stands of *Phragmites* (i.e. untreated) as well as the small, young, sparsely distributed shoots (i.e. when they regenerate following treatment). Such mapping would require a remote-sensing approach that is cost-effective, repeatable, and produce results that maximize both producers' (mapping accuracy on the map makers' or the producers' perspective, complements the level of omission error or the false negatives) and users' (mapping accuracy on the map users' perspective, complements the level of commission error or the false positives) accuracies, since both false negatives and false positives are unacceptable at high levels. In this study, we compare classification accuracies associated with two multispectral products (commercially available, high resolution WorldView 2/WorldView3 (WV 2/3) and the freely available, moderate resolution Sentinel 2 (S2) images) using sub-pixel image classification methods to determine the relative usefulness of these image products for mapping the distribution of *Phragmites* in three Lake Erie marshes that had been colonized since the late 1990s (Wilcox et al. 2003). At the time of image acquisition, the patterns of *Phragmites* distribution varied across the three sites. One wetland had low-density stands of young shoots a year following herbicide treatment, whereas another had large, dense mature *Phragmites* stands that had not yet been chemically treated, and a third had a mixture of both chemically treated and untreated areas. Our goal is to experiment with sub-pixel techniques used previously, mostly with hyperspectral images, and apply them to multispectral images to obtain accuracies > 80% for all *Phragmites* density classes across the three Lake Erie wetlands.

3.3. Methods

3.3.1. Study sites

Two of the three Lake Erie wetlands, Big Creek National Wildlife Area (BCNWA; 42°35'N 80°27'W) and Crown Marsh (CM; 42°35'N 80°24'W) occur in Long Point (LP) Wetland Complex, which is internationally recognized as an UNESCO World Biosphere Reserve and under the Ramsar Convention as an internationally important wetland (Ministry of Natural Resources and Forestry 2019) (Fig. 3.1). BCNWA covers an area of 771 ha and consist of the Big Creek unit (615 ha) and the Hahn Marsh Unit (156 ha). It is federally owned and managed by the Environment and Climate Change Canada. CM is about 2 km East to the BCNWA and covers approximately 708.2 ha. It is owned by the Province of Ontario and is normally accessible to the public throughout the year. These wetlands are characterised by emergent aquatic vegetation, mainly Cattail (*Typha* sp.), *Phragmites*, and Bulrushes (*Juncus* sp.) (Long Point Crown Marsh Rehabilitation Steering Committee 2007) and meadow marsh dominated by *Calamagrostis canadensis* (Yuckin and Rooney 2019). The third wetland, Rondeau Bay Marsh (RBM; 42°17'N 81°52'W), is managed by the province of Ontario, and is located further west on the north shore of Lake Erie, covering an area of 1800 ha (Fig. 3.1). RBM is characterized by Carolinian forests, sandy peninsula, and marsh (Mann and Nelson 1980). The drier parts of the marsh are dominated by *Cephalanthus occidentalis*, *Salix*, and *Cornus* spp. Other than *Phragmites*, the emergent plants included monocultures of *Typha latifolia*, *T. angustifolia*, *T.* x *glauca* and *Zizania aquatica* and the marshes with deeper standing

water was dominated by aquatic species of Cyperaceae, *Nuphar advena,* and *Nymphaea odorata* (Finkelstein and Davis 2006).

3.3.2. Remote Sensing data

WV, which is operated by DigitalGlobe, is a fourth-generation, optical and commercial earth-observation satellite series, with the highest spatial resolution (30 cm for WV3 and 40 cm for WV2) of all existing optical satellites available for research (Kurihara et al. 2018). WV3 has revisit frequency less than 1 day at 40°N latitude and 4.5 days at 20° off-nadir or less while for WV2, revisit frequency is 1.1 days and 3.7 days at 20° off-nadir (Satellite Image Corporation 2017a). A cloud-free WV3 image was acquired on 4th July 2018 for BCNWA and CM sites and WV2 image was acquired on 5th September 2018 for RBM site. WV3 images consist of one panchromatic band (445-808 nm spectral resolution and 30 cm spatial resolution) and eight multispectral bands (1.2 m spatial resolution), including the coastal blue (397-454 m), blue (445-517 nm), green (507-586 nm), yellow (580-629 nm), red (626-696 nm), red edge (698-749 nm), Near InfraRed 1 (NIR 1; 765-899 nm) and NIR 2 (857-1039 nm) bands. For the WV2 images, the panchromatic band is 40 cm spatial resolution (464-801 nm) with 8 multispectral bands (1.8 m spatial resolution); coastal blue (401-453 m), blue (447-508 nm), green (511-581 nm), yellow (588-629 nm), red (629-689 nm), red edge (704-744 nm), NIR 1 (772-890 nm) and NIR 2 (862-954 nm) (Nikolakopoulos and Oikonomidis 2015).

S2 is a satellite owned by the European Space Agency (ESA), designed for studies based on terrestrial observations. It consists of two satellites, Sentinel-2A (launched in 2015) and Sentinel-2B (launched in 2017). S2 provide revisit time of 5 days at the equator

(European Space Agency 2020). The images for BCNWA and CM sites were acquired on 6th July 2018 and for RBM site on 28th August 2018. S2 images consist of four 10-m resolution bands (Blue; 490 nm, Green; 560 nm, Red; 665nm, and NIR; 842 nm), six 20-m resolution bands (Vegetation red edge; 705 nm, 74 nm, 783 nm, Narrow NIR; 865 nm, Short Wave InfraRed 1 (SWIR 1); 1610 nm, SWIR 2; 2190 nm), and three 60-m resolution bands (Coastal aerosols; 443 nm, Water vapor; 945 nm, and SWIR Cirrus; 1375 nm).

3.3.3. Ground truth data

We conducted field sampling in the summers of 2018 and 2019 at the BCNWA and CM to record locations of *Phragmites* as ground truth data. In the field, we established 1.5 × 1.5 m quadrats in the *Phragmites* patches and visually recorded percentage cover of *Phragmites*. Then we cut all the standing *Phragmites* stems within the quadrat and weighed them using a Xcalibur Spring Scale. Stand height of *Phragmites* was estimated by cutting down the tallest shoot at its base, laying it on the ground, and measuring them with a tape measure (to the nearest cm). We recorded the coordinates of the quadrats using Garmin eTrex handheld GPS (Garmin and subsidiaries). In total for both years, we collected *Phragmites* information from 58 quadrats in BCNWA and 89 quadrats in CM. In addition to field sampling, we used high-resolution image interpretation to identify land-cover classes on inaccessible areas. We used the sensefly eBee (Parrot, Cheseaux-Lausanne, Switzerland (SenseFly 2020b), equipped with the Parrot Sequoia+ camera (SenseFly 2020) to acquire Unmanned Aerial Vehicle (UAV; 13 cm resolution) images in July 2019. We used this high-resolution UAV image and the

pansharpened WV3 image (30 cm spatial resolution; same image used in image classification) to collect ground reference for land-cover classes for both classification and accuracy assessment for areas with limited access. We identified these classes through both knowledge in the field and visual comparison of manually digitized UAV image acquired in late summer 2015 (Marcaccio et al. 2016). In addition, we also used 15 *Phragmites* treatment locations corresponding to a spraying program conducted between September to October in 2018 by Nature Conservancy Canada (NCC) to validate the image classification.

Field data used as ground reference for RBM were collected by Angoh et al., (841 quadrats; unpublished data) as part of their study to examine the effect of *Phragmites* on turtle habitats. They used 2×2 m quadrats and counted the number of dead and live *Phragmites* stems and Cattail stems within the quadrat and recorded the dominant species and landcover types within the quadrat. Of these 841 quadrats, 313 contained *Phragmites*. In addition to the field data, we used locations from manual interpretation of pansharpened WV2 image (40 cm spatial resolution, same image used for the image classification) and obtained 10 locations where *Phragmites* had been treated in 2018 (data provided by Ontario Parks).

3.3.4. Remote sensing data processing

We conducted all image pre-processing and processing with the software ENVI 5.5 (L3Harris Geospatial 2020). We performed radiometric correction and atmospheric correction (ENVI FLAASH correction) to obtain surface reflectance values for both WV2/3 and S2 images. Reflectance values were rescaled from 0 to 1 after FLAASH

correction. For S2 images, we separately preprocessed the 20-m resolution bands, resampled them to 10-m resolution and stacked them with the preprocessed 10-m bands prior to image analysis.

We performed sub-pixel image classification using spectral mixture analysis to detect *Phragmites*. In the spectral mixture analysis, it is assumed that the mixed pixel spectrum is a linear combination of the spectral signatures of the component classes of the pixel (Adams et al. 1985). Mixture Tuned Match Filtering (MTMF) is a method used in spectral mixture analysis which performs partial spectral unmixing (Boardman et al. 1995). In this technique, only the pure spectral signature (endmember) of the target landcover class needs to be defined. The image is then filtered for the defined endmember spectrum and the unknown background spectra are supressed (Boardman 1998; Boardman and Kruse 2011; Brelsford and Shepherd 2013). The three steps in MTMF includes: i) Minimum Noise Fraction (MNF) transformation to minimize and decorrelate noise, ii) Match Filtering (MF) to estimate the abundance of the target class, and iii) Mixture Tuning (MT) to separate false positives from the MF step (Boardman 1998; Boardman and Kruse 2011). The MTMF produces two outputs at the end of the analysis, the MF score image, and the infeasibility image. The MF score represents the relative abundance of the target class within a pixel. It ranges from 0 to 1 where a score of 1 represents a perfect match between the endmember and the sub-pixel abundance or 100% of the target class within the pixel. The infeasibility scores are in noise sigma units and provide the feasibility of the MF results (Harris Geospatial Solutions, Inc 2020).

First, we performed Minimum Noise Fraction (MNF) transformation for both pre-processed WV2/3 and S2 images to reduce image dimensionality. After the MNF transformation, we performed the MTMF followed by image classification. We evaluated the eigen value plots and the classification results with various combinations of MNF bands and based on these results, chose the first four or five bands for further analysis (additional MNF bands added unwanted noise to the classification). For the MTMF, we extracted spectral endmembers using the field observations. Again, we repeated the classification with *Phragmites* endmember alone and with different combinations of endmembers of the other classes and checked for accuracy. Then we selected the endmember combination that provided the highest classification accuracy.

After the MTMF transformation, we classified the images using both Maximum Likelihood (ML) and Support Vector Machines (SVM) classification methods. We applied 5×5 majority filter for all classes except for *Phragmites* and then compared the results. For image classification and endmember extraction, we used *Phragmites* locations collected in the field in addition to locations obtained from the image interpretation (73 locations for the LP and 38 locations for the RBM); we used all *Phragmites* quadrat data collected in the field and the *Phragmites* treatment locations for accuracy assessment (162 locations for the LP and 323 locations for the RBM). Therefore, there was no overlap between classification and accuracy assessment locations.

After image classification, we imported landcover maps that provided the highest mapping accuracy into ArcMap 10.4.1 and evaluated the mapping accuracy of *Phragmites* cover, stem count, height, and weight using the quadrat data collected during

field work. To enable analyses, we divided percentage cover data into five equal intervals (i.e. 20% increments). Height information were sorted into four categories (<1m, 1-2m, 2-3m, and >3 m) as were weight data (0-2kg, 2-4kg, 4-6kg, and >6 kg). Although we performed image classification of BCNWA and CM together (i.e. a single image was acquired for both sites), we calculated percent cover and analyzed the height and weight data separately for the two sites. For the RBM site, we sorted the live stem counts per quadrat into six categories (0, 1-25, 25-50, 50-75, 75-100, and >100), before calculating mapping accuracies.

We used Fragstats 4.2 to extract patch area, Largest Patch Index (LPI), and radius of gyration of each patch for the three sites separately using the maps with highest classification accuracy. We analysed the data using the JMP 15 software and created plots in MS Excel and in JMP.

3.4. Results

3.4.1. *Phragmites* and wetland land cover mapping

After analyzing different endmember combinations, we obtained the highest classification accuracy with the combination that included *Phragmites*, trees/shrubs (mixed forest for RBM site), and open land. Accuracy obtained for this combination was higher than that for the *Phragmites* endmember alone. Therefore, we used this combination of classes for the rest of the study (i.e. all combinations of sites and sensors).

For the BCNWA and CM sites, we classified the image into eight land cover classes; *Phragmites*, Cattail organic shallow marsh, mixed organic shallow marsh, trees/shrubs, open land, open water, submerged shallow aquatic shallow marsh, and

floating vegetation (Fig. 3.2). We classified the RBM site also into eight classes: *Phragmites*, Cattail organic shallow marsh, floating vegetation, meadow marsh, mixed forest, open land, open water, and organic thicket swamp (Fig. 3.3). The overall, user's and producer's accuracies were higher for WV2/3 than for S2, regardless of classification method (Table 3.1). For WV2/3 images only, ML classification produced higher classification accuracy than did SVM. The SVM classification resulted in high commission error of *Phragmites* for both LP and RBM sites (Table 3.1; Fig. 3.2 and 3.3). By comparison, SVM produced higher accuracy than did ML classification for S2 images. Based on these results, we used the ML classification for the WV2/3 images and SVM classification for the S2 images in *Phragmites* cover, stem count, height, and weight analysis.

3.4.2. *Phragmites* percentage cover and stem count analysis

The MF score of *Phragmites* increased with percentage cover and stem count (Fig. 3.4 and 3.5); however, whereas significant positive regressions between MF score and percentage cover were found for all WV2/3 images, only the S2 image for BC was associated with a significant regression. Classification of S2 images were generally associated with comparatively low accuracies (Table 3.1), with no significant positive correlation between MF scores and percentage cover or stem counts (Fig. 3.4 and 3.5). Despite the statistical significance, the regression coefficient between the MF score and percentage cover of *Phragmites* was relatively low (Fig. 3.4). This is due to the spectral similarities between *Phragmites* and other vegetation classes. We observed lower MF scores for some locations with 100% *Phragmites* cover (as reported in the field) because

the actual image pixels could be mixed with different reflectance signals such as shadows cast by *Phragmites* itself or by adjacent taller vegetation, non-leaf reflectance from large inflorescences, dried leaves and stalks, glare from open water etc. We observed a similar trend with the stem count data for the RBM site, in which the regression coefficient between MF score and the live stem count of *Phragmites* was very low (Fig. 3.5). The dead stems in majority of the quadrats at the RBM site and other reflectance signals associated with non-*Phragmites* vegetation may explain the low range of MF scores.

Although accuracies for the five density categories varied for the two LP sites, some generalizations can be made. First, regardless of the site, we obtained higher accuracies with the WV3 image (Fig. 3.6 a and c) than with the S2 image (Fig. 3.6 b and d). Secondly, in all cases, the lowest density category (<20% cover) failed to meet the threshold accuracy of 80% (Fig. 3.6). For BCNWA, four of the remaining density categories achieved acceptable accuracies with the WV3 image compared with three with the S2 image (Fig. 3.6a vs Fig. 3.6c). Inaccurate classifications for the highest density (80-100% cover) were caused by confusion between *Phragmites* and Cattail and in a few cases, between a patch of high-density *Phragmites* and trees/shrubs. For CM, acceptable accuracies were only achieved with the WV3 image in the two highest density categories, whereas all accuracies were < 80% with the S2 image (Fig. 3.6b vs 3.6d).

For the RBM site, we had stem counts instead of percentage cover data. The WV2 image yielded >80% accuracies for quadrats with greater than 25 *Phragmites* stems (Fig. 3.7). An accuracy of 93.3% was obtained for quadrats with over 100 live *Phragmites* stems, and 53.4% for the lowest category with fewer than 25 live stems. For quadrats

containing non-living *Phragmites* stems, we obtained an accuracy of 50.0%. For S2 images, accuracy for the highest count category (>100 live stem) was only 73.3% (4 of 15 quadrats had been misclassified), and accuracies for all other categories were lower than 65%.

We observed a significant positive correlation between percentage cover of *Phragmites* and live stem weight and height for both BCNWA (r=0.58 and r=0.71 respectively) and CM (r=0.84 and r=0.79 respectively) sites. Therefore, we analysed the classification accuracy of *Phragmites* sorted by weight and height. With the WV3 images, we found >80% accuracy for all height categories over 1 m. We obtained accuracy of 75.0% for plants <1 m tall at the BCNWA site (Fig. 3.8a). By contrast, the highest accuracy (86.7%) for the S2 image was obtained for the 1-2 m category, while plants shorter than 1m, taller than 3m, and between 2-3 m were associated with much lower accuracies of 62.5%, 71.4% and 82.1%, respectively (Fig. 3.8b). We did not have any quadrat data over 3 m height category for the CM site. We obtained 100% accuracy for the height category of 2-3 m and very low accuracy for 0-1 m height category (7.7%; Fig. 3.8e). We obtained a similar trend with the S2 images, where highest accuracy was obtained for the intermediate category (2-3 m; 85.7%), and lowest accuracy was obtained for quadrats with plant heights <1 m (7.7%; Fig. 3.8f). Based on the results, accuracy for both WV3 and S2 images generally improved with increasing plant height.

We also compared accuracies between WV3 and S2 for classifying *Phragmites* weights in the two LP sites. For BCNWA, accuracies for all four weight categories met the target of 80% when WV3 image was used (Fig. 3.8c), whereas only two categories

met this target when the S2 image was used (Fig. 3.8d). For CM, accuracies for only three of the weight categories were >80% when WV3 image was used (Fig. 3.8g), whereas none of the categories had acceptable accuracies when the S2 image was used (Fig. 3.8h). Therefore, in general, accuracies were much better for the WV3 than the S2 image.

3.4.3. *Phragmites* patch characteristics

We studied the patch characteristics using the maps produced using the WV2/3 images as it provided the highest mapping accuracy. The patch sizes of *Phragmites* in this study ranged from very small (2 m^2) to extremely large (40 ha) patches. The two largest patches were found in RBM (40.33 ha) and in BCNWA (26.89 ha). By far, however, the majority (>80% of the 58081 patches) of these *Phragmites* patches were < 100 m^2 at the BCNWA site. In comparison, 70% of 17889 *Phragmites* stands in CM and 50% of the 50191 stands in RBM had an area < 100 m^2. The radius of gyration, which is a measure of the spatial extent of a habitat patch (defined as a mean distance between each cell in the patch and the patch's centroid) differed significantly among the three sites. RBM, with the greatest total area occupied by *Phragmites*, also had the highest radius of gyration (Fig. 3.9a and 3.9b). The calculated geometric mean patch size of *Phragmites* in both LP wetlands was < 5 m^2 while that in RBM was more than double (>10 m^2; Figure 3.9c). When we compared the LPI for the three sites, CM, BCNWA, and RBM sites have 0.8%, 2.2%, and 2.5% respectively. Overall, these results indicate that the RBM site had comparatively larger *Phragmites* patches, and fewer small-sized stands compared with the LP sites.

3.5. Discussion

Our study is the first to use subpixel image classification using MTMF with multispectral satellite images to map *Phragmites*, and we have been able to achieve up to 90% accuracy across landscapes containing patches that range from very large size of 40 ha to very small sparse stands of 2 m^2. We achieved higher classification accuracy by using spectral endmembers that were defined for trees/shrubs and open land in addition to *Phragmites* instead of *Phragmites* endmember alone. We focused on developing simple, cost-effective methods that could be used in sites with a range of patch sizes and distributions so that the protocol can be repeated across many different wetlands by environmental agencies. Our goal was to obtain accurate maps of both low density or young *Phragmites* stands as well as expansive, large stands so that the same protocol can be used for initial assessment as well as effectiveness monitoring. We found that the best combination at no-cost involves the use of S2 images and SVM classification while the best combination with highest mapping accuracy involves the commercially available WV2/3 images and use of ML classification.

In all respects, classification of WV2/3 images produced higher overall and *Phragmites* accuracies than did classification of S2 images. This difference in performance is directly related to the higher spatial resolution of WV2/3 (1.8 m and 1.2 m) compared with S2 (10 m and 20 m) which results in higher spectral mixing in the latter. When we compared the two sites, RBM had slightly lower accuracy than did LP sites, and this difference also may have been due to slightly lower spatial resolution of WV2 compared with WV3. Spectral resolution may also have affected the results since

we used 8 bands of WV2/3 (from 400 – 1040 nm wavelength) compared with 10 bands of S2 (from 490 – 2190 nm wavelength). Although S2 images have a greater number of bands covering a larger wavelength region, the spatial resolution appeared to have considerably reduced the accuracy of image classification.

We observed some classification confusion of *Phragmites* with Cattail, open water, and trees/shrubs. In our study sites, Cattail is most similar to *Phragmites* in terms of being tall, unbranched, and forming dense monospecific stands, with somewhat similar leaf arrangement when compared to other vegetation classes. Given that they have similar habitat requirements, they are often found in mixed stands, and these morphological similarities may have resulted in similar reflectance signals that resulted in classification confusions between *Phragmites* and Cattail (Rupasinghe and Chow-Fraser 2019). Initially, we included meadow marsh in our classification for the LP sites as this is an important wetland category, but this increased *Phragmites* omission error. Meadow marsh at LP sites consisted of mixed plant species such as grasses, sedges, emergent shrubs, and upland plant species and can be highly confused with *Phragmites* when mapped with satellite images (Rupasinghe and Chow-Fraser 2019). The meadow marsh class was mostly confused with young and lower density *Phragmites* patches due to spectral similarities. Therefore, we excluded meadow marsh from the final classification of the LP sites because our main target was to improve *Phragmites* producers' and users' accuracies. Due to this modification, vegetation in the meadow marsh habitat was incorrectly classified as Cattail or mixed organic shallow marsh, but only infrequently as young, low density *Phragmites*. As our intention was to map low density *Phragmites* as

accurately as possible for management purposes, missing meadow marsh was not considered a significant problem. This confusion, however, was not observed at the RBM site mainly because the *Phragmites* stands at RBM are large and dense and therefore not easily confused with spectral characteristics of meadow marsh.

We also observed misclassifications between *Phragmites* and trees/shrubs in some locations. This occurred in some extremely dense *Phragmites* patches. Confusion of *Phragmites* with open water occurred in areas where *Phragmites* was beginning to colonize in shallow water and had low plant density. Spectral reflectance of sunlight by water can also interfere with the signal produced by *Phragmites* and lead to misclassifications. Finally, we were able to improve the accuracy of the classification by removing or masking out ecologically irrelevant classes such as built-up areas, roads, and agricultural fields. This is because the bright signals of these classes often interfered with vegetation classes, especially when the glare from water caused misclassifications and reduced the overall accuracy.

We were relatively successful in classifying *Phragmites* stands according to height and weight. When *Phragmites* stands are dense, they produced purer reflectance signals that were not mixed with those of other classes. Mature *Phragmites* can grow up to 3-4 m high and reach densities of 200 live and 300 dry stands per square meter under optimal conditions (Hara et al. 1993; Poulin et al. 2010). Optimal conditions for *Phragmites* are freshwater bodies with seasonal fluctuations of 30 cm (Deegan et al. 2007) and all our study sites provide these ideal conditions for *Phragmites* colonization. According to Hara et al., (1993), *Phragmites* does not increase shoot diameter, and increase in shoot weight

is parallel to increase in shoot height. At younger stages, *Phragmites* shoots use carbohydrates from the rhizomes, accumulated during the previous growing season. Therefore, younger shoots are smaller and have fewer number of small leaves (Hara et al. 1993). Furthermore, density and height of *Phragmites* stands could also be affected by environmental conditions such as water level fluctuations. We obtained acceptable accuracy for even the lowest height and weight category with the WV3 images. Our study confirms that WV2/3 could be effectively used for mapping even young or smaller *Phragmites* stands; however, S2 could only be used to map older, denser, or larger *Phragmites* stands with less spectral mixing.

Timing of image acquisition and plant phenology are important considerations in *Phragmites* mapping (Rupasinghe and Chow-Fraser 2019). *Phragmites* produce the most unique, detectable signal that can be separated from other vegetation classes (especially Cattail and meadow marsh) during the peak summer period. The distinct inflorescence, the unique green color due to the high chlorophyll concentration, the leaf arrangement, and the high water-use efficiency of *Phragmites* during this period all could be combined to produce this unique spectral signature. Use of images collected in late summer is also beneficial as the *Phragmites* treatment is usually conducted in September to October and this provides most up-to-date map. Use of Short-Wave IR bands may also improve the classification accuracy (Rupasinghe and Chow-Fraser 2019). One obvious limitation of WV2/3 is the potentially high cost of acquiring images to map large invasion areas.

We have shown that besides differences in resolution of satellite images, we can attribute some of the variation in mapping accuracies among the three sites to differences

in treatment history along with amount of field data, and the timing of image acquisition. Since the entire CM had been treated in the fall of 2017 and the image was acquired in July the following year, there were no mature stands but many small stands that had either escaped treatment or had recently regenerated. Therefore, there was interference from water reflectance in many inundated areas that were absent in the other two sites. By comparison, mature stands in the diked area of BCNWA could be mapped accurately because they were large and dense and had not yet been treated at the time of image acquisition. We had relatively few RBM data to train and validate the classification of small sparse stands of common reed, whereas such data had been specifically collected in CM and BCWNA, and this may also explain differences in mapping accuracies. According to Rupasinghe and Chow-Fraser (2019), images acquired in July and early August was best for minimizing confusion between *Phragmites* and *Typha* and were associated with highest accuracies for *Phragmites*. Therefore, all else being equal, the July image for LP could explain the better performance than the September image for RBM.

3.6. Conclusion

Tracking *Phragmites* distribution, determining the borders of the patches, and estimating the extent of invaded area are common objectives of invasive plant management programs. The conventional approach is to map the distribution using field surveys, which are extremely labour intensive, and which may produce results that are biased against smaller and mixed *Phragmites* stands depending on the thoroughness of the observer. Mapping approaches with remote sensing technology can overcome these

challenges by providing comprehensive coverage of both small and large study areas, even if they are difficult to access by boat or by road. Accurate distribution of relatively small *Phragmites* stands are difficult to obtain, but they are very valuable to managers because both mechanical and chemical treatment are most effective when populations are small and sparsely distributed. Using commercially purchased high-resolution satellite images, we were able to map younger, less dense, or smaller *Phragmites* stands as well as the mature, dense, and larger *Phragmites* stands with overall accuracy greater than 80%. By comparison, satellite images from S2 that are available at no cost could be used to accurately map large, high density *Phragmites* stands, but this approach is only useful when general estimation of *Phragmites* cover is required over large spatial extents. The mapping accuracy is dependent on the *Phragmites* patch characteristics, other wetland plant species, and the site conditions. We recommend masking out ecologically irrelevant or adjacent land-cover classes (e.g. agricultural lands, roads, and buildings) to reduce classification errors and computational time. Use of spectral unmixing of WV2/3 is a promising method for detection of *Phragmites* in wetlands, especially for detecting new *Phragmites* growth in treated areas and for routine mapping and regular updating purposes.

3.7. Acknowledgements

Authors would like to thank Dr. James Marcaccio, Jordan DeBoer, and Dr. Chantel Markle for support with UAV image acquisition and field data collection. We would like to thank Jennifer Angoh (Trent University) and Dr. Christina Davy (Trent University and Ontario Ministry of Natural Resources and Forestry) for sharing field data

from the RBM site. We are grateful to the Nature Conservancy of Canada for providing partial funding for this study. We would also like to thank Canadian Wildlife Service and Ministry of Environment and Climate Change Canada for providing permission to conduct field work at the BCNWA site. We are grateful to the Nature Conservancy of Canada and Parks Ontario for the *Phragmites* treatment locations data for this study. We would like to express our gratitude to the reviewers and Associate Editor for providing valuable comments and suggestions to improve our manuscript.

3.8. Literature Cited

Adam E, Mutanga O, Rugege D (2010) Multispectral and hyperspectral remote sensing for identification and mapping of wetland vegetation: a review. Wetl Ecol Manag 18:281–296. https://doi.org/DOI 10.1007/s11273-009-9169-z

Adams JB, Smith MO, Johnson PE (1985) Spectral mixture modeling: a new analysis of rock and soil types at the Viking Lander 1 site. J Geophys Res 91:8098–8112. https://doi.org/doi.org/10.1029/JB091iB08p08098

Ailstock MS, Norman CM, Bushmann PJ (2001) Common Reed *Phragmites australis*: Control and Effects Upon Biodiversity in Freshwater Nontidal Wetlands. Restor Ecol 9:49–59. https://doi.org/10.1046/j.1526-100x.2001.009001049.x

Albert A, Brisson J, Belzile F, et al (2015) Strategies for a successful plant invasion: the reproduction of *Phragmites australis* in north-eastern North America. J Ecol 103:1529–1537. https://doi.org/10.1111/1365-2745.12473

Avers B, Fahlsing R, Kafcas E, et al (2007) A guide to the control and management of invasive *Phragmites*. Mich Dep Environ Qual Lansing

Bachmann CM, Donato TF, Lamela GM, et al (2002) Automatic classification of land cover on Smith Island, VA, using HyMAP imagery. IEEE Trans Geosci Remote Sens 40:2313–2330. https://doi.org/10.1109/TGRS.2002.804834

Boardman JW (1998) Leveraging the high dimensionality of AVIRIS data for improved sub-pixel target unmixing and rejection of false positives: mixture tuned matched filtering. In: Summaries of the seventh JPL Airborne Geoscience Workshop, JPL Publication, 1998. NASA Jet Propulsion Laboratory, pp 55–56

Boardman JW, Kruse FA (2011) Analysis of imaging spectrometer data using N-dimensional geometry and a mixture-tuned matched filtering approach. IEEE Trans Geosci Remote Sens 49:4138–4152. https://doi.org/10.1109/TGRS.2011.2161585

Boardman JW, Kruse FA, Green RO (1995) Mapping target signatures via partial unmixing of AVIRIS data. In: JPL Airborne Earth Science Workshop. pp 23–26

Bolton RM, Brooks RJ (2010) Impact of the seasonal invasion of *Phragmites australis* (common reed) on turtle reproductive success. Chelonian Conserv Biol 9:238–243. https://doi.org/10.2744/CCB-0793.1

Bourgeau-Chavez L, Endres S, Battaglia M, et al (2015) Development of a bi-national Great Lakes coastal wetland and land use map using three-season PALSAR and Landsat imagery. Remote Sens 7:8655–8682. https://doi.org/10.3390/rs70708655

Brelsford C, Shepherd D (2013) Using mixture tuned match filtering to measure changes in subpixel vegetation area in Las Vegas, Nevada. In: Remote Sensing and

Modeling of Ecosystems for Sustainability X. International Society for Optics and Photonics, San Diego, California, United States, p 88690B

Brisson J, de Blois S, Lavoie C (2010) Roadside as invasion pathway for common reed (*Phragmites australis*). Invasive Plant Sci Manag 3:506–514. https://doi.org/10.1614/IPSM-09-050.1

Burgess ND, Evans CE (1989) The management of reedbeds for birds. RSPB, Information Press, Sandy, Oxford, UK

Campbell JB (2002) Introduction to remote sensing 3rd ed, 3rd edn. The Guilford Press. New York, New York, USA

Chambers RM, Meyerson LA, Saltonstall K (1999) Expansion of *Phragmites australis* into tidal wetlands of North America. Aquat Bot 64:261–273. https://doi.org/10.1016/S0304-3770(99)00055-8

Cook CE, McCluskey AM, Chambers RM (2018) Impacts of invasive *Phragmites australis* on diamondback terrapin nesting in Chesapeake Bay. Estuaries Coasts 41:966–973. https://doi.org/DOI 10.1007/s12237-017-0325-z

Deegan BM, White SD, Ganf GG (2007) The influence of water level fluctuations on the growth of four emergent macrophyte species. Aquat Bot 86:309–315. https://doi.org/10.1016/j.aquabot.2006.11.006

Derr JF (2008) Common reed (*Phragmites australis*) response to mowing and herbicide application. Invasive Plant Sci Manag 1:12–16. https://doi.org/10.1614/IPSM-07-001.1.

European Space Agency (2020) Sentinel-2 Missions Resolution and Swath Sentinel Handbook. https://sentinel.esa.int/web/sentinel/missions/sentinel-2/instrument-payload/resolution-and-swath. Accessed 2 Mar 2020

Finkelstein SA, Davis AM (2006) Paleoenvironmental records of water level and climatic changes from the middle to late holocene at a Lake Erie coastal wetland, Ontario, Canada. Quat Res 65:33–43. https://doi.org/10.1016/j.yqres.2005.08.021

Gagnon Lupien N, Gauthier G, Lavoie C (2015) Effect of the invasive common reed on the abundance, richness and diversity of birds in freshwater marshes. Anim Conserv 18:32–43. https://doi.org/10.1111/acv.12135

Garmin, subsidiaries GL or its Garmin eTrex® 10 | Outdoor GPS. In: Garmin. https://buy.garmin.com/en-CA/CA/p/87768. Accessed 18 Apr 2020

Gilbert J (2015) Rondeau Provincial Park Invasive *Phragmites* Management Program 2008–2014 Summary Report and Recommended Next Steps

Gilbert J, Vidler N, Cloud Sr P, et al (2014) *Phragmites australis* at the crossroads: why we cannot afford to ignore this invasion. In: Proceedings of great lakes wetlands day. Toronto, Ontario, Canada, pp 78–84

Hara T, van Der Toorn J, Mook JH (1993) Growth Dynamics and Size Structure of Shoots of *Phragmites Australis*, a Clonal Plant. J Ecol 81:47–60. https://doi.org/10.2307/2261223

Harris Geospatial Solutions, Inc (2020) Mixture Tuned Matched Filtering. https://www.harrisgeospatial.com/docs/MTMF.html. Accessed 21 Mar 2020

Kurihara J, Takahashi Y, Sakamoto Y, et al (2018) HPT: A High Spatial Resolution Multispectral Sensor for Microsatellite Remote Sensing. Sensors 18:. https://doi.org/10.3390/s18020619

L3Harris Geospatial (2020) ENVI - The Leading Geospatial Image Analysis Software. https://www.harrisgeospatial.com/Software-Technology/ENVI. Accessed 25 Mar 2020

Lambert AM, Dudley TL, Saltonstall K (2010) Ecology and impacts of the large-statured invasive grasses Arundo donax and *Phragmites australis* in North America. Invasive Plant Sci Manag 3:489–494. https://doi.org/10.1614/IPSM-D-10-00031.1

Lass LW, Prather TS, Glenn NF, et al (2005) A review of remote sensing of invasive weeds and example of the early detection of spotted knapweed (*Centaurea maculosa*) and baby's breath (*Gypsophila paniculata*) with a hyperspectral sensor. Weed Sci 53:242–251. https://doi.org/10.1614/WS-04-044R2

Lathrop RG, Windham L, Montesano P (2003) Does *Phragmites* expansion alter the structure and function of marsh landscapes? Patterns and processes revisited. Estuaries 26:423–435. https://doi.org/DOI: 10.1007/BF02823719

Long Point Crown Marsh Rehabilitation Steering Committee (2007) Toward Rehabilitation of the Crown Marsh - Long Point, Lake Erie, Ontario. Ontario Ministry of Natural Resources, University of Western Ontario, Long Point Waterfowl & Wetlands Research Fund, Long Point Waterfowlers Association, Bird Studies Canada, Bird Studies Canada

Lopez RD, Edmonds CM, Neale AC, et al (2004) Accuracy assessments of airborne hyperspectral data for mapping opportunistic plant species in freshwater coastal wetlands. In: In Remote Sensing and GIS Accuracy Assessment, Edited by: Lunetta, R. S. and Lyon, J. G. CRC Press, Boca Raton, Florida, USA, pp 253–267

Mal TK, Narine L (2004) The biology of Canadian weeds. 129. *Phragmites australis* (Cav.) Trin. ex Steud. Can J Plant Sci 84:365–396. https://doi.org/10.4141/P01-172

Mann DL, Nelson JG (1980) Ideology and wildlands management: The case of Rondeau Provincial Park, Ontario. Environ Manage 4:111–124. https://doi.org/10.1007/BF01866508

Marcaccio JV, Markle CE, Chow-Fraser P (2016) Use of fixed-wing and multi-rotor unmanned aerial vehicles to map dynamic changes in a freshwater marsh. J Unmanned Veh Syst 4:193–202. https://doi.org/10.1139/juvs-2015-0016

Markle CE, Chow-Fraser P (2018) Effects of European common reed on Blanding's turtle spatial ecology. J Wildl Manag 82:857–864. https://doi.org/10.1002/jwmg.21435

Marks M, Lapin B, Randall J (1994) *Phragmites australis* (*P. communis*): threats, management and monitoring. Nat Areas J 14:285–294

McNabb CD, Batterson TR (1991) Occurrence of the common reed, *Phragmites australis*, along roadsides in Lower Michigan. Mich Acad USA 23:211– 220

Meyerson LA, Saltonstall K, Windham L, et al (2000) A comparison of *Phragmites australis* in freshwater and brackish marsh environments in North America. Wetl Ecol Manag 8:89–103. https://doi.org/10.1023/A:1008432200133

Ministry of Natural Resources and Forestry (2019) Invasive *Phragmites* Control at Long Point Region and Rondeau Provincial Park Implementation Plan - 2019. Ministry of Natural Resources and Forestry, Ministry of Environment, Conservation and Park, Canadian Wildlife Service

Nikolakopoulos K, Oikonomidis D (2015) Quality assessment of ten fusion techniques applied on Worldview-2. Eur J Remote Sens 48:141–167. https://doi.org/10.5721/EuJRS20154809

Phillips RL, Beeri O, DeKeyser ES (2005) Remote wetland assessment for Missouri Coteau prairie glacial basins. Wetlands 25:335–349. https://doi.org/10.1672/10

Poulin B, Davranche A, Lefebvre G (2010) Ecological assessment of *Phragmites australis* wetlands using multi-season SPOT-5 scenes. Remote Sens Environ 114:1602–1609. https://doi.org/10.1016/j.rse.2010.02.014

Rodríguez M, Brisson J (2015) Pollutant removal efficiency of native versus exotic common reed (*Phragmites australis*) in North American treatment wetlands. Ecol Eng 74:364–370. https://doi.org/10.1016/j.ecoleng.2014.11.005

Rupasinghe P, Markle C, Marcaccio J, Chow-Fraser P (2017) Determination of treatment effectiveness of *Phragmites autralis* at Rondeau Bay Provincial Park, ON. In: Proceedings of CASIOPA. Georgian Bay Hotel & Conference Centre, Collingwood, ON, p 24

Rupasinghe PA, Chow-Fraser P (2019) Identification of most spectrally distinguishable phenological stage of invasive *Phramites australis* in Lake Erie wetlands (Canada)

for accurate mapping using multispectral satellite imagery. Wetl Ecol Manag 27:513–538. https://doi.org/10.1007/s11273-019-09675-2

Rutchey K, Vilchek L (1999) Air photointerpretation and satellite imagery analysis techniques for mapping cattail coverage in a northern Everglades impoundment. Photogramm Eng Remote Sens 65:185–191

Saltonstall K (2002) Cryptic invasion by a non-native genotype of the common reed, P*hragmites australis*, into North America. Proc Natl Acad Sci 99:2445–2449. https://doi.org/10.1073/pnas.032477999

Satellite Image Corporation (2017a) WorldView-3 Satellite Sensor. https://www.satimagingcorp.com/satellite-sensors/worldview-3/. Accessed 2 Mar 2020

Sawaya KE, Olmanson LG, Heinert NJ, et al (2003) Extending satellite remote sensing to local scales: land and water resource monitoring using high-resolution imagery. Remote Sens Environ 88:144–156. https://doi.org/10.1016/j.rse.2003.04.006

Schmidt KS, Skidmore AK (2001) Exploring spectral discrimination of grass species in African rangelands. Int J Remote Sens 22:3421–3434. https://doi.org/10.1080/01431160152609245

SenseFly (2020b) senseFly - eBee Classic. In: senseFly. https://www.sensefly.com/homepage/ebee-small. Accessed 18 Apr 2020

SenseFly (2020) senseFly - Parrot Sequoia+. In: senseFly. https://www.sensefly.com/camera/parrot-sequoia. Accessed 18 Apr 2020

Taddeo S, Blois SD (2012) Coexistence of introduced and native common reed (*Phragmites australis*) in freshwater wetlands. Écoscience 19:99–105. https://doi.org/10.2980/19-2-3468

Uddin MN, Robinson RW, Caridi D, Al Harun MAY (2014) Suppression of native *Melaleuca ericifolia* by the invasive *Phragmites australis* through allelopathic root exudates. Am J Bot 101:479–487. https://doi.org/10.3732/ajb.1400021

Vretare V, Weisner SE, Strand JA, Granéli W (2001) Phenotypic plasticity in *Phragmites australis* as a functional response to water depth. Aquat Bot 69:127–145. https://doi.org/10.1016/S0304-3770(01)00134-6

Weinstein MP, Balletto JH (1999) Does the common reed, *Phragmites australis*, affect essential fish habitat? Estuaries 22:793–802. https://doi.org/10.2307/1353112

Weisner SEB, Strand JA (1996) Rhizome architecture in *Phragmites australis* in relation to water depth: Implications for within-plant oxygen transport distances. Folia Geobot 31:91–97. https://doi.org/10.1007/BF02803998

Wilcox KL, Petrie SA, Maynard LA, Meyer SW (2003) Historical distribution and abundance of *Phragmites australis* at long point, Lake Erie, Ontario. J Gt Lakes Res 29:664–680. https://doi.org/DOI: 10.1016/S0380-1330(03)70469-9

Williams AEP, Hunt Jr ER (2004) Accuracy assessment for detection of leafy spurge with hyperspectral imagery. Rangel Ecol Manag 57:106–112. https://doi.org/10.2111/1551-5028(2004)057[0106:AAFDOL]2.0.CO;2

Williams AP, Hunt Jr ER (2002) Estimation of leafy spurge cover from hyperspectral imagery using mixture tuned matched filtering. Remote Sens Environ 82:446–456. https://doi.org/10.1016/S0034-4257(02)00061-5

Yuckin S, Rooney R (2019) Significant Increase in Nutrient Stocks Following *Phragmites australis* Invasion of Freshwater Meadow Marsh but Not of Cattail Marsh. Front Environ Sci 7:. https://doi.org/10.3389/fenvs.2019.00112

Table 3.1 Overall, *Phragmites* users' and producers' accuracy for different combinations of WV2/3 and S2 images and SVM and ML classification methods.

		WV3		**S 2**	
Site	Classification Accuracy	**SVM**	**ML**	**SVM**	**ML**
BCNWA and CM	Overall Accuracy %	69.75	**93.08**	**74.68**	72.15
	Kappa	0.6162	**0.9062**	**0.6832**	0.6467
	Phragmites producers' Accuracy %	95.07	**92.72**	**76.32**	79.82
	Phragmites Users' accuracy %	41.77	**89.29**	**85.29**	79.13
		WV2		**S2**	
		SVM	**ML**	**SVM**	**ML**
RBM	Overall Accuracy %	75.77	**86.37**	**74.25**	70.86
	Kappa	0.6869	**0.8220**	**0.6927**	0.6503
	Phragmites producers' Accuracy %	95.14	**88.43**	**79.17**	48.57
	Phragmites Users' accuracy %	61.94	**84.29**	**69.09**	70.15

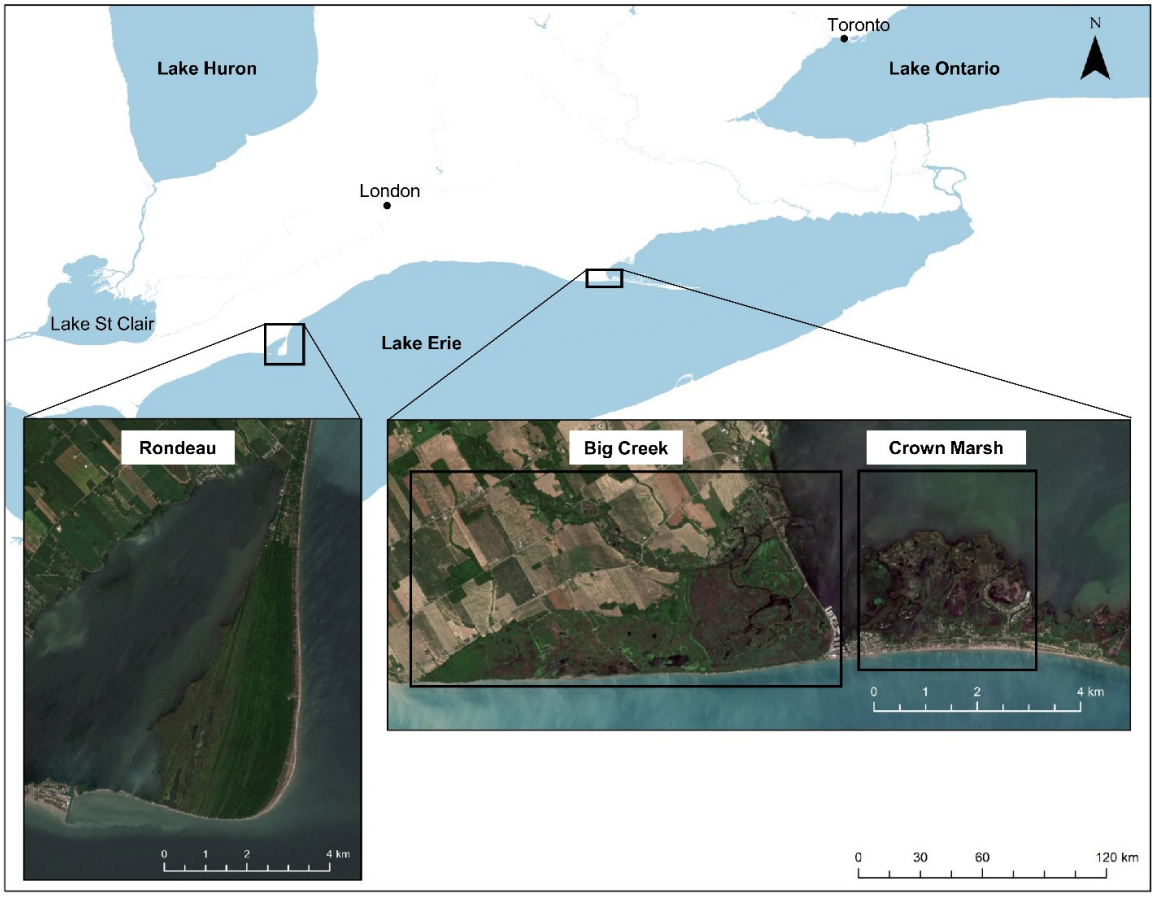

Fig 3.1 Map of the study sites located in the north shore of Lake Erie

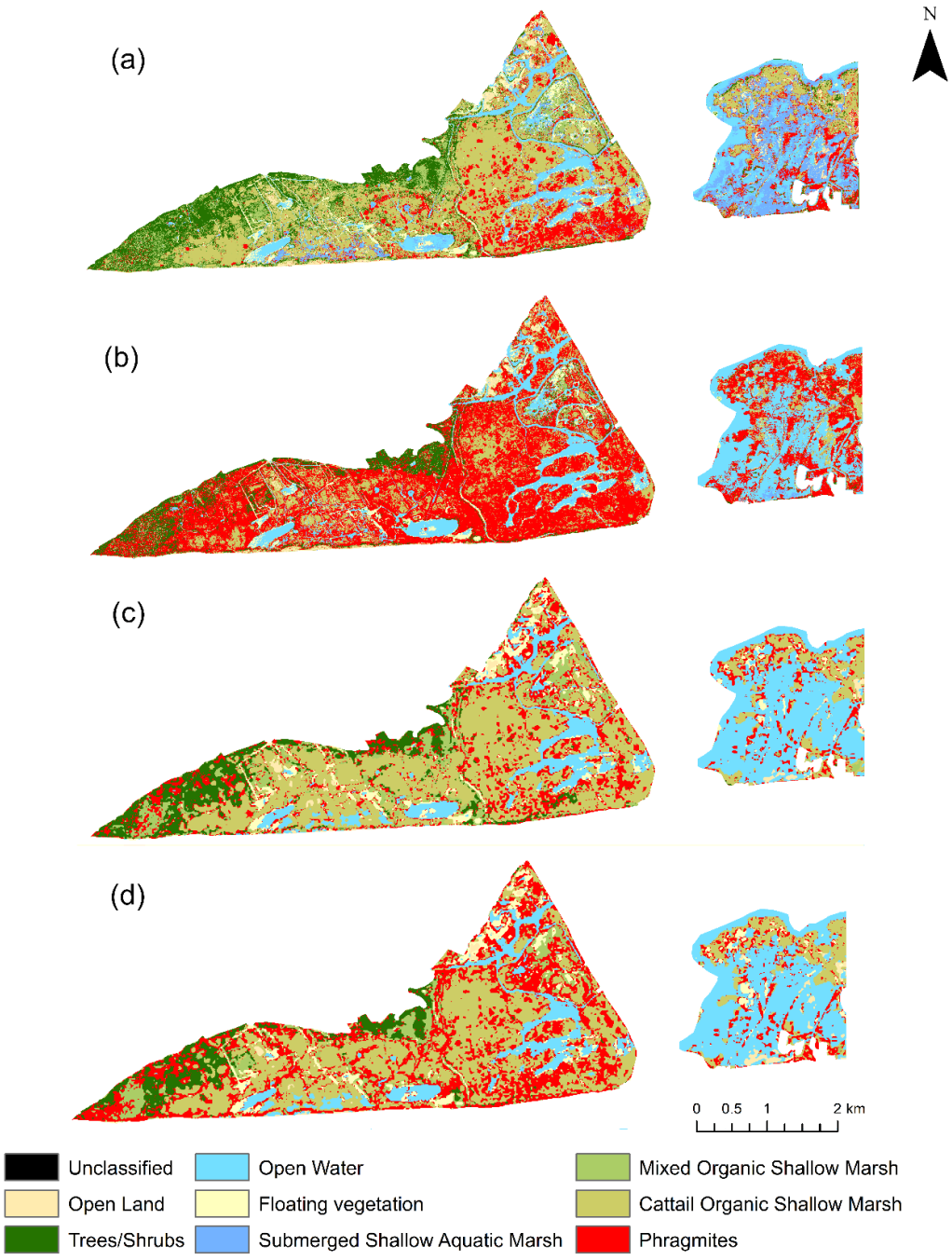

Fig 3.2 Classified images of BCNWA and CM sites with (a) WV3 images-ML classification, (b) WV3 images -SVM classification, (c) S2 images-ML classification (d) S2 images-SVM classification

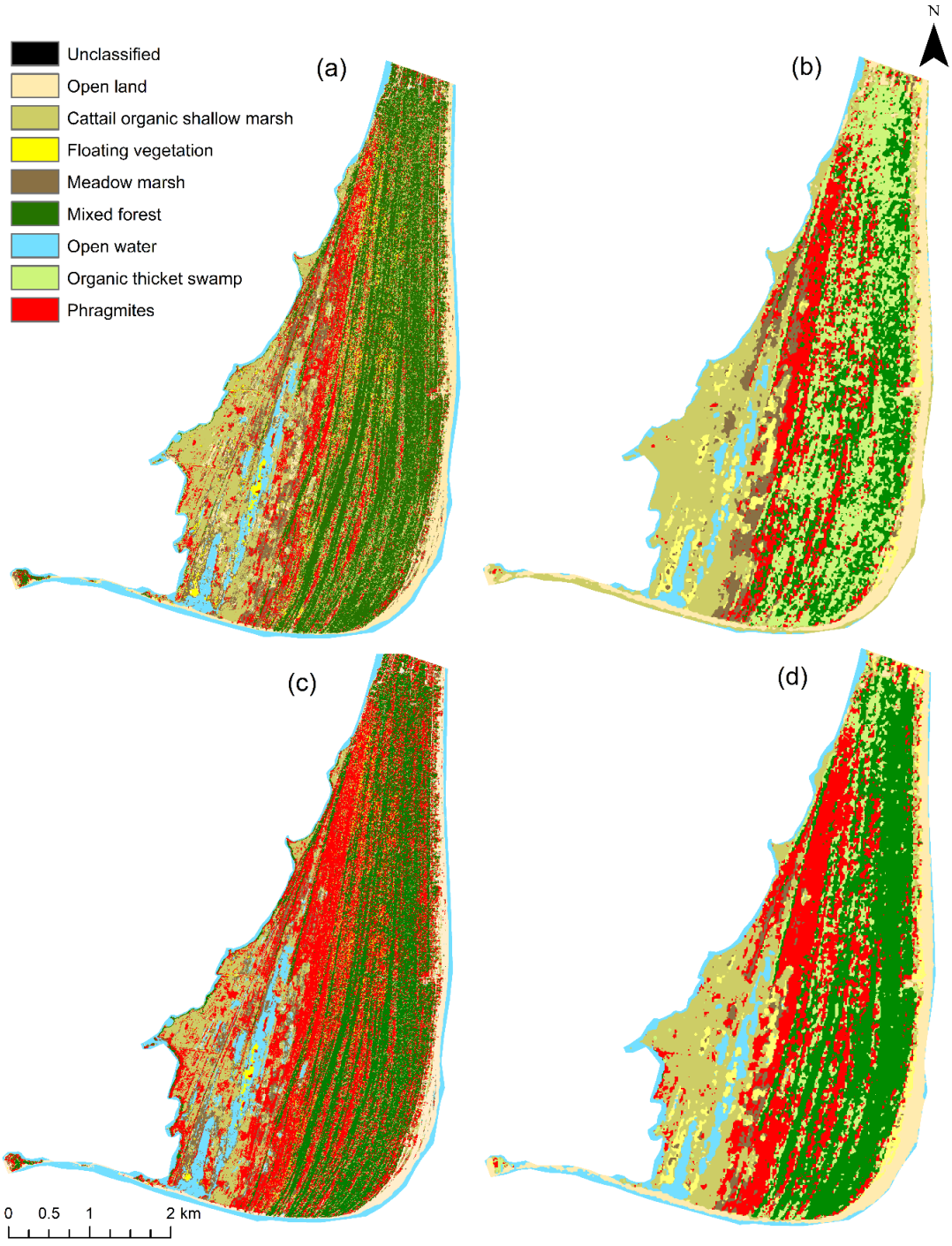

Fig 3.3 Classified images of RBM site with (a) WV2 images-ML classification (b) S2 images-ML classification (c) WV2 images-SVM classification (d) S2 images-SVM classification

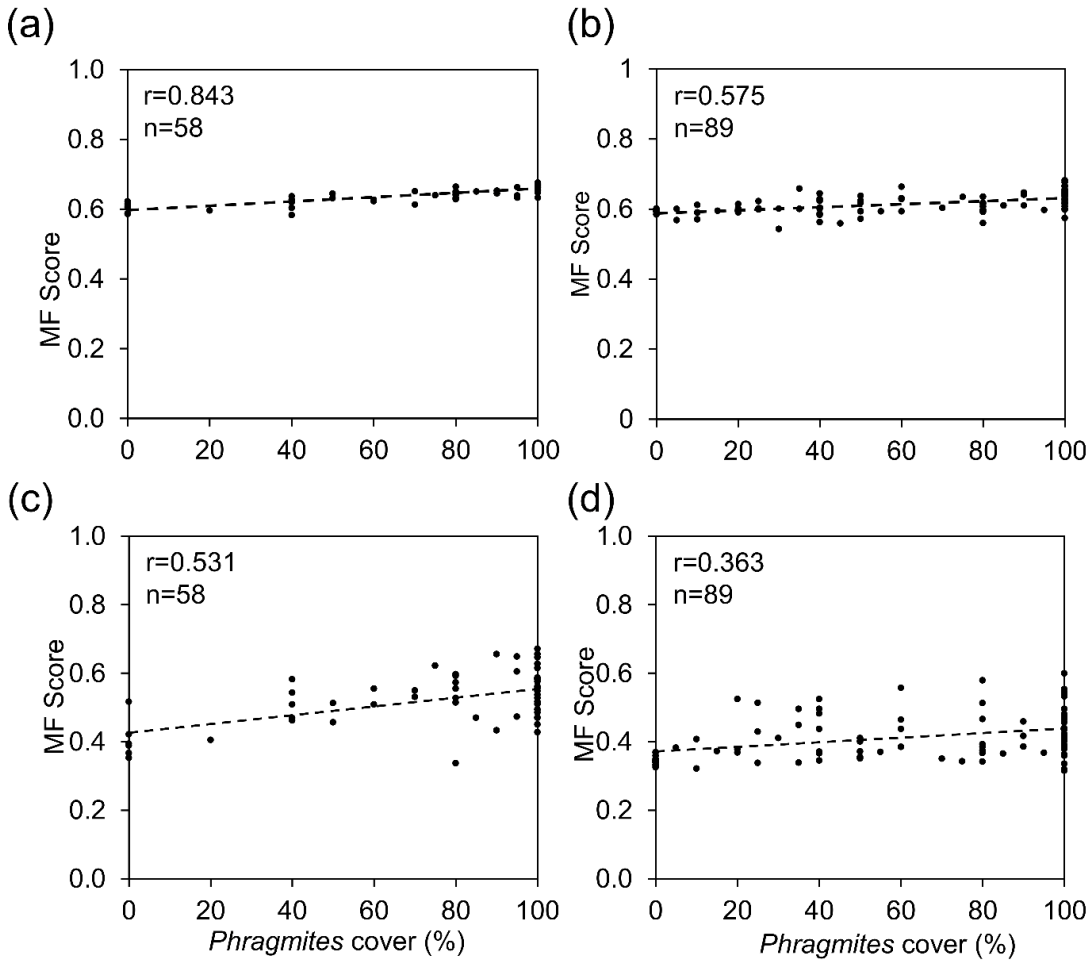

Fig 3.4 Linear regression plots of MF scores versus *Phragmites* percent cover associated with WV3 images for (a) BCNWA and (b) CM sites; corresponding regression plots associated with S2 images for (c) BCNWA and (d) CM sites

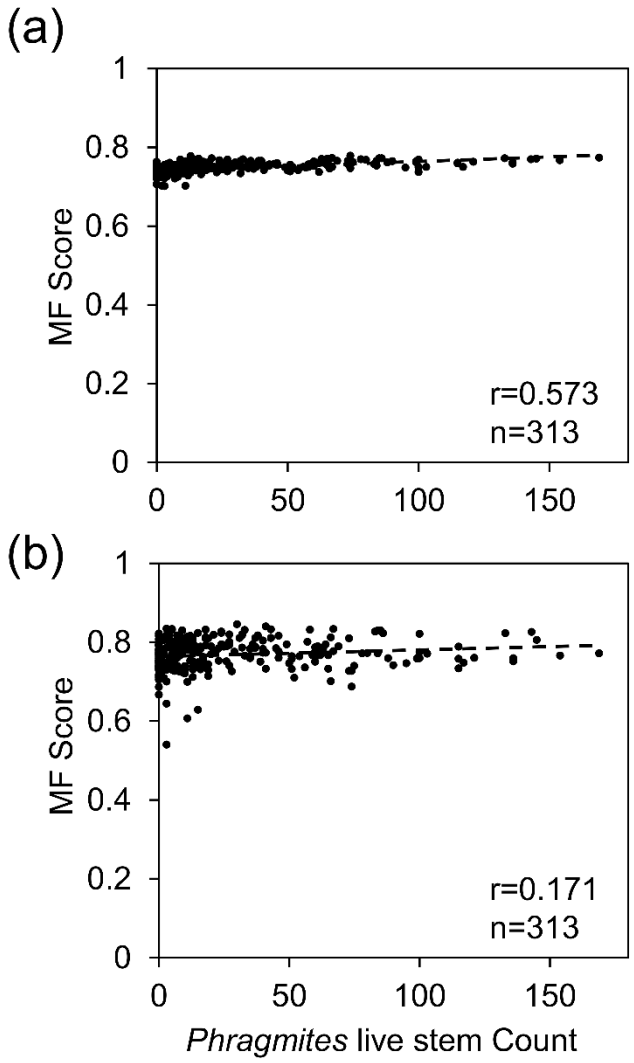

Fig 3.5 Linear regression plots of MF scores versus *Phragmites* stem counts obtained with (a) WV2 and (b) S2 images for the RBM site

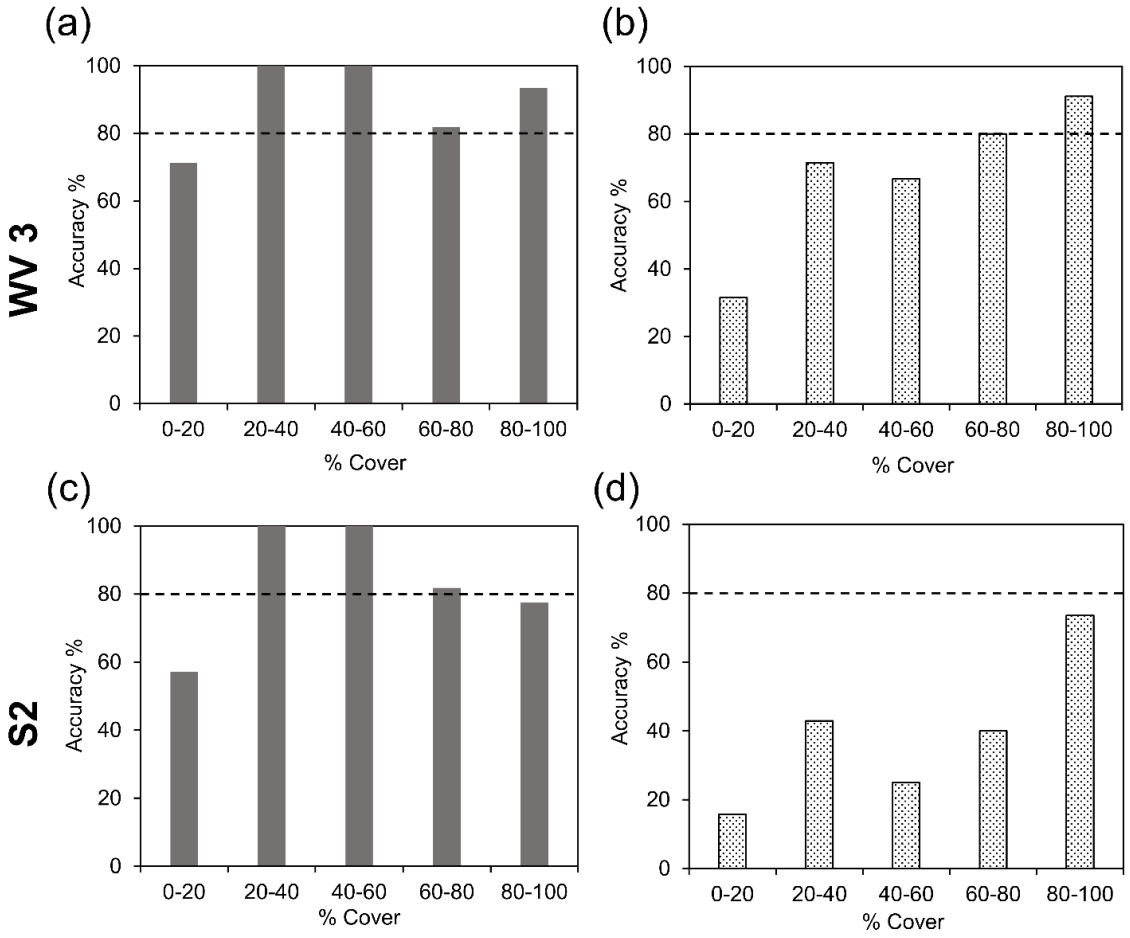

Fig 3.6 Comparison of mapping accuracies for *Phragmites* in five density categories for BCNWA (solid bars) and CM (stippled bars) using ML classification with WV3 (top panels) and S2 images (bottom panels)

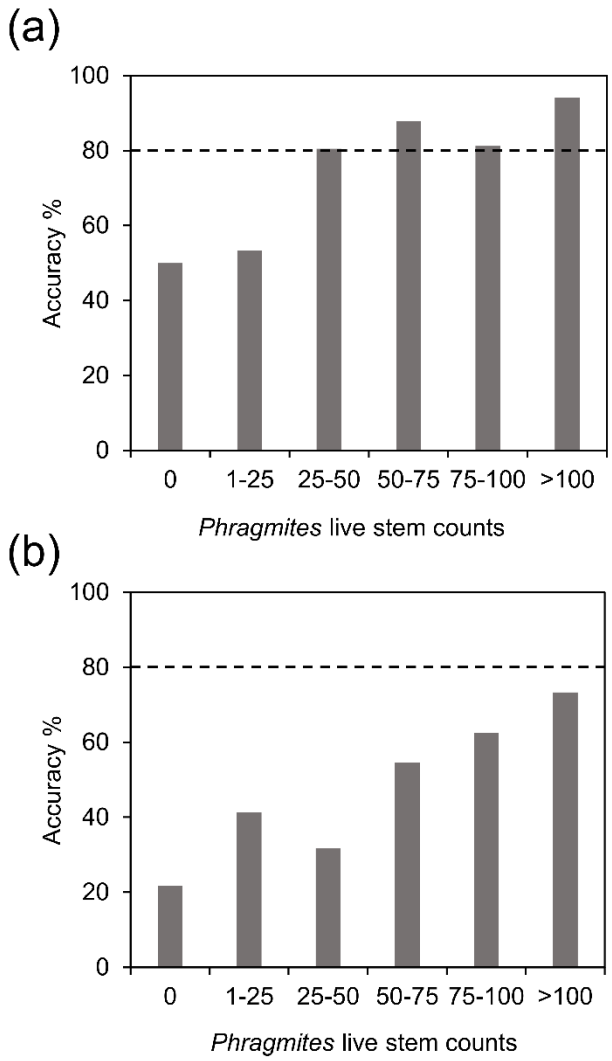

Fig 3.7 Mapping accuracies of live *Phragmites* in six stem count categories for the RBM site using (a) WV2 image-ML classification and (b) S2 image-SVM classification

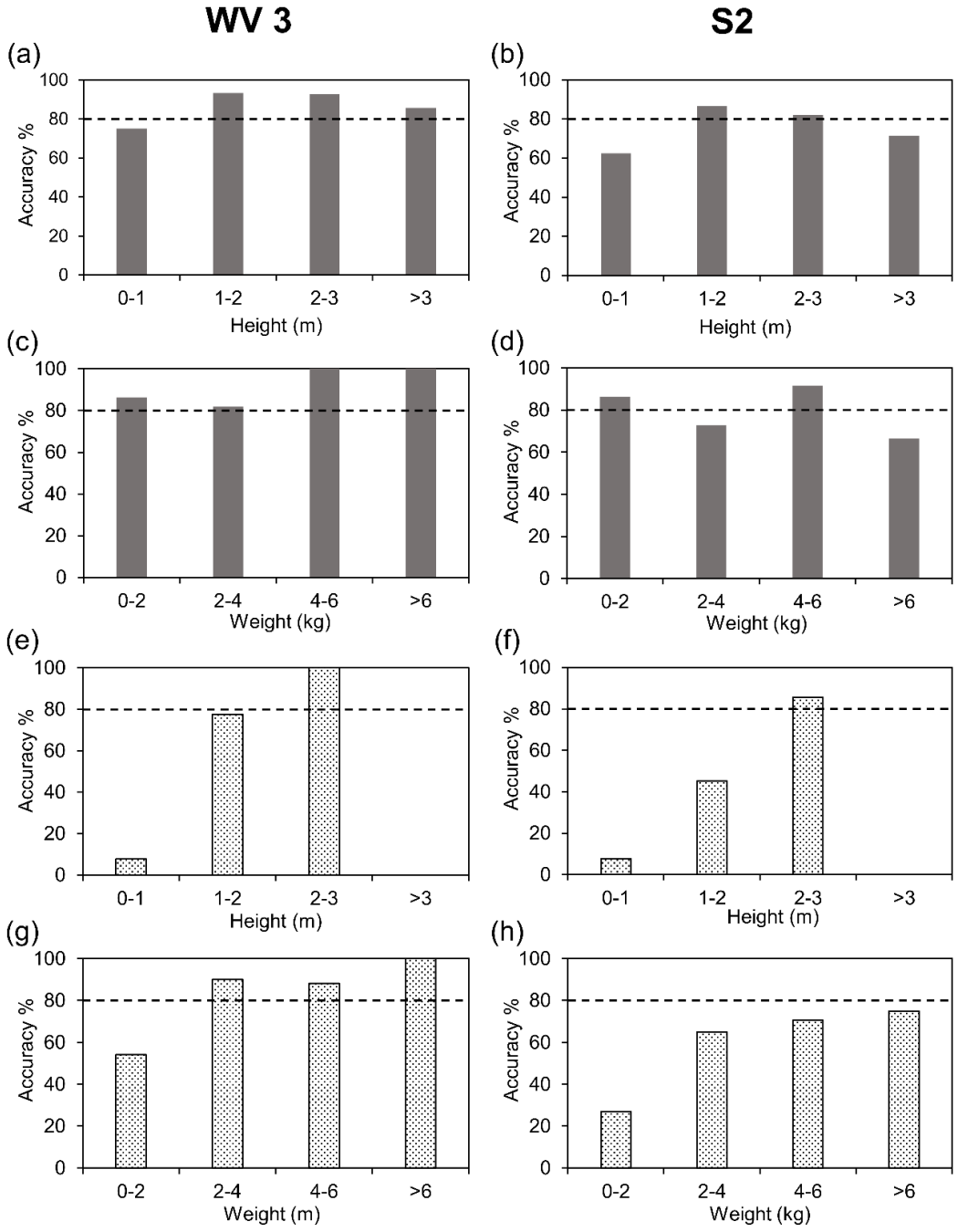

Fig 3.8 Mapping accuracies of height and weight of *Phragmites* for BCNWA (solid bars) and CM (stippled bars) using WV3 (all left panels) and S2 (all right panels). (Note: no data for >3 m height category in CM site)

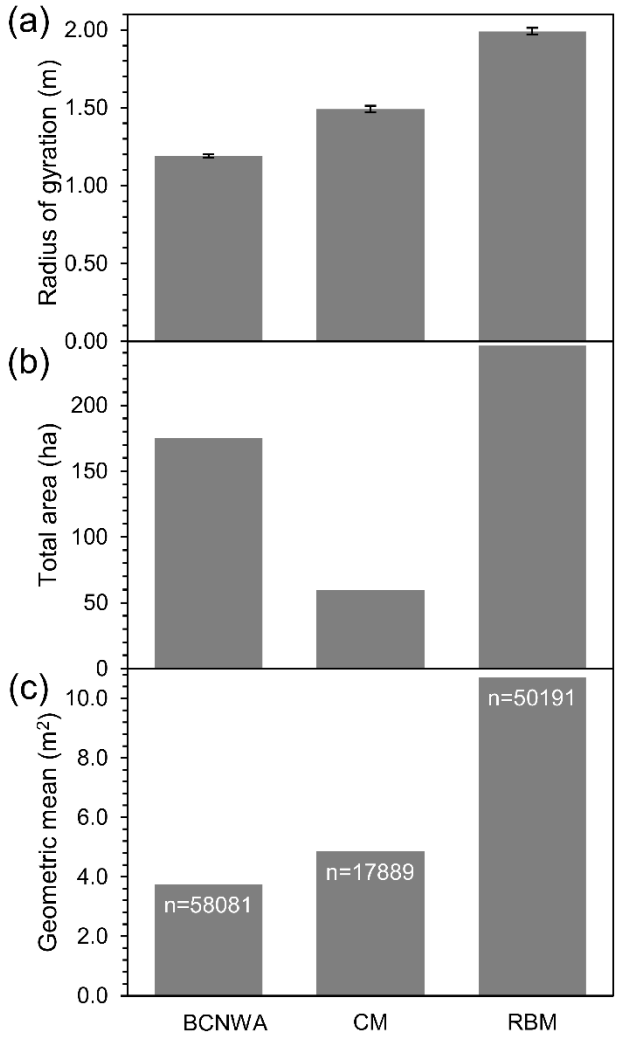

Fig 3.9 Comparison of (a) mean Radius of Gyration, (b) mean total area occupied by *Phragmites* and (c) geometric mean size of *Phragmites* stands in the three wetlands in this study. Data were calculated from classification of WV2/3 images with the ML classification

Chapter 4. Relating pre-fire canopy species and proximity to water features to burn severity of boreal wildfires in northern Alberta, Canada

By,

Prabha Amali Rupasinghe and Patricia Chow-Fraser

Rupasinghe, P. A., & Chow-Fraser, P. (2021). Relating pre-fire canopy species and proximity to water features to burn severity of boreal wildfires in northern Alberta, Canada. *Forest Ecology and Management*. *Under review, manuscript number* FORECO-D-21-00141

4.1. Abstract

Increased global temperature, drought, and extreme weather have increased the frequency and intensity of wildfires in Canadian Boreal forests. We examined how burn severity was related to canopy species composition and proximity to water in six large boreal forest stands across northern Alberta (two in the Bistcho Lake region, three in Wood Buffalo National park, and one in the Richardson backcountry) and a smaller stand close to the town of Slave Lake (204 - 5217 km^2). We used Landsat 5, 7, and 8 satellite images that included two phenological stages (spring, summer, or fall), followed by Support Vector Machines (SVM) classification to map the distribution of pre-fire canopy species. To quantify the burn severity of each fire, we used the Landsat images to calculate the differenced Normalized Burn Ratio (dNBR); we then combined dNBR for all affected areas to develop the Standardized Burn Impact Score (SBIS), that quantifies the average impact of each fire based on the size of the burned area and the mean burn severity per pixel. In general, pre-fire dominance of coniferous species (jack pine and spruce) led to higher SBIS values while pre-fire dominance of broad-leaved species (aspen, birch, and poplar) led to lower values. Mean burn severity and SBIS values increased when fire outbreaks occurred at a distance of 1 km or greater from water features (e.g. lakes, rivers, streams, wetlands). By integrating burn impact over very large temporal and spatial scales, we have confirmed the general influence of pre-fire canopy species on burn severity, and the ameliorating effect of water features on fire behavior at the landscape level.

Keywords: Boreal forests, Remote sensing, Wildfire, canopy species mapping, Landsat

Highlights

- Pre-fire species composition and distance to water features affect burn severity.
- Deciduous species reduce the wildfire potential while coniferous species enhance.
- Water features reduce wildfire potential and burn impact.
- Remote sensing provides useful methods to study wildfire behavior in large areas.

4.2. Introduction

Boreal forests are wilderness areas in northern circumpolar regions, where freezing temperatures occur for 6 to 8 months of the year (Mery et al., 2010). This biome encompasses ~30% of the global forested area and occurs in the northernmost regions of Canada, Russia, and the United States (Gauthier et al., 2015). They contain more surface freshwater than any other biome in the world (Mery et al., 2010). They store approximately 66% of the world's carbon in the soil, peat, and permafrost deposits and therefore, play a major role in global carbon cycling (Kasischke et al., 1995; Pan et al., 2011). They are also involved in global climate regulation through energy and water exchange (Steffen et al., 2015). Boreal forests also provide great societal value by supporting fishing, hunting, leisure or spiritual pursuits, and economic opportunities to many rural communities as well as indigenous people throughout the world (Gauthier et al., 2015).

Boreal forests usually have low plant diversity with dominant gymnosperms such as white and black spruce, jack pine, balsam and douglas fir, and tamarack and varying proportions of angiosperms such as trembling aspen, balsam poplar, and white birch (Alberta Forest service, 1985; Mery et al., 2010; Shorohova et al., 2011). The canopy

species are capable of reaching a minimum height of 5 m with a canopy cover of 10% (Gauthier et al., 2015). These forests are adapted to short, hot growing seasons, and long winters with extreme weather conditions (Matsuura, 2010). Furthermore, these forests are characterized by various disturbances including wildfire, insect infestations, and windthrow hazards, which are essential processes that maintain the structure and diversity of boreal forests (Gauthier et al., 2015).

Wildfire is considered the most widespread disturbances in boreal forests that shape their structure, composition, and function, as well as influence rates and processes of ecological succession and encroachment (Lentile et al., 2006). Major factors that affect fire activity include availability and type of fuel, ignition agents, topography, and human activities, and climate conditions (Johnson et al., 2001; Schoennagel et al., 2004). Flannigan *et al.* (2005) suggested that climate change can increase the area burned, the length of the fire season, the intensity as well as the severity of the fire; they predicted that the amount of burned area in Canada may increase by 74 to 118% by the end of the century. Given the importance of boreal forests, there is an urgent need to understand how specific factors contribute to the frequency and severity of wildfires and to monitor how boreal forests are responding to adverse effects of climate change (Chu & Guo, 2014).

Severity and impact of wildfire in remote locations are determined by a number of pre-fire conditions such as the distribution of pre-fire canopy species, local topography, fire weather, and fuel load and structure (Boucher et al., 2017; Krawchuk et al., 2016; Lydersen et al., 2017; Whitman et al., 2018). These factors are challenging to study because they require examination of multiple fire outbreaks occurring over large temporal

and spatial scales that preclude the use of field studies. Even if logistical challenges can be overcome, severe fires can completely remove all traces of vegetation present before the fire. Therefore, remote sensing provides the best and most cost-effective means to understand fire behavior and pre-fire conditions over larger spatial scales (Akther and Hassan, 2011; Hall et al., 2008; Whitman et al., 2018).

Multispectral remote sensing is widely used to map burn severity in North America (Barrett et al., 2011; Hall et al., 2008; Murphy et al., 2008; Whitman et al., 2018). Differenced Normalized Burn Ratio (dNBR) (Key and Benson, 2005), Relativized dNBR (RdNBR) (Miller and Thode, 2007), and Relativized Burn Ratio (RBR) (Parks et al., 2014) are some of the common indices used to map burn severity. Besides mapping burn severity, remote sensing has also been used to map post-fire changes in landcover and vegetation recovery processes following fire outbreaks (Cumming 2001; Hammill and Bradstock 2006; Hall *et al.* 2008; Chu and Guo 2014; Chu *et al.* 2016; Fernández-García *et al.* 2018). By comparison, the use of remote sensing to examine pre-fire conditions is attempted less, especially for fires occurring in remote areas where there are no ground truth data prior to the fire.

Wildfires in boreal forests of northern Alberta have been large and frequent in recent decades (Stocks et al., 2002), and a warming climate has been implicated as an important driver (Flannigan et al., 2009). Other variables such as the pre-fire composition of canopy species and proximity to water features (e.g. rivers, streams, lakes, wetlands) may influence burn severity at the stand level that could be important for managing wildlife habitat and for understanding fire behavior. Given that human activities

generally resulted in a decrease in wildfire activity between 1980 and 2010 in Alberta's boreal forests (Robinne et al. 2016), studies should differentiate between remote wildfires and those located near human settlements.

The primary objective of this study was to use remote sensing to quantify the effects of pre-fire canopy species composition and proximity of water features on burn severity of multiple fire outbreaks occurring in boreal forests of northern Alberta. To minimize the variation in pre-fire conditions, we included fire events that occurred over an 11-y period between 2004 and 2015, and for which the minimum pre-fire period exceeded two decades. To ensure our results have wide applicability, we chose four major areas in northern Alberta that experience a range of human activities from minimal disturbance in a large national park to a forest stand located near a small town. To allow comparison of wildfire activity for each outbreak, we created an index, the Standardized Burn Index Score (SBIS) that quantifies the average impact of each fire based on the size of the burned area and the mean burn severity per pixel. Overall, our goal was to provide a simple, cost-effective technique to quantify burn impact and fire behavior to investigate changes in fire regimes over large spatial and temporal scales.

4.3. Methods

4.3.1. Study sites

Our largest site is Wood Buffalo National Park (WB), Canada's largest National Park, and also one of the largest in the world (Lat 58.943 Lon -112.788; Fig. 4.1; Parks Canada 2020). The Park covers 44, 807 km^2 area in total and is characterized by large, undisturbed grass and sedge meadows, wetlands and prairie, and boreal forests (UNESCO World Heritage Center, 2020). This park is very remote and is subject to minimal anthropogenic stress, except for flow regulation, water withdrawal, industrial discharge,

and effects of climate change, which originate from outside the park (UNESCO World Heritage Center, 2020). The Richardson (RC) Wildland Provincial Park is located 150 km southeast of WB National Park (Lat 57.999 Lon -111.141; Fig. 4.1), and is part of the largest sand dune complex in Canada, with paleo-parabolic dunes and riparian areas along the Athabasca River, and boreal forests (Alberta Parks 2018). Bistcho Lake (BL) is located in northwestern Alberta (Lat 59.672, Lon -119.143; Fig. 4.1), and is characterized by wetlands, including *Sphagnum* peat bogs, channel fens, and large tracts of mixed wood boreal forests (Alberta Wilderness Association 2020). Other than wildfires, this area has been disturbed by clear-cut logging and extensive petroleum and natural gas exploration for many years. Whereas only 22% of the Richardson area is disturbed by human activities, 61% of the Bitscho Lake area is anthropogenically disturbed with linear features (Canadian Parks and Wilderness Society Northern Alberta, 2016). The last study site is the Lesser Slave Lake region (LSL), located in the central part of Alberta, about 250 km northwest of the city of Edmonton (1.43 million as of 2019). The LSL fire occurred close to the Town of Slave Lake, near oil, gas, and forestry operations. In addition to the forest fire, 56 properties in the outskirts and one-third of the town were destroyed by this fire (Botey and Kulig, 2014).

In total, we studied seven fire outbreaks: two at BL, three in WB national park, one each in the RC and LSL region. All fire outbreaks occurred after 2004, during the summer months. The burned areas varied from 204 to 5217 km^2. There were multiple fire-years in BL (2004 and 2012) and WB (2007, 2012, and 2015 in WB) whereas both RC and LSL were single fire outbreaks that occurred in 2011 (Table 4.1).

4.3.2. Image data

We used Landsat 5, 7, and 8 multispectral images for burn-severity calculation and species mapping. Landsat is owned by the United States Geological Survey (USGS) and the National Aeronautics and Space Administration (NASA) and is the longest earth observing satellite series. Landsat 5 operated from March 1984 to January 2013. For this study, we used six bands of Landsat 5 Thematic Mapper (TM): blue (0.45-0.52 μm), green (0.52-0.60 μm), red (0.63-0.69 μm), two Near-Infrared (NIR) bands (0.76-0.90 and 0.76-0.90 μm), and Mid-Infrared (2.08-2.35 μm) (USGS, 2016a). Landsat 7 was launched in April 1999 and is still functioning. We used seven bands of Landsat 7: blue (0.45-0.52 μm), green (0.52-0.60 μm), red (0.63-0.69 μm), two NIR (0.77-0.90 and 1.55-1.75 μm), and Mid-Infrared (2.08-2.35 μm) (USGS, 2016b). Landsat 8 is the newest satellite of the series which was launched in February 2013. We used seven bands of Landsat 8 Operations Land Imager (OLI): coastal aerosols (0.43-0.45 μm), blue (0.45-0.51 μm), green (0.53-0.59 μm), red (0.64-0.67 μm), NIR (0.85-0.88 μm), and two Shortwave Infrared (SWIR) bands (1.57-1.65 and 2.11-2.29 μm). All images have a 30-m spatial resolution.

We downloaded summertime cloud-free images, or those with minimum cloud cover from Earth Explorer to map burn severity (Table 4.2). Whenever possible, we selected images acquired in late July and early August; however, if cloud-free images were unavailable during the preferred time, we used images as early as June and as late as September. For species mapping, we downloaded additional images either acquired in spring or fall (further explained in section 2.4). For the Landsat 7 images, we used an

additional image acquired as close as possible in date to the first image to fill data gaps caused by a sensor-borne error. We used ENVI 5.5 (Harris Geospatial Solutions) to preprocess and process reflectance values in our images. We performed radiometric correction and atmospheric correction (ENVI FLAASH) and masked clouds, shadows cast by clouds, and thick haze in the images.

4.3.3. Mapping burn severity

We calculated the differenced Normalized Burn Ratio (dNBR; equations 4.1 and 4.2) to map burn severity (Key and Benson, 2005) using the preprocessed Landsat images collected before and after the fire outbreak (Table 4.1).

$$NBR = \frac{(NIR - SWIR)}{(NIR + SWIR)} \quad [4.1]$$

$$NBR = NBR_{prefire} - NBR_{postfire} \quad [4.2]$$

Where NIR and SWIR are the corresponding image bands and the $NBR_{prefire}$ and $NBR_{postfire}$ are the corresponding NBR calculated for images acquired before and after the fire event. The dNBR values were imported into ArcMap 10.4.1 and these were classified into burn-severity classes according to guidelines in Table 4.3. We used the shapefiles of the burn footprint available from the National Wildfire Database (NFDB)(Natural Resources Canada, 2017) to determine the size and the borders of the burned area for each fire outbreak.

4.3.4. Mapping canopy species distribution

4.3.4.1. Ground reference data

To map the distribution of canopy species before the fire event, we used ground reference data from Phase 3 of the forest inventory monochrome maps created by Alberta Township Systems (ATS) (Alberta Government, 2019). In total, three forest inventories were conducted in Alberta; Phase 1 included most of the publicly owned forested lands, while Phase 2 covered lands with commercial timber commitments. Phase 3 is the most recent inventory that was initiated in 1970 and was completed in 1984. It covered both forests on publicly owned lands as well as areas of active timber harvesting (Alberta Forest service, 1985) and included greater detail on canopy species. Data for these maps were derived from aerial photographs and were combined with field data that documented stand volumes and growth estimations. Photointerpretation was conducted manually (minimum stand size of 2 ha) and included species composition (based on ground surveys), crown density, height, date of stand origin, site index class, and coniferous commercialism class (Alberta Forest service, 1985).

We first digitized the species locations from the monochrome maps using ArcGIS. For this step, we used locations that had been affected by fire outbreaks as well as the unaffected areas between 1985 to 2017. We avoided using mixed-species locations, and only used locations corresponding to a single species. The forest inventory data did not cover the northernmost part of Alberta entirely, therefore we only had ground reference partially for WB and BL burned areas. In that case, we used more species locations from neighboring regions as ground references and used them in image classification and

validation. We used 70% of the digitized ground-truth locations for image classification and saved the remaining 30% for accuracy assessment.

4.3.4.2. Image classification

The Landsat images collected in two seasons, either spring and summer, fall and summer, or spring and fall, were stacked together as one image prior to image classification (see Table 4.4). We followed the methods developed by Liu *et al.* (2002) and used the Support Vector Machines (SVM) in ENVI 5.5 to classify images. Using this procedure, we produced classified images beginning in 1985 until each fire outbreak in our study. We combined the dominant deciduous species (aspen, birch, and poplar) into one class because our classification was unable to accurately discriminate among these species. We were also unable to discriminate between white and black spruce and combined them into a single class to improve classification accuracy. Our final classification scheme included three taxon classes and two non-vegetated classes: deciduous (aspen, birch, or poplar), spruce (black or white), jack pine, water, and unvegetated area. After obtaining a satisfactory level of classification accuracy for 1985, we used the same Regions Of Interest (ROIs) to classify the images collected before the fire outbreak, and for every year we carefully checked the ROIs and excluded them if they were located within clouds, shadows of clouds, clear cuts, or areas that appeared to have been disturbed. Given that our study sites had minimal human disturbance, we assumed that the forest canopy species composition in the ground reference locations did not change between 1985/1986 up to the fire year unless there was a visible physical

disturbance. After the image classification, we applied a 3 by 3 majority filter to smooth out the classified images.

4.3.5. Standardized Burn Impact Score (SBIS)

We developed SBIS to characterize the impact of each fire outbreak using the equation below.

$$SBIS = Average\ dNBR\ per\ km^2 \times Total\ area\ burned\ (km^2) \quad [4.3]$$

For each fire outbreak, we extracted dNBR values for all the pixels within the burned area and calculated the average dNBR values to be used in the equation. We calculated the total burned area using the burned area shapefiles downloaded from Natural Resources Canada (2017). We calculated this score for each of the 21 fire outbreaks within the study locations.

4.3.6. Pre-fire species composition data analysis

Following the image classification, we conducted the further analysis in ArcMap 10.4.1. We clipped the classified maps with the fire footprint (Natural Resources Canada, 2017) and intersected it with the reclassified dNBR maps to combine pre-fire canopy species distribution with the burn severity levels (section 2.3). Then we calculated the area of each taxon class and used these area values for further statistical analysis.

Then we extracted the species composition within 21 smaller fire events regardless of the burn severity category and analyzed the relationship between species composition and dNBR and SBIS using regression analysis. We conducted all analyses with Microsoft (MS) Excel, Minitab 19, or JMP 15 software.

4.3.7. Burn severity and impact in relation to proximity to water features

We extracted the water features from classified maps (section 2.4.2) and modified these visually to minimize the classification errors using ArcGIS to investigate the effect of water features such as rivers, lakes, and ponds on the burn severity. We created multiple ring buffers around water features at 50, 100, 150, 200, 250, 500, 1000, 1500, and 2000 m intervals. Then we extracted the dNBR values within each of the buffers for 21 smaller fire outbreaks. We calculated average dNBR and SBIS for all fire events and regressed these values against proximity to water features.

4.4. Results

4.4.1. Burn severity and Impact

Burn severity and areal extent of the fire for the seven site-events varied greatly (Fig. 4.2). The RC fire in 2011 was the largest, burning a total area of 4942.0 km^2 according to our assessment using dNBR for the affected area (5217 km^2) recorded by the NFDB. This was followed by the WB fire in 2015, which burned a total of 2871.06 km^2; the entire affected area recorded by the NFDB was burned (Figures 4.2 a and b). Although the LSL fire was the smallest, with only 154.01 km^2 burned out of the recorded area of 203.63 km^2 (Figure 4.2b), it had a disproportionately large area with high burn severity (45.24%; Fig. 4.2c). The BL 2004 fire had the second-largest percentage area of high burn severity, given the total burned area reported in the NFDB (37.38%; Figure 4.2c). The WB 2007 fire burned with the lowest severity, with only 0.32% of the total area associated with high burn severity while 54.58% was associated with low burn severity (Fig. 4.2c). Overall, most locations experienced moderate-high and high severity

burns except for the WB 2007 and 2012 fires, which had low and moderate-low severity fires in the majority of the burned area. When the total affected area recorded by the NFDB is considered, LSL and WB 2007 site-events had more unburned than burned areas according to our approach of burn mapping using dNBR. When average dNBR for the site-events are considered, WB 2007 fire had the lowest dNBR value (0.073), followed by the LSL fire (0.157). By contrast, the highest average dNBR was for the BL 2004 fire (0.643). However, when the total affected area is combined with the dNBR through SBIS, the least burn impact was on the LSL fire (35,496.03), followed by the WB 2007 fire (58,856.68). The highest burn impact was for the RC fire (2,029,980.823).

4.4.2. Burn severity and pre-fire species distribution

In majority of cases, we obtained greater than 75% overall accuracy and for canopy species alone (Table 4.5). The use of two seasons' images improved mapping accuracy by about 20% over than when single images were used; however, since there were a limited number of cloud-free images over two seasons in the same year, we could not create a continuous time series of species maps from 1985 to the year of the fire outbreak.

In all cases, coniferous species dominated the pre-fire canopy, occupying more than half of the area. RC was the largest burned area (5217.36 km^2), which had a pre-fire composition consisting of >80% jack pine (Fig. 4.2b and 4.3). Areas with low burn severity coincided with areas occupied by the deciduous taxa, accounting for <6% cover and pre-fire unvegetated areas (Fig. 4.3 and 4.4). By contrast, the pre-fire canopy in burned areas at WB during 2007, 2012, and 2015 were dominated by spruce (73, 58%,

and 57% respectively). The WB fires consisted of multiple fire outbreaks, two in 2007, seven in 2012, and six in 2015 (Table 4.1). The pre-fire species in the BL area was also dominated by spruce, which occupied 54% and 76% of the burned areas in 2004 and 2012, respectively (Fig. 4.3 and 4.4); the higher coniferous cover in the latter year may reflect the higher area burned in 2012 (1706 km^2) compared with that in 2004 (1308 km^2) (Fig. 4.2b). The smallest fire in this study occurred near Lesser Slave Lake (LSL), where spruce occupied 59% of the pre-fire canopy (Fig. 4.2b and 4.3).

In general, the burn severity categories appeared to be dependent on the pre-fire species distribution; in areas dominated by aspen, birch, or poplar, burn severity categories remained low or moderate-low, whereas in areas dominated either by spruce or jack pine, burn severity levels reached high or moderate-high categories (Fig. 4.4). We also pooled all sites to statistically test the relationship between burn severity and species distribution of the forest canopy (Fig. 4.5). There was a significant negative relationship when burn severity was regressed against the percentage cover of deciduous taxa in the pre-fire forest stands (Fig. 4.5a; Table 4.6). In contrast, we found a significant positive relationship when burn severity was regressed against the percentage cover of spruce in the pre-fire forest stands (Fig. 4.5b; Table 4.6).

We found a significant positive correlation between burn duration and total burned area ($r=0.62$; $p=0.003$). When average dNBR values were regressed against burn duration, percent cover of deciduous, and percent cover of coniferous species, we did not find any significant relationship (Fig. 4.6 a, b, and c, respectively). By contrast, we found

a significant non-linear relationship between SBIS and burn duration, coniferous species, and the areal cover of deciduous species (Fig. 4.6 d, e, and f, respectively).

4.4.3. Burn severity and impact in relation to proximity to water features

We observed a strong logarithmic relationship between average dNBR and the distance from water features (R^2=0.76, Fig 4.7a). dNBR increased sharply from 0 to 150m, reaching a plateau at 1 km away from water features. When individual fire outbreaks were considered, we found significant relationships for 13 of the 21 fire outbreaks; regression analysis for six of the WB and two of the BL fire outbreaks, however, did not result in any significant relationship.

As we did not observe a change in dNBR after a distance of 1 km, we investigated the relationship between SBIS value and the effect of water features within 1 km of fire outbreaks. We obtained a highly significant linear relationship (R^2=0.9686) between average SBIS for all fire outbreaks and their distance to water features (Fig. 4.7b). When individual fire outbreaks were considered, we obtained highly significant (R^2>0.95) relationships between SBIS and distance to water features for all 21 fires regardless of burn severity.

4.5. Discussion

Wildfires are the main stand-renewing disturbance in boreal forests (Parisien et al., 2005). Fire regimes are variable over both space and time. To understand these dynamic systems, quantification of fire magnitude in terms of both burn severity and impact is essential. Acquiring burn severity data is often challenging in remote regions of northern Alberta due to limited access and the high cost of surveying. This becomes even

more challenging when investigating historical fire outbreaks since the affected areas have been in recovery for many years or even decades. Remote sensing can overcome these challenges and maybe the only viable option in the Canadian boreal region (Boucher et al., 2017; Hall et al., 2008; San-Miguel et al., 2016; Soverel et al., 2010; Whitman et al., 2018).

In this study, we used dNBR, a widely used index of burn severity developed by (Key and Benson, 2005). This index was first developed in 1996 following a wildfire at Glacial National Park, the USA in 1994. More recently, the Composite Burn Index (CBI) was developed to field validate the burn severity index (Key and Benson, 2005). Since then, dNBR has been widely investigated, used with various satellite sensors (eg: Landsat, AVIRIS, MODIS), and calibrated with field measurements (Chuvieco et al., 2006; Cocke et al., 2005; Keeley, 2009; Kokaly et al., 2007), making it the index of choice for mapping burn severity throughout North America (Hall et al., 2008; Loboda et al., 2007; San-Miguel et al., 2016; Soverel et al., 2010). For this study, the burn severity categories derived through dNBR corresponded well with the degree of vegetation changes in affected areas investigated using Normalized Difference Vegetation Index (NDVI) and Leaf Area Index (LAI) (Rupasinghe and Chow-Fraser, unpublished data).

Despite the high accuracy and widespread use of dNBR, the index only gives a measure of burn severity of an image pixel. Therefore, the results are presented in a format of a map or graph. By calculating the average dNBR value for all pixels in the burned area, we were able to integrate the impact of a particular fire outbreak into a standardized score, the Standardized Burn Index Score (SBIS), which is simple to

calculate and use. We were able to use this index to rank the severity of fire outbreaks, regardless of their size, and to relate SBIS values to pre-fire conditions to produce a generalized understanding of how the type of pre-fire canopy species contribute to burn severity.

Fire season in Alberta usually starts in early April and ends in late September and most of the fires occur in the northern region (Tymstra et al., 2005). All the fire outbreaks we investigated occurred in this time window. Majority of the fire events we investigated experienced moderate-high to high severity fires. The WB and RC fires, however, were exceptions, with moderate or low burn severity in most of the affected areas. The forests in the footprint of the WB 2007 and RC 2011 fires had experienced partial burns in the early 1950s and 1980s, respectively (Alberta wildfire, 2020). These earlier fires may have reduced fuel accumulation and prevented high burn intensity in the more recent fires. Similarly, the 2012 outbreak in WB was not due to a single large fire but seven smaller fire outbreaks with less severe burns, likely because the area had been surrounded by many historical fires and the meanders of the Peace river had acted as natural fire barriers. Although we did not investigate it, these anomalies may also have been due to site-to-site variation in weather conditions (precipitation and temperature).

It is also important to consider the influence of anthropogenic disturbances (e.g. oil explorations, human settlements) as well as fire management. Among the fire events studied within regions, WB was the least affected by anthropogenic activity, and this was followed by the RC fire. These two regions are in protected areas and have minimal to no impact from oil and gas exploration and human development. The BL area, however, is

severely affected by both gas and oil exploration as well as logging, with a very high density of seismic lines. Of the four regions, the LSL fire was the most affected by anthropogenic activity and fire management. This fire outbreak was the smallest, and in fact, about 25% of the affected area recorded by the NFDB was not mapped as being burned by dNBR, although there was high burn severity, probably due to the higher amount of accumulated fuel in the forest.

The LSL fire was anomalous to the other three regions, likely because of its proximity to the town of Slave Lake. Despite the high burn severity, if we considered both the area burned and mean severity together, the LSL fire exerted the least impact overall. According to Robinne et al., (2016), human activities are expected to reduce fire activity close to human settlements. Human involvement in fire suppression and management makes natural fire behavior more complex to understand and for which to predict future trajectories (Robinne et al., 2016; Thompson and Calkin, 2011). The burned area at the LSL area is also characterized by a high density of seismic lines. Although the effect of oil and gas exploration and seismic lines on wildfire activity is still unclear, many specialists expect them to have a non-negligible effect as these lines are grass-dominated areas and can act as 'flashy' fuels where fire can spread rapidly (Robinne et al., 2016). Nevertheless, the influence of human involvement and oil and gas exploration, especially the seismic lines on the wildfire activity should be studied further (Krawchuk et al., 2009).

In this study, we found the pre-fire composition of canopy species in forests to have a significant effect on burn severity. Cumming (2001) also used Alberta Phase 3

inventory (Alberta Forest service, 1985) to investigate the relationship between the forest type and wildfire in northeastern Alberta. They used Volronoi polygonization as approximate digitization of the forest stand boundaries followed by statistical and modeling approaches. In the current study, we used remote-sensing image classification followed by GIS-based analysis to achieve the same objective. The use of multitemporal images from the Landsat satellite alone with the automated image classification approaches considerably reduced the need for time-consuming digitizing as well as person-related errors. Furthermore, we were able to obtain a good level of accuracy for overall and target species mapping. Despite differences in methods used, Cumming (2001) reported similar results to ours, where deciduous stands burnt at a lower rate while black spruce stands burned at the highest rate.

According to literature, aspen stands usually do not sustain crown fires because fires reaching the crown tend to drop to the ground and burn as surface fire, thereby making them act as natural barriers to fires (Cumming, 2001; DeByle and Winokur, 1985; Jones and DeByle, 1985). Trembling aspen, balsam poplar, and white birch, the most common deciduous stands in boreal forest stands of northern Alberta, have physiological and morphological characteristics (e.g.: high crown base height, high leaf and stem moisture content, smooth bark) that make them ineffective in spreading wildfires (Alberta Government, 2012). Coniferous species such as spruce and pines, on the other hand, have characteristics that can help spread wildfires; they occur in high density, accumulate needles on the forest floor as fuel, and have rough, loose bark, low-lying branches, and high rates of dead branches that help convey the fire up to the crown (Alberta

Government, 2012; Thompson et al., 2017). Therefore, forest stands with a higher proportion of deciduous species prior to the fire will sustain less severe burns.

Boreal forests consist of many freshwater reserves and approximately 25% of the boreal forest cover in western Canada is characterized by wetlands (Mery et al., 2010; Tarnocai et al., 2011; Thompson et al., 2017). Several studies have investigated the effect of wetland cover and fuel loading levels in wetlands and have reported negative relationships with wildfire susceptibility and severity (Johnston et al., 2015; Schneider et al., 2016; Thompson et al., 2017; Whitman et al., 2018). According to Thompson et al., (2017), the fuel in wetlands may show site-level differences in fuel moisture, phenology, and access to groundwater and may contribute to burning if profound droughts occur. Johnston et al., (2015) reported that the potential of high-frequency fire in graminoid-dominant wetlands is only possible in about 80 years after a significant fire outbreak. Despite these documented findings, the effect of water features on the spread of fire and burn severity is still poorly understood. Our results suggest that regardless of land cover (e.g. wetland or forested), water features up to 1 km distance from vegetation can protect and/or ameliorate fire damage. Therefore, water features and wetland communities in the boreal region play an important role in controlling the spread of severe fires, especially under the increased frequency of wildfires due to global climate change.

When relating the pre-fire species composition with the burn severity, we did not observe any relationship with the commonly used index, dNBR. However, SBIS captured the relationship with pre-fire species composition as well as the duration of the fire, indicating that the combination of the burned extent and burn severity are important for

understanding fire behavior. Furthermore, we obtained a stronger relationship between distance from water features and SBIS than for dNBR. This indicates that the burn impact provides a better measure of the importance of water features in fire behavior than that of burn severity. We, therefore, recommend using SBIS over dNBR when describing the relationship between burn impact and pre-fire conditions.

4.6. Conclusion

Changes in fire regimes due to global climate change in the boreal region has both social and ecological ramifications. Understanding pre-fire conditions that lead to severe fires may help us forecast future wildfire trajectories. To make a more generalized understanding of fire regime changes, wildfires need to be investigated over large spatial scales and over longer time spans. We used remote-sensing techniques to study pre-fire conditions on burn severity and burn impact using 21 fire outbreaks in four boreal forest regions in northern Alberta. To map the pre-fire distribution of canopy species in the burned areas, we successfully employed remote sensing approaches with multitemporal Landsat images. We created the SBIS by combining dNBR (commonly used index of burn severity) and total burned area of different fire outbreaks and used them to understand the relationships between pre-fire conditions and burn impact. Our results confirm that areas dominated by conifers lead to more severe fires while those occupied by deciduous species can reduce burn severity. We have demonstrated a cost-effective means to map species distribution in remote forested areas that may help forest managers to develop more up-to-date forest maps. Our study also shows the importance of water

features in the boreal region in reducing or inhibiting the spread of wildfires, regardless of the type of nearby ecosystems or plant communities.

4.7. Acknowledgments

We would like to thank Dr. Michael Waddington and Dr. Francoise-Nicolas Robinne for sharing their experience on wildfire and for providing valuable references and data sources. We also thank Jordan DeBoer, Yuxin Zang, and Sherry Chen for the assistance with image pre-processing and digitizing. The project was funded by Boreal Water Futures (BWF) of Global Water Futures (GWF).

4.8. Literature cited

Akther, M.S., Hassan, Q.K., 2011. Remote Sensing-Based Assessment of Fire Danger Conditions Over Boreal Forest. IEEE J. Sel. Top. Appl. Earth Observations Remote Sensing 4, 992–999. https://doi.org/10.1109/JSTARS.2011.2165940

Alberta Forest service, 1985. Alberta Phase 3 Forest Inventory; An OverView (No. ENR Report No. I/86). Alberta Energy and Natural Resources, Edmonton, Alberta, Canada.

Alberta Government, 2019. West of 4th Meridian - Historical Forest Inventory - Phase 3 Maps - Open Government [WWW Document]. URL https://open.alberta.ca/dataset/gda-dfa530fd-1e9d-4649-a984-fe3560a2fb93 (accessed 8.6.20).

Alberta Government, 2012. How Different Tree Species Impact the Spread of Wildfire.

Alberta Parks, 2018. Information & Facilities - Richardson Wildland Provincial Park | Alberta Parks [WWW Document]. URL

https://www.albertaparks.ca/parks/northeast/richardson-wpp/information-facilities/ (accessed 8.5.20).

Alberta Wilderness Association, 2020. Bistcho is a remote and serene wilderness region in the far northwestern corner of Alberta. [WWW Document]. Alberta Wilderness Association. URL https://albertawilderness.ca/issues/wildlands/areas-of-concern/bistcho/ (accessed 8.5.20).

Alberta wildfire, 2020. Spatial Wildfire Data | AAF - Agriculture and Forestry [WWW Document]. URL https://wildfire.alberta.ca/resources/historical-data/spatial-wildfire-data.aspx (accessed 12.24.20).

Barrett, K., McGuire, A.D., Hoy, E.E., Kasischke, E.S., 2011. Potential shifts in dominant forest cover in interior Alaska driven by variations in fire severity. Ecological applications 21, 2380–2396. https://doi.org/10.1890/10-0896.1

Botey, A. P., Kulig, J.C., 2014. Family Functioning Following Wildfires: Recovering from the 2011 Slave Lake Fires. J Child Fam Stud 23, 1471–1483. https://doi.org/10.1007/s10826-013-9802-6

Boucher, J., Beaudoin, A., Hébert, C., Guindon, L., Bauce, É., 2017. Assessing the potential of the differenced Normalized Burn Ratio (dNBR) for estimating burn severity in eastern Canadian boreal forests. International Journal of Wildland Fire 26, 32–45.

Canadian Parks and Wilderness Society Northern Alberta, 2016. Alberta's Caribou: a guide to range planning. Vol 2: Little Smoky.

Chu, T., Guo, X., 2014. Remote sensing techniques in monitoring post-fire effects and patterns of forest recovery in boreal forest regions: A review. Remote Sensing 6, 470–520. https://doi.org/10.3390/rs6010470

Chu, T., Guo, X., Takeda, K., 2016. Remote sensing approach to detect post-fire vegetation regrowth in Siberian boreal larch forest. Ecological Indicators 62, 32–46. https://doi.org/10.1016/j.ecolind.2015.11.026

Chuvieco, E., Riaño, D., Danson, F.M., Martin, P., 2006. Use of a radiative transfer model to simulate the postfire spectral response to burn severity. Journal of Geophysical Research:Biogeosciences 111.https://doi.org/10.1029/2005JG000143

Cocke, A., Fulé, P., Crouse, J., 2005. Comparison of burn severity assessment using Differenced Normalized Burn Ratio and ground data. International Journal of Wildland Fire 14, 189–198. https://doi.org/10.1071/WF04010

Cumming, S.G., 2001. Forest Type and Wildfire in the Alberta Boreal Mixedwood: What Do Fires Burn? Ecological Applications 11, 97–110. https://doi.org/10.1890/1051-0761(2001)011[0097:FTAWIT]2.0.CO;2

DeByle, N.V., Winokur, R.P., 1985. Aspen: ecology and management in the western United States (No. RM-119). US Department of Agriculture, Forest Service, Rocky Mountain Forest and Range Experiment Station, Fort Collins, Colorado, USA.

Fernández-García, V., Quintano, C., Taboada, A., Marcos, E., Calvo, L., Fernández-Manso, A., 2018. Remote sensing applied to the study of fire regime attributes and

their influence on post-fire greenness recovery in pine ecosystems. Remote Sensing 10, 733. https://doi.org/733; https://doi.org/10.3390/rs10050733

Flannigan, M.D., Logan, K.A., Amiro, B.D., Skinner, W.R., Stocks, B.J., 2005. Future area burned in Canada. Climatic change 72, 1–16. https://doi.org/10.1007/s10584-005-5935-y

Flannigan, M., Stocks, B., Turetsky, M., Wotton, M., 2009. Impacts of climate change on fire activity and fire management in the circumboreal forest. Global change biology 15, 549–560. https://doi.org/10.1111/j.1365-2486.2008.01660.x

Gauthier, S., Bernier, P., Kuuluvainen, T., Shvidenko, A.Z., Schepaschenko, D.G., 2015. Boreal forest health and global change. Science 349, 819–822. https://doi.org/DOI: 10.1126/science.aaa9092

Hall, R.J., Freeburn, J.T., De Groot, W.J., Pritchard, J.M., Lynham, T.J., Landry, R., 2008. Remote sensing of burn severity: experience from western Canada boreal fires. International Journal of Wildland Fire 17, 476–489. https://doi.org/10.1071/WF08013

Hammill, K.A., Bradstock, R.A., 2006. Remote sensing of fire severity in the Blue Mountains: influence of vegetation type and inferring fire intensity. International Journal of Wildland Fire 15, 213–226. https://doi.org/10.1071/WF05051

Johnson, E.A., Miyanishi, K., Bridge, S.R.J., 2001. Wildfire regime in the boreal forest and the idea of suppression and fuel buildup. Conservation Biology 15, 1554–1557.

Johnston, D.C., Turetsky, M.R., Benscoter, B.W., Wotton, B.M., 2015. Fuel load, structure, and potential fire behaviour in black spruce bogs. Canadian Journal of Forest Research 45, 888–899. https://doi.org/10.1139/cjfr-2014-0334

Jones, J.R., DeByle, N.V., 1985. Genetics and variation in Aspen: Ecology and Management in the Western United States (Technical report No. RM-119). USDA Forest Service, Rocky Mountain Forest and Range Experiment Station, Fort Collins, CO.

Kasischke, E.S., Christensen Jr, N.L., Stocks, B.J., 1995. Fire, global warming, and the carbon balance of boreal forests. Ecological applications 5, 437–451. https://doi.org/10.2307/1942034

Keeley, J., 2009. Fire intensity, fire severity and burn severity: A brief review and suggested usage. International Journal of Wildland Fire 18, 116–126. https://doi.org/10.1071/WF07049

Key, C.H., Benson, N.C., 2005. Landscape assessment: ground measure of severity, the Composite Burn Index; and remote sensing of severity, the Normalized Burn Ratio. FIREMON: Fire effects monitoring and inventory system 2004.

Kokaly, R.F., Rockwell, B.W., Haire, S.L., King, T.V., 2007. Characterization of post-fire surface cover, soils, and burn severity at the Cerro Grande Fire, New Mexico, using hyperspectral and multispectral remote sensing. Remote Sensing of Environment 106, 305–325. https://doi.org/10.1016/j.rse.2006.08.006

Krawchuk, M.A., Cumming, S.G., Flannigan, M.D., 2009. Predicted changes in fire weather suggest increases in lightning fire initiation and future area burned in the

mixedwood boreal forest. Climatic change 92, 83–97. https://doi.org/DOI 10.1007/s10584-008-9460-7

Krawchuk, M.A., Haire, S.L., Coop, J., Parisien, M.A., Whitman, E., Chong, G., Miller, C., 2016. Topographic and fire weather controls of fire refugia in forested ecosystems of northwestern North America. Ecosphere 7, 1–18. https://doi.org/10.1002/ecs2.1632

Lentile, L.B., Holden, Z.A., Smith, A.M., Falkowski, M.J., Hudak, A.T., Morgan, P., Lewis, S.A., Gessler, P.E., Benson, N.C., 2006. Remote sensing techniques to assess active fire characteristics and post-fire effects. International Journal of Wildland Fire 15, 319–345. https://doi.org/10.1071/WF05097

Liu, Q.J., Takamura, T., Takeuchi, N., Shao, G., 2002. Mapping of boreal vegetation of a temperate mountain in China by multitemporal Landsat TM imagery. International Journal of Remote Sensing 23, 3385–3405. https://doi.org/10.1080/01431160110076171

Loboda, T., O'Neal, K.J., Csiszar, I., 2007. Regionally adaptable dNBR-based algorithm for burned area mapping from MODIS data. Remote Sensing of Environment 109, 429–442. https://doi.org/10.1016/j.rse.2007.01.017

Lydersen, J.M., Collins, B.M., Brooks, M.L., Matchett, J.R., Shive, K.L., Povak, N.A., Kane, V.R., Smith, D.F., 2017. Evidence of fuels management and fire weather influencing fire severity in an extreme fire event. Ecological Applications 27, 2013–2030. https://doi.org/10.1002/eap.1586

Matsuura, Y., 2010. Soil carbon and nitrogen storage in Siberian permafrost region/A. Osawa, OA Zyryanova, Y. Matsuura, T. Kajimoto, RW Wein. Permafrost Ecosystems: Siberian Larch Forests.-Ecological studies 209, 149–163.

Mery, G., Katila, P., Galloway, G., Alfaro, R.I., Kanninen, M., Lobovikov, M., Varjo, J., 2010. Forests and society-responding to global drivers of change, IUFRO World Series. International Union of Forest Research Organizations (IUFRO), Vantaa, Finland.

Miller, J.D., Thode, A.E., 2007. Quantifying burn severity in a heterogeneous landscape with a relative version of the delta Normalized Burn Ratio (dNBR). Remote Sensing of Environment 109, 66–80. https://doi.org/10.1016/j.rse.2006.12.006

Murphy, K., Reynolds, J., Koltun, J., 2008. Evaluating the ability of the differenced Normalized Burn Ratio (dNBR) to predict ecologically significant burn severity in Alaskan boreal forests. INTERNATIONAL JOURNAL OF WILDLAND FIRE 17, 490–499. https://doi.org/10.1071/WF08050

Natural Resources Canada, 2017. Canadian Wildland Fire Information System | CWFIS Datamart [WWW Document]. URL https://cwfis.cfs.nrcan.gc.ca/datamart (accessed 8.6.20).

Pan, Y., Birdsey, R.A., Fang, J., Houghton, R., Kauppi, P.E., Kurz, W.A., Phillips, O.L., Shvidenko, A., Lewis, S.L., Canadell, J.G., 2011. A large and persistent carbon sink in the world's forests. Science 333, 988–993. https://doi.org/DOI: 10.1126/science.1201609 Article

Parisien, M.-A., Kafka, V., Hirsch, K., Todd, J., Lavoie, S., Maczek, P., 2005. Mapping Wildfire Susceptibility with the BURN-P3 Simulation Model (No. NOR-X-405). Natural Resources Canada, Canadian Forest Service, Northern Forestry Centre.

Parks Canada, Government of Canada, 2020. Wood Buffalo National Park [WWW Document]. URL https://www.pc.gc.ca/en/pn-np/nt/woodbuffalo(accessed 8.5.20).

Parks, S.A., Dillon, G.K., Miller, C., 2014. A new metric for quantifying burn severity: the relativized burn ratio. Remote Sensing 6, 1827–1844. https://doi.org/10.3390/rs6031827

Robinne, F.-N., Parisien, M.-A., Flannigan, M., 2016. Anthropogenic influence on wildfire activity in Alberta, Canada. Int. J. Wildland Fire 25, 1131–1143. https://doi.org/10.1071/WF16058

San-Miguel, I., Andison, D., Coops, N., Rickbeil, G., 2016. Predicting post-fire canopy mortality in the boreal forest from dNBR derived from time series of Landsat data. International Journal of Wildland Fire 25. https://doi.org/10.1071/WF15226

Schneider, R.R., Devito, K., Kettridge, N., Bayne, E., 2016. Moving beyond bioclimatic envelope models: integrating upland forest and peatland processes to predict ecosystem transitions under climate change in the western Canadian boreal plain. Ecohydrology 9, 899–908. https://doi.org/10.1002/eco.1707

Schoennagel, T., Veblen, T.T., Romme, W.H., 2004. The interaction of fire, fuels, and climate across Rocky Mountain forests. BioScience 54, 661–676. https://doi.org/10.1641/0006-3568(2004)054[0661:TIOFFA]2.0.CO;2

Shorohova, E., Kneeshaw, D., Kuuluvainen, T., Gauthier, S., 2011. Variability and dynamics of old-growth forests in the circumbolear zone: implications for conservation, restoration and management. Silva Fenn 45, 785–806. https://doi.org/10.14214/sf.72doi:10.14214/sf.72

Soverel, N.O., Perrakis, D.D.B., Coops, N.C., 2010. Estimating burn severity from Landsat dNBR and RdNBR indices across western Canada. Remote Sensing of Environment 114, 1896–1909. https://doi.org/10.1016/j.rse.2010.03.013

Steffen, W., Richardson, K., Rockström, J., Cornell, S.E., Fetzer, I., Bennett, E.M., Biggs, R., Carpenter, S.R., De Vries, W., De Wit, C.A., 2015. Planetary boundaries: Guiding human development on a changing planet. Science 347. https://doi.org/DOI: 10.1126/science.1259855

Stocks, B.J., Mason, J.A., Todd, J.B., Bosch, E.M., Wotton, B.M., Amiro, B.D., Flannigan, M.D., Hirsch, K.G., Logan, K.A., Martell, D.L., 2002. Large forest fires in Canada, 1959–1997. Journal of geophysical research 108, FFR5.1-FFR5.12. https://doi.org/10.1029/2001JD000484

Tarnocai, C., Kettles, I.M., Lacelle, B., 2011. Peatlands of Canada; Geological Survey of Canada, Open File 6561; map, scale 1: 6 500 000. Natural Resources of Canada/Ressources naturelles Canada.

Thompson, D.K., Parisien, M.-A., Morin, J., Millard, K., Larsen, C.P.S., Simpson, B.N., 2017. Fuel accumulation in a high-frequency boreal wildfire regime: from wetland to upland. Can. J. For. Res. 47, 957–964. https://doi.org/10.1139/cjfr-2016-0475

Thompson, M.P., Calkin, D.E., 2011. Uncertainty and risk in wildland fire management: a review. Journal of environmental management 92, 1895–1909. https://doi.org/10.1016/j.jenvman.2011.03.015

Tymstra, C., Wang, D., Rogeau, M.-P., 2005. Alberta wildfire regime analysis (Wildfire Science and Technology Report No. PFFC-01-5). Alberta Department of Sustainable Resource Development, Forest Protection Division, Edmonton AB.

UNESCO World Heritage Center, 2020. Wood Buffalo National Park [WWW Document]. UNESCO World Heritage Centre. URL https://whc.unesco.org/en/list/256/ (accessed 8.5.20).

USGS, 2016a. Landsat Missions; Landsat 5 [WWW Document]. Fact Sheet. URL https://www.usgs.gov/core-science-systems/nli/landsat/landsat-5?qt-science_support_page_related_con=0#qt-science_support_page_related_con (accessed 8.5.20).

USGS, 2016b. Landsat Missions; Landsat 7 [WWW Document]. Fact Sheet. URL https://www.usgs.gov/core-science-systems/nli/landsat/landsat-7?qt-science_support_page_related_con=0#qt-science_support_page_related_con (accessed 8.5.20).

Whitman, E., Parisien, M.-A., Thompson, D.K., Hall, R.J., Skakun, R.S., Flannigan, M.D., 2018. Variability and drivers of burn severity in the northwestern Canadian boreal forest. Ecosphere 9, e02128. https://doi.org/10.1002/ecs2.2128

Table 4.1 Start and end dates and burn duration of different fire outbreaks in this study. (Note: LSL, RC, WB, and BL stand for the slave lake, Richardson, wood buffalo, and bistcho lake respectively)

Fire event	Start date	End date	Burn duration (d)
WB 2007	2007-05-29	2007-07-13	45
	2007-05-29	2007-08-01	64
WB 2012	2012-05-26	2012-09-28	125
	2012-06-08	2012-08-08	61
	2012-07-09	2012-07-28	19
	2012-07-10	2012-07-16	6
	2012-07-10	2012-08-22	43
	2012-07-13	2012-08-22	40
WB 2015	2015-06-06	2015-07-12	36
	2015-06-26	2015-09-12	78
	2015-06-24	2015-09-12	80
	2015-05-28	2015-10-01	126
	2015-06-18	2015-08-11	54
	2015-06-05	2015-07-05	30
LSL 2011	2011-05-04	2011-05-17	13
RC 2011	2011-05-14	2011-07-06	53
BL 2004	2004-07-15	2004-08-10	26
	2004-07-22	2004-08-16	25
	2004-07-12	2004-09-26	76
BL2012	2012-06-22	2012-10-07	107
	2012-08-12	2012-09-23	42

Table 4.2 Year and location of fires in the study, and satellite images used in associated burn severity analyses. L5, L7, and L8 refer to Landsat 5, Landsat 7, and Landsat 8, respectively. (Note: LSL, RC, WB, and BL stand for the slave lake, Richardson, wood buffalo, and bistcho lake respectively)

Year of fire	Location of fire	Image used before the fire		Image used after the fire	
		Date acquired	Sensor	Date acquired	Sensor
2011	LSL	2010/06/19	L7	2011/08/09	L7
		2010/07/21	L7	2011/08/25	L7
2011	RC	2010/07/23	L7	2011/09/04	L5
		2010/08/24	L7		
2007	WB	2006/09/04	L5	2008/06/21	L5
2012	WB	2011/09/10	L7	2013/08/06	L8
2015	WB	2014/09/10	L8	2015/09/29	L8
2004	BL	2003/08/30	L5	2005/08/12	L5
		2003/09/01	L5		
2012	BL	2011/09/14	L5	2013/07/10	L8
				2013/09/03	L8

Table 4.3 Burn Severity categories according to U.S. Geological Survey FireMon program (Key and Benson, 2005).

dNBR value	Burn Severity Category
< -0.25	High post-fire regrowth
-0.25 to -0.1	Low post-fire regrowth
-0.1 to 0.1	Unburned
0.1 to 0.22	Low burn severity
0.22 to 0.44	Low-moderate burn severity
0.44 to 0.66	Moderate-high burn severity
>0.66	High burn severity

Table 4.4 Satellite images used for tree species mapping before and after fires at LSL (2011), RC (2011), WB (2007, 2012, 2015), and BL (2004, 2012). L5, L7, and L8 refer to Landsat 5, Landsat 7, and Landsat 8, respectively.

Fire	Focal year	First season image		Second season image	
		Date acquired	Sensor	Date acquired	Sensor
LSL	1986	1986/06/02	L5	1986/08/28	L5
	2010	2010/06/20	L5	2010/09/24	L5
RC	1985	1985/07/03	L5	1985/08/18 &	L5
				1985/09/28	L5
	2010	2010/07/22 &	L5	2010/10/03	L5
		2010/07/24	L5		
WB	1985	1985/07/17 &	L5	1985/09/10	L5
		1985/07/31	L5		
	1997	1997/06/23	L5	1997/08/26	L5
	1998	1998/06/10	L5	1998/08/26	L5
BL	1985	1985/06/02	L5	1985/08/21	L5
	2002	2002/06/09	L7	2002/09/13	L7
	2006	2006/06/12	L5	2006/08/31	L5
	2008	2008/05/16	L5	2008/07/03	L5

Table 4.5 Overall and canopy species mapping accuracy of time series species maps for 2011 LSL, the 2011 RC, the 2007, 2012, and 2015 WB, and the 2004, and 2012 BL fires.

Fire	Focal year	All Classes		Canopy species	
		Overall accuracy (%)	Kappa	Overall accuracy (%)	Kappa
LSL	1986	82.13	0.75	79.38	0.67
	2010	80.92	0.74	80.44	0.61
RC	1985	92.65	0.88	91.66	0.72
	2010	88.20	0.80	85.21	0.73
WB	1985	90.09	0.87	83.75	0.66
	1997	66.05	0.55	65.76	0.57
	1998	82.47	0.76	77.22	0.59
BL	1985	88.89	0.76	89.81	0.67
	2002	79.53	0.68	84.60	0.55
	2006	79.38	0.66	83.98	0.69
	2008	77.75	0.64	78.02	0.60

Table 4.6 Summary statistics for linear regression analyses relating % total area burned to burn severity category for the four sites and when data from all sites were pooled. Regression equations were determined separately for coniferous and deciduous species. (The significant values are indicated with *).

Location	Species	Regression coefficient	R-square	P-value
LSL	Spruce	16.014	0.93*	0.0001*
	Aspen, birch, or Poplar	-14.384	0.93*	<0.0001*
RC	Jack pine	6.192	0.78*	0.1146
	Aspen, birch, or Poplar	-5.102	0.78*	0.1196
WB	Spruce	7.694	0.29	0.0007*
	Aspen, birch, or Poplar	-6.066	0.21	0.0045*
BL	Spruce	8.521	0.33	0.0014*
	Aspen, birch, or Poplar	-8.841	0.39	0.0003*
All Sites	Spruce or Pine	+8.795	0.31	<0.0001*
	Aspen, birch, or Poplar	-7.913	0.30	<0.0001*

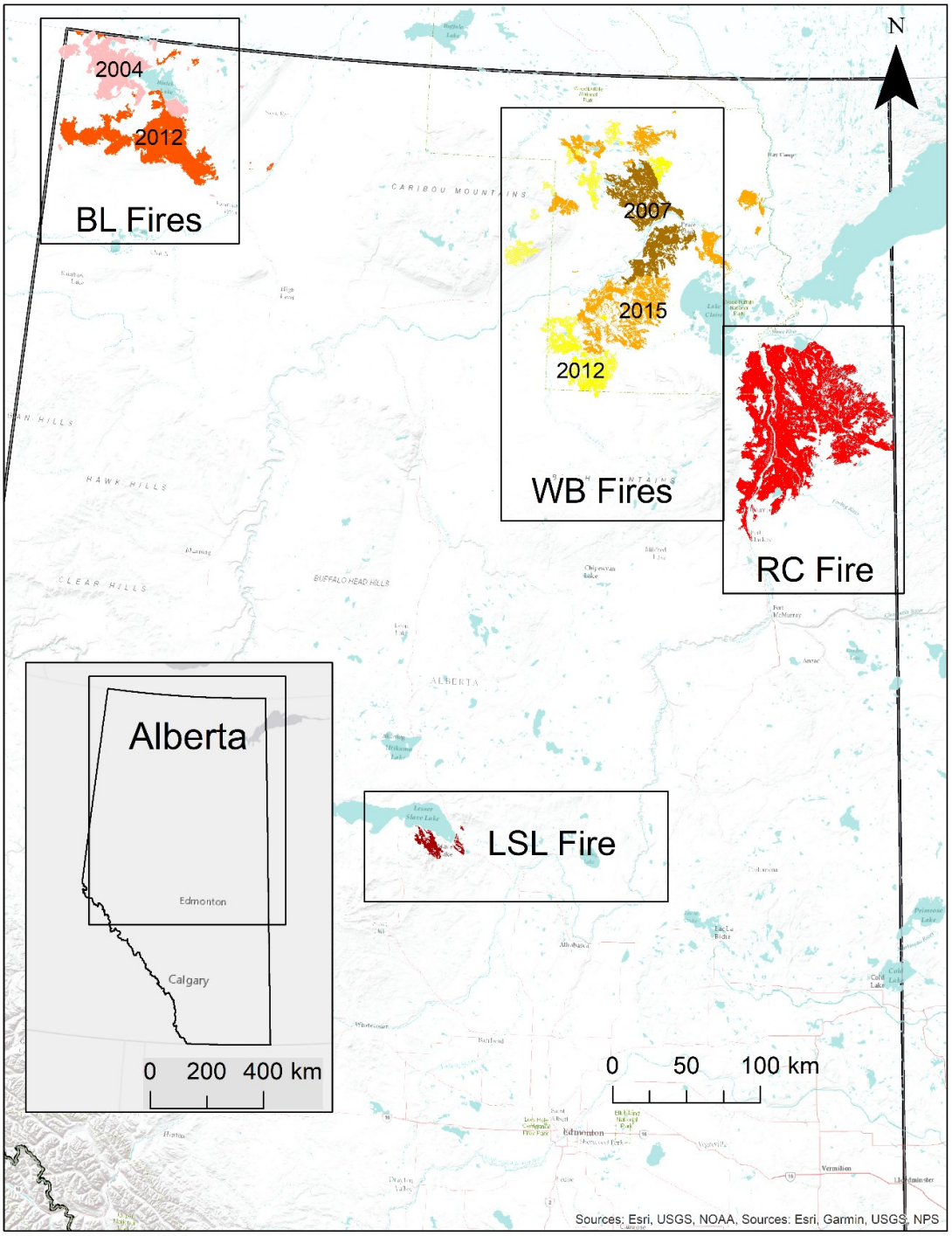

Figure 4.1 Location of study sites in this study.

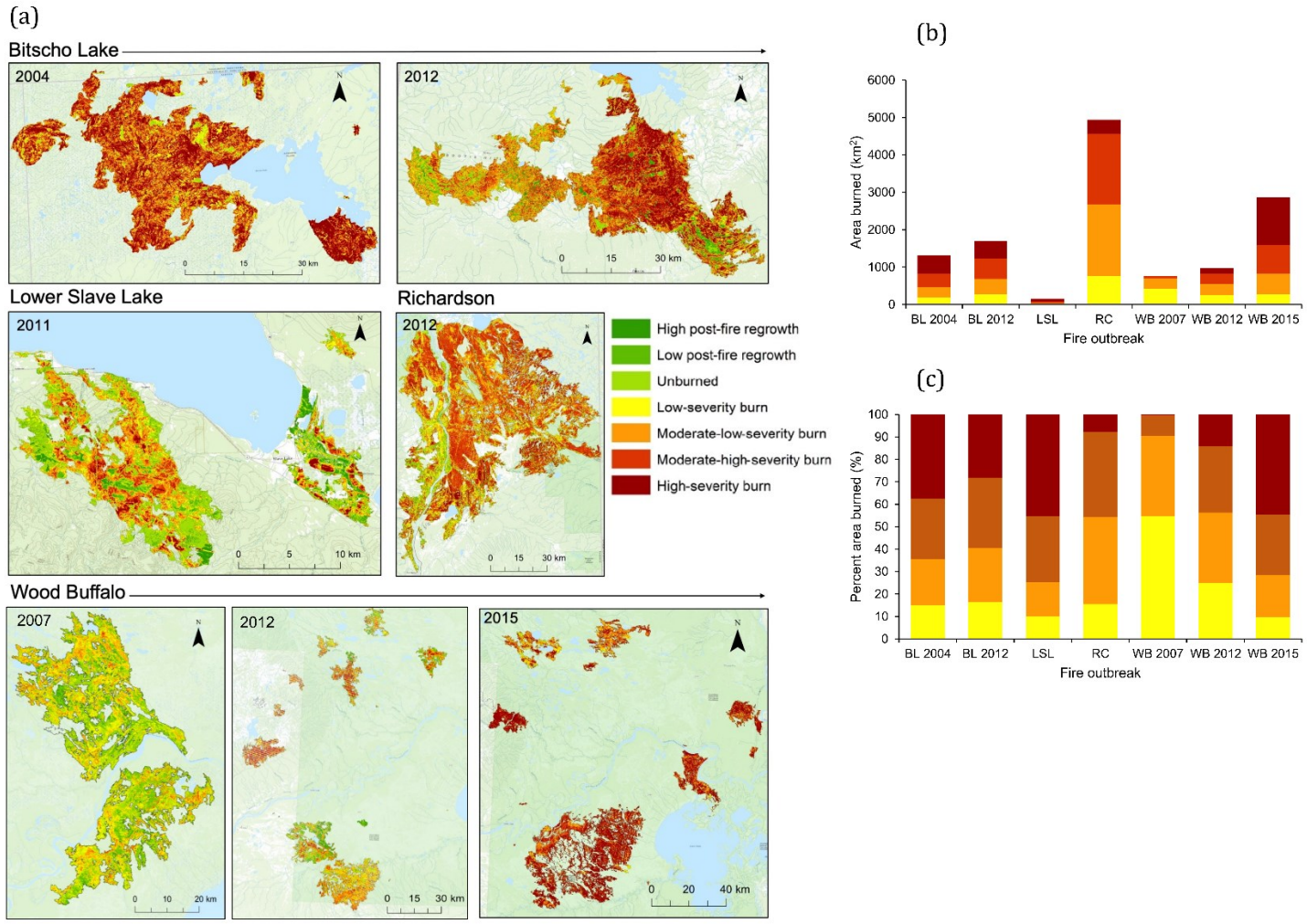

Figure 4.2 Comparison of burn severity of the study sites (a) burn severity maps of fire events based on dNBR values, (b) areas burned at different burn severity levels determined from dNBR, and (c) percent area burned at each burn severity level. (Base map: ESRI topographic base map).

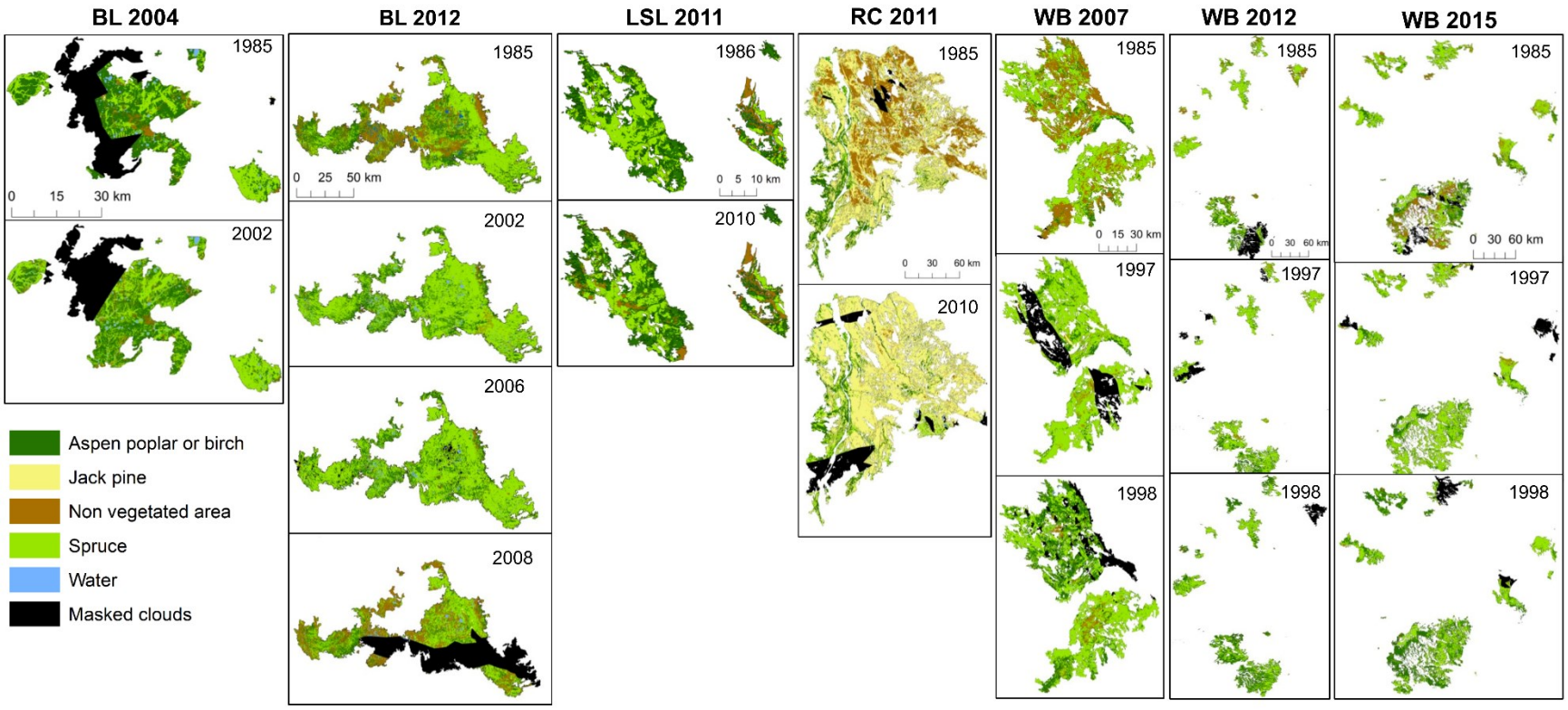

Figure 4.3 Time series maps showing the distribution of tree species within the wildfire footprints before fire events in this study.

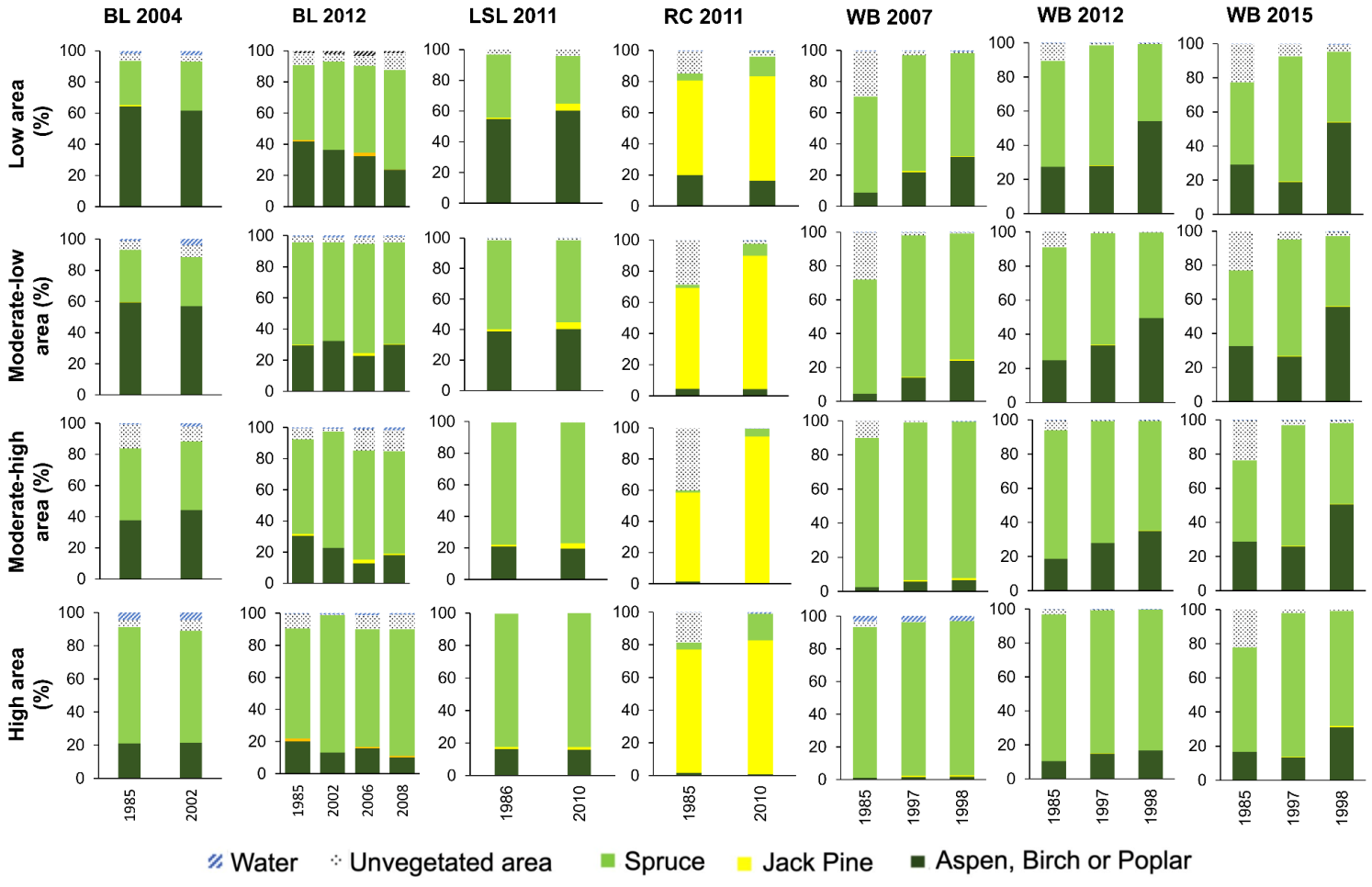

Figure 4.4 Percentage change in landcover classes for four burn-severity categories corresponding to the Bitscho Lake (BL), Lower Slave Lake (LSL), Richardson (RC), and Wood Buffalo (WB) fires

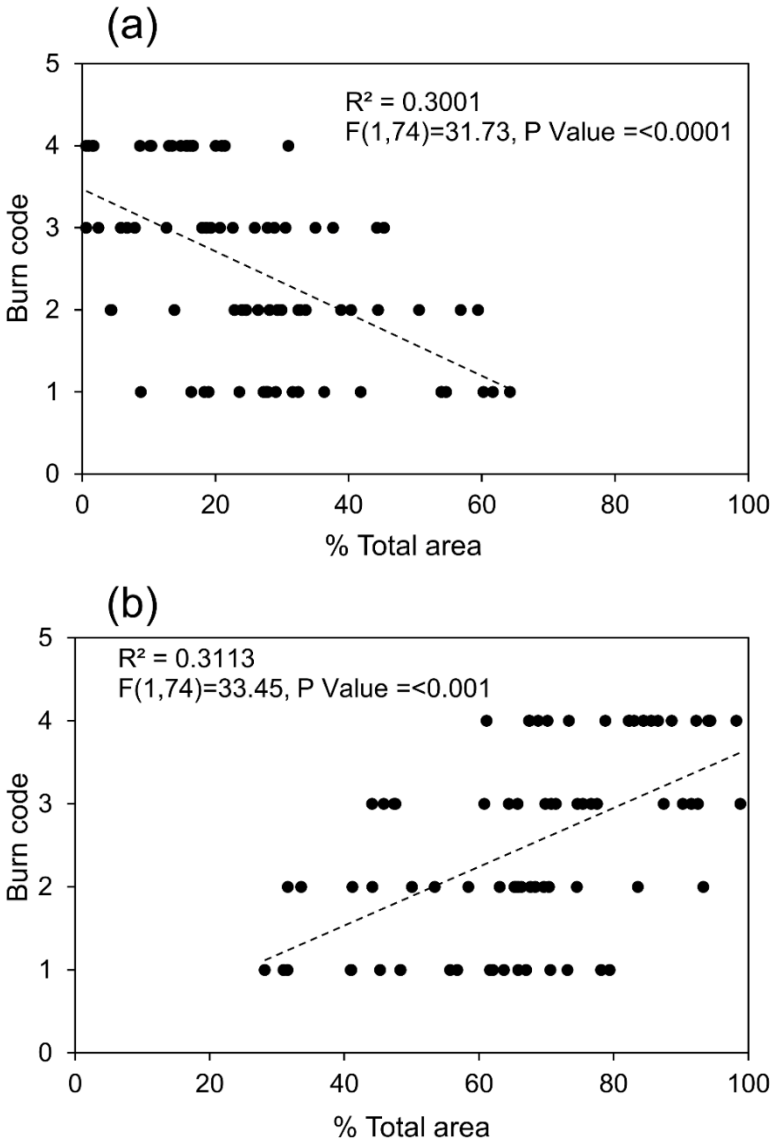

Figure 4.5 Distribution of burn severity (Burn codes: 1-Low, 2-Moderate-low, 3-Moderate-high, 4-High severity) vs percentage area occupied by a) deciduous and b) coniferous canopy taxa at forest stands in this study.

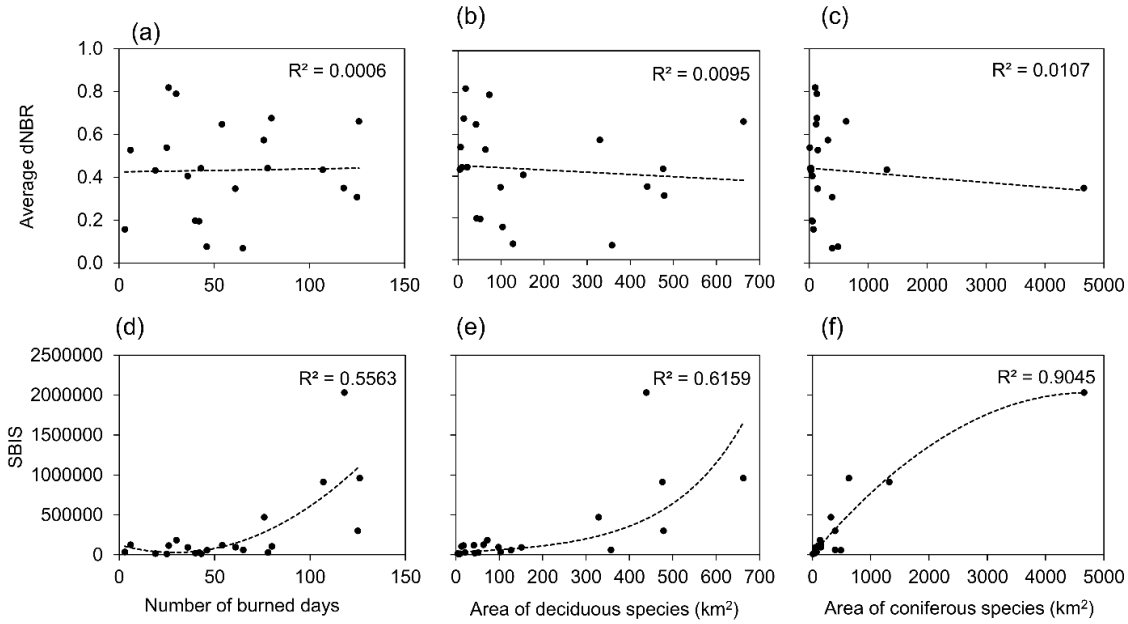

Figure 4.6 Linear regression of burn severity (dNBR) against (a) burn duration, (b) percent area of deciduous species, and (c) percent area of coniferous species; non-linear regression of burn impact score (SBIS) against (d) burn duration, (e) area of deciduous species, and (f) area of coniferous species.

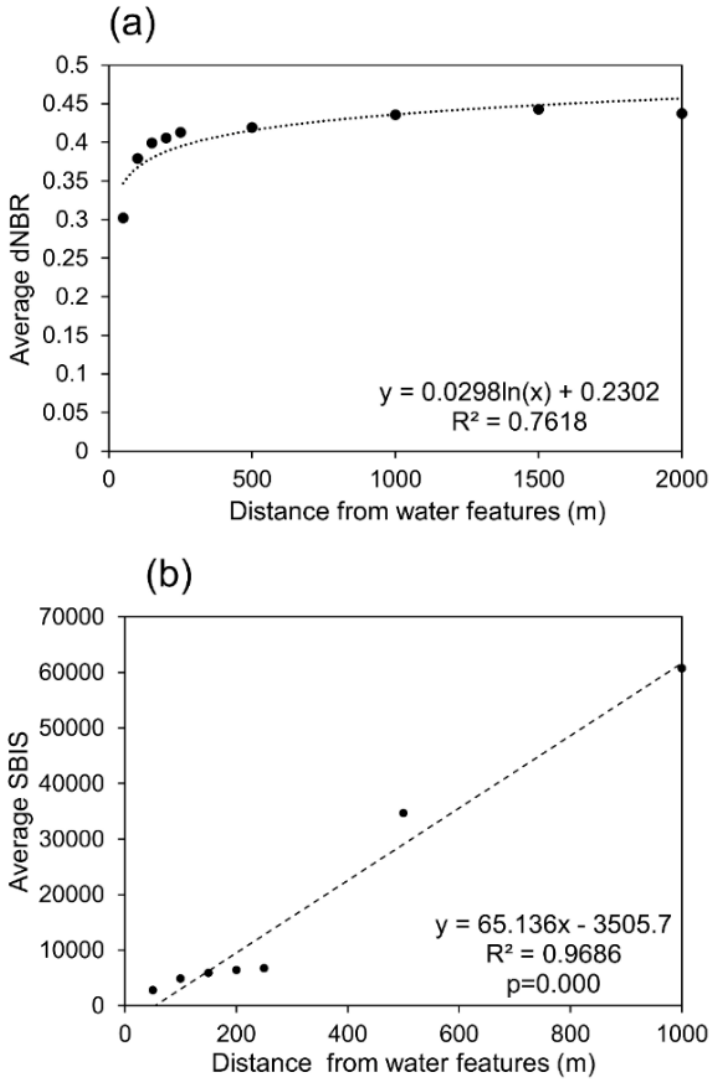

Figure 4.7 Regression analysis of (a) dNBR and (b) SBIS of fire outbreaks against proximity to water features

Chapter 5. Effect of anthropogenic impact on post-fire vegetation recovery of Alberta's boreal forests using time-series Landsat data

By,

Prabha Amali Rupasinghe and Patricia Chow-Fraser

Presented as a manuscript

5.1. Abstract

Wildfires are the dominant stand-renewing disturbance factor in Canadian boreal forests and play an important role in altering forest succession, biogeochemical cycling, and carbon sequestration. Natural fires spread unevenly through the landscape, but human-made structures and activity can influence these natural patterns. Here, we use remote sensing and GIS techniques to investigate the post-fire recovery of seven wildfires in Alberta, that are influenced by human activity to varying degrees. The 2011 fire close to Lesser Slave Lake (LSL) was most influenced by human activities, the 2004 and 2012 fires in the Bistcho Lake region (BL) were exposed to moderate impact, while the 2011 fire in the Richardson (RC) backcountry, and three in Wood Buffalo National park (WB; 2007, 2012, 2015) were exposed to the least amount of human impact. We used differenced Normalized Burn Ratio (dNBR) to map the burn severity of the selected fire outbreaks, and then used available time-series images to calculate indices of vegetation greenness (Normalized Difference Vegetation Index; NDVI), area of vertical leaf layers (Leaf Area Index; LAI), and mapped canopy species distribution using images collected in two seasons to determine canopy species recovery rates. The LSL fire had the fastest recovery rate according to both vegetation indices; we also found that spruce thinning occurred in areas that experienced low burn severity after the fire. Areas that experienced low burn severity recovered faster than areas that experienced high burn severity, and recovery was faster for coniferous than for deciduous species. Such differences in recovery rates, however, were more evident with fire outbreaks of moderate and low human impact than with fire outbreaks with high human impact. We also observed an

ameliorating effect on the recovery and burn severity of the areas closer to the water features, however, this effect was not evident in the human impacted sites. Future models of wildfire behavior should account for possible deviations from the natural post-fire recovery processes whenever human activities are involved.

5.2. Introduction

Wildfires are the most common disturbance in boreal forests, shaping the forest structure and species composition, forming landscape patterns, and controlling energy flow and biogeochemical cycles (Goldammer & Furyaev, 1996). The Forest disturbance and recovery process are considered as a primary mechanism in the regulation of the carbon cycle (Cao et al., 2011). Increased global temperatures, however, have increased fire activity in Canada since about 1970 (Gillett et al., 2004). Many studies suggest that the increased temperatures will likely increase fire activity in the 21st century, increasing both the frequency of fires and total area burned (Flannigan et al., 2009; Girardin & Mudelsee, 2008; Yang et al., 2011). According to Hansen et al., (2013), 3.6% of biome-level boreal forests were lost between 2000 and 2012, with the largest losses in Canada (5.6% of Canadian boreal forests), and the majority of these due to wildfires (FAO, 2015). The ecological effects of wildfires in boreal fires are highly variable and are difficult to predict (Chu & Guo, 2014). Wildfires are influenced by many natural factors such as fire regimes, vegetation cover, permafrost conditions, topography, soil, properties, and climate (Chu & Guo, 2014; de Groot et al., 2013).

The pressure from large-scale human activity is increasing in the boreal forests in western Canada due to natural resource exploitation and urbanization (Government of

Canada, 2009; Robinne et al., 2016). This increasing human activity has also altered the wildfire activity through various processes such as higher ignition density in areas with higher human activity, landscape fragmentation, and fire suppression and management (Gralewicz et al., 2012; Stocks et al., 2002). The province of Alberta is especially affected by the oil and gas industry and timber extraction. According to Robinne et al., (2016), the influence of anthropogenic influence shows a diversity of responses in wildfire activity rather than the generally accepted decrease with a higher level of human activity. Despite the acknowledged complexity and importance of anthropogenic activity on ecological processes related to wildfire, this has remained a poorly understood issue (Chen et al., 2014; Mann et al., 2016; Robinne et al., 2016).

The northernmost boreal forests in Canada are mostly unmanaged and have not been properly surveyed (Gillis et al., 2005; Wulder et al., 2004). These forests are generally low in production value and distant from human settlements or activity. Logging is also minimal in these regions and therefore, wildfires are the key stand-renewing disturbance in these regions. Furthermore, no fire suppression or management is carried out in these remote, forested regions (Magnussen & Wulder, 2012). Southern regions in comparison are regularly surveyed for strategic planning for forest management and harvesting and therefore are more disturbed by human activity (Magnussen & Wulder, 2012). Therefore, the boreal forests of the province of Alberta experience a variety of human influence and as a result, the impact and response to wildfire may also vary depending on their location.

Global climate change and human activity not only affect wildfire frequency and severity but also affect the post-fire recovery process. Forest succession following fire outbreaks is an important process that determines the biophysical, biological, and biochemical characteristics of the forested ecosystems (Liu et al., 2008). These successional characteristics and recovery rates may vary depending on many factors such as size and severity of the fire, climatic conditions, fire intervals, species characteristics, and pre-and post-fire forest conditions (Furyaev et al., 2001). According to Johnstone et al., (2004), tree recruitment in North American boreal forests occurs within 3 to 10 years from the fire outbreak, and observations of the first five years of recovery could be used to predict the recovery trajectories for another two or three decades following the fire. The successional process may lead to similar forest composition as before the fire; however, it may also lead to ecosystem shifts depending on the extent of disturbance and post-fire recovery trajectories. An example of these ecological effects is the potential shift of conifer dominant boreal forests into deciduous forests as a result of more frequent high severity fires during the last two decades (Barrett et al., 2011). Furthermore, the species composition and the structure of boreal forests are also influenced by the drainage (Serbin et al., 2013); increased global temperatures have increased the drying of forested vegetation (Mbogga et al., 2010), making soil water availability an important factor in the forest recovery process. To better understand shifts in fire regimes and successional dynamics, the underlying causes, impacts, and long-term ecosystem conditions (e.g. forest structure, composition, and health status) need to be studied at relatively large spatial and temporal scales (Food and Agriculture Organization (FAO), 2010).

Changing patterns of wildfire disturbance as well as recovery processes need to be studied at regional scales that are only feasible with Remote Sensing (RS) approaches. Burned landscapes display obvious physical and spectral changes such as canopy consumption, ground charring, and soil color alterations, that could be easily detected through RS-based techniques (White et al., 1996). RS techniques have been developed since the mid-1980s to assess and manage wildfires (Lentile et al., 2006). These techniques allow the assessment of different temporal phases of wildfires including the ecosystem response before, during, and after the fire (Lentile et al., 2006). Previous studies have used RS-based indices, as well as statistical or modeling approaches to map burn severity and to investigate post-fire recovery processes. These studies have used RS data such as optical images, Synthetic Aperture Radar (SAR), and Light Detection and Ranging (LiDAR) (Chu & Guo, 2014; Cuevas-González et al., 2009; Hislop et al., 2018; Samiappan et al., 2019; Serbin et al., 2013; Tanase et al., 2011). Among these, optical satellite data from sensors such as Landsat and MODIS (Cleugh et al., 2007) are especially useful, as these are available at no cost and cover a long period, making them useful for long-term monitoring purposes.

This study was conducted specifically to address the paucity of information on how human activities affect post-fire recovery processes in the boreal forests of Canada. We chose fire outbreaks in four regions of northern Alberta that vary with respect to the influence of human activities, ranging from a fire that was started by arson in the town of Slave Lake to several wildfires that occurred in remote parts of Wood Buffalo National Park. We tested for the effect of human activities on the post-fire recovery process while

accounting for potential influences of proximity to water features (wetlands, lakes, streams), given that this factor had a significant effect on burn severity (Rupasinghe and Chow-Fraser, 2021; CH 3). We investigated the post-fire recovery process using time-series Landsat images to calculate indices of vegetation greenness and area of vertical leaf layers and to determine canopy species recovery rates. Our results will fill an important knowledge gap to inform managers how human involvement may alter natural post-fire recovery processes in Alberta's boreal forests.

5.3. Methods

5.3.1. Study sites

Fire outbreaks in this study occurred in four regions of northern Alberta (Fig. 5.1, Table 5.1). The 2011 Slave Lake fire was started by arson and burned an area of 202.25 km^2 in the Municipal District of Lesser Slave Lake (LSL; Flat Top Complex Wildfire Review Committee, 2012). Being subjected to the highest level of fire management, it is the smallest fire in this study and also the most human-influenced, affecting hundreds of homes near the town Slave Lake as well as the adjacent forested areas. This area is also affected by the oil and gas industry and has a high density of seismic lines. Two wildfires that occurred close to the Bistcho Lake region in 2004 and 2012 (BL2004 and BL2012) were located in remote areas of northern Alberta. The affected areas were relatively large (1371.53 km^2 for the fire in 2004 and 2142. 94 km^2 for the fire in 2012), with no fire management. This area experienced moderate human influence related to the oil and gas exploration and the associated high-density seismic lines. The 2011 Richardson fire (RC) occurred in northeastern Alberta close to Lake Athabasca and is the largest fire outbreak

(5217 km^2) in this study. Only a very small area in the southernmost region of the burned area was affected by seismic lines, while the remaining burned area was not influenced by human activities. We examined three additional fire outbreaks in Wood Buffalo National Park that occurred in 2007, 2012, and 2015 (WB 2007, WB 2012, and WB 2015) and that were located about 150 km northeast of the RC fire. This region was not influenced by any anthropogenic activity. Based on these site descriptions, we considered the RC and WB fires to have the lowest human impact, the LSL to have the highest human impact, and the BL fires to have an intermediate level of impact (Table 5.1).

5.3.2. Image data

We used cloud-free time-series Landsat 5, 7, and 8 multispectral images collected before and after years following each fire outbreak until 2018 to investigate the burn severity levels and post-fire recovery process (Table 5.2). We gave priority to peak summer month images (ie. July and August); however, when no cloud-free images were available, we extended our image search up to late May until late September. When required, we used an additional image collected close to the desired date to fill image gaps caused by the known error of the Landsat 7 sensor. After downloading the images, we performed radiometric correction and FLAASH atmospheric correction using ENVI 5.5 (Harris Geospatial Solutions). We adjusted the pixel values of the FLAASH product to range from 0 to 1. We used reflectance images for all RS-based analyses. Furthermore, we masked the clouds, cloud shades, the thick haze that had not been removed by atmospheric correction, and data gaps of some Landsat 7 images when no cloud-free

images close to the desired date were available, or when data gaps were not fully covered by a second image.

5.3.3. Mapping burn severity

We identified the affected area using a shapefile downloaded from the National Wildfire Database (NFDB) (Natural Resources Canada, 2017). Then we used differenced Normalized burn ratio (dNBR) to map the burn severity of all fire outbreaks (Key & Benson, 2005). We classified the dNBR images into burn severity levels following the categories defined by the United States Geological Survey FireMon Program (Key & Benson, 2005) using ArcMap 10.4.1. We created 30 random points for each of the four burn severity categories (low, moderate to low, moderate to high, and high burn severity) for all seven fire outbreaks separately to be used in post-fire recovery analysis.

5.3.4. Post-fire recovery using vegetation indices

We calculated the Normalized difference Vegetation Index (NDVI) and Leaf Area Index (LAI) using the pre-built functions in ENVI 5.5 for the time series, reflectance images. NDVI gives a measure of vegetation greenness as an indicator of vegetation health (Rouse et al., 1974) while LAI gives a measure of the area of vertical leaf layers per unit area, hence a direct measure of the recovery of canopy species (Watson, 1947; Zheng & Moskal, 2009). We calculated NDVI and LAI using time-series Landsat images collected each year before and following the fire outbreak. Then we exported the images to ArcGIS and used the random points that were generated for each burn severity category (described in the previous section) to extract the indices values of all time-series images. Here, we carefully observed the data points for each of the time-series images

and excluded any points that fell within the masked areas. For further data analysis, we combined the data for two severity categories; "low" and "moderate-low" severity were combined together as the "low severity" category while "moderate-high" and "high" severity were combined as the "high severity" category. After extracting the index values, we used Eq. 5.1 to calculate the recovery:

$$\%\ Recovery\ rate = \frac{post - fire\ index\ value}{Pre - fire\ index\ value} \times 100 \qquad \text{[Eq. 5.1]}$$

5.3.5. Post-fire recovery of canopy species

We used multi-temporal Landsat images collected in two seasons (spring and summer, fall and summer, or spring and fall; Table 5.3; Liu et al., 2002), and applied the Support Vector Machines (SVM) classification to map the canopy species distribution. We used manually digitized canopy species locations from Phase 3 of the forest inventory monochrome maps from Alberta Township Systems (ATS) (Alberta Government, 2019) as a ground reference for the species mapping. These maps were completed in 1984 (Alberta Forest service, 1985) and therefore we used images collected in 1985 or 1986 (depending on the availability of cloud-free images, no cloud-free images were available for 1984) to create an initial species map for each study site. Then we created time-series species maps until 2018 using the same ground reference locations used for 1985/6 and we assumed that the ground reference data did not change over time unless a visual disturbance occurred in each location. The three categories of canopy species were "deciduous species" (aspen, birch or poplar), "jack pine", and "spruce" (black or white), and two additional categories were "non-vegetated" areas and "water". We obtained ground reference for the two non-vegetation categories through manual interpretation of

the images. We carefully observed every ground reference location and eliminated locations that visually appeared to be disturbed or located on the masked areas for each image in the time series. The time series, however, was not continuous due to lack of cloud-free images for two seasons in majority of the years in the time series. We used 70% of the ground reference locations for image classification and the rest of the locations for accuracy assessment.

Using ArcMap, we overlayed time series species maps on the burn severity maps and extracted the pre-and post-fire species distribution data for each burn-severity category. Then we calculated the species recovery rates using Eq 5.2.

$$Species\ recovery\ rate = \frac{Percentage\ change\ in\ aerial\ cover\ since\ the\ fire\ outbreak}{Number\ of\ years\ since\ the\ fire} \quad \text{[Eq. 5.2]}$$

Therefore, the species recovery rate was calculated as the percentage increase in area per year. Here, we did not have species maps soon after the fire for any of the studied fire outbreaks due to lack of cloud-free images. Therefore, we assumed zero canopy cover soon after the fire when we calculated the species recovery rates. We calculated recovery rates separately for four burn-severity categories (low, moderate-low, moderate-high, and high) for the deciduous species, jack pine, and spruce. For further data analysis, we combined all fire outbreaks except for the LSL fire, which was most influenced by human activities.

5.3.6. Post-fire recovery rates with distance to water features

We evaluated the effect of proximity to water features on the post-fire recovery process by creating buffer zones around water features such as wetlands, ponds, and

rivers (derived from maps explained in the previous section) at distances of 50, 100, 150, 200, 250, 500, 1000, 1500, and 2000 m. Then we collected the NDVI values at 30 randomly chosen locations for each burn-severity category in each buffer zone as a proxy for vegetation recovery. Similar to image classification, we repeated the data extraction for each of the time-series images and carefully avoided collecting data points located on masked areas. We further extracted the area values of each burn-severity class within each buffer zone using the dNBR image that was created to evaluate the burn severity. For data analysis, we combined the ‘low’ and ‘moderate-low’ severity categories as well as the ‘moderate-high’ and 'high' severity categories into 'low' and 'high', respectively. We conducted the data analysis separately for the three human impact levels assuming LSL to be associated with the highest human impact, BL2004 and BL 2012 to have a moderate impact, and RC and WB2007, WB2012, and WB2015 to have the lowest human impact.

5.4. Results

5.4.1. Post-fire recovery using vegetation indices

Regardless of the degree of anthropogenic impact, both NDVI and LAI scores gradually increased following the fire outbreak (Fig. 5.2). In all cases, however, the LAI scores recovered faster than did NDVI scores. Areas that experienced lower burn severity also recovered faster when compared with areas that experienced higher burn severity in all fire outbreaks. Overall, however, we observed an erratic recovery pattern in all study fire events regardless of the level of human impact, much of which can be explained by differences in image acquisition dates (Table 5.2).

In terms of NDVI scores, the four sites associated with the least human impact (WB2007, WB2012, WB2015, and RC) recovered slower than did sites associated with moderate and high human impact (Fig. 5.2a). This was despite the fact that the WB2007 had the lowest burn severity among all study fire outbreaks (average dNBR of 0.073), with only 0.32% of the burned area experiencing high burn severity. The other sites in this group (RC and WB2012) had moderate burn severity levels (average dNBR of 0.350 and 0.375 respectively) and only a small proportion of the burned area had a high-severity burn (7.69% and 14.11% respectively). The WB2015 fire experienced higher burn severity (average dNBR of 0.604) with 44.72% of the area experiencing high burn severity. Overall, NDVI scores for high severity burns did not reach pre-fire levels (i.e. 100% recovery) even after eleven years following the fire, and their recovery rates lagged behind those of low-severity burns. By contrast, the LAI scores recovered at a faster rate, with mean values in areas of low-severity burn reaching pre-fire levels after two years, while those in areas of high-severity burn recovering to 100% of pre-burn values within three years. The recovery rate of LAI scores in areas of high severity caught up with those in areas of low-severity burn after 10 years of the fire outbreak.

The two fire outbreaks associated with a moderate level of human impact experienced relatively high burn severity (37.4% and 28.2% high-severity burn in BL2004 and BL2012, respectively; and average dNBR of 0.643 and 0.315, respectively). Both NDVI and LAI scores recovered rapidly (Fig. 5.2b), and there appeared to be less separation between low- and high-severity recovery rates after 6 years, when compared to the low human impact fires (Fig. 5.2a). NDVI scores in areas with low-severity burn

reached 100% of pre-fire values within six years, while those in areas with high-severity burn eventually reached pre-fire values within eight years. The recovery rate of the high-severity burn never caught up with those of the low-severity burn throughout the study period. By comparison, the recovery of LAI scores in the area of high-severity exceeded the rate of the low-severity burn after only six years following the fire. Similar to earlier observations, LAI scores also recovered faster than NDVI scores; in areas with a low-severity burn, recovery was 100% of the pre-fire level after only two years, while the recovery in areas of high-severity burn took more than four years.

LSL, which had the highest impact on human activity, had an average dNBR value of 0.16, with a relatively large area of 49.62 km^2 that remained unburned within the affected area. Despite its small size, the fire experienced high burn severity in almost half of the burned area (45.24%). Nevertheless, we observed faster recovery in LSL compared with the moderate and low-impact sites (Fig. 5.2c). The NDVI score reached its initial greenness (i.e., 100% mean recovery) in approximately 5 years, while the LAI score recovered to the pre-fire level within a year. The recovery rate of NDVI of the high-severity burn areas eventually matched that of the low-severity burn area within two years, while that for LAI took approximately four years. The LAI score increased to 150% of the pre-fire value within seven years after the fire outbreak.

5.4.2. Post-fire recovery of canopy species

We obtained relatively good accuracies for the overall and individual species mapping using two-season images, with over 75% accuracy for the majority of the years (Table 5.4). We were unable to create continuous time-series maps of canopy species

distribution because of the lack of cloud-free images for two seasons in each year following 1985 (Fig. 5.3). Prior to the fire events, the dominant canopy species in the LSL and BL forests were spruce and deciduous taxa including aspen, poplar, or birch. By contrast, the RC forest was dominated by jack pine and a smaller amount of deciduous taxa, and relatively little spruce. The WB forests were dominated by spruce with a smaller percentage cover of deciduous taxa. In all cases, the fire removed a substantial amount of the forest cover, revealing large contiguous unvegetated areas in the years immediately following the fires. There was a gradual increase in forest cover in all cases except LSL, which showed a more rapid and erratic recovery pattern.

To fully understand the species recovery process, we had to also consider the spatial variability of burn severity as well as the canopy species. We, therefore, sorted the data according to the four categories of burn severity (i.e. low, moderate-low, moderate-high, and high) and then determined the proportion of canopy species in each year following each fire outbreak. In all cases, we observed that the proportion of unvegetated area increased as we progressed from the low burn-severity to high burn-severity category; the data for LSL was particularly illustrative of this with 100% of the vegetation cover removed in the high-severity area, compared with almost 50% of the vegetation remaining in the low-severity area (Fig. 5.4). For fires that occurred before 2012, we had six or more years of post-fire recovery information. The proportion and species of trees that grew back in the footprint of the BL2004, RC2011, and WB007 fires resembled the pre-fire conditions, whereas the post-fire proportion for the LSL fire had changed to one dominated by deciduous taxa with a very small proportion of spruce and jack pine. This

figure also clearly shows the slow recovery rate of the BL2004 fire in all burn-severity categories, especially when compared to LSL and WB2007.

We combined the low and moderate human impact sites to compare against the high human impact site (Fig. 5.5). For the combined outbreaks, we observed the inverse relationship between burn severity and recovery rate noted earlier (Fig. 5.5a). The LSL site, however, showed an opposite trend where the highest overall species recovery was observed in areas that experienced high-severity burn (Fig. 5.5b). When recovery rates of different species were compared, spruce had the highest recovery rate for WB and BL fire outbreaks, and jack pine had the highest recovery rate in the RC fire (Fig. 5.5c). In all cases, the highest recovery rate was observed for areas that experienced low burn severity. The LSL site in contrast had a higher recovery rate of deciduous species compared to spruce and jack pine (Fig. 5.5d). Furthermore, a higher recovery rate was observed for areas that had high-severity burn.

We used linear regression to further study the relationship between post-fire species recovery rate and the area of burned canopy. Deciduous species recovery rate had a negative trend with the burned canopy area (R^2=0.185, p=0.022). In contrast, the recovery of jack pine was positively related to the burned area (R^2=0.345, p=0.001). We also analyzed the relationship between spruce and the pre-fire aerial cover of deciduous species and observed a positive trend (R^2=0.373, p=0.0006). Similarly, we observed a positive relationship between the areal cover of jack pine before the fire and the recovery rate of jack pine following the fire (R^2=0.449, p=<0.0001).

5.4.3. Post-fire recovery rates with distance to water features

In wildfire outbreaks that experienced only low human impact, we found that areas closer to water features had a more rapid rate of NDVI recovery compared to areas further away from water features, regardless of burn severity (Fig. 5.6a). In areas influenced by moderate and high human impact, however, we did not find any ameliorating effect of water features on the recovery of forests based on NDVI scores (Fig. 5.6b and c). We further examined the effect of distance to water features on the area of different burn severity levels by grouping data according to the three levels of human impact. For low-impact sites, we found a direct relationship between burn severity and distance to water features up to 2 km away (Fig. 5.7a). This relationship was not as evident for the areas with moderate human impact, where burn severity had been overall much higher than that in low-impact sites (Fig 5.7b). In the high-impact sites, however, the ameliorating effect of water features was only evident up to 500 m distance from the burned area, and beyond that distance, there was an apparent inverse relationship (Fig. 5.7c). Another striking result was that overall, the high-impact site had disproportionately more areas that were either unburnt or only experienced low burn severity compared with moderate- and low-impact sites.

5.5. Discussion

Quantifying post-fire health recovery is a prerequisite to measuring forests' resilience to a major disturbance event. The study of the post-fire recovery process in boreal forests is challenging because it requires examination that extends over large spatial scales and long-time frames. RS techniques and approaches are the appropriate

tools to understand the post-fire recovery processes in Canadian boreal forests (Chu & Guo, 2014; Jones et al., 2013; Peckham et al., 2008). In this paper, we have developed an RS strategy to compare sites across a large region to elucidate the effects of human activities on the post-fire recovery patterns of four boreal forest regions in Alberta.

Despite being the smallest fire, the LSL fire incurred the greatest economic loss of $700 million, because it affected the town of Slave Lake (Chowdhury & Hassan, 2013; Flat Top Complex Wildfire Review Committee, 2012). This area is fire-prone, with a history of fires in 2008, 2001, 1998, and 1968; however, the footprint of these previous fires did not overlap with that of the 2011 fire (Flat Top Complex Wildfire Review Committee, 2012). The impact of human activities included a high degree of fire management to prevent loss of lives and property and to minimize fire damage in the forest (Flat Top Complex Wildfire Review Committee, 2012), as well as a high density of seismic lines within the affected area that are known to take a much longer time to recover from disturbances (e.g. Dabros et al., 2017; Robinne et al., 2016). We will explore the effects of these human activities separately and show how they may artificially influence the pattern of recovery that is very different from the natural patterns exhibited by sites experiencing low human impact.

The LSL fire was different from the other fires in a number of ways. First, the recovery rate of the LSL fire (as indicated by NDVI and LAI) was comparatively faster than those in regions with moderate or low human impact. Secondly, it affected a much smaller area compared to other fires, and thirdly, a higher proportion of the affected area had remained unburned or had only experienced low-severity burns. All these factors

helped to quicken the overall recovery process. Whereas the other fires showed a direct relationship between time to full recovery and burn severity, the recovery rate of the LSL fire in areas experiencing high-severity burn actually recovered faster than those in areas with a low-severity burn. The more rapid recovery of the deciduous canopy species compared with the coniferous species also contradicted the observations seen for the other six fire outbreaks. We attribute both of these anomalous trends to the accelerated fuel management recommended by the Flat Top Complex Wildfire Review Committee (2012) and the subsequent shift in priority to thinning and converting coniferous stands, especially the black spruce stands, to deciduous species to minimize future wildfire risk in the LSL region. This explains our observed post-fire disappearance of spruce in areas that had remained unburned and those areas experiencing low burn severity, and inadvertently obliterated any differential between recovery rates of areas with low-severity and high-severity burns. Therefore, actions were taken by people both with respect to fire suppression during the fire and conifer thinning to minimize the risk of future wildfires after the fire resulted in anomalous fire-recovery patterns.

Boreal forests cover approximately 60% of the province of Alberta but most of the forested areas are disturbed and fragmented by industrial forestry and harvesting, agriculture, transportation, and communication corridors, as well as the oil and gas industry (Dabros et al., 2017). Seismic lines are used in these wilderness areas to identify and map geological structures that contain oil and gas prior to drilling (Dabros et al., 2017; Stern et al., 2018). These seismic lines are long, narrow clearings (5-10 m wide) that have been associated with very slow recovery rates lasting over decades (Dabros et

al., 2017). When wind-driven wildfires in Alberta occur during the springtime, dry grass from the previous year could act as 'flashy' fuels to quickly spread the fire over the large network of seismic lines (Flat Top Complex Wildfire Review Committee, 2012; Robinne et al., 2016). The BL region is characterized by the highest density of seismic lines in Alberta (Stern et al., 2018). This region is also affected by commercial logging. Nevertheless, no fire management occurs in these forests as it is located in very remote parts of northwestern Alberta. The high density of seismic lines may explain why both BL fires experienced proportionately more high-severity burns than either the RC or WB fires that were associated with low human impact. In addition, regions that experienced higher severity fires recovered at comparatively lower rates than regions that experienced low severity fires, reflecting the lack of firefighting strategies that characterized the LSL fire.

Wood Buffalo National Park is Canada's largest National Park and is characterized by meadows, wetlands and prairies, and boreal forest stands (Parks Canada, 2020; UNESCO World Heritage Center, 2020). This region has minimal human influence and no fire management of any kind. Similarly, Richardson Wildland Provincial Park is characterized by wetlands, peat bogs, and mixed-wood boreal forests and has minimal human influence. Therefore, we considered both WB and RC to be low human impact sites. It is important to note that footprints of historic fires occurred in close proximity to these fire outbreaks or overlapped partially with both of the affected areas. Despite these similarities between sites, WB is spruce-dominated while RC is jack pine-dominated. The WB2007 fire burned with the lowest burn severity, while the WB2015 fire had the

highest burn severity; the RC2011 and WB2012 fires burned at similar levels of severity that were intermediate. Differences in burn-severity levels may have been a result of weather variations between years. In general, the NDVI and LAI index scores indicated a slower recovery rate compared with sites experiencing moderate and high human impact. Chen et al., (2014) also reported that coniferous species under artificial regeneration can grow significantly faster than artificial promotion recovery and natural regeneration in China. We also suggest that under natural conditions, recovery rates following wildfires proceed more slowly than when areas are influenced by human activities, and that these differ according to burn-severity levels. The advantage of the slower recovery rates means that fuel accumulation rates are slower, and therefore durations between fire recurrence are longer.

Johnstone et al., (2004) reported that the majority of tree establishment following wildfires in 36 permanent boreal forest plots occurred within three to seven years, with a decrease in aspen and pine density after ten years. We had data for 14 years of post-fire recovery for BL2004, 11 years for WB2007, and less than 10 years for all other sites. The BL fires followed a similar trend described by Johnstone et al., (2004), with both NDVI and LAI scores peaking at about nine years, but for the WB2007 fire, health levels did not peak even after the eleventh year of recovery. In the majority of cases, however, we observed a 100% mean recovery between two to six years following the fire outbreak. In all cases, we observed higher recovery rates with LAI scores than with NDVI. Past studies appear to have favored the use of NDVI in vegetation monitoring (Chu & Guo, 2014; Goetz et al., 2006; Serbin et al., 2013) over the use of LAI (Boer et al., 2008; Chen

et al., 2014; Chu & Guo, 2014). NDVI provides a measure of vegetation greenness, rather than a change in vegetation biomass and may reach its maximum before the ecosystem is fully recovered to its original state prior to the fire (Tanase et al., 2011; Wang et al., 2005). Therefore, the use of NDVI could be limited to the first decade of post-fire recovery depending on the location (Tanase et al., 2011). LAI on the other hand provides the ratio of leaf area per unit surface area on the ground (Zheng & Moskal, 2009) and could be related to processes such as photosynthesis, evapotranspiration, and carbon fluxes.

Mapping canopy species in fire-impacted and remote boreal forests can be difficult because of the lack of ground reference and the high cost of high-resolution images to cover a large spatial extent in a study such as ours. We opted to use Landsat images that are cost-free, available throughout the year for dates going back to the 1980s; however, the post-fire images that we obtained in the more recent decade yielded comparatively low accuracies. This is because of fewer ground reference points since we had to exclude locations in the burned areas for post-fire image classification. Accuracies for images with partial cloud cover were also lower because we had to reduce some of the ground reference locations.

There have been relatively few studies on the influence of water features on the post-fire recovery process, even though several recent studies have investigated the influence of wetlands on wildfire susceptibility and severity (Johnston et al., 2015; Thompson et al., 2017; Whitman et al., 2018). We observed slightly higher post-fire recovery rates and higher proportions of low severity or unburned areas closer to water

features than in areas further away from water, but this was only evident in the two regions with low human impact. This relationship was not evident or very weak for the regions with moderate or high human impact. Water features can provide refugia from the fire or help in the recovery process due to the higher water tables (Thompson et al., 2017). Although proximity to water features appears to influence the recovery process, our results suggest that fire management practices and the occurrence of seismic lines can and do interfere with any potential ameliorating effect.

5.6. Conclusions

Fire activity in the boreal forests of western Canada has drastically increased during the last few decades as a result of global climate change. These fires not only impact the wilderness regions but also influence human settlements and cause tremendous economic losses. On the other hand, human activity influences both natural wildfire occurrences as well as the post-fire recovery processes. Despite the level of human influence on these natural processes, the effect of anthropogenic activity on the post-fire recovery process in the boreal region is poorly understood. In this study, we investigated the post-fire recovery processes in the boreal forests of Alberta using RS-based techniques for locations with varying levels of human impact. The fire outbreak associated with the highest level of human impact (including fire management and high density of seismic lines) recovered fastest and suffered least from the ecological impacts of fire. Fire outbreaks with minimum human impact (too remote for fire management and no construction of seismic lines) were associated with the slowest recovery rate, while those experiencing moderate levels of human impact (high density of seismic lines

but no fire management) had intermediate rates of recovery. We used a simple two-season mapping approach to determine the pre-and post-fire canopy species distribution using Landsat images. These mapping approaches were consistent with patterns of natural canopy species recovery as well as effects of wildfire management strategies. We also documented ameliorating effects of water features on burn severity but found that human activities interfered with this relationship. We have developed a standardized RS strategy to compare sites across a large fire-prone region to generalize the influence of anthropogenic activities on both fire behavior and post-fire recovery patterns in Alberta's boreal forests.

5.7. Acknowledgments

The authors would like to thank Dr. Michael Waddington and Dr. Francoise-Nicolas Robinne for their feedback and for providing data sources. The authors also acknowledge J. DeBoer, Y. Zang, and S. Chen for the assistance on RS-based analysis. The project was funded by the Boreal Water Futures (BWF) of Global Water Futures (GWF).

5.8. Literature cited

Alberta Forest service. (1985). *Alberta Phase 3 Forest Inventory; An OverView* (ENR Report No. I/86). Alberta Energy and Natural Resources. https://open.alberta.ca/dataset/gda-dfa530fd-1e9d-4649-a984-fe3560a2fb93#detailed

Alberta Government. (2019). *West of 4th Meridian—Historical Forest Inventory—Phase 3 Maps—Open Government*. https://open.alberta.ca/dataset/gda-dfa530fd-1e9d-4649-a984-fe3560a2fb93

Barrett, K., McGuire, A. D., Hoy, E. E., & Kasischke, E. S. (2011). Potential shifts in dominant forest cover in interior Alaska driven by variations in fire severity. *Ecological Applications*, *21*(7), 2380–2396. https://doi.org/10.1890/10-0896.1

Boer, M. M., Macfarlane, C., Norris, J., Sadler, R. J., Wallace, J., & Grierson, P. F. (2008). Mapping burned areas and burn severity patterns in SW Australian eucalypt forest using remotely-sensed changes in leaf area index. *Remote Sensing of Environment*, *112*(12), 4358–4369.

Cao, C., Chen, W., Li, G., Jia, H., Ji, W., Xu, M., Gao, M., Ni, X., Zhao, J., & Zheng, S. (2011). The retrieval of shrub fractional cover based on a geometric-optical model in combination with linear spectral mixture analysis. *Canadian Journal of Remote Sensing*, *37*(4), 348–358.

Chen, W., Moriya, K., Sakai, T., Koyama, L., & Cao, C. (2014). Monitoring of post-fire forest recovery under different restoration modes based on time series Landsat data. *European Journal of Remote Sensing*, *47*(1), 153–168. https://doi.org/10.5721/EuJRS20144710

Chowdhury, E. H., & Hassan, Q. K. (2013). Use of remote sensing-derived variables in developing a forest fire danger forecasting system. *Natural Hazards*, *67*(2), 321–334.

Chu, T., & Guo, X. (2014). Remote sensing techniques in monitoring post-fire effects and patterns of forest recovery in boreal forest regions: A review. *Remote Sensing*, *6*(1), 470–520. https://doi.org/10.3390/rs6010470

Cleugh, H. A., Leuning, R., Mu, Q., & Running, S. W. (2007). Regional evaporation estimates from flux tower and MODIS satellite data. *Remote Sensing of Environment*, *106*(3), 285–304.

Cuevas-González, M., Gerard, F., Balzter, H., & Riaño, D. (2009). Analysing forest recovery after wildfire disturbance in boreal Siberia using remotely sensed vegetation indices. *Global Change Biology*, *15*(3), 561–577. https://doi.org/10.1111/j.1365-2486.2008.01784.x

Dabros, A., Hammond, H. J., Pinzon, J., Pinno, B., & Langor, D. (2017). Edge influence of low-impact seismic lines for oil exploration on upland forest vegetation in northern Alberta (Canada). *Forest Ecology and Management*, *400*, 278–288.

de Groot, W. J., Cantin, A. S., Flannigan, M. D., Soja, A. J., Gowman, L. M., & Newbery, A. (2013). A comparison of Canadian and Russian boreal forest fire regimes. *Forest Ecology and Management*, *294*, 23–34.

FAO, (Food and Agriculture Organizations of the United Nations). (2015). *Global forest resources assessment 2015.* http://www.fao.org/3/a-i4808e.pdf

Flannigan, M. D., Krawchuk, M. A., de Groot, W. J., Wotton, B. M., & Gowman, L. M. (2009). Implications of changing climate for global wildland fire. *International Journal of Wildland Fire*, *18*(5), 483–507.

Flat Top Complex Wildfire Review Committee. (2012). *Flat top complex, Submitted to the Minister of Alberta Environment and Sustainable Resource Development* (Pub No. T/272; p. 95). https://open.alberta.ca/dataset/a73f7285-020d-41d1-af5f-cf54faa381f1/resource/add3bd4b-5465-4797-bb09-64f8bdb1231e/download/flattopcomplex-wildfirereviewcommittee-a-may18-2012.pdf

Food and Agriculture Organization (FAO). (2010). *Global Forest Resources Assessment 2010—Main Report* (N Food and Agriculture Organization of the United Nations (FAO) Forestry Paper; FAO Volume 163).

Furyaev, V. V., Vaganov, E. A., Tchebakova, N. M., & Valendik, E. N. (2001). Effects of fire and climate on successions and structural changes in the Siberian boreal forest. *Eurasian Journal of Forest Research*, *2*, 1–15.

Gillett, N. P., Weaver, A. J., Zwiers, F. W., & Flannigan, M. D. (2004). Detecting the effect of climate change on Canadian forest fires. *Geophysical Research Letters*, *31*(18).

Gillis, M. D., Omule, A. Y., & Brierley, T. (2005). Monitoring Canada's forests: The national forest inventory. *The Forestry Chronicle*, *81*(2), 214–221.

Girardin, M. P., & Mudelsee, M. (2008). Past and future changes in Canadian boreal wildfire activity. *Ecological Applications*, *18*(2), 391–406.

Goetz, S. J., Fiske, G. J., & Bunn, A. G. (2006). Using satellite time-series data sets to analyze fire disturbance and forest recovery across Canada. *Remote Sensing of Environment*, *101*(3), 352–365.

Goldammer, J. G., & Furyaev, V. V. (1996). Fire in ecosystems of boreal Eurasia: Ecological impacts and links to the global system. In *Fire in ecosystems of Boreal Eurasia* (pp. 1–20). Springer.

Government of Canada, P. S. and P. C. (2009). *Canada's northern strategy: Our north, our heritage, our future : R3-72/2008-PDF - Government of Canada Publications - Canada.ca*. http://publications.gc.ca/site/eng/9.674653/publication.html?wbdisable=true

Gralewicz, N. J., Nelson, T. A., & Wulder, M. A. (2012). Factors influencing national scale wildfire susceptibility in Canada. *Forest Ecology and Management*, *265*, 20–29.

Hansen, M. C., Potapov, P. V., Moore, R., Hancher, M., Turubanova, S. A., Tyukavina, A., Thau, D., Stehman, S. V., Goetz, S. J., & Loveland, T. R. (2013). High-resolution global maps of 21st-century forest cover change. *Science*, *342*(6160), 850–853.

Hislop, S., Jones, S., Soto-Berelov, M., Skidmore, A., Haywood, A., & Nguyen, T. H. (2018). Using landsat spectral indices in time-series to assess wildfire disturbance and recovery. *Remote Sensing*, *10*(3), 460.

Johnston, D. C., Turetsky, M. R., Benscoter, B. W., & Wotton, B. M. (2015). Fuel load, structure, and potential fire behaviour in black spruce bogs. *Canadian Journal of Forest Research*, *45*(7), 888–899. https://doi.org/10.1139/cjfr-2014-0334

Johnstone, J. F., Chapin Iii, F. S., Foote, J., Kemmett, S., Price, K., & Viereck, L. (2004). Decadal observations of tree regeneration following fire in boreal forests. *Canadian Journal of Forest Research*, *34*(2), 267–273.

Jones, M. O., Kimball, J. S., & Jones, L. A. (2013). Satellite microwave detection of boreal forest recovery from the extreme 2004 wildfires in Alaska and Canada. *Global Change Biology*, *19*(10), 3111–3122. https://doi.org/10.1111/gcb.12288

Key, C. H., & Benson, N. C. (2005). Landscape assessment: Ground measure of severity, the Composite Burn Index; and remote sensing of severity, the Normalized Burn Ratio. *FIREMON: Fire Effects Monitoring and Inventory System*, *2004*.

Lentile, L. B., Holden, Z. A., Smith, A. M., Falkowski, M. J., Hudak, A. T., Morgan, P., Lewis, S. A., Gessler, P. E., & Benson, N. C. (2006). Remote sensing techniques to assess active fire characteristics and post-fire effects. *International Journal of Wildland Fire*, *15*(3), 319–345. https://doi.org/10.1071/WF05097

Liu, Q. J., Takamura, T., Takeuchi, N., & Shao, G. (2002). Mapping of boreal vegetation of a temperate mountain in China by multitemporal Landsat TM imagery. *International Journal of Remote Sensing*, *23*(17), 3385–3405. https://doi.org/10.1080/01431160110076171

Liu, W., Song, C., Schroeder, T. A., & Cohen, W. B. (2008). Predicting forest successional stages using multitemporal Landsat imagery with forest inventory and analysis data. *International Journal of Remote Sensing*, *29*(13), 3855–3872.

Magnussen, S., & Wulder, M. A. (2012). Post-fire canopy height recovery in Canada's boreal forests using Airborne Laser Scanner (ALS). *Remote Sensing*, *4*(6), 1600–1616.

Mann, M. L., Batllori, E., Moritz, M. A., Waller, E. K., Berck, P., Flint, A. L., Flint, L. E., & Dolfi, E. (2016). Incorporating anthropogenic influences into fire probability models: Effects of human activity and climate change on fire activity in California. *PLoS One*, *11*(4), e0153589.

Mbogga, M. S., Wang, X., & Hamann, A. (2010). Bioclimate envelope model predictions for natural resource management: Dealing with uncertainty. *Journal of Applied Ecology*, *47*(4), 731–740.

Natural Resources Canada. (2017). *Canadian Wildland Fire Information System | CWFIS Datamart*. https://cwfis.cfs.nrcan.gc.ca/datamart

Parks Canada, G. of C. (2020, May 29). *Wood Buffalo National Park*. https://www.pc.gc.ca/en/pn-np/nt/woodbuffalo

Peckham, S. D., Ahl, D. E., Serbin, S. P., & Gower, S. T. (2008). Fire-induced changes in green-up and leaf maturity of the Canadian boreal forest. *Remote Sensing of Environment*, *112*(9), 3594–3603.

Robinne, F.-N., Parisien, M.-A., & Flannigan, M. (2016). Anthropogenic influence on wildfire activity in Alberta, Canada. *International Journal of Wildland Fire*, *25*(11), 1131–1143. https://doi.org/10.1071/WF16058

Rouse, J. W., Haas, R. H., Schell, J. A., & Deering, D. W. (1974). Monitoring vegetation systems in the Great Plains with ERTS. *NASA Special Publication*, *351*, 301–317.

Samiappan, S., Hathcock, L., Turnage, G., McCraine, C., Pitchford, J., & Moorhead, R. (2019). Remote sensing of wildfire using a small unmanned aerial system: Post-fire mapping, vegetation recovery and damage analysis in Grand Bay, Mississippi/Alabama, USA. *Drones*, *3*(2), 43.

Serbin, S. P., Ahl, D. E., & Gower, S. T. (2013). Spatial and temporal validation of the MODIS LAI and FPAR products across a boreal forest wildfire chronosequence. *Remote Sensing of Environment*, *133*, 71–84.

Stern, E. R., Riva, F., & Nielsen, S. E. (2018). Effects of narrow linear disturbances on light and wind patterns in fragmented boreal forests in northeastern Alberta. *Forests*, *9*(8), 486.

Stocks, B. J., Mason, J. A., Todd, J. B., Bosch, E. M., Wotton, B. M., Amiro, B. D., Flannigan, M. D., Hirsch, K. G., Logan, K. A., & Martell, D. L. (2002). Large forest fires in Canada, 1959–1997. *Journal of Geophysical Research: Atmospheres*, *108*(D1), FFR5.1-FFR5.12. https://doi.org/10.1029/2001JD000484

Tanase, M., de la Riva, J., Santoro, M., Pérez-Cabello, F., & Kasischke, E. (2011). Sensitivity of SAR data to post-fire forest regrowth in Mediterranean and boreal forests. *Remote Sensing of Environment*, *115*(8), 2075–2085. https://doi.org/10.1016/j.rse.2011.04.009

Thompson, D. K., Parisien, M.-A., Morin, J., Millard, K., Larsen, C. P. S., & Simpson, B. N. (2017). Fuel accumulation in a high-frequency boreal wildfire regime: From wetland to upland. *Canadian Journal of Forest Research*, *47*(7), 957–964. https://doi.org/10.1139/cjfr-2016-0475

UNESCO World Heritage Center. (2020). *Wood Buffalo National Park*. UNESCO World Heritage Centre. https://whc.unesco.org/en/list/256/

Wang, Q., Adiku, S., Tenhunen, J., & Granier, A. (2005). On the relationship of NDVI with leaf area index in a deciduous forest site. *Remote Sensing of Environment*, *94*(2), 244–255.

Watson, D. J. (1947). Comparative physiological studies on the growth of field crops: I. Variation in net assimilation rate and leaf area between species and varieties, and within and between years. *Annals of Botany*, *11*(41), 41–76.

White, J., Ryan, K., Key, C., & Running, S. (1996). Remote Sensing of Forest Fire Severity and Vegetation Recovery. *International Journal of Wildland Fire*, *6*(3), 125. https://doi.org/10.1071/WF9960125

Whitman, E., Parisien, M.-A., Thompson, D. K., Hall, R. J., Skakun, R. S., & Flannigan, M. D. (2018). Variability and drivers of burn severity in the northwestern Canadian boreal forest. *Ecosphere*, *9*(2), e02128. https://doi.org/10.1002/ecs2.2128

Wulder, M. A., Kurz, W. A., & Gillis, M. (2004). National level forest monitoring and modeling in Canada. *Progress in Planning*, *61*(4), 365–381.

Yang, G., Di, X., Guo, Q., Shu, Z., Zeng, T., Yu, H., & Wang, C. (2011). The impact of climate change on forest fire danger rating in China's boreal forest. *Journal of Forestry Research*, *22*(2), 249–257.

Zheng, G., & Moskal, L. M. (2009). Retrieving leaf area index (LAI) using remote sensing: Theories, methods and sensors. *Sensors*, *9*(4), 2719–2745.

Table 5.1 Duration and number of fires, total affected areas, and level of human impact associated with each fire event in this study.

Fire event	Fire Season	Number of fire outbreaks	Total affected area (km^2)	Level of human impact
LSL 2011	2011-05-04 to 2011-05-17	1	202.25	High
BL 2004	2004-07-12 to 2004-09-26	3	1371.50	Moderate
BL2012	2012-06-22 to 2012-09-23	2	2142.60	Moderate
RC 2011	2011-05-14 to 2011-07-06	1	5217.00	Low
WB 2007	2007-05-29 to 2007-08-01	2	1702.00	Low
WB 2012	2012-05-26 to 2012-09-28	7	1372.10	Low
WB 2015	2015-05/28 to 2015-10-01	6	2937.4	Low

Table 5.2 Landsat images used for the time series data analysis (Note: L5, L7, and L8 stands for Landsat 5, Landsat 7, and Landsat 8)

Period	Image dates and sensors						
	LSL	BL2004	BL2012	RC	WB2007	WB2012	WB2015
Before	2010/06/09 L7 2010/07/21 L7	2003/08/30 L5 2003/09/01 L5	2011/09/14 L5	2010/07/23 L7 2010/08/24 L7	2006/09/04 L5	2009/08/11 L5	2014/05/14 L8 2014/06/13 L8
During	2011/08/09 L7 2011/08/25 L7	2004/09/26 L5	2012/05/28 L7 2012/08/07 L7	2011/09/04 L5	2007/06/03 L5 2007/07/21 L5	2010/06/12 L7 2010/06/19 L7	2015/09/29 L8
Post 1	2012/08/11 L7 2012/08/20 L7	2005/08/12 L5	2013/07/10 L7	2012/06/26 L7 2012/07/28 L7	2008/08/08 L5	2011/09/10 L7	2016/09/06 L8 2016/08/23 L8
Post 2	2013/08/06 L8	2006/08/31 L5	2014/06/26 L7	2013/08/17 L8 2013/08/31 L8	2009/08/11 L5	2012/08/27 L7	2017/08/01 L8
Post 3	2014/07/01 L8	2007/08/18 L5	2015/05/20 L8	2014/08/04 L8	2010/06/12 L7 2010/06/19 L7	2013/06/03 L8	2018/07/27 L8

Post 4	2015/08/12 L8	2008/07/03 L5	2016/05/22 L8	2015/08/30 L8	2011/09/10 L7	2014/05/14 L8 2014/06/13 L8	-
Post 5	2016/08/30L8	2009/08/15 L5	2017/08/29 L8	2016/08/09 L8 2016/08/23 L8	2012/08/27 L7	2015/09/29 L8	-
Post 6	2017/07/25 L7	2010/05/29 L5	2018/05/21 L8	2017/08/28 L8	2013/06/03 L8	2016/09/06 L8 2016/08/23 L8	-
Post 7	2018/07/28 L8	2011/09/14 L5	-	2018/07/05 L8	2014/05/14 L8 2014/06/13 L8	2017/08/01 L8	-
Post 8	-	2012/05/28 L7 2012/08/07 L7	-	-	2015/09/29 L8	2018/07/27 L8	-
Post 9	-	2013/07/10 L7	-	-	2016/09/06 L8 2016/08/23 L8	-	-
Post 10	-	2014/06/26 L7	-	-	2017/08/01 L8	-	-

Post 11	-	2015/05/20 L8	-	-	2018/07/27 L8	-	-
Post 12	-	2016/05/22 L8	-	-	-	-	-
Post 13	-	2017/08/29 L8	-	-	-	-	-
Post 14	-	2018/05/21 L8	-	-	-	-	-

Table 5.3 Satellite images used for tree species mapping before and after the LSL, RC, WB 2007, 2012, and 2015, and the BL 2004 and 2012. (Note: L5, L7, and L8 refer to Landsat 5, Landsat 7, and Landsat 8, respectively).

Fire	Year	First season image		Second season image	
		Date	Sensor	Date	Sensor
LSL Fire	1986	1986/06/02	L5	1986/08/28	L5
	2010	2010/06/20	L5	2010/09/24	L5
	2011	2011/07/25	L5	2011/09/27	L5
	2013	2013/06/28	L8	2013/08/31	L8
	2015	2015/05/17	L8	2015/08/12	L8
	2016	2016/06/20	L8	2016/08/30	L8
	2017	2017/05/29	L8	2017/07/25	L8
RC Fire	1985	1985/07/03	L5	1985/08/18 1985/09/28	L5 L5
	2010	2010/07/22 2010/07/24	L5 L5	2010/10/03	L5
	2015	2015/08/30	L8	2015/10/01	L8
	2017	2017/06/25	L8	2017/08/26	L8
WB Fires	1985	1985/07/17 1985/07/31	L5 L5	1985/09/10	L5
	1997	1997/06/23	L5	1997/08/26	L5
	1998	1998/06/10	L5	1998/08/26	L5
	2017	2017/08/01	L8	2017/09/18	L8
BL Fires	1985	1985/06/02	L5	1985/08/21	L5
	2002	2002/06/09	L7	2002/09/13	L7
	2006	2006/06/12	L5	2006/08/31	L5
	2008	2008/05/16	L5	2008/07/03	L5

	2016	2016/05/22 2016/06/07	L8 L8	2016/07/18	L8

Table 5.4 Overall and canopy species mapping accuracy of time series species maps for LSL, RC, WB 2007, 2012, and 2015, and the BL 2004 and 2012 fires.

Fire	Focal year	All Classes		Canopy species	
		Overall accuracy (%)	Kappa	Overall accuracy (%)	Kappa
LSL	1986	82.13	0.75	79.38	0.57
	2010	80.92	0.74	80.44	0.61
	2011	81.93	0.75	77.74	0.54
	2013	78.51	0.71	78.47	0.57
	2015	82.22	0.76	75.74	0.48
	2016	79.28	0.72	73.65	0.47
	2017	80.68	0.74	73.99	0.47
RC	1985	92.65	0.88	91.66	0.72
	2010	88.20	0.80	85.21	0.73
	2015	68.20	0.55	72.62	0.47
	2017	65.41	0.51	75.48	0.43
WB	1985	90.09	0.87	83.75	0.66
	1997	66.05	0.55	65.76	0.57
	1998	82.47	0.76	77.22	0.51
	2017	80.26	0.73	76.19	0.49
BL	1985	88.89	0.76	89.81	0.67
	2002	79.53	0.68	84.60	0.55
	2006	79.38	0.66	83.98	0.69
	2008	77.75	0.64	78.02	0.60
	2016	88.25	0.83	80.54	0.61

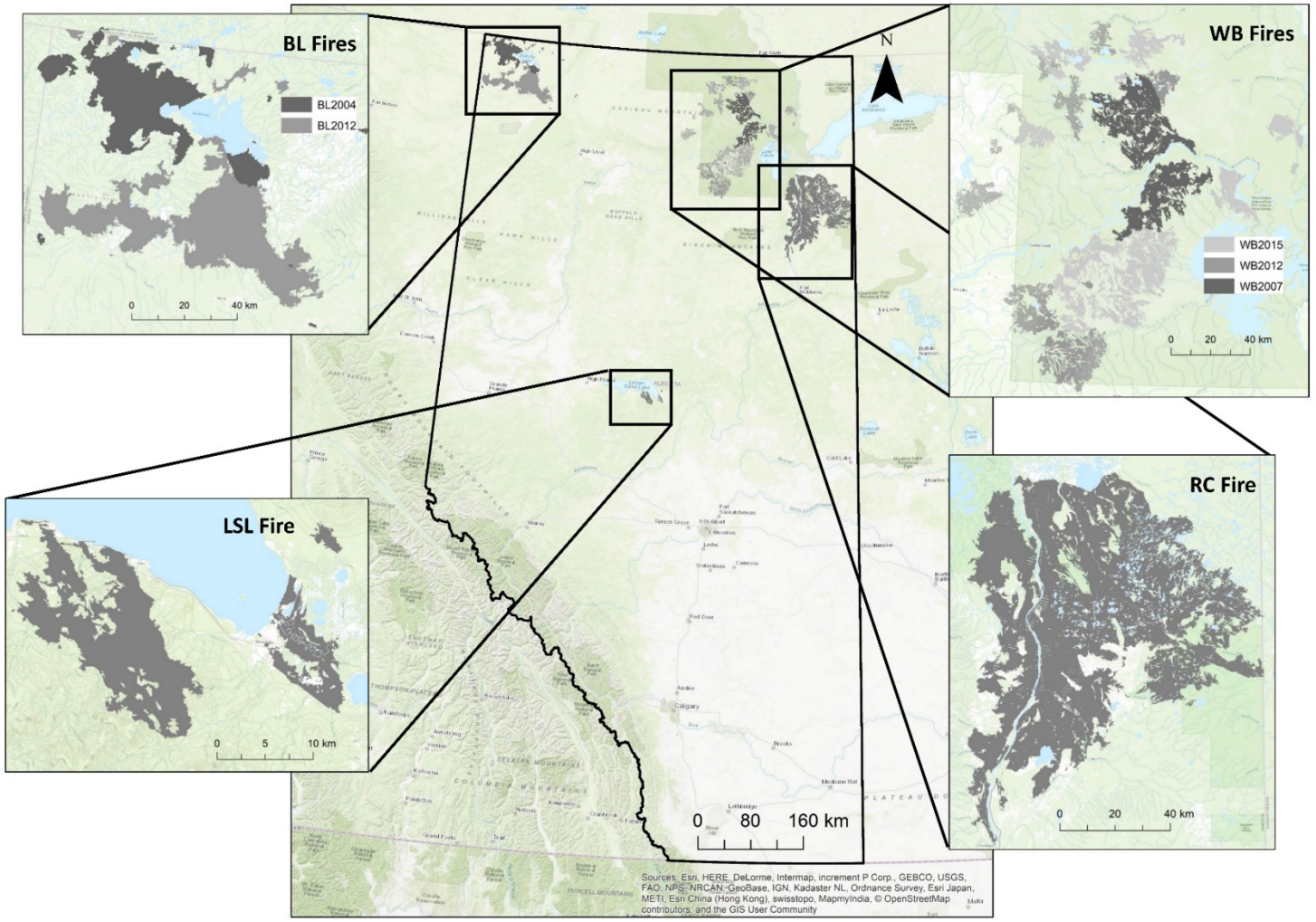

Fig 5.1 Location of fire events in four regions of Alberta's boreal forests in this study (Base map: ESRI topographic maps).

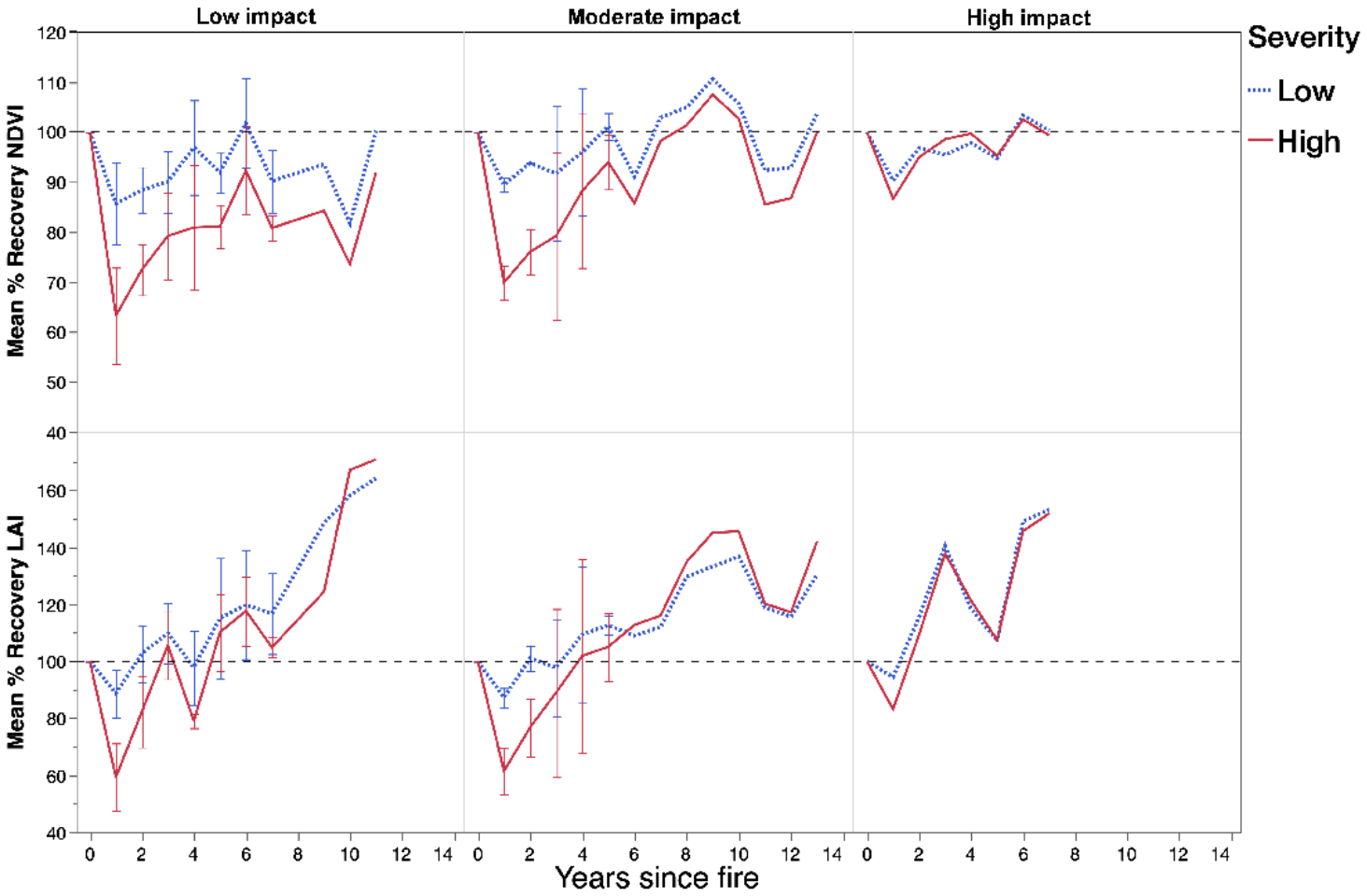

Fig 5.2 Mean percent recovery using NDVI (top panel) and LAI (bottom panel) for (a) low, (b) moderate, and (c) high levels of human impact. Lines join means (± SE) calculated for each year where applicable.

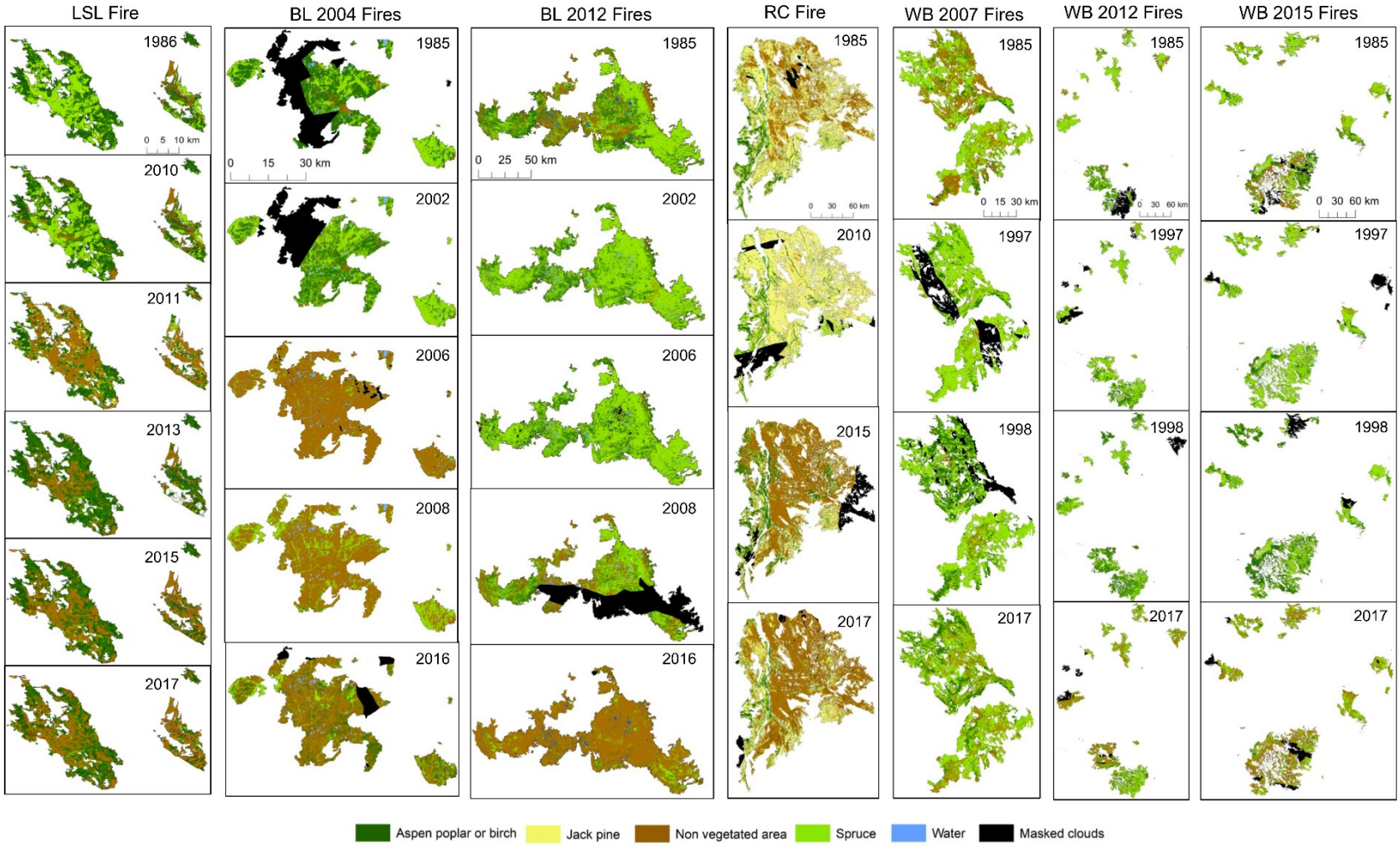

Fig 5.3 Time-series maps of canopy species distributed in areas affected by the seven fire outbreaks in this study.

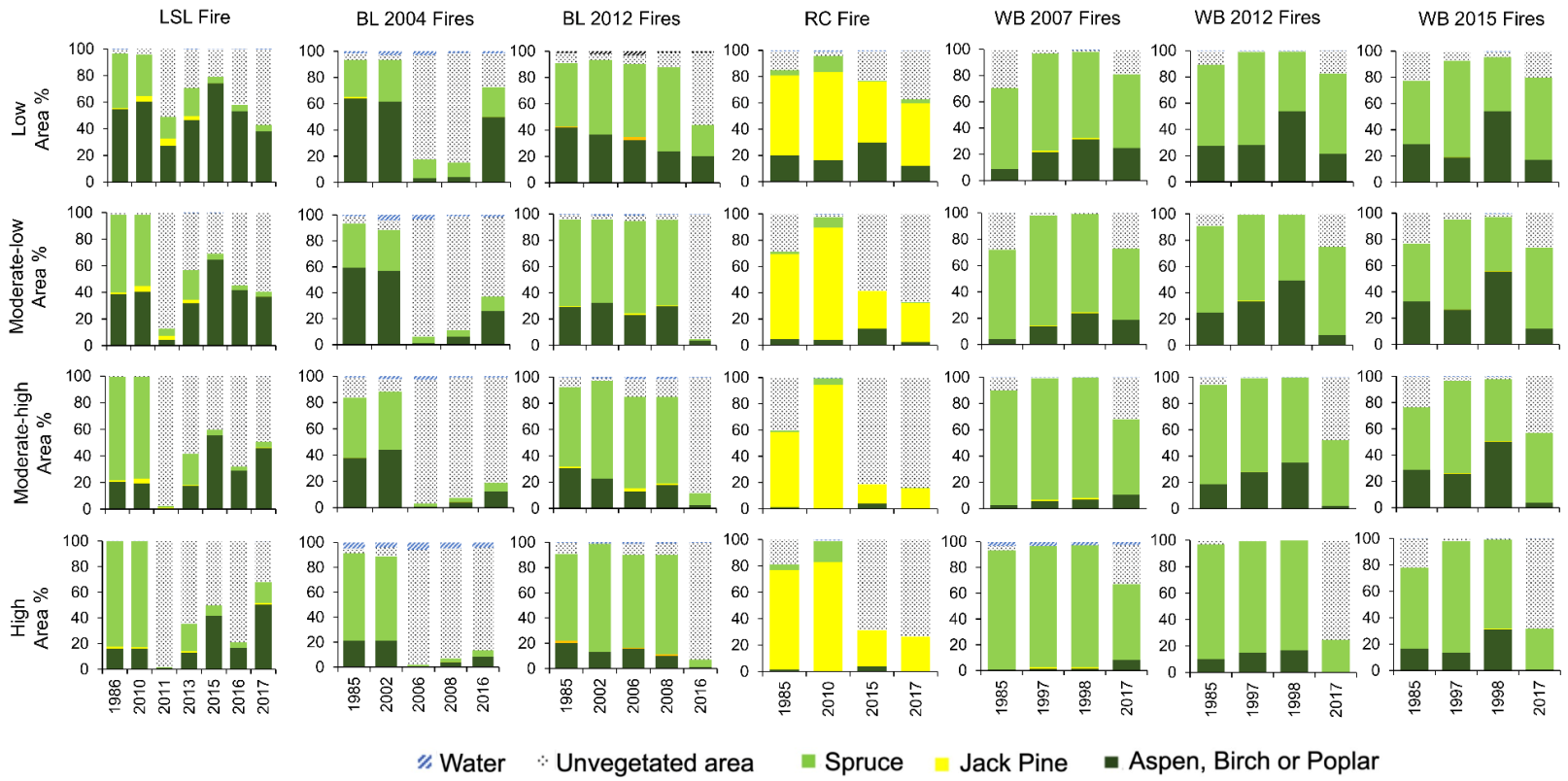

Fig 5.4 Change in percentage cover of canopy species over time in each of the seven fire outbreaks in this study, after sorting the data by the degree of burn severity (i.e. low, moderate-low, moderate-high, and high severity).

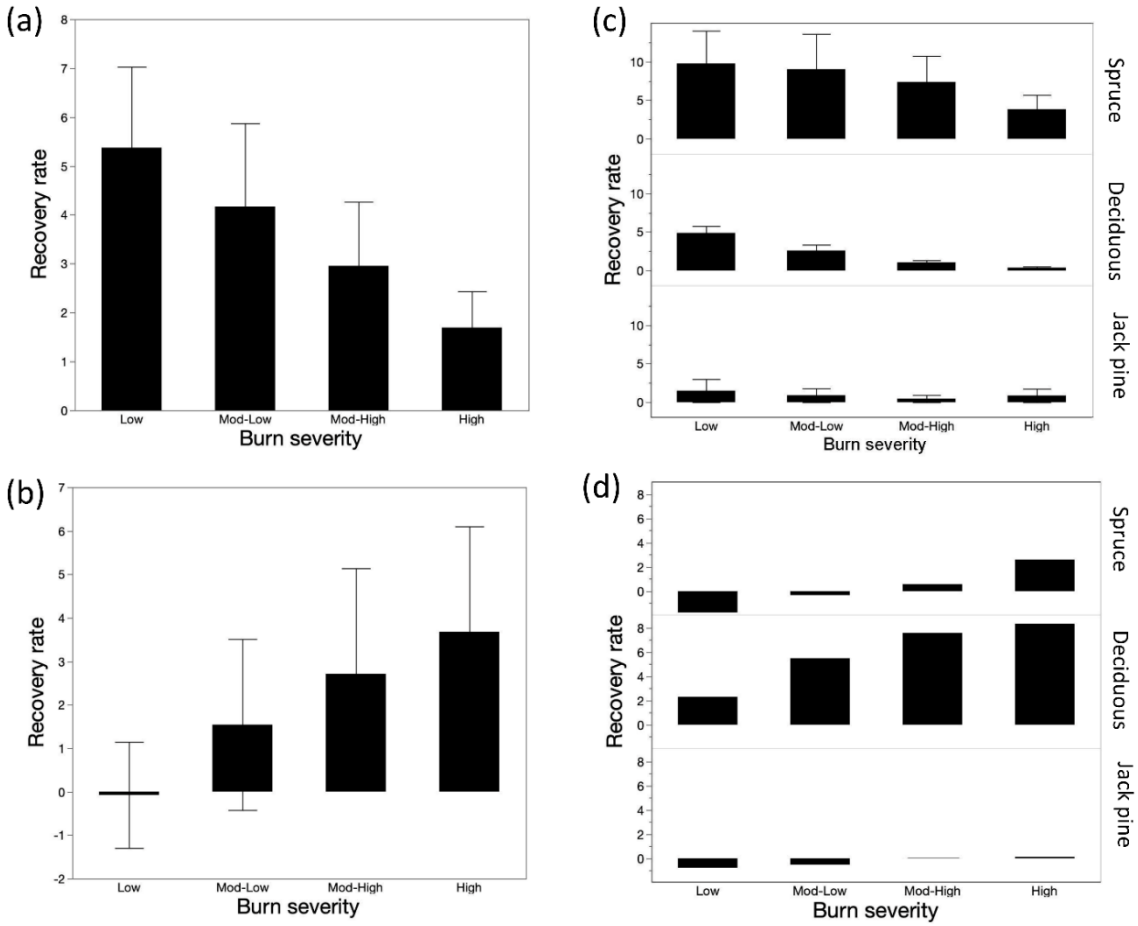

Fig 5.5 Recovery rate of canopy species for different levels of burn severity when all canopy species were considered within (a) moderate and low human-impacted sites and (b) only high human-impacted site. The recovery rate of canopy species for the same information plotted in (a) and (b) but shown separately for the dominant coniferous and deciduous taxa in (c) moderate and low human-impacted sites and (d) high human-impacted site.

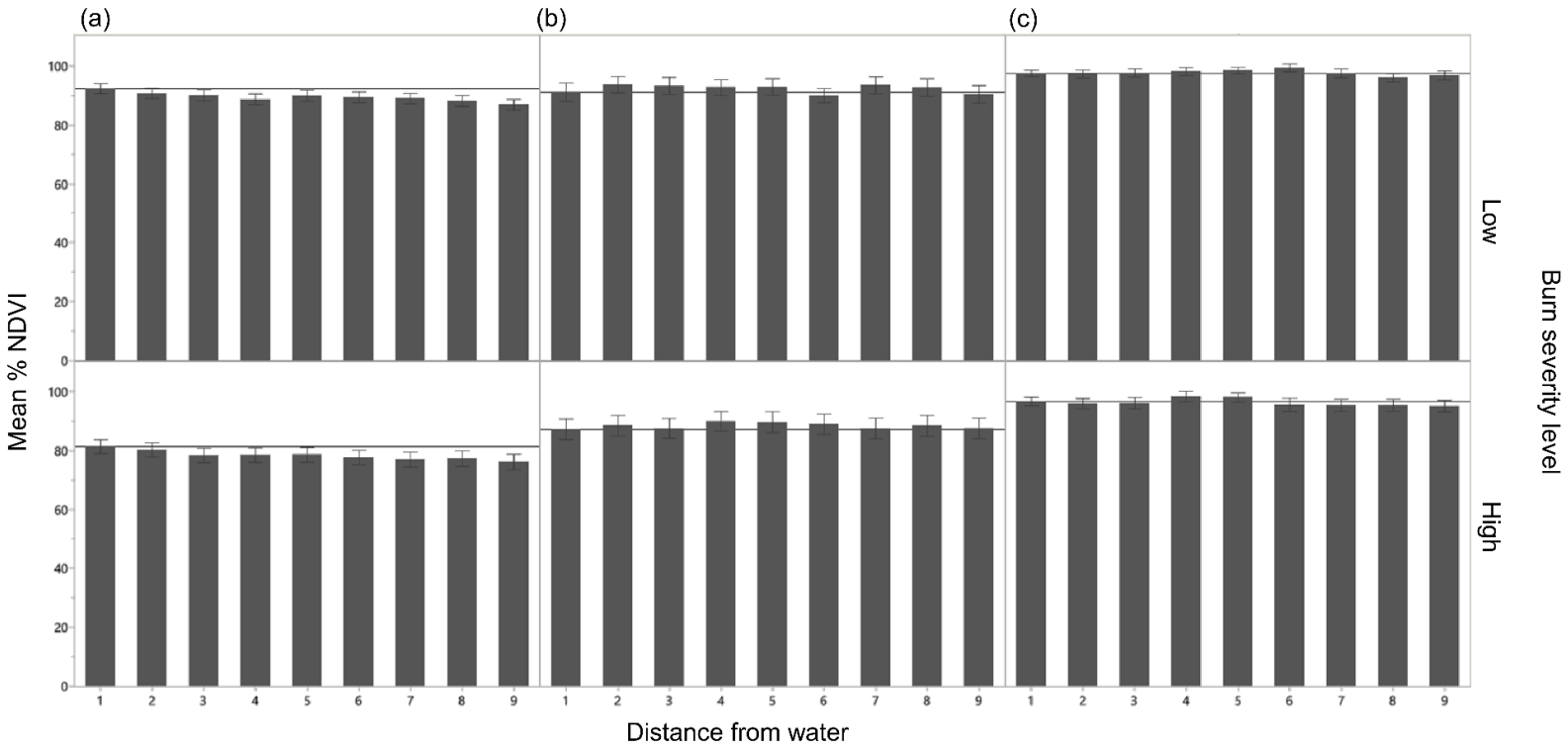

Fig 5.6 Mean percent recovery of pre-burn NDVI scores as a function of distance from water features for low burn-severity level (top panel) and high burn-severity level (bottom panel) for regions experiencing (a) low, (b) moderate, and (c) high human impact. (Note: categories 1 to 9 on the X-axis corresponds to 50, 100, 150, 200, 250, 500, 1000, 1500, and 200 m buffer zones from water features, respectively)

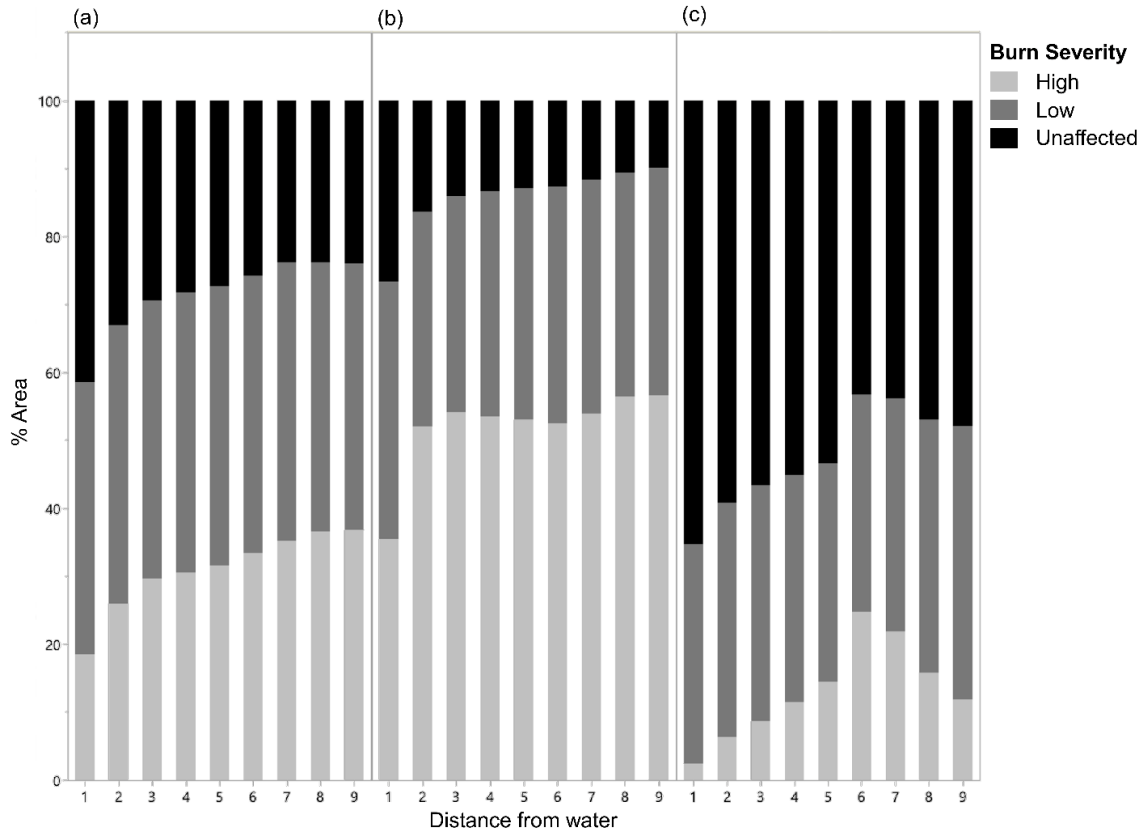

Fig 5.7 Percent area of unburned, low, and high burn-severity levels sorted by distance from water features for (a) low, (b) moderate, and (c) high human impact levels (Note: categories of 1 to 9 on the X-axis corresponds to 50, 100, 150, 200, 250, 500, 1000, 1500, and 200 m buffer zones from water features, respectively).

Chapter 6. Conclusions and Recommendations

6.1. Summary

Ecosystems are affected by different stress factors of both natural and anthropogenic origin. In the past few decades, not only the stress factors of anthropogenic origin have increased, but also the stress factors of natural origin have enhanced due to human activity. The overall objective of my thesis was to develop novel GIS- and RS-based methodologies to understand and manage a stress factor of anthropogenic origin in wetland ecosystems and a stress factor of natural origin on the terrestrial ecosystems. Chapters 2 and 3 investigated the mapping strategies to identify invasive *Phragmites* on Lake Erie Wetlands for effective management. Chapters 4 and 5 evaluated the pre-and post-fire effects of wildfires on the boreal forests of Alberta.

In Chapter 2, we investigated the phenological stage of *Phragmites* that produce the most unique spectral signature using a time series of freely available moderate resolution Landsat and Sentinel 2 images using two highly invaded Lake Erie wetlands. We identified late summer and fall to be the best period to map *Phragmites* using RS-based classification approaches as *Phragmites* produced the most unique signature during this time of the year. Green, NIR, and SWIR reflectance of *Phragmites* differed from the two most confused vegetation classes with *Phragmites,* cattail and meadow marsh, during this time of the year. Meadow marsh produced a more different signature than *Phragmites* in the winter months, but there was more confusion with other vegetation classes and therefore, the overall mapping accuracy was reduced. We were able to obtain better mapping accuracy when meadow marsh mapped in winter was combined with maps of

other classes produced using images acquired in summer months. We further extended the findings of this research to investigate the *Phragmites* treatment effectiveness, to identify *Phragmites* distribution in inland wetlands and roadsides of Norfolk county, and to map *Phragmites* distribution in roadside ditches of major highways using multitemporal Sentinel 2 images successfully in three separate projects that are not a part of this thesis. Overall, our study shows that moderate resolution images could be effectively used to map large *Phragmites* stands if the images are collected at right time with the right bands.

In Chapter 3, we further investigated the *Phragmites* mapping approaches to map small, less dense *Phragmites* stands in the same Lake Erie wetland. Here, we used commercially available, high-resolution WV2/3 images and freely available, moderate resolution Sentinel 2 images to map *Phragmites* using sub-pixel image classification techniques. With WV2/3 images, we were able to map both large and relatively small, less density *Phragmites* stands with accuracy levels above 80%. However, Sentinel 2 images only gave an acceptable level of accuracy for the large, *Phragmites* mono stands. We used the mapping protocols developed during this study to map the *Phragmites* distribution in the Long Point wetlands complex and aided the treatment programs in the summer of 2020 and treatment planning of summer 2021. We also used the maps produced in this study to aid habitat identification of at-risk turtle species (Angoh et al. Unpublished data).

In Chapter 4, we investigated how canopy species distribution and proximity to water features affect the burn severity of wildfires in Alberta using novel mapping

approaches developed using time-series Landsat images. We were able to successfully map the distribution of deciduous species (aspen, birch, or poplar), spruce (black or white), and jack pine using Landsat images collected in two seasons with a good level of accuracy. Our results suggest that the coniferous species lead to high burn severity while deciduous species lead to low burn severity. We also created a novel score, SBIS, by combining the average dNBR of a fire outbreak and the total area burned. This index helps to easily compare the burn impact of different fire outbreaks and it showed a better correlation with pre-fire canopy species distribution. We also found that the water features such as lakes, rivers, and ponds can reduce the burn impact up to 1 km distance from them. Overall, this study shows that the pre-fire canopy species distribution and distance to water features can influence the burn severity levels and the burn impact and aids to understand the behavior of fire over large spatial scales.

In Chapter 5 we evaluated the post-fire recovery of the same fire events that we studied in Chapter 4. Here, we specifically looked at the influence of human impact (proximity to human settlements and density of seismic lines) on the post-fire recovery process in three impact levels: high (fire management and seismic lines), moderate (only seismic lines, no fire management), and low (no fire management or seismic lines) using two RS-based indices and species recovery rates. We also explored the influence of water features on the post-fire recovery process. Our results show that the fire outbreak with high human impact recovered faster than the sites with moderate and low human impact and had the least burn impact. The sites that had a low human impact had the slowest recovery and the sites with moderate human influence had a moderate level of recovery

rates. Our species level recovery analysis reflected the fire management practices in the site with the highest human influence to prevent possible future fire outbreaks. This analysis also showed the natural recovery process in the moderate and low human impact sites where recovery rates of coniferous species were faster than the deciduous species. Our study also shows an ameliorating effect of water features such as lakes and rivers in the sites that had low human influence, but human activities may interfere with this effect. Overall, this study provides a new insight to understand how human interference can affect the natural post-fire recovery process in the boreal forests of Alberta.

6.2. Recommendations

Based on the findings of this thesis, we propose several recommendations in mapping and managing *Phragmites* in affected areas and on documenting and managing wildfires in western Canada.

1. For effective *Phragmites* mapping strategies, I recommend using images acquired in late summer or fall periods, regardless of the sensor used. Also, I recommend using SWIR bands if available in the sensor used, because our study shows that the SWIR signal differs from the signal of the confused vegetation classes, most probably as a result of water use efficiency of *Phragmites* during this time of the year.
2. If the wetland classes other than *Phragmites* are of interest, I recommend using images collected in winter, preferably February or March (snow-covered images) to map meadow marsh and then combine it with the maps produced using the

images acquired in summer/fall periods. This will improve the mapping accuracy of both *Phragmites* and meadow marsh as well as the other wetland vegetation.

3. I also recommend using the optimum level of ground reference to aid the classification process, regardless of the classification method being used. I observed a significant improvement in classification accuracy levels when the number of ground reference points is increased. However, the accuracy levels went down after a certain threshold with the addition of further points. Therefore, I recommend repeated classification and accuracy assessment as well as spectral separability analysis with varying amounts of ground reference points to identify the optimum level of ground reference to produce the most accurate maps.
4. I also recommend masking out the ecologically irrelevant land cover classes such as roads, agricultural lands, and build-up areas to avoid unwanted misclassifications within the area of interest. Mapping wetland vegetation could be challenging due to spectrally similar yet, ecologically different vegetation communities. Also, the high level of reflectance from water interferes with the vegetation signal and leads to misclassifications. This is especially problematic when locations with bright water reflectance are present and that often confuses with the bright signal from the buildings, most possibly the glass or highly reflective surfaces. Removal of the irrelevant, neighboring classes can improve the classification accuracies of these confused vegetation classes and reduce the image processing time.

5. I recommend using SBIS over dNBR when comparing different fire outbreaks and describing different pre-fire conditions. This novel score combined the burn severity with the area that is being burnt and therefore gives a more generalized idea about the impact of the fire outbreak.
6. The canopy species mapping approach we used in this study is relatively simple to use yet effective. Furthermore, we were able to map the canopy species at their regrowth after fire using the ground reference from the neighboring, unaffected regions. Therefore, I recommend using this mapping approach to map forested regions in remote parts of western Canada using the ground reference from the areas that are being surveyed.
7. Human activities such as fire management and oil and gas exploration affect the natural fire regimes and recovery processes. The human factor in understanding wildfires in boreal forests is becoming increasingly important due to enhanced human activity in these forested regions. Therefore, I recommend considering the influence of human activity in developing models to predict the future of fire regimes and recovery trajectories.

6.3. Future Work

Upon completion of this thesis, I have identified several new research projects to be conducted in the future. These new research projects involve both repeated use of the methodologies developed in this thesis and developing new RS-based methodologies to understand ecological questions that are important in managing ecosystem health and stress.

1. Global climate change has affected the wetland ecosystems and their species communities. According to Eller et al., (2017), *Phragmites* show high phenotypic plasticity and can well respond to climate change. The *Phragmites* mapping protocols developed with free satellite data in my second chapter could be used to map the *Phragmites* distribution in wetland ecosystems over the past two decades to investigate its growth patterns and rates in relation to changing climate conditions. This would aid the prediction of future *Phragmites* invasion trajectories and develop effective management strategies.
2. Climate change mediated surface water level fluctuations have caused serious ecological impacts in the Great Lakes ecosystems (Gronewold et al., 2013). In addition to climate change-related water level changes, *Phragmites* invasions also alter the hydrological regimes in the invaded Great Lakes wetlands (Lathrop et al., 2003; Meyerson et al., 2000) and may result in devastating effects on the native vegetation communities and may alter the habitats of wetland fauna. Fine-scale *Phragmites* mapping protocols with WV2/3 images developed in chapter 3 could be used to understand these hydrological and vegetation community shifts in relation to global climate change. Furthermore, the mapping approaches we developed could be used in other high-resolution images from Unmanned Aerial Vehicles (UAV) or hyperspectral images to investigate the effect of *Phragmites* invasions on hydrological alterations within the wetland ecosystems.
3. The distribution of native *Phragmites* haplotype in Ontario is poorly understood. The rapid spread of the invasive haplotype may over-compete the native

haplotype and may displace it from its original habitats. Therefore, mapping the distribution of the native *Phragmites* haplotype is essential for conservation purposes. RS-based mapping protocols need to be developed to distinguish between the native and invasive *Phragmites* haplotypes and the distribution of the native haplotype needs to be mapped and documented.

4. *Phragmites* is treated in affected wetlands annually using both chemical and mechanical methods (Gilbert, 2015). The image classification methods developed in this thesis could be used to study the treatment effectiveness in the invaded wetlands using RS-based change detection techniques. These methods also could be used to compare the effectiveness of different treatment methods.
5. The effect of seismic lines on the boreal vegetation communities and wildfire is poorly understood (Robinne et al., 2016). The species mapping protocols and the RS-based approaches we developed to understand the pre-and post-fire conditions could be used to understand the effect of seismic lines in detail on wildfire impact and post-fire health recovery trajectories.
6. The RS-based techniques we used for Alberta could be used to study the fire outbreaks in different geographical and ecological settings to investigate the repeatability of our methods as well as to understand the ecological importance and influence of wildfires in these settings. Parry sound 33 fire that occurred in the summer of 2018 in Ontario is one such example. This fire affected forested and wetlands ecosystems of northeastern Georgian bay (Markle et al., 2020), and

it is a good case study to investigate the effect of wetlands and water features on the fire severity levels as well as the post-fire recovery processes.

7. Wildfire activity in western Canada is highly influenced by climatic variations. Linking the climate variables such as annual temperature and precipitation to the fire distribution and post-fire recovery patterns we investigated in this study may provide a better understanding of the changing fire dynamics and influence of human activity on fire regimes.

6.4. Literature cited

Eller, F., Skálová, H., Caplan, J. S., Bhattarai, G. P., Burger, M. K., Cronin, J. T., Guo, W.-Y., Guo, X., Hazelton, E. L. G., Kettenring, K. M., Lambertini, C., McCormick, M. K., Meyerson, L. A., Mozdzer, T. J., Pyšek, P., Sorrell, B. K., Whigham, D. F., & Brix, H. (2017). Cosmopolitan Species As Models for Ecophysiological Responses to Global Change: The Common Reed Phragmites australis. *Frontiers in Plant Science*, *8*. https://doi.org/10.3389/fpls.2017.01833

Gilbert, J. (2015). *Rondeau Provincial Park Invasive Phragmites Management Program 2008–2014 Summary Report and Recommended Next Steps*. Unpublished manuscript.

Gronewold, A. D., Fortin, V., Lofgren, B., Clites, A., Stow, C. A., & Quinn, F. (2013). Coasts, water levels, and climate change: A Great Lakes perspective. *Climatic Change*, *120*(4), 697–711. https://doi.org/10.1007/s10584-013-0840-2

Lathrop, R. G., Windham, L., & Montesano, P. (2003). Does Phragmites expansion alter the structure and function of marsh landscapes? Patterns and processes revisited. *Estuaries*, *26*(2), 423–435. https://doi.org/DOI: 10.1007/BF02823719

Markle, C. E., Wilkinson, S. L., & Waddington, J. M. (2020). Initial Effects of Wildfire on Freshwater Turtle Nesting Habitat. *The Journal of Wildlife Management*, *84*(7), 1373–1383. https://doi.org/10.1002/jwmg.21921

Meyerson, L. A., Saltonstall, K., Windham, L., Kiviat, E., & Findlay, S. (2000). A comparison of Phragmites australisin freshwater and brackish marsh environments in North America. *Wetlands Ecology and Management*, *8*(2–3), 89–103. https://doi.org/10.1023/A:1008432200133

Robinne, F.-N., Parisien, M.-A., & Flannigan, M. (2016). Anthropogenic influence on wildfire activity in Alberta, Canada. *International Journal of Wildland Fire*, *25*(11), 1131–1143. https://doi.org/10.1071/WF16058

Chapter 7/Appendix A: Use of World View 3 (WV 3) satellite imagery for early detection of invasive *Phragmites australis* in roadway corridors in Ontario

By,

Prabha Amali Rupasinghe and Patricia Chow-Fraser

Rupasinghe, P.A., & Chow-Fraser, P. (2018). Use of World View 3 (WV 3) satellite imagery for early detection of invasive *Phragmites australis* in roadway corridors in Ontario. Report prepared for the Ontario Ministry of Transportation, St. Catharine's, ON. 23 pages.

7.1. Abstract

We tested the suitability of high-resolution (80 cm) multi-spectral satellite data from World View 3 (WV 3) to detect small patches of invasive *Phragmites* within 20-m buffer of the centre-line of the road. We used ENVI 5.5 to classify the image into seven classes: roads, trees, *Phragmites,* roadsides, ground, grass, and agriculture. We applied the Mixture-Tuned Match Filtering (MTMF) procedure to the image, which is a spectral unmixing method in which the target features could be separated out from the other background features in mixed pixels. The highest confusion with *Phragmites* were with grasses and agricultural lands. Accuracy of the *Phragmites* classification was higher for the MTMF image (81.6% producer's and 75.6% user's accuracy) than for the reflectance image (73.7% producer's and 71.4% user's accuracy), while overall accuracy was 84.4% and 74.6%, for the MTMF and the reflectance image, respectively. We conclude that WV 3 can be used in early-detection programs, as long as the procedure is applied to a relatively small area in wetlands (maximum 100 ha) or roadsides (4-km segment) to increase accuracy and publishing requirements necessary to achieve the best possible product.

Keywords: Invasive *Phragmites*, early detection, road maintenance, remote sensing

7.2. Executive Summary

Phragmites australis (the common reed) is a taxonomically diverse perennial grass, with 27 genetically distinct groups throughout the world, 11 of which are found in North America. One of the European haplotypes, M, is an aggressive invader in coastal

wetlands and roadway corridors and have been growing at the expense of native vegetation in many coastal marshes of the lower Great Lakes. This invasive *Phragmites* has also been invading the roadway corridors in southwestern Ontario over the past decade. Currently, no provincial agencies include an early-detection program as part of their overall control strategy to manage invasive *Phragmites* in wetlands or roadways. An early-detection program would be beneficial since efficacy of herbicide treatment is known to be better when *Phragmites* patches are small and sparse than when they are large and dense.

Some recent studies have explored the use of high-resolution multispectral satellite data such as IKONOS, QuickBird, WorldView 2 and 3 (WV 3) for species-level mapping. Although these multispectral data have relatively low spectral resolution, the images have higher temporal resolution and the image availability is higher. Hence these data are very useful in largescale *Phragmites* mapping and monitoring. In this paper, we tested the suitability of high-resolution (80 cm) multi-spectral satellite data from World View 3 (WV 3) to detect small patches of invasive *Phragmites* in wetlands and roadside corridors. These results should inform MTO of the feasibility of using WV 3 in early detection programs.

We selected Norfolk County for this study because it is situated on the north shore of Lake Erie, where there are several small towns connected by approximately 4,100 kms of roads, of which 83% are in rural areas. There are also several large coastal wetland complexes including the Big Creek National Wildlife Area (BCNWA), where we have ground-truth data of invasive *Phragmites* from an ancillary study. Big Creek wetland is

located west of Hwy 59 at the base of Long Point Bay on Lake Erie, in the municipality of Norfolk County.

WV 3, which is operated by DigitalGlobe, is a fourth-generation, optical and commercial earth-observation satellite, with the highest spatial resolution (30 cm panchromatic and 1.24 m multispectral) of all existing optical satellites available for research. A cloud-free WV 3 image was acquired in 07th July 2016. The image covered an area of 437 km^2, which includes Big Creek Marsh and other parts of the Long Point watershed. The training data for image classification and accuracy assessment of invasive *Phragmites* in the BCWNA were manually digitized from an image (8-cm resolution) acquired with an Unmanned Aerial Vehicle (UAV; Sensefly eBee) in late summer 2015. We selected a sample area of 1 × 1 km^2 within the wetland that contained large *Phragmites* patches as well as many of the most common wetland classes. We also selected a 4-km stretch of arterial 2 lane road (Hwy 59) that included six spraying locations to test the usefulness of WV 3 for mapping *Phragmites* in roadsides. These relatively smaller areas were chosen to increase our classification accuracy.

Image pre-processing and processing was conducted with the software ENVI 5.5 (Harris Geospatial). Radiometric correction and atmospheric correction (ENVI QUAC correction) were performed for the image data to obtain surface reflectance values. Minimum Noise Fraction (MNF) transformation was performed for the pre-processed WV 3 image to reduce image dimensionality. Then Mixture-Tuned Match Filtering (MTMF) was applied to the image. MTMF is a partial un-mixing algorithm for the mixed pixels so that the relative fraction of the reflectance of the target feature can be separated

out from the background. MTMF reduces the image classification errors (especially omission errors) when detecting *Phragmites* and makes it possible to detect smaller, less dense patches. After MTMF transformation, we classified the image using maximum likelihood classification. The reflectance image was also classified with the maximum likelihood classification and was compared against the classification with MTMF transformation. For roadsides, we created a 20-m buffer around the center-line of the road to avoid having to classify complex features in the image such as built-up areas. Ground-truthing data were obtained as described above. Random points that were not used as training data for the classification were used for the accuracy assessment.

Using ENVI 5.5, we classified the wetland image into seven classes: Cattail Organic Shallow Marsh, Floating Leaved Sallow Aquatic Marsh, Meadow Marsh, Mixed Organic Shallow Marsh, Open water, invasive *Phragmites*, and roads with overall accuracy of 87.4% for the MTMF image and 89.8% for the reflectance image. We also classified the road image into seven classes: roads, trees, *Phragmites,* roadsides, ground, grass, and agriculture. The highest confusion with *Phragmites* were with grasses and agricultural lands. Accuracy of the *Phragmites* classification was higher for the MTMF image (81.6% producer's and 75.6% user's accuracy) than for the reflectance image (73.7% producer's and 71.4% user's accuracy), while overall accuracy was 84.4% and 74.6%, for the MTMF and the reflectance image, respectively.

One challenge we experienced with WV 3 was the considerable time and skill required to pre-process the image initially. After determining the exact mapping protocol, however, the processing time was significantly reduced; nevertheless, some knowledge

and expertise in remote sensing and ecology would still be required for anyone considering using our approach. Furthermore, we emphasize that ground-truth data collected at the appropriate time is essential for accurate estimation of *Phragmites* in both wetlands and roadsides. We conclude that WV 3 can be used in early-detection programs, as long as the procedure is applied to a relatively small area in wetlands (maximum 100 ha) or roadsides (4-km segment) to increase accuracy.

7.3. Introduction

Phragmites australis (Cav.) Trin. ex Steudel (the common reed) is a perennial grass that grows in aquatic, semi-aquatic, and terrestrial habitats throughout the world. Saltonstall (2002) identified 27 genetically distinct groups (haplotypes) worldwide, of which 11 have been found in North America. Over the past 2 decades, the European haplotype M began to make rapid incursions into Canada and the U.S., especially into coastal wetlands of the Laurentian Great Lakes (Wilcox et al. 2003; Tulbure et al. 2007; Wilcox 2012; Bourgeau-Chavez et al. 2015), and along highway corridors (Saltonstall 2002; Lelong et al. 2007). This haplotype exhibits invasive characteristics, including its ability to aggressively colonize exposed mud flats sexually (through seeds), and then expand asexually (through rhizomes) to form dense monocultures that inhibit biodiversity of other plants and wildlife (Meyerson et al. 2000a; Markle and Chow-Fraser 2018). Its rapid spread has been attributed to it being a superior competitor against other emergent vegetation (Rickey and Anderson 2004; Uddin et al. 2014) and to being more tolerant of disturbances (e.g. road maintenance and changes in hydrologic regimes) and stress (e.g.

increased salinity due to road de-icing salts) (McNabb & Batterson,1991; Marks et al.,1994; Chambers et al. 1999; Saltonstall 2002).

Roadsides provide suitable conditions for invasive *Phragmites* to establish. Most roadsides are bordered by drainage ditches that form a linear network of 'wetlands' (Jodoin et al. 2008). Over the past 50 years, *Phragmites* has expanded in these roadside ditches in both Canada and the U.S. (Meyerson et al. 2000b). Studies have documented a dramatic expansion of invasive *Phragmites* throughout Quebec following the construction of a road network (Jodoin et al. 2008; Brisson et al. 2010). Even though these ditches can facilitate the spread of *Phragmites* into nearby ecosystems, only a few studies have been conducted to investigate how infested roadways influence the invasion pattern of *Phragmites* in adjacent wetlands (Richburg et al. 2001; Maheu-Giroux & de Blois 2007).

A big challenge to those trying to study the effects of roadside *Phragmites* invasions on ecosystems is lack of an efficient method to map *Phragmites* accurately in the narrow linear wetlands along road sides or highway medians. In past studies, investigators relied on visual surveys while driving on roads to map *Phragmites* distributions (Lelong et al. 2007; Jodoin et al. 2008). Such an approach necessarily limits the geographic coverage of the study area. Remote sensing is the most appropriate approach to use for mapping *Phragmites* along roadsides, especially for areas that are difficult to survey safely (Davranche et al. 2009), such as sides and medians of busy highways and roads. Since herbicide treatments are more effective when *Phragmites* stands are small, it would be beneficial to have an early detection system that could identify and eradicate new patches in a timely manner before they can spread and become

dense. Fortunately, a number of remote sensing options are now available both for routine monitoring and for early detection purposes.

Airborne sensors such as AVIRIS, CASI, HyMap, and PROBE-1 have been used successfully in species level mapping (Schmidt and Skidmore, 2001). These approaches are however limited by the relatively small geographic coverage, and the low temporal resolution of image acquisition. Some recent studies have explored the use of high-resolution multispectral satellite data such as IKONOS, QuickBird, WorldView 2 and 3 (WV 3) for species-level mapping (Adam et al. 2010; Li et al. 2015; Mustafa & Habeeb, 2014). Although these multispectral data have lower spectral resolution, the images have higher temporal resolution and the image availability is higher. Hence these data are very useful in large-scale *Phragmites* mapping and monitoring.

7.4. Objectives

The goal of this study is to test the feasibility of using WV 3 satellite data to detect young, less dense and small *Phragmites* patches occurring in both wetland complexes and along roadsides of Norfolk County.

7.5. Methodology

7.5.1. Study sites

We selected Norfolk County for this study because it is situated on the north shore of Lake Erie, where there are several small towns and numerous recreational destinations (Niewójt, 2007) as well as several large coastal wetland complexes including the Big Creek National Wildlife Area (BCNWA), where we have ground-truth data of invasive

Phragmites from an ancillary study (Marcaccio et al. 2016). Approximately 4,100 km of roads currently exist in Norfolk County, of which 83% percent are in rural areas ("Asset-Management-Plan-Roads.pdf," n.d.). Big Creek wetland is located west of Hwy 59 at the base of Long Point Bay on Lake Erie, in the municipality of Norfolk county (Ashley & Robinson 1996). In 1982, the Long Point wetlands were declared to be "Wetlands of International Importance" and was designated a "World Biosphere Reserve" by the Man and the Biosphere Program of UNESCO.

7.5.2. Remote sensing data

WV 3, which is operated by DigitalGlobe, is a fourth-generation, optical and commercial earth-observation satellite, with the highest spatial resolution (30 cm panchromatic) of all existing optical satellites available for research. A cloud-free WV 3 image was acquired in 07th July 2016. The image covers an area of 437 km^2, which includes Big Creek Marsh and other parts of the Long Point watershed (Figure 7.1). The image consists of one panchromatic band (445-808 nm spectral resolution and 30 cm spatial resolution) and eight multispectral bands (80 cm spatial resolution), including the coastal blue (397-454 m), blue (445-517 nm), green (507-586 nm), yellow (580-629 nm), red (626-696 nm), red edge (698-749 nm), Near InfraRed 1 (NIR 1; 765-899 nm) and NIR 2 (857-1039 nm) bands. The range of available spectral bands and high spatial resolution makes WV 3 suitable for a wide range of applications including vegetation monitoring, coastal monitoring, mineral exploration and species-level mapping (Kruse & Perry, 2013; Wang, Zhang, Lin, & Fang, 2015).

7.5.3. Ground Truth Data

The training data for image classification and accuracy assessment of invasive *Phragmites* in the BCWNA were manually digitized from an image (8-cm resolution) acquired with an Unmanned Aerial Vehicle (UAV; Sensefly eBee) in late summer 2015 (Marcaccio et al. 2016). We selected a sample area of 1 × 1 km2 within the wetland that contained large *Phragmites* patches as well as many of the most common wetland classes. We selected a 4-km stretch of arterial 2 lane road (Hwy 59) that included six spraying locations to test the usefulness of WV 3 for mapping *Phragmites* in roadsides. (Figure 7.1). These relatively smaller areas were chosen to increase our classification accuracy. Training data for image classification and accuracy assessment of invasive *Phragmites* in roadsides of Norfolk County were geographic coordinates corresponding to *Phragmites* stands that had been sprayed during the summer of 2017 (E. Clelland, Nature Conservancy Canada, unpub. data). We also consulted Google street View to determine accuracy of Phragmites being classified on these roads.

7.5.4. Remote sensing processing

Image pre-processing and processing was conducted with the software ENVI 5.5 (Harris Geospatial). Radiometric correction and atmospheric correction (ENVI QUAC correction) were performed for the image data to obtain surface reflectance values. Minimum Noise Fraction (MNF) transformation was performed for the pre-processed WV 3 image to reduce image dimensionality. Then Mixture-Tuned Match Filtering (MTMF) was applied to the image. MTMF is a partial un-mixing algorithm for the mixed pixels so that the relative fraction of the reflectance of the target feature can be separated

out from the background. This technique produces two images that represent percent target feature abundance and a measure of feasibility without prior knowledge of the reflectance of the background features (Lass et al., 2005; Parker Williams & Hunt Jr.2004). MTMF reduces the image classification errors (especially omission errors) when detecting *Phragmites* and makes it possible to detect smaller, less dense patches. The endmembers for the MTMF classification were extracted from the reflectance image. After MTMF transformation, we classified the image using maximum likelihood classification using a separate set of ground truth data. The reflectance image was also classified with the maximum likelihood classification and was compared against the classification with MTMF transformation. For roadsides, we created a 20-m buffer around the centerline of the road to avoid having to classify complex features in the image such as built-up areas. Ground-truth data were obtained as described above. For the accuracy assessment, we used a set of randomly generated points for locations that were not used as training data for the classification.

7.6. Results and Discussion

7.6.1. Early detection of *Phragmites* in wetlands

We classified features in both the reflectance and MTMF transformed images into seven classes (Table 7.1). Overall accuracy of the reflectance image reached 89.75% and that of the MTMF image was slightly lower at 87.39%.

Both overall accuracy and that for *Phragmites* alone were slightly lower for the MTMF transformed image. Manual digitization of the UAV image only captured the dense, large, and distinct *Phragmites* patches but not the smaller less dense patches that

are important for early detection purposes. The MTMF transformation, however, detected smaller, less dense, presumably younger *Phragmites* patches (Figure 7.2 b and c). Most of the smaller *Phragmites* stands detected by the MTMF transformation occurred in areas classified as meadow marsh by the reflectance image and the manual digitization. These findings indicate that Phragmites is likely invading areas initially covered by meadow marsh and cattail.

7.6.2. Early detection of *Phragmites* in roadsides

We classified features in the image of the roadside buffer into seven classes (Table 7.2). Classification of the reflectance image gave an overall accuracy of 74.6% while that of the MTMF image yielded a higher accuracy of 84.4%. Highest confusion with *Phragmites* were with grasses and agricultural lands. Unlike wetlands, however, accuracy of roadsides was higher for the MTMF than for the reflectance image. Since MTMF reduces the confusion between agricultural lands and *Phragmites*, we obtained higher overall accuracy and Phragmites accuracy for the MTMF image than with the reflectance image (Table 7.2). In a preliminary study, we used a buffer size of 50 m, and obtained a much lower classification accuracy compared to the 20-m buffer we used in this study. Therefore, we recommend using the smallest buffer size possible for the road type of interest, to avoid having to classify additional features such as buildings and paved areas.

Despite the relatively high commission error, five of the six sprayed locations in the selected area had *Phragmites* detected by both the reflectance and MTMF image. Since the spray locations were centroids with no details on the length of the *Phragmites*

patch that had been sprayed or which side of the road had been sprayed, we consulted Google Street View to obtain ancillary information to confirm the presence of Phragmites. Since the Google Street View image had been collected in August 2013, three years prior to acquisition of the WV 3 image, and four years prior to the herbicide spraying, we were not surprised to see relatively low cover of *Phragmites* on this road segment in the Google Street View. Only three of the sprayed locations in 2017 actually showed *Phragmites* in 2013. We examined all locations where *Phragmites* were eventually sprayed in 2017 and noted that they were either roadside ditches or small ponds that could easily be colonized by *Phragmites* (Figure 7.4). Some locations had cattail, and some had short grass species and shrubs, making them good candidates to be invaded by *Phragmites* after three growing seasons. There were, however, two sprayed locations that did not show any signs of invasion in 2013 (e.g. Figure 7.4 c and d). This shows that *Phragmites* can invade suitable habitats relatively quickly. Without more updated field truth, we will not be able to obtain a more valid accuracy assessment. It goes without saying that better results could have been obtained if the timing of image acquisition and field truth had been synchronized.

We were able to use an automated classification protocol in ENVI 5.5 to accurately map very small, sparsely growing patches of *Phragmites* in wetlands and roadsides in a WV 3 satellite image of Norfolk County. Timing of image acquisition and plant phenology play a major role in *Phragmites* mapping (Rupasinghe and Chow-Fraser, unpub. data). *Phragmites* produced the most unique, detectable signal that separated it from other vegetation classes (especially cattail and meadow marsh) during the peak

summer period. We believe that the distinct inflorescence, the unique green color due to the high chlorophyll concentration, the leaf arrangement, and the high water-use efficiency of the plant during this period all combine to produce this unique spectral signature. We observed more confusion between *Phragmites* and agricultural lands, especially corn fields when mapping during fall or spring using pixel-based classification methods; however, object-based classification may improve the classification accuracy if fall or spring-time images are used. Several studies reported higher accuracy if images acquired in different months or from different sensors are combined to detect individual species (Hill et al. 2010; Li et al. 2014; Li et al. 2015). Use of Short-Wave IR bands may also improve the classification accuracy. One obvious limitation of WV 3 is the high cost of the images—which makes it less attractive for mapping large invasion areas. Therefore, use of WV 3 images are feasible for early-detection purposes, and other free or low-cost satellite images should be used to map large infested areas.

Airborne, hyperspectral images had been successfully used in species-level mapping in previous studies (Schmidt & Skidmore, 2001). The high spectral resolution of these data provides sufficient details for vegetation mapping, especially for the smaller weed and grass species. However, these data often have limited coverage and are not convenient for frequent monitoring purposes. Soft classification algorithms such as Linear Spectral Unmixing (LSU), MTMF, and Bayesian Probability have been used successfully to detect invasive weed species with hyperspectral imagery (Williams & Hunt Jr 2004; Shafii et al. 2004; Lass et al. 2005). These algorithms separate out defined signatures (endmembers) from the background in the mixed pixels. These mixed

reflectance values often produce high omission errors of the target features. Commission errors may also arise if spectrally similar classes occur in the same image. MTMF helps to distinguish smaller, less dense *Phragmites* patches from these mixed pixels and can help to reduce commission error due to occurrence of similar classes such as when corn and *Phragmites* in roadsides occur in the same pixel. Therefore, use of spectral unmixing of WV 3 is a promising method for early detection of *Phragmites* in both wetlands and roadways.

One challenge we experienced with WV 3 was the considerable time and skill required to pre-process the image initially. After determining the exact mapping protocol, however, the processing time was significantly reduced (see Table 7.3); nevertheless, some knowledge and expertise in remote sensing and ecology would still be required for anyone considering using our approach. Furthermore, we emphasize that ground-truth data and the images collected at the summer time where *Phragmites* stand out from the other wetland classes is essential for accurate estimation of *Phragmites* in both wetlands and roadsides.

7.7. Conclusions and Recommendations

Our study shows that the high-resolution multispectral satellite data from WV 3 could be successfully used for early detection. Sub-pixel classification is capable of detecting less dense, smaller *Phragmites* patches in both wetlands and roadsides and reduces the omission error. Moreover, this method resulted in less confusion between *Phragmites* and agricultural lands and built-up areas. Therefore, commission error is also reduced for *Phragmites* detection in roadsides.

We recommend using relatively small areas for both wetlands and roadsides. Specifically, we recommend using a smaller buffer size as possible around roads (e.g. 20-m for two-lane) to avoid confusion with complex land-cover classes such as built-up areas. Furthermore, we recommend using as many ground-truth points as possible to increase accuracy. Object-based classification and use of combination of images collected in different months may also increase overall accuracy.

7.8. Acknowledgements

This research was funded by HIIFP Grant to P. Chow-Fraser. We thank Barbara Macdonell for her unwavering support for this project.

7.9. References

Adam, E., Mutanga, O., & Rugege, D. (2010). Multispectral and hyperspectral remote sensing for identification and mapping of wetland vegetation: a review. *Wetlands Ecology and Management*, *18*(3), 281–296.

Ashley, E. P., & Robinson, J. T. (1996). Road mortality of amphibians, reptiles and other wildlife on the Long Point Causeway, Lake Erie, Ontario. *Canadian Field Naturalist*, *110*(3), 403–412.

Asset-Management-Plan-Roads.pdf. (n.d.). Retrieved from http://www.norfolkcounty.ca/download/government/public_works/Asset-Management-Plan-Roads.pdf

Brisson, J., de Blois, S., & Lavoie, C. (2010). Roadside as invasion pathway for common reed (Phragmites australis). *Invasive Plant Science and Management*, *3*(4), 506–514.

Bourgeau-Chavez et al. 2015 Development of a Bi-National Great Lakes Coastal Wetland and Land Use Map Using Three-Season PALSAR and Landsat Imagery. *Remote Sensing*: 7, 8655-8682; doi:10.3390/rs70708655

Chambers, R. M., Meyerson, L. A., & Saltonstall, K. (1999). Expansion of *Phragmites australis* into tidal wetlands of North America. *Aquatic Botany*, *64*(3–4), 261–273.

Davranche, A., Lefebvre, G., & Poulin, B. (2009). Radiometric Normalization of SPOT-5 Scenes. *Photogrammetric Engineering & Remote Sensing*, *75*(6), 723-728.

Hazelton, E. L., Mozdzer, T. J., Burdick, D. M., Kettenring, K. M., & Whigham, D. F. (2014). *Phragmites australis* management in the United States: 40 years of methods and outcomes. *AoB Plants*, *6*.

Hill, R. A., Wilson, A. K., George, M., & Hinsley, S. A. (2010). Mapping tree species in temperate deciduous woodland using time-series multi-spectral data. *Applied Vegetation Science*, *13*(1), 86–99.

Jodoin, Y., Lavoie, C., Villeneuve, P., Theriault, M., Beaulieu, J., & Belzile, F. (2008). Highways as corridors and habitats for the invasive common reed *Phragmites australis* in Quebec, Canada. *Journal of Applied Ecology*, *45*(2), 459–466. https://doi.org/10.1111/j.1365-2664.2007.01362.x

Kruse, F. A., & Perry, S. L. (2013). Mineral Mapping Using Simulated Worldview-3 Short-Wave-Infrared Imagery. *Remote Sensing*, *5*(6), 2688–2703. https://doi.org/10.3390/rs5062688

Lass, L. W., Prather, T. S., Glenn, N. F., Weber, K. T., Mundt, J. T., & Pettingill, J. (2005). A review of remote sensing of invasive weeds and example of the early detection of spotted knapweed (*Centaurea maculosa*) and babysbreath (*Gypsophila paniculata*) with a hyperspectral sensor. *Weed Science*, *53*(2), 242–251.

Lelong, B., Lavoie, C., Jodoin, Y. and Belzile, F. 2007. Expansion pathways of the exotic common reed (*Phragmites australis*): a historical and genetic analysis. *Diversity and Distributions* 13: 430-437.

Li, D., Ke, Y., Gong, H., Chen, B., & Zhu, L. (2014). Tree species classification based on WorldView-2 imagery in complex urban environment. In *Earth Observation and Remote Sensing Applications (EORSA), 2014 3rd International Workshop on* (pp. 326–330). IEEE.

Li, D., Ke, Y., Gong, H., & Li, X. (2015). Object-Based Urban Tree Species Classification Using Bi-Temporal WorldView-2 and WorldView-3 Images. *Remote Sensing*, *7*(12), 16917–16937. https://doi.org/10.3390/rs71215861

Maheu-Giroux, M., & de Blois, S. (2007). Landscape ecology of *Phragmites australis* invasion in networks of linear wetlands. *Landscape Ecology*, *22*(2), 285–301.

Marks, M., Lapin, B., & Randall, J. (1994). *Phragmites australis* (P. communis): threats, management and monitoring. *Natural Areas Journal*, *14*(4), 285–294.

Marcaccio, J.V., Markle, C.E. and Chow-Fraser, P. 2016. Use of fixed-wing and multi-rotor unmanned aerial vehicles to map dynamic changes in a freshwater marsh. *J. Unmanned Veh. Syst.* 4: 193–202 (2016) dx.doi.org/10.1139/juvs-2015-0016

Markle, C.E. and Chow-Fraser, P. 2018 Effects of European Common Reed on Blanding's Turtle Spatial Ecology. *The Journal of Wildlife Management;* DOI: 10.1002/jwmg.21435

McNabb, C. D., & Batterson, T. R. (1991). Occurrence of the common reed, *Phragmites australis*, along roadsides in Lower Michigan. *Michigan Academician (USA)*.

Meyerson, L. A., Saltonstall, K., Windham, L., Kiviat, E., & Findlay, S. (2000a). A comparison of *Phragmites australis* in freshwater and brackish marsh environments in North America. *Wetlands Ecology and Management*, *8*(2–3), 89–103.

Meyerson, L. A., Saltonstall, K., Windham, L., Kiviat, E., & Findlay, S. (2000b). A comparison of *Phragmites australis* in freshwater and brackish marsh environments in North America. *Wetlands Ecology and Management, 8*(2–3), 89–103.

Mustafa, Y. T., & Habeeb, H. N. (2014). Object based technique for delineating and mapping 15 tree species using VHR WorldView-2 imagery. In *Remote Sensing for Agriculture, Ecosystems, and Hydrology XVI* (Vol. 9239, p. 92390G). International Society for Optics and Photonics.

Niewójt, L. (2007). From waste land to Canada's tobacco production heartland: Landscape change in Norfolk County, Ontario. *Landscape Research*, *32*(3), 355–377.

Parker Williams, A. E., & Hunt Jr, E. R. (2004). Accuracy assessment for detection of leafy spurge with hyperspectral imagery. *Journal of Range Management*, *57*(1), 106–112.

Rickey, M.A. and Anderson, R.C. 2004. Effects of nitrogen addition on the invasive grass *Phragmites australis* and a native competitor *Spartina pectinata*. Journal of Applied Ecology. 41: 888–896

Richburg, J. A., Patterson III, W. A., & Lowenstein, F. (2001). Effects of road salt and *Phragmites australis* invasion on the vegetation of a western Massachusetts calcareous lake-basin fen. *Wetlands*, *21*(2), 247–255.

Saltonstall, K. (2002). Cryptic invasion by a non-native genotype of the common reed, *Phragmites australis,* into North America. *Proceedings of the National Academy of Sciences*, *99*(4), 2445–2449.

Schmidt, K. S., & Skidmore, A. K. (2001). Exploring spectral discrimination of grass species in African rangelands. *International Journal of Remote Sensing*, *22*(17), 3421–3434.

Shafii, B., Price, W. J., Prather, T. S., Lass, L. W., & Thill, D. C. (2004). Using landscape characteristics as prior information for Bayesian classification of yellow starthistle. *Weed Science*, *52*(6), 948–953.

Tulbure, M.G., Johnston, C.A. and Auger, D.L. 2007. Rapid Invasion of a Great Lakes Coastal Wetland by Non-native *Phragmites australis* and *Typha*. *J. Great Lakes Res.* 33 (Special Issue 3): 269–279.

Uddin, N., Robinson, R.W., Caridi, D. and Al Harun, A.Y. 2014. Suppression of native *Melaleuca ericifolia* by the invasive *Phragmites australis* through allelopathic root exudates. *Am J. Botany* 101(3): 1–9,

Wang, T., Zhang, H., Lin, H., & Fang, C. (2015). Textural–Spectral Feature-Based Species Classification of Mangroves in Mai Po Nature Reserve from Worldview-3 Imagery. *Remote Sensing*, 8(1), 24. https://doi.org/10.3390/rs8010024

Wilcox, K. L., Petrie, S. A., Maynard, L. A., & Meyer, S. W. (2003). Historical distribution and abundance of *Phragmites australis* at long point, Lake Erie, Ontario. *Journal of Great Lakes Research*, 29(4), 664–680.

Wilcox, D.A. 2012. Response of wetland vegetation to the post-1986 decrease in Lake St. Clair water levels: Seed-bank emergence and beginnings of the *Phragmites australis* invasion. *Journal of Great Lakes Research*, 38: 270-277.

Table 7.1 Summary of classification accuracies for wetlands in the BCWNA. Data for *Phragmites* have been bolded for emphasis.

Class	Reflectance image		MTMF image	
	Producer's accuracy (%)	User's Accuracy (%)	Producer's accuracy (%)	User's Accuracy (%)
Cattail Organic Shallow Marsh	98.99	81.59	99.71	73.38
Meadow Marsh	72.60	97.21	62.82	100.00
Mixed Organic Shallow Marsh	91.73	54.96	89.93	56.56
Open Water	100	100.00	100.00	99.53
Phragmites	**80.21**	**99.62**	**77.32**	**95.66**
Roads	100.00	100.00	100.00	100.00
Floating Leaved Shallow Aquatic Marsh	100.00	96.68	99.47	99.21

Table 7.2 Summary of classification accuracies for roadsides using WV 3. Data for *Phragmites* are bolded for emphasis.

Class	Reflectance image		MTMF image	
	Producer's accuracy (%)	User's Accuracy (%)	Producer's accuracy (%)	User's Accuracy (%)
Roads	100.00	100.00	100	100
Trees	100.00	57.44	97.00	79.89
Phragmites	**73.73**	**71.43**	**81.57**	**75.64**
Road side	95.45	75.00	100	95.65
Ground	96.09	96.09	99.29	88.36
Grass	73.60	82.09	71.85	85.50
Agriculture	39.89	84.03	80.87	86.82

Table 7.3 Overall utility of WV 3 for early detection of *Phragmites* per km^2

Parameter	Details
Cost of imagery (Panchromatic + 8 band multispectral)	$ 23 CAD with minimum area of 25 km^2 (with academic discount)
Time for preprocessing	~ 2 months initially and ~1 hour afterwards
Time for image classification	~ 1.5 month initially and ~5 hours afterwards
Image availability	Temporal resolution is 4.5 days (clear image availability depends on the weather conditions and the cloud cover)
Training data for image classification	At least 5 random locations for each class included in classification. More training locations would provide higher accuracy.
Ground truth for accuracy assessment	At least 5 random locations for each class included in classification. More training locations would provide higher accuracy.
Software	Require specific remote sensing software such as ENVI, PCI Geomatica, ERDAS IMAGINE etc. that may cost >5000 CAD

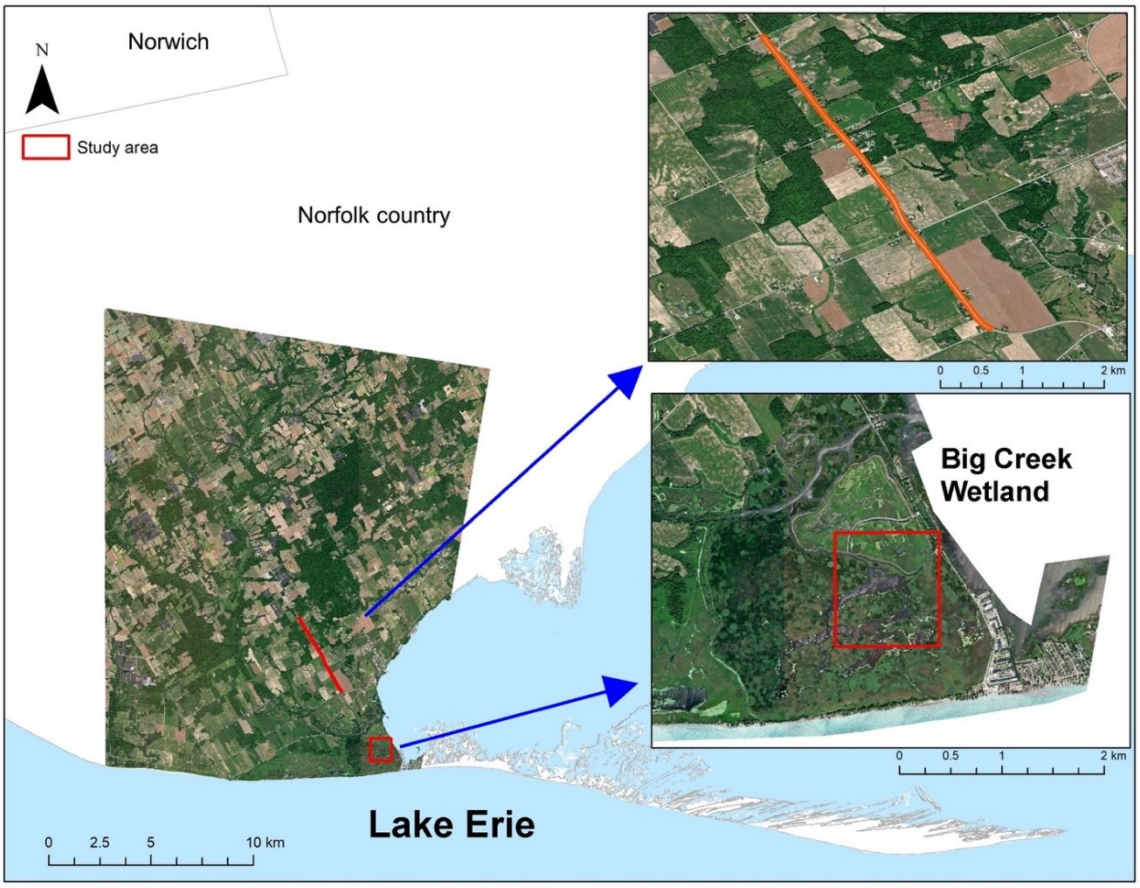

Figure 7.1 Footprint of the WV 3 image used in this study showing Big Creek Wetland (bottom right inset) and the road segment (top right inset) that was classified.

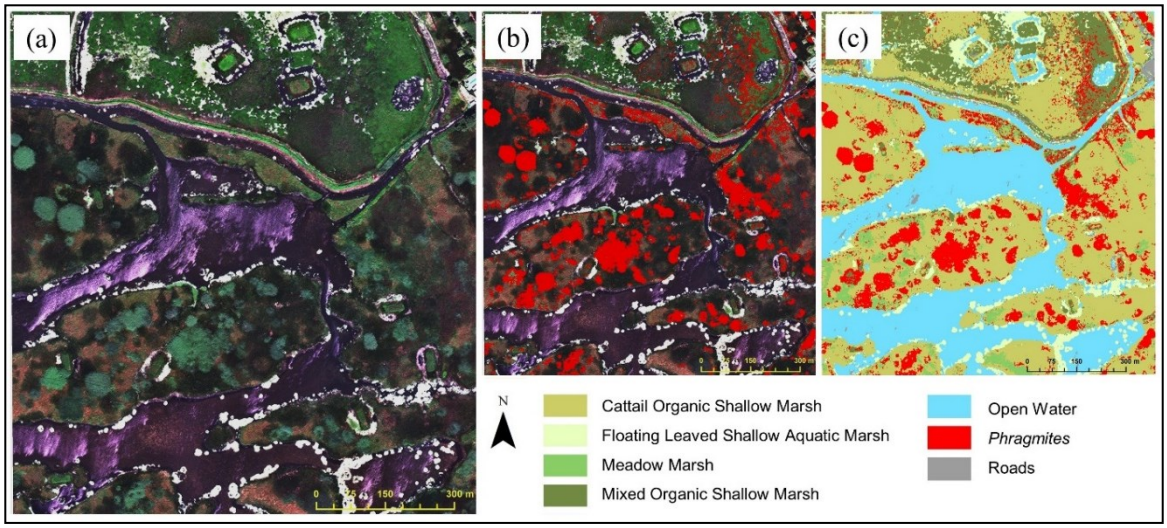

Figure 7.2 Different views of a segment of the WV3 image of Big Creek National Wildlife Area showing (a) the unclassified true color image in which *Phragmites* appears as distinct blue-green spherical units (b) *Phragmites* detected through MTMF image, (c) *Phragmites* classified in red in the MTMF image. The legend for classification only refers to (b) and (c).

Figure 7.3 (a) True color WV3 image showing region of interest that was classified (b) one road segment and 20-m buffer used in the classification (c) classified image for the MTMF image pertaining to (b). The legend only pertains to (c).

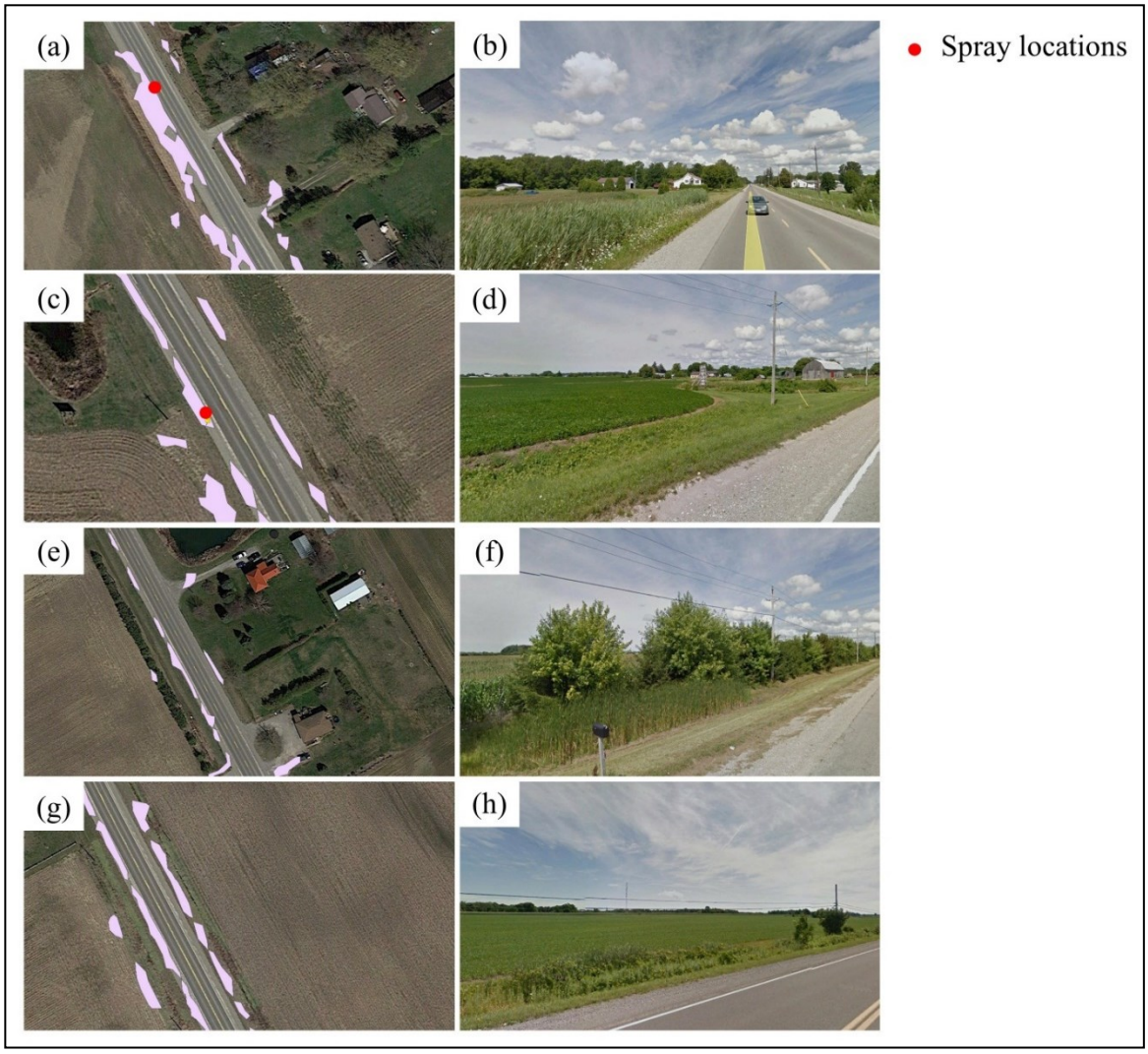

Figure 7.4 WV3 images of road segments acquired in July 2016 overlain with classified *Phragmites* stands (pink polygons) in the 20-m buffer (left panels) shown with corresponding Google Street View taken in August 2013 at each of these locations (right panels). The red circle indicates locations on the road where herbicide spraying had taken place during July 2017. (a) and (b): Sprayed location where *Phragmites* was confirmed in the 2013 Street View; (c) and (d): Sprayed location where *Phragmites* had not been detected in 2013 Street; (e) and (f): Location of classified *Phragmites* patches in 2016

that showed presence of *Phragmites* in the corresponding 2013 Google Street View; and (g) and (h): Location of classified *Phragmites* patches that did not show *Phragmites* in corresponding Street View, but that had suitable habitat for invasion of *Phragmites* after three seasons.

Glossary

Term	Definition	Reference
Burn severity	Degree to which a site has been altered or disrupted by fire; loosely, a product of fire intensity and residence time	(NWCG, 2005)
Ecosystem disturbance	A cause: a physical force, agent, or process, either abiotic or biotic, causing a perturbation (which includes stress) in an ecological component or system; relative to a specified reference state and system; defined by specific characteristic	(Rykiel, 1985)
Ecosystem health	A comprehensive, multi-scale, dynamic, hierarchical measure of system resilience, organization, and vigor	(Costanza & Mageau, 1999)
Ecosystem productivity	The rate of whole-ecosystem biomass production	(Fridley, 2001)
Ecosystem stress	an external force or factor, or stimulus that causes changes in the ecosystem, or causes the ecosystem to respond, or entrains ecosystemic dysfunctions that may exhibit symptoms	(Rapport et al., 1985)
Fire intensity	Rate of spread of the fire edge multiplied by the amount of fuel consumed by flaming combustion and the heat yield of the fuel	(Byram, 1959)
Fire regime	The features of historic, natural fires that have been typical for a particular ecosystem or set of ecosystems	(Pyne et al., 1996)

Fire weather	Weather conditions that influence fire ignition, behavior and suppression	(National Park Service | USDA Forest Service, n.d.)
GIS	A computer system for managing spatial data and is capable of capturing, input, manipulate, transform, visualize, combine, query, analyze, model, and output spatial data	(Bonham-Carter, 1994)
Healthy ecosystem	A healthy ecosystem is one that is sustainable, it has the ability to maintain its structure (organization) and function (vigor) over time in the face of external stress (resilience).	(Costanza & Mageau, 1999)
Organization	the number and diversity of interactions between the components of the system	(Costanza, 2012)
Resilience	An ecosystem's ability to maintain its structure and pattern of behavior in the presence of stress	(Holling, 1973)
RS	The technology of acquiring data through a device which is located at a distance from the object, and analysis of the data for interpreting the physical attributes of the object	(Gupta, 2017)
Species richness	The number of species within a defined region	(Moore, 2013)
Vigor	A measure of an ecosystem's activity, metabolism or primary productivity	(Costanza, 2012)

Literature cited

Bonham-Carter, G. F. (1994). *Geographic Information Systems for Geoscientists: Modelling with GIS* (First Edition, Vol. 13). Elsevier.

Byram, G. M. (1959). *Combustion of forest fuels. In 'Forest fire: Control and use'.(Ed. KP Davis) pp. 61–89*. McGraw-Hill: New York.

Costanza, R. (2012). Ecosystem health and ecological engineering. *Ecological Engineering*, *45*, 24–29. https://doi.org/10.1016/j.ecoleng.2012.03.023

Costanza, R., & Mageau, M. (1999). What is a healthy ecosystem? *Aquatic Ecology*, *33*(1), 105–115.

Fridley, J. D. (2001). The influence of species diversity on ecosystem productivity: How, where, and why? *Oikos*, *93*(3), 514–526. https://doi.org/10.1034/j.1600-0706.2001.930318.x

Gupta, R. P. (2017). *Remote Sensing Geology* (3rd Edition). Springer. https://books.google.ca/books?id=lERADwAAQBAJ&printsec=copyright&source=gbs_pub_info_r#v=onepage&q&f=false

Holling, C. S. (1973). Resilience and Stability of Ecological Systems. *Annual Review of Ecology and Systematics*, *4*(1), 1–23. https://doi.org/10.1146/annurev.es.04.110173.000245

Moore, J. C. (2013). *Diversity, taxonomic versus functional*.

National Park Service | USDA Forest Service. (n.d.). *Fire Terminology*. Retrieved April 16, 2021, from https://www.fs.fed.us/nwacfire/home/terminology.html

NWCG, [National Wildfire Coordinating Group]. (2005). *Glossary of Wildland Fire Terminology. National Interagency Fire Center. Boise, Idaho*. https://www.nwcg.gov/

Pyne, S. J., Andrews, P. L., & Laven, R. D. (1996). *Introduction to wildland fire, revised* (2nd ed.). John Wiley and Sons, Inc.

Rapport, J. D., Regier, H. A., & Hutchinson, T. C. (1985). Ecosystem Behavior Under Stress. *The American Naturalist*, *125*(5), 617–640. JSTOR.

Rykiel, E. J. (1985). Towards a definition of ecological disturbance. *Australian Journal of Ecology*, *10*(3), 361–365. https://doi.org/10.1111/j.1442-9993.1985.tb00897.x